Southern Methodist University

SMU Scholar

Physics Theses and Dissertations | Physics

Summer 8-6-2019

Massive elementary particles in the Standard Model and its supersymmetric triplet Higgs extension

Keping Xie
Southern Methodist University, kepingx@smu.edu

Follow this and additional works at: https://scholar.smu.edu/hum_sci_physics_etds

 Part of the Elementary Particles and Fields and String Theory Commons

Recommended Citation

Xie, Keping, "Massive elementary particles in the Standard Model and its supersymmetric triplet Higgs extension" (2019). *Physics Theses and Dissertations*. 7.
https://scholar.smu.edu/hum_sci_physics_etds/7

This Dissertation is brought to you for free and open access by the Physics at SMU Scholar. It has been accepted for inclusion in Physics Theses and Dissertations by an authorized administrator of SMU Scholar. For more information, please visit http://digitalrepository.smu.edu.

MASSIVE ELEMENTARY PARTICLES IN THE STANDARD MODEL
AND ITS SUPERSYMMETRIC TRIPLET HIGGS EXTENSION

Approved by:

Dr. Pavel M. Nadolsky, Advisor
Southern Methodist University

Dr. Roberto Vega, Advisor
Southern Methodist University

Dr. Stephen J. Sekula, Committee Chair
Southern Methodist University

Dr. John M. Campbell, Committee Member
Fermi National Accelerator Laboratory

Dr. Chien-Peng Yuan, Committee Member
Michigan State University

MASSIVE ELEMENTARY PARTICLES IN THE STANDARD MODEL AND ITS SUPERSYMMETRIC TRIPLET HIGGS EXTENSION

A Dissertation Presented to the Graduate Faculty of the

Dedman College of Humanities and Sciences

Southern Methodist University

in

Partial Fulfillment of the Requirements

for the degree of

Doctor of Philosophy

with a

Major in Physics

by

Keping Xie

(B.S., Physics, Peking University)

August 6, 2019

Copyright (2019)

Keping Xie

All Rights Reserved

ACKNOWLEDGMENTS

This dissertation would not have been possible without the mentoring of my advisors, Pavel Nadolsky and Roberto Vega. They have been constantly teaching me not only the research skills but also the balance between work and leisure in my academic life. They guide me a lot on my journey into particle physics to explore the unknown universe. Both of them introduced me a great many excellent collaborators, who shape my understanding of science. It was always a pleasure to work as Roberto's teaching assistant (TA) in my first year here at SMU. Special thanks to Pavel for continuously supporting me with research-assistant (RA) fellowship in the past 4 years. Also, gratitude to him for providing me plenty of travel funds to participate in many conferences, workshops, and summer schools.

It is my honor to have Stephen Sekula as an experimentalist to serve as my dissertation committee chair. He has done a lot for us in the past five years, including assigning the TA tasks, maintaining the computing system, and organizing students to attend the Texas sections of APS (American physics society) meetings. We had some good experience together, such as giving a joint seminar and participating in the SUSY 2015 and the APS April Meeting 2019. Many thanks to John Campbell for the service as one of the external members in my committee. With his kindness to be my host, I visited Fermilab for one and a half years. It was a great opportunity to expose myself to the particle-physics community, and I took this advantage to communicate with a lot of scholars, including faculties and visitors in the Theoretical Physics Department, and experimentalists in various groups such as CMS, NOvA. Gratitude to C.-P. Yuan to serve as another external member. With his support, I visited Michigan State University serval times. Each time, we had a great time there collaborating on the CTEQ-TEA projects and meeting with his colleagues, students, and family members.

I would like to express my appreciation to all of my collaborators. They are Roberto Vega-Morales, Bowen Wang, Sayip Dulat, Tie-Jiun Hou, Jun Gao, Marco Guzzi, Jan Winter, Tim Hobbs, Joey Huston, Carl Schmidt, Daniel Stump, Jon Pumplin, Bo-Ting Wang, and Walter

Giele. I had many extensive discussions with Tie-Jiun on many topics, not limited to our projects. He guided me in many technical skills, such as `Fortran`, Unix scripts, `gnuplot`, and the CTEQ fitting package. Marco helped me with `xFitter`. Jun guided me about the `Mathematica` package `MP4LHC`. Walter instructed me about the OpenMP/MPI parallelization. Roberto Vega-Morales gave me many suggestions during my postdoc application. I collaborated with Bowen about a higher-order calculation for deep inelastic scattering.

I have to acknowledge the Department of Physics at SMU for providing me the opportunity to accomplish my Ph.D. degree. Thanks to Lacey Breaux and Michele Hill for their administrative work. Special Memoriam to Kent Hornbostel, who served as the Director of Graduate Studies, but unfortunately passed away in 2018. Also gratitude to all other faculties in our department, especially Ryszard Stroynowski, Fredrik Olness, Jingbo Ye, Thomas Coan, Jodi Cooley, Roberto Kehoe. Meanwhile, I would like to deliver my thanks to all the other students in our department. They are Huanzhao Liu, Tingting Cao, Hang Qiu, Biao Wang, Li Zhou, Xiandong Zhao, Ryan Staten, Daniel Jardin, Peilong Wang, Matthew Feickert, Madalyn McKay, Matthew Stein.

Thanks to Linda Evans for helping me with my English proficiency during the seminars for international TAs. Thanks to Paula Walvoord for providing me a cozy house to live and a lot of conveniences. Thanks to Mandy Pathak for organizing the Chi Alpha to host the weekly dinners for international students. Thanks to John Wheeler for working together for many overnights. Thanks to Mia Guo for many delightful discussions and encouragements. Thanks to the PKU Alumni Association at DFW for many gatherings. Thanks to the DASH Running Club for organizing us to train and to participate in marathon races.

Last but not least, I own my inexpressible gratitude to all my family members, who always constantly support me in pursuing my academic career. Their love and encouragement always give me magnificent power to overcome the difficulties in my life oversea.

Xie, Keping B.S., Physics, Peking University

Massive elementary particles in the Standard Model and its supersymmetric triplet Higgs extension

Advisors: Dr. Pavel M. Nadolsky, Dr. Roberto Vega
Doctor of Philosophy degree conferred August 6, 2019
Dissertation completed August 6, 2019

In this dissertation, we focus on massive elementary particles in the Standard Model and its supersymmetric triplet Higgs extension.

In the first part, we start with a review of electroweak (EW) sector in the Standard Model. Motivated by nonzero neutrino masses, we consider triplet scalars in addition to the Standard Model. The vacuum expectation values of scalar triplets are strongly constrained by the ρ parameter, extracted from electroweak precision measurements. Therefore, we introduce a custodial symmetry to weaken this constraint and obtain the well-known Georgi-Machacek (GM) Model. The GM model still requires fine-tuning to satisfy the ρ parameter constraint. It is because the custodial symmetry is broken by the hypercharge gauge interaction, which leads to quadratic divergences in the quantum corrections to the ρ parameter, starting at the 1-loop level. By adopting supersymmetry (SUSY), which solves the quadratic divergence problem in quantum corrections both to the ρ parameter and to the squared mass of Higgs simultaneously, we obtain the Supersymmetric Custodial Triplet Model (SCTM). It doubles the GM scalar fields with the *mirror*-GM sector. In the limit of large dimensionful parameters, B-terms, the *mirror*-GM particles are decoupled, and the spectrum of the GM-like particles looks the same as that in the GM model at the electroweak scale. We dub this limit as the "supersymmetric GM (SGM) model", which serves as a weakly coupled origin for the GM model. Incorporating the gauge-mediated supersymmetry breaking (GMSB) mechanism, we perform a phenomenological study for a pair of benchmark scenarios to illustrate when the SGM model can behave in the same way as the GM model, and when the GM and SGM models are distinguishable. When confronting the experimental diphoton data, we take the GM and SGM models as explicit examples to show how a light exotic Higgs boson

can escape the current experimental constraints through cancellations between different loop contributions to the effective couplings, or via decaying into the invisible sector.

In the second part, we focus on massive particle production, both in DIS experiments and at hadron-hadron colliders. By applying the QCD factorization theorem, hadronic cross sections can be factorized as convolutions of long-distance parton distribution functions (PDFs) and short-distance partonic cross sections. The partonic cross section can be obtained through perturbative calculations, thanks to the asymptotic freedom of the strong interaction. The universal PDFs have to be extracted from experimental data and are gradually becoming the largest uncertainty source that obscures the discovery of the new physics, especially at hadron colliders. Precise determinations of the PDFs require us to treat the massive quarks correctly. We discuss various factorization schemes to deal with the massive quarks in DIS, and we perform the calculations of the DIS structure functions in the intermediate-mass scheme at N3LO. We develop a new method called the SACOT-MPS (Simplified-ACOT with massive phase space) scheme to deal with heavy-quark production at hadron colliders, and we apply it to the $B^{\pm}$ production at the LHCb experiment.

TABLE OF CONTENTS

LIST OF FIGURES

LIST OF TABLES

This dissertation is dedicated to my beloved family:

Guozhen Xie (grandpa),

Fuxiang Li (grandma),

Enlong Xie (dad),

Juzhen Shu (mom),

Shuqiong Xie (sister).

Notations and Conventions

In this dissertation, we will work in the natural units, where

$$\hbar = c = 1. \tag{0.1}$$

All the physical units can be related to the mass dimension,

$$[L] = [T] = [M]^{-1}, \quad [p] = [E] = [M]. \tag{0.2}$$

The mass dimensions for scalar, spinor and vector fields respectively are

$$[\phi] = [M], \quad [\psi] = [M]^{3/2}, \quad [V] = M. \tag{0.3}$$

We take the west coast (timelike) convention of the Minkowski metric,

$$g_{\mu\nu} = g^{\mu\nu} = \text{diag}(1, -1, -1, -1). \tag{0.4}$$

Usually, the Greek indices $(\mu, \nu, \alpha, \cdots)$ run over $0, 1, 2, 3$, and the Roman indices $(i, j, k \cdots)$ denote only the three spatial components $1, 2, 3$. The four-vector is defined as

$$x^\mu = (x^0, \vec{x}), \quad x_\mu = g_{\mu\nu} x^\nu = (x^0, -\vec{x}), \tag{0.5}$$

where the repeated indices are summed implicitly. The dot product is defined as

$$p \cdot x = p^\mu g_{\mu\nu} x^\nu = p^0 x^0 - \vec{p} \cdot \vec{x}. \tag{0.6}$$

The Pauli matrices are defined as

$$\sigma^1 = \tau^1 = \begin{pmatrix} 0 & 1 \\ 1 & 0 \end{pmatrix}, \quad \sigma^2 = \tau^2 = \begin{pmatrix} 0 & -i \\ i & 0 \end{pmatrix}, \quad \sigma^3 = \tau^3 = \begin{pmatrix} 1 & 0 \\ 0 & -1 \end{pmatrix}. \tag{0.7}$$

The generators of the $SU(2)$ group are $T^i = \tau^i/2$, which satisfy $[T^i, T^j] = i\epsilon^{ijk} T^k$, where ϵ^{ijk} is the fully antisymmetric tensor.

Most of the time, we take the Weyl (chiral) basis of Dirac's gamma matrices,

$$\gamma^0 = \begin{pmatrix} 0 & I_2 \\ I_2 & 0 \end{pmatrix}, \quad \gamma^k = \begin{pmatrix} 0 & \sigma^k \\ -\sigma^k & 0 \end{pmatrix}, \quad \gamma^5 = \begin{pmatrix} -I_2 & 0 \\ 0 & I_2 \end{pmatrix}, \tag{0.8}$$

where I_2 is the identity matrix in 2×2 dimensions. Usually, we define $\sigma^0 = \bar{\sigma}^0 = I_2$ and $\bar{\sigma}^k = -\sigma^k$. The chiral projecting operators are defined as $P_{L,R} = \frac{1 \mp \gamma^5}{2}$, which satisfy $P_{L,R}^2 = P_{L,R}$.

Chapter 1

Introduction

1.1 The known and unknown

So far, we know that the matter in our universe is made of atoms that bind nuclei and electrons together through electromagnetic force. Nuclei, in turn, consist of protons and neutrons, together named as nucleons. Nucleons are bound objects composed of quarks and gluon fields held together by the strong interactions. This hierarchy structure of the universe is sketched in Figure 1.1. A free neutron is not stable and therefore will decay into an electron, a proton, and an invisible neutrino. The decay is mediated by the so-called weak interactions. These 3 kinds of interactions (electromagnetic, weak, and strong) are successfully unified in the **Standard Model** (SM) of elementary particles and fields. The SM is based on the symmetries of nature and a quantum gauge theory which reflects these symmetries. It is not yet understood how to write a consistent quantum theory for gravity, which remains the major stumbling block for unifying all four forces under one fundamental theory. It is not even clear whether such a theory exist. It is the goal of theoretical particle physics to sort these questions out and perhaps find the so-called theory of everything (TOE) or the final theory. String theory appears to provide a possible direction, but it remains to be seen what form the ultimate TOE will take.

The term "Standard Model" was first coined by Abraham Pais and Sam Treiman [2], with reference to Steven Weinberg's electroweak theory [3], which embraces the idea of Yang-Mills' gauge field theory [4] and **spontaneous symmetry breaking** (SSB) [5, 6] realized through the Higgs mechanism [7, 8, 9]. Weak gauge fields acquire mass by absorbing degrees of freedom of the massless Goldstone bosons. The SM predictions were tentatively established by experiments in the early 1980s, especially by the discovery of W/Z bosons by the UA1 [10, 11], and UA2 [12, 13] experiments at CERN. In 2012, the last unknown piece

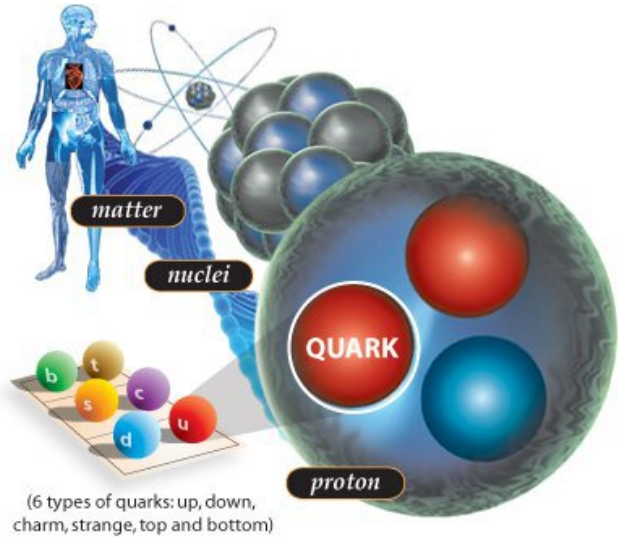

Figure 1.1: The composition of matter in our universe. This figure is taken from website [1].

of the Standard Model, the Higgs boson, was discovered by the ATLAS [14] and CMS [15] collaborations at the Large Hadron Collider (LHC). These discoveries symbolized a great triumph of the Standard Model.

However, even though the Standard Model is proven to be a great success, it is not the end of the story to explain all the phenomena observed in our universe. In spite of that, the SM is a self-consistent renormalizable theory, it can be only considered as an effective field theory (EFT) valid at the electroweak scale. There are many hints that the SM is not even close to the final theory since it fails to explain many puzzling observations about our universe. Here we briefly rephrase some of them, without going in all the details.

- **Neutrino mass**: The original version of the Standard Model predicts neutrinos to be massless. Conversely, neutrino oscillation experiments suggest that neutrinos must have a nonzero mass. However, thinking more carefully, we realize it is not a serious problem, considering that the quarks and charged leptons are massive. In the Standard Model, the fermions obtain mass through the Yukawa interactions with the Higgs boson. The neutrino in the original Standard Model must be massless, because of the missing of the right-handed neutrinos. This hint suggested the modified version to solve this problem by adding the right-handed neutrinos to the Standard Model. Similarly to

the right-handed up-type quarks, the right-handed neutrinos couple to the Higgs boson through the Yukawa interaction in a gauge-symmetry preserving way. After the Higgs field develops the vacuum expectation value (VEV) during the Electroweak Symmetry Breaking (EWSB), the neutrinos automatically obtain mass that is proportional to the Higgs VEV and the Yukawa coupling. In such a way, we add more particle contents and more parameters to the Standard Model.

- **Hierarchy problem**: Different from the neutrino mass puzzle which is driven by experiments, the hierarchy problem emerges from a theoretical argument of the naturalness principle. Once Planck obtained his famous constant h (or reduced one $\hbar$), he realized that the gravitational force must merge quantum mechanics at the Planck scale of order 10^{19} GeV. The weak force is characterized by the electroweak (EW) scale (around 100 GeV). There is a large discrepancy between the aspects of the gravitational and weak force. In the Standard Model, the squared mass of Higgs boson acquires quantum corrections that result in quadratic divergence at scales much larger than the EW scale. If there is no new physics between the Planck and EW scales, one would expect that the corrections would be inevitably large compared to the observed value at the EW scale unless there exists an incredible cancellation between the quadratic divergence and the Lagrangian bare mass. This fine-tuning problem suggests that new physics is hiding somewhere behind the corner. By now, people have come up with several solutions to this hierarchy problem, among which supersymmetry is perhaps the most prospective one.
- **Dark Matter**: Astrophysical observations, including spinning galaxies, gravitational lensing, and colliding galaxies, suggest that 85% of the matter (27% of the total energy density) in our universe is dark matter, which cannot be explained by the particle content of the Standard Model. The observations of the cosmological large-scale structure indicate that the dark matter should be cold, that is, the dark matter moves relatively slow compared to the speed of light. We are not sure what the Dark Matter consists of, but a lot of candidates can make it work, among which, the WIMPs (weakly interacting massive particles) are most explored ones, both theoretically and experimentally. Supersymmetric extensions of the Standard Model predict a lot of new particles, and

the lightest supersymmetric particle (LSP) satisfies the Dark Matter properties, which is being tested by the current and future direct detection experiments.

- **Matter-antimatter asymmetry**: According to astronomical observations, the stars and gas in our universe are made up of visible matter (proton, neutron, and electron). In comparison, the antimatter (positron, anti-proton, etc) is only produced artificially in laboratories. This imbalance of the baryonic and antibaryonic matter in our observable universe implies a baryogenesis process, which violates the baryon number conservation and charge-parity (CP) symmetry. In the Standard Model, the phase δ in the CKM matrix is the only known source of CP-violation. However, it is too small to explain the observed matter-antimatter asymmetry. We need more CP-violation sources, which must come from BSM physics.
- **Quantization of gravity**. The Standard Model does not include graviton which accounts for the quantization of gravity. More generally speaking, a quantum field theory (QFT) cannot canonically quantize gravitation, which is described by a classical theory called general relativity. The fundamental structure of gravity is not the same as the other three forces. We hope string theory or loop quantum gravity can provide us with an answer to this puzzle.
- **Inflation**: The isotropy and homogeneity of our visible universe, revealed by the cosmic microwave background (CMB) radiation, requires a stage of extremely rapid expansion called the inflationary epoch right after the big bang. The Standard Model does not contain the fields accounting for inflation.
- **Cosmological constant**: The zero-point energy of the quantum field theory is much larger (120 orders of magnitude higher) than the observed vacuum energy density. The Standard Model cannot help us to understand this many-orders-of-magnitude discrepancy between theory and observation.
- **Dark Energy**: We observe that the present-day universe is expanding at an accelerating rate, which suggests that 68% of the total energy in the observable universe is in a hypothesized unknown energy form, called dark energy. Otherwise, the expansion of our universe should be slowing down because of the gravitational attraction.

- **Strong CP problem**: The strong interaction is described by quantum chromodynamics (QCD), which could allow a Charge-Parity violation (CPV) term $\theta \frac{g^2}{32\pi^2} G_{\mu\nu} \tilde{G}^{\mu\nu}$. However, the experimental measurement of the neutron electric dipole moment (EDM)
$$d_n \simeq \theta \frac{e m_q}{M_N^2} < 3 \times 10^{-26}\,\text{ecm}, \tag{1.1}$$
which suggests $\theta < 10^{-9}$. This is another example of a fine-tuning problem. We hope that a pseudo-scalar particle called axion in Peccei-Quinn symmetry will provide us with a satisfactory answer.
- **Ad hoc parameters**: The Standard Model contains 18 free parameters:
$$\lambda, \mu, g_{1,2,3}, m_{e,\mu,\tau}, m_{d,u,s,c,b,t}, \theta_{12,13,23}, \delta. \tag{1.2}$$
If we count the θ as yet another parameter, we would have 19 parameters in total. Now, we realize that neutrinos have mass discovered by oscillation experiments. Therefore, we need to add 7 more parameters into this model:
$$m_{1,2,3}, \theta'_{12,13,23}, \delta'. \tag{1.3}$$
If the neutrino is a Majorana fermion, we would have 2 additional phase factors, $\alpha_{1,2}$. Therefore, the extended Standard Model contains 26-28 parameters in total, and all of them should be determined in experiments. It is rather unsatisfying that a fundamental theory would suffer from such a plethora of free parameters with such a large range of values. Moreover, we found that there exists a hierarchy structure among the 3 generations of the leptons and quarks,
$$m_e < m_\mu < m_\tau, \qquad m_{d,u} < m_{s,c} < m_{b,t}. \tag{1.4}$$
We do not yet know whether neutrinos satisfy the hierarchy structure, i.e., $m_1 < m_2 < m_3$, and we have no explanation for this hierarchy within the Standard Model.
- **Generations**: All the quarks and leptons that have been discovered can be classified into three generations distinguished by the scale of their masses. However, the observed Universe appears to be composed entirely of just quarks and leptons in the first generation. This generation can form a complete and consistent (anomaly free) theory by itself. The other generations only manifest themselves involving collisions at high energies. The Standard Model fails to explain why there should be exactly three generations.

Of course, this is not a complete list of all the problems that the SM suffers from. Each problem motivates us to search for new physics **beyond the Standard Model** (BSM). One strategy to follow is to modify or extend the SM and to see ways in which the predictions of these extended models differ from those of the SM. The modifications should be driven by their adequateness in resolving some of the issues or weakness of the SM listed above.

1.2 Organization of this dissertation

Our target is to deal with massive elementary particles in the Standard Model and its BSM extensions. We divide this dissertation into two parts. In the first part, we cover various heavy particles in the framework of triplet Higgs models and the supersymmetric versions. In order to produce these new particles, we need hadron colliders. And the production of heavy particles, both in the SM and new physics, is based on our understanding of perturbative quantum chromodynamics, which is the main subject of our second part.

1.2.1 Higgs triplet Models

In the first part of this dissertation, we start with the Standard Model and explore the modifications of which extended the Higgs sector to include, in addition to the usual SM doublet representation, triplet representations of $SU(2)$. Several intimations lead us to scalar triplets. First, scalar triplets possess the potential to provide neutrinos with nonzero masses through Yukawa interactions of the scalar triplets' coupling to the Majorana neutrinos, which is well-known as the Type-II seesaw mechanism [16, 17], which is discussed in Chapter 3. A natural source for this mechanism can be provided by the Left-Right symmetric models [18]. Second, the seesaw Yukawa interactions violate lepton number and therefore satisfy one of the Sakharov's conditions [19] on global quantum number generation in the evolution of the Universe. Triplet models also encompass the possibility of charge-parity (CP) violation, either explicitly or spontaneously, which satisfy another Sakharov's condition. These two conditions lead us to the leptogenesis [20], which can be converted into the baryogenesis [21] through a nonperturbative process called sphaleron [22]. Third, triplet models naturally arise in the Higgs composite models and Little Higgs models. Finally, scalar triplet models contain rich phenomenology with new particles (such as doubly charged scalars $H^{\pm\pm}$) and

new couplings to vector bosons (such as HVV or HHV), which can be directly measured at current and future colliders.

In general, the vacuum expectation values (VEVs) of the neutral components of the scalar triplets are strongly constrained by electroweak precision measurements, and ρ parameter is one of the biggest constraints [23]. However, these constraints are strongly weakened if the triplet scalar representations are added in such a way as to obey the accidental $SU(2)$ custodial symmetry of the SM. The implication of imposing a custodial symmetry is that one must add at least one real and one complex triplet representations. Such a model was first proposed by Georgi and Machacek [24], and is commonly known as the Georgi-Machacek (GM) Model. The GM model, nevertheless, still requires fine-tuning in order to satisfy the ρ parameter constraints. Similarly to the SM, the solution to this additional naturalness problem is supersymmetry, as discussed in Chapter 4. Therefore, we supersymmetrize the GM model, and obtain the Supersymmetric Custodial Triplet Model, in Chapter 5. We study a particular limit of dimensionful parameters for this model which, in the scalar sector, reproduces the spectrum of the GM model at energies in the TeV range. We dub this limit as the Supersymmetry GM (SGM) model.

In Chapter 6, we assume gauge-mediate supersymmetry breaking (GMSB) [25] and perform a phenomenological study for a pair of benchmark scenarios to illustrate when the SGM model can mimic the GM model, and when they are distinguishable. When confronting the experimental diphoton data, in Chapter 7, we take the GM and SGM models as explicit examples to show how light exotic Higgs boson can escape the current experimental constraints through different loop contributions to the effective couplings, or via decaying into the invisible sector. The lightest supersymmetric particle (LSP) in the SGM model is very stable. It behaves like a WIMP (weakly interacted massive particles) and therefore is a good candidate for dark matter. We explore the direct detection constraints from various dark-matter search experiments. We leave this possibility for future study.

1.2.2 Massive particle production

We would like to test our new physics models at colliders. Direct evidence must come from the production of massive particles predicted by these models at colliders. Hadron colliders

are the most powerful machines which can push the energy up to its highest frontier. In history, the heaviest fundamental particles were discovered at hadron colliders, such as W, Z boson at the UA1 [10, 11] and UA2 [12, 13], bottom quark at the Fermilab E288 [26], and top quark at the Tevatron [27, 28]. The latest discovery of this kind is the Higgs boson discovered at the LHC in 2012 [14, 15]. All these big discoveries rely heavily on hadron colliders, which will continue to be the most powerful tools to explore new physics in the future.

Understanding of the production of massive particles at hadron colliders is based on the **QCD factorization theorem**. In perturbative Quantum Chromodynamics (pQCD), we can separate a cross-section for hadron collisions into 2 parts: a soft part to characterize the long-distance interaction and a hard part for the short-distance one. The hard partonic cross-section can be calculated through perturbative expansion, thanks to the asymptotic freedom of the non-Abelian SU(3) gauge. In contrast, the long-distance interaction cannot be calculated from the first principle, due to its nonperturbative behavior. Fortunately, we can parameterize it by universal parton distribution functions (PDFs), which can be extracted from benchmark experiments, such as deep inelastic scattering (DIS), and fixed-target collisions. In Chapter 8, we first consider the Higgs production through gluon-gluon fusion (ggF) as an example to illustrate the framework of factorization theorem. After discussing the general features of the factorization formalism, we talk briefly about the Drell-Yan process, which was the first application of the factorization theorem to hadron-hadron collisions. Then, we move on to deep inelastic scattering, which provides the most precise information to constrain the PDFs in our global analysis. We also summarize some sum rules of the PDFs and higher-order corrections, taking DIS structure functions as an example.

In history, DIS played a key role in the development of QCD. In modern theory, the DIS data serve as a backbone for describing the partonic structure of the proton, which is described by PDFs. Precise determinations of PDFs require to correctly include massive heavy quarks in DIS structure functions. In Chapter 9, we compare various factorization schemes to deal with heavy-quark mass dependence. Then, we apply one of them, the

intermediate-mass (IM) scheme, to calculate the DIS structure functions up to N3LO. In Chapter 10, we extend these schemes to the hadron-hadron collider case.

Let's see how we tackle these problems, and how far we can get.

Part I

Electroweak sector in the Standard Model and beyond

Chapter 2

Electroweak physics in the Standard Model

The Standard Model is a very successful model in particle physics, which has been tested to be correct up to very high precision. It describes three of the four known fundamental forces (the electromagnetic, weak and strong interactions, but not including gravity) and classifies all known elementary particles in our universe. We will review the electroweak (EW) physics of the Standard Model in this chapter, mostly by following Chong Sheng Li's lecture notes on *Quantum Gauge Field Theory* [29].

2.1 Gauge groups

The fundamental particles in the Standard Model can be classified into 3 categories: spin-1/2 fermion, spin-0 scalar, and spin-1 vector boson, all illustrated in Figure 2.1. The scalar particle called Higgs Boson is responsible for the Spontaneous Symmetry Breaking (SSB) through the Higgs Mechanism [30, 8]. A vector boson mediates gauge interactions and, therefore, is called a gauge boson. There are 3 kinds of gauge interactions, described by the direct product of 3 gauge groups $SU(3)_c \otimes SU(2)_L \otimes U(1)_Y$. The $SU(3)_c$ is the color group, where subscripts c stands for color charge carried only by quarks. The subscript L in the isospin group $SU(2)_L$ indicates left-handedness (chirality). It means the weak force only acts on the left-handed fermions (including quarks and leptons) and the Higgs boson. Y in the Abelian group $U(1)_Y$ represents the hyper-charge, which is carried by all the fermions and scalars. The electroweak group $SU(2)_L \otimes U(1)_Y$ is spontaneously broken. However, the electric charge $Q = T_L^3 + Y/2$ is conserved, where $T_L^3 = \tau^3/2$ is the third generator for the isospin group $SU(2)_L$. That is to say,

$$SU(2)_L \otimes U(1)_Y \xrightarrow{\text{SSB}} U(1)_Q : \tag{2.1}$$

the EW group is broken into an Abelian gauge group $U(1)_Q$, i.e., Quantum Electrodynamics (QED) responsible for electromagnetic interactions. On the other hand, the strong interaction symmetry described by $SU(3)_c$ group, also called Quantum Chromodynamics (QCD),

is unbroken. We first review EW theory in this chapter and leave QCD to the second part of this dissertation.

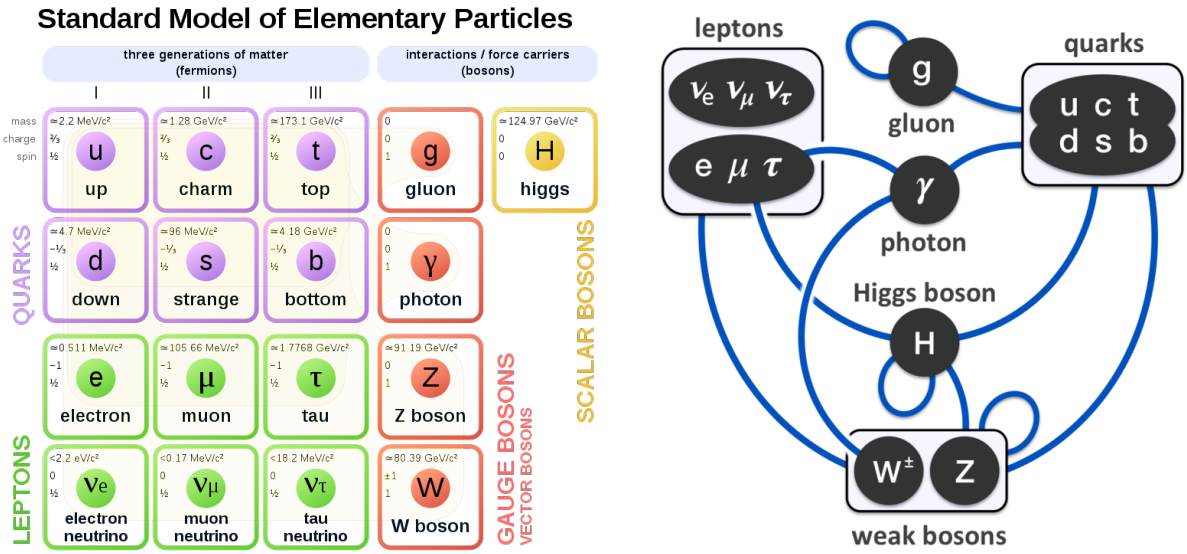

Figure 2.1: The elementary particles and the interactions in the Standard Model. The table and plot are taken from WIKIPEDIA [31].

2.2 Elementary particles

The Standard Model contains 12 kinds of fermions, shown in Figure 2.1. We can organize them into $SU(2)_L$ representations and the corresponding hypercharges,

$$\begin{aligned} q_L &= \begin{pmatrix} u_L \\ d_L \end{pmatrix} (Y = \frac{1}{3}), \qquad d_R(Y = -\frac{2}{3}), \quad u_R(Y = \frac{4}{3}), \\ l_L &= \begin{pmatrix} \nu_L \\ e_L \end{pmatrix} (Y = -1), \qquad e_R(Y = -2). \end{aligned} \tag{2.2}$$

The gauge transformation under $SU(2)_L \otimes U(1)_Y$ are respectively

$$\psi_L \to e^{-i\vec{\theta}\cdot\frac{\vec{\tau}}{2} - i\beta\frac{Y}{2}}\psi_L, \quad \psi_R \to e^{-i\beta\frac{Y}{2}}\psi_R, \tag{2.3}$$

where $\vec{\tau}$ is the Pauli matrices, and $\vec{\theta}, \beta$ are the group transformation parameters. Here ψ_L denotes isospin doublets q_L, l_L, and ψ_R represents isospin singlets d_R, u_R, e_R. The gauge-invariant Lagrangian for the fermion sector can be written as

$$\mathcal{L}_f = i\bar{\psi}_L \not{D}\psi_L + i\bar{\psi}_R \not{D}\psi_R, \tag{2.4}$$

where the Feynman d-slash is $\not{D} = \gamma^\mu D_\mu$. The covariant derivatives are defined as

$$D_\mu \psi_L = (\partial_\mu - i g_1 \frac{Y}{2} B_\mu - i g_2 \frac{\tau^i}{2} W_\mu^i)\psi_L, \quad D_\mu \psi_R = (\partial_\mu - i g_1 \frac{Y}{2} B_\mu)\psi_R. \tag{2.5}$$

B_μ and W_μ^i represent the corresponding gauge field of $U(1)_Y$ and $SU(2)_L$, and $g_{1,2}$ are the gauge couplings. The Lagrangian for the gauge field can be written as

$$\mathcal{L}_g = -\frac{1}{4} B^{\mu\nu} B_{\mu\nu} - \frac{1}{4} W_i^{\mu\nu} W_{\mu\nu}^i, \tag{2.6}$$

where $W_{\mu\nu}^i$ and $B_{\mu\nu}$ are the field strength tensors for the weak isospin and hypercharge field,

$$B_{\mu\nu} = \partial_\mu B_\nu - \partial_\nu B_\mu, \quad W_{\mu\nu}^i = \partial_\mu W_\nu^i - \partial_\nu W_\mu^i + g_2 \epsilon^{ijk} W_\mu^j W_\nu^k. \tag{2.7}$$

The ϵ^{ijk} is the fully antisymmetric tensor.

2.3 Higgs sector

In the unbroken phase, the Higgs Boson is a $SU(2)_L$ doublet with hypercharge $Y = 1$,

$$\Phi = \begin{pmatrix} H^+ \\ H^0 \end{pmatrix} (Y = 1). \tag{2.8}$$

The corresponding covariant derivative is

$$D_\mu \Phi = (\partial_\mu - i g_1 \frac{1}{2} B_\mu - i g_2 \frac{\tau^i}{2} W^i)\Phi. \tag{2.9}$$

Therefore, the Higgs sector in the SM Lagrangian can be written as

$$\mathcal{L}_H = (D_\mu \Phi)^\dagger (D_\mu \Phi) - V(\Phi), \quad V(\Phi) = -\mu^2 \Phi^\dagger \Phi + \lambda (\Phi^\dagger \Phi)^2. \tag{2.10}$$

When $\mu^2 > 0$ and $\lambda > 0$, the Higgs potential looks like Figure 2.2. By rolling to a lower-

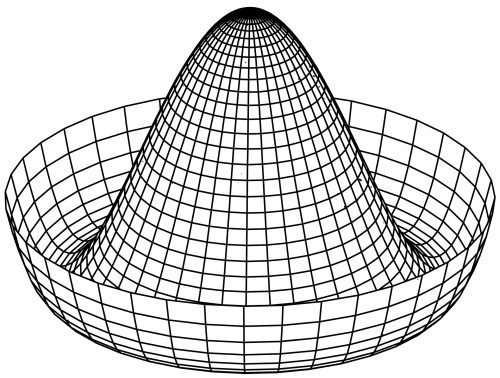

Figure 2.2: A sketch of the "Mexican hat" potential of Higgs $V(\Phi)$. This plot is taken from WIKIPEDIA [32].

energy state at the brim of the "Mexican hat", the Higgs field develops a vacuum expectation

value (VEV) as

$$\langle\Phi\rangle_0 \equiv \langle 0|\Phi|0\rangle = \frac{1}{\sqrt{2}}\begin{pmatrix}0\\ v\end{pmatrix}, \quad v = \sqrt{\frac{\mu^2}{\lambda}}. \tag{2.11}$$

We can easily check that the gauge symmetry is broken in the vacuum state $\langle\Phi\rangle_0$,

$$T_L^i\langle\Phi\rangle_0 \neq 0, (i=1,2,3), \quad Y\langle\Phi\rangle_0 \neq 0. \tag{2.12}$$

where $T_L^i = \tau^i/2$. However, the vacuum is invariant under action of the electric charge operator Q:

$$Q\langle\Phi\rangle_0 = (T_L^3 + \frac{Y}{2})\langle\Phi\rangle_0 = \begin{pmatrix}1 & 0\\ 0 & 0\end{pmatrix}\frac{1}{\sqrt{2}}\begin{pmatrix}0\\ v\end{pmatrix} = 0. \tag{2.13}$$

It means the EW gauge symmetry breaks down to a smaller group $SU(2)_L \otimes U(1)_Y \to U(1)_Q$, which can be interpreted as the Abelian group describing the quantum electrodynamics (QED).

We can shift the Higgs boson in the neighborhood of its VEV $\Phi = \langle\Phi\rangle_0 + \begin{pmatrix}H^+\\ \frac{h_R+ih_I}{\sqrt{2}}\end{pmatrix}$. The Higgs potential can be expressed as

$$V(\Phi) = -\frac{\mu^4}{4\lambda} + \mu^2 h_R^2 + \sqrt{\lambda}\mu h_R(h_R^2 + h_I^2 + 2H^+H^-) + \frac{\lambda}{4}(h_R^2 + h_I^2 + 2H^+H^-)^2. \tag{2.14}$$

Therefore, we obtain three massless Goldstone boson h_I and $H^\pm$, and one massive Higgs boson with mass $m_H = \sqrt{2}\mu = \sqrt{2\lambda}v$. In the unitary gauge, we can parameterize the Higgs boson as

$$\begin{aligned}\Phi &= U^{-1}(\zeta)\begin{pmatrix}0\\ \frac{v+\eta}{\sqrt{2}}\end{pmatrix} = \exp\Big(i\vec{\zeta}\cdot\vec{\tau}/v\Big)\begin{pmatrix}0\\ \frac{v+\eta}{\sqrt{2}}\end{pmatrix}\\ &\approx \frac{v}{\sqrt{2}} + \frac{1}{\sqrt{2}}\begin{pmatrix}\zeta_2 + i\zeta_1\\ \eta - i\zeta_3\end{pmatrix} = \langle\Phi\rangle_0 + \frac{1}{\sqrt{2}}\begin{pmatrix}i\sqrt{2}w^+\\ \eta - iz^0\end{pmatrix}.\end{aligned} \tag{2.15}$$

We can see easily that $w^\pm$ and z^0 are Goldstone bosons. They are absorbed into gauge bosons that consequently acquire mass. The VEVs for these shifted fields are

$$\langle 0|\zeta_i|0\rangle = \langle 0|\eta|0\rangle = 0. \tag{2.16}$$

We redefine the Higgs field in the unitary gauge,

$$\Phi' = U(\zeta)\Phi = \begin{pmatrix}0\\ \frac{v+\eta}{\sqrt{2}}\end{pmatrix} = \frac{v+\eta}{\sqrt{2}}\chi, \quad \chi = \begin{pmatrix}0\\ 1\end{pmatrix}. \tag{2.17}$$

The Higgs sector can be rewritten as

$$\mathcal{L}_H = (D_\mu \Phi')^\dagger (D^\mu \Phi') - V(\Phi') \tag{2.18}$$

where

$$D_\mu \Phi' = (\partial_\mu - i g_1 \frac{1}{2} B'_\mu - i g_2 \frac{1}{2} \vec{\tau} \cdot \vec{W}'_\mu) \frac{v+\eta}{\sqrt{2}} \chi, \quad V(\Phi') = \mu^2 \eta^2 + \lambda v \eta^3 + \frac{1}{4} \eta^4. \tag{2.19}$$

We have dropped the zero-point energy $-\frac{1}{4}\lambda v^4$ in $V(\Phi')$. We obtain the mass of the gauge boson in the $|D_\mu \Phi'|^2$ term,

$$\begin{aligned} &\frac{v^2}{2} \chi^\dagger (g_1 \frac{1}{2} B'_\mu + g_2 \frac{1}{2} \vec{\tau} \cdot \vec{W}')(g_1 \frac{1}{2} B'^\mu + g_2 \frac{1}{2} \vec{\tau} \cdot \vec{W}'^\mu) \chi \\ =&\frac{v^2}{8} \left\{ g_2^2 \left[(W'^1_\mu)^2 + (W'^2_\mu)^2 \right] + (g_2 W'^3_\mu - g_1 B'_\mu)^2 \right\} \\ =&m_W^2 W^+_\mu W^{-\mu} + \frac{1}{2} m_Z^2 Z_\mu Z^\mu. \end{aligned} \tag{2.20}$$

where

$$W^\pm_\mu = \frac{1}{\sqrt{2}} (W'^1_\mu \mp i W'^2_\mu), \quad m_W^2 = \frac{1}{4} g_2^2 v^2 \tag{2.21}$$

Conversely, we find that the vector boson of the gauge eigenstate can be expressed as the mass eigenstate (physical state) as

$$W'^1_\mu = \frac{1}{\sqrt{2}} (W^+_\mu + W^-_\mu), \quad W'^2_\mu = \frac{i}{\sqrt{2}} (W^+_\mu - W^-_\mu). \tag{2.22}$$

For the neutral vector boson, we have unbroken $U(1)_Q$ symmetry $Q\langle\Phi\rangle_0 = 0$, which corresponds to the massless gauge boson, or photon A^μ.

$$\begin{aligned} \frac{1}{2} m_Z^2 Z_\mu Z^\mu &= \frac{v^2}{8} (g_2 W'^3_\mu - g_1 B'_\mu)^2 \\ &= \frac{v^2}{8} (W'^3_\mu, B'_\mu) \begin{pmatrix} g_2^2 & -g_1 g_2 \\ -g_1 g_2 & g_2^2 \end{pmatrix} \begin{pmatrix} W'^{3\mu} \\ B'^\mu \end{pmatrix} \\ &= \frac{1}{2} (Z_\mu, A_\mu) \begin{pmatrix} m_Z^2 & 0 \\ 0 & 0 \end{pmatrix} \begin{pmatrix} Z^\mu \\ A^\mu \end{pmatrix}. \end{aligned} \tag{2.23}$$

The physical gauge fields

$$\begin{pmatrix} Z_\mu \\ A_\mu \end{pmatrix} = \begin{pmatrix} \cos\theta_W & -\sin\theta_W \\ \sin\theta_W & \cos\theta_W \end{pmatrix} \begin{pmatrix} W'^3_\mu \\ B'_\mu \end{pmatrix}, \quad m_Z^2 = \frac{1}{4}(g_1^2 + g_2^2) v^2. \tag{2.24}$$

where $\theta_W = \arctan(g_1/g_2)$ is the Weinberg angle. Conversely, the gauge eigenstates of the vector boson can be expressed in terms of the mass eigenstates as

$$W'^3_\mu = c_W Z_\mu + s_W A_\mu, \quad B'_\mu = -s_W Z_\mu + c_W A_\mu, \tag{2.25}$$

where $s_W \equiv \sin\theta_W$ and $c_W \equiv \cos\theta_W$.

2.4 Yukawa sector

When we introduce the Yukawa interaction,

$$\mathcal{L}_Y = y_i^e \bar{e}_R \Phi^\dagger l_L + y_{ij}^d \bar{d}_{Ri} \Phi^\dagger q_{Lj} + y_{ij}^u \bar{u}_R \tilde{\Phi}^\dagger q_{Lj} + \text{h.c.}, \ (\text{where } \tilde{\Phi} = i\tau_2 \Phi^*), \tag{2.26}$$

the fermion will obtain mass after the Higgs boson develops a VEV. In the unitary gauge, we have

$$\Phi = \frac{1}{\sqrt{2}} \begin{pmatrix} 0 \\ v+\eta \end{pmatrix}, \quad \tilde{\Phi} = \frac{1}{\sqrt{2}} \begin{pmatrix} v+\eta \\ 0 \end{pmatrix}. \tag{2.27}$$

Therefore, the fermions acquire mass proportional to the Higgs VEV,

$$m_i^e = \frac{1}{\sqrt{2}} y_i^e v, \quad M_{ij}^d = \frac{1}{\sqrt{2}} y_{ij}^d v, \quad M_{ij}^u = \frac{1}{\sqrt{2}} y_{ij}^u v. \tag{2.28}$$

The original version of the Standard Model developed by Steven Weinberg [3] does not include the right-handed neutrinos. As a result, the neutrinos $\nu_{e,\mu,\tau}$ could only be left-handed and massless. But this is not the case in our real world, as explained later.

Under the CP transform, we have

$$\bar{e}_R \Phi^\dagger l_L \xleftrightarrow{\text{CP}} \text{h.c.} \tag{2.29}$$

Therefore, if we have $y^e \neq y^{e*}$, the Yukawa interactions will break the CP symmetry explicitly. However, if we do not have mixing among different generations, then, equivalently speaking, the Yukawa coupling matrix y_{ij}^e is diagonal,

$$y_{ij}^e = y_i^e \delta_{ij} = |y_i^e| e^{i\alpha_i} \delta_{ij}. \tag{2.30}$$

In this case, one can absorb the phase $e^{i\alpha_i}$ into the redefined field of the Dirac fermion (electron here). This redefinition would be equivalent to having the real Yukawa coupling $y_i^e = y_i^{e*}$ that conserves the CP symmetry as a result. However, our real world is not so simple. We realize that y_{ij} must be complex and also non-diagonal in order to be responsible for the CP violation discovered in neutral K-meson decays [33]. Taking the quark sector as an example, we have the mass term as

$$(\bar{u}_1, \bar{u}_2, \bar{u}_3)_R M^u \begin{pmatrix} u_1 \\ u_2 \\ u_3 \end{pmatrix}_L + (\bar{d}_1, \bar{d}_2, \bar{d}_3)_R M^d \begin{pmatrix} d_1 \\ d_2 \\ d_3 \end{pmatrix}_L + \text{h.c.} \tag{2.31}$$

The mass matrices M_{ij}^d and M_{ij}^u contain 9×2 complex matrix elements. We can diagonalize the mass matrix by multiplying it by matrix A from the left and matrix B from the right,

as

$$\begin{aligned} A^\dagger M B &= D, & B^\dagger M^\dagger A &= D^\dagger, \\ A^\dagger M M^\dagger A &= D D^\dagger, & B^\dagger M^\dagger M B &= D^\dagger D. \end{aligned} \tag{2.32}$$

The solution for these equation is $M = ADB^\dagger$. Therefore, before the EWSB, we can write the isospin gauge eigenstates (u_1, u_2, u_3) and (d_1, d_2, d_3) in terms of the mass eigenstates (u, c, t) and (d, s, b) as

$$\begin{pmatrix} u_1 \\ u_2 \\ u_3 \end{pmatrix}_{L,R} = U_{L,R} \begin{pmatrix} u \\ c \\ t \end{pmatrix}_{L,R}, \quad \begin{pmatrix} d_1 \\ d_2 \\ d_3 \end{pmatrix}_{L,R} = D_{L,R} \begin{pmatrix} d \\ s \\ b \end{pmatrix}_{L,R}, \tag{2.33}$$

which diagonalizes the mass matrices

$$U_R^\dagger M^u U_L = \begin{pmatrix} m_u & 0 & 0 \\ 0 & m_c & 0 \\ 0 & 0 & m_t \end{pmatrix}, \quad D_R^\dagger M^d D_L = \begin{pmatrix} m_d & 0 & 0 \\ 0 & m_s & 0 \\ 0 & 0 & m_b \end{pmatrix}. \tag{2.34}$$

Here $U_{L,R}, D_{L,R}$ are unitary matrices. Therefore, we can rewrite the Yukawa interaction for the quark sector in terms of mass eigenstates as

$$\begin{aligned} \mathcal{L}_Y &= (\bar{d}_1, \bar{d}_2, \bar{d}_3)_R M^d \begin{pmatrix} d_1 \\ d_2 \\ d_3 \end{pmatrix}_L \left(1 + \frac{\eta}{v}\right) + (\bar{u}_1, \bar{u}_2, \bar{u}_3)_R M^u \begin{pmatrix} u_1 \\ u_2 \\ u_3 \end{pmatrix}_L \left(1 + \frac{\eta}{v}\right) + \text{h.c.} \\ &= (\bar{d}, \bar{s}, \bar{b})_R D_R^\dagger M^d D_L \begin{pmatrix} d \\ s \\ b \end{pmatrix}_L \left(1 + \frac{\eta}{v}\right) + (\bar{u}, \bar{c}, \bar{t})_R U_R^\dagger M^u U_L \begin{pmatrix} u \\ c \\ t \end{pmatrix}_L \left(1 + \frac{\eta}{v}\right) + \text{h.c.} \\ &= (\bar{d}, \bar{s}, \bar{b})_R \begin{pmatrix} m_d & 0 & 0 \\ 0 & m_s & 0 \\ 0 & 0 & m_b \end{pmatrix} \begin{pmatrix} d \\ s \\ b \end{pmatrix}_L \left(1 + \frac{\eta}{v}\right) + (\bar{u}, \bar{c}, \bar{t})_R \begin{pmatrix} m_u & 0 & 0 \\ 0 & m_c & 0 \\ 0 & 0 & m_t \end{pmatrix} \begin{pmatrix} u \\ c \\ t \end{pmatrix}_L \left(1 + \frac{\eta}{v}\right) + \text{h.c.} \\ &= \sum_i (m_d^i \bar{d}_R^i d_L^i + m_u^i \bar{u}_R^i u_L^i) \left(1 + \frac{\eta}{v}\right) + \text{h.c.} = \sum_i (m_d^i \bar{d}^i d^i + m_u^i \bar{u}^i u^i) \left(1 + \frac{\eta}{v}\right). \end{aligned} \tag{2.35}$$

Here $m_d^i \bar{d}^i d^i + m_u^i \bar{u}^i u^i$ is the Dirac mass term for quarks, where i runs over (d, s, b) for down-type and (u, c, t) for up-type quarks in the sums. The weak charge current can be written

in terms of the mass eigenstates as well

$$J_\mu^+ = (\bar{u}_1, \bar{u}_2, \bar{u}_3)_L \gamma_\mu \begin{pmatrix} d_1 \\ d_2 \\ d_3 \end{pmatrix}_L = (\bar{u}, \bar{c}, \bar{t})_L U_L^\dagger D_L \gamma_\mu \begin{pmatrix} d \\ s \\ t \end{pmatrix}_L \tag{2.36}$$

We can define a unitary 3×3 matrix $V = U_L^\dagger D_L$, which is called Cabibbo-Kobayashi-Maskawa (CKM) mixing matrix. The CKM matrix can be parameterized in terms of three Euler angles ($\theta_{12,13,23}$) and one CP-violation phase δ,

$$\begin{aligned} V &= \begin{pmatrix} 1 & 0 & 0 \\ 0 & c_{23} & s_{23} \\ 0 & -s_{23} & c_{23} \end{pmatrix} \begin{pmatrix} c_{13} & 0 & s_{13}e^{-i\delta} \\ 0 & 1 & 0 \\ -s_{13}e^{-i\delta} & 0 & c_{13} \end{pmatrix} \begin{pmatrix} c_{12} & s_{12} & 0 \\ -s_{12} & c_{12} & 0 \\ 0 & 0 & 1 \end{pmatrix} \\ &= \begin{pmatrix} c_{12}c_{13} & s_{12}c_{13} & s_{13}e^{-i\delta} \\ -s_{12}c_{23} - c_{12}s_{23}s_{13}e^{i\delta} & c_{12}c_{23} - s_{12}s_{23}s_{13}e^{i\delta} & s_{23}c_{13} \\ s_{12}s_{23} - c_{12}c_{23}s_{13}e^{i\delta} & -c_{12}s_{23} - s_{12}c_{23}s_{13}e^{i\delta} & c_{23}c_{13} \end{pmatrix}, \end{aligned} \tag{2.37}$$

where $c_{ij} = \cos\theta_{ij}$ and $s_{ij} = \sin\theta_{ij}$. As a result, there is only one degree of freedom (the δ phase here) corresponding to the CP violation in the SM. If we only have 2 generations, the CKM matrix would be reduced to the 2×2 Cabibbo rotation matrix

$$V = \begin{pmatrix} \cos\theta_c & \sin\theta_c \\ -\sin\theta_c & \cos\theta_c \end{pmatrix}. \tag{2.38}$$

In such case, there is no degree of freedom accounting for the CP violation. We need at least 3 generations to get the CP-breaking effect.

2.5 The SM parameters

Up to this stage, we are able to count all parameters in the Standard Model. First, we have 3 gauge couplings $g_{1,2,3}$ corresponding to the 3 gauge groups. In the Higgs sector, we have 2 parameters μ^2, λ. In the Yukawa sector, we have the masses corresponding to all the massive fermions,

$$m_e, m_\mu, m_\tau, m_d, m_s, m_b, m_u, m_c, m_t. \tag{2.39}$$

The CKM matrix has 4 parameters, $\theta_{12}, \theta_{13}, \theta_{23}, \delta$. Therefore, we have 18 parameters so far in the SM, and all of them correspond to observables which have to be determined from the experimental measurements. As we mentioned in Chapter 1, no symmetry forbids the

strong CP violation term $\theta \frac{g_3^2}{32\pi^2} G_{\mu\nu}\tilde{G}^{\mu\nu}$ in the QCD, and the θ value also has to be measured experimentally. That is why someone quote that the SM contains 19 free parameters in total, depending on how you count.

As we know, neutrino oscillations were first implied by the solar neutrino problem [34, 35], then observed by the Super-Kamiokande Observatory (SuperK) [36] and the Sudbury Neutrino Observatories (SNO) [37]. From these experiments, we know that neutrinos have mass: therefore, we have to add the right-handed neutrinos ν_R and the corresponding Yukawa couplings y^ν_{ij} to the Standard Model in order to account for this effect:

$$\mathcal{L}_\nu = y^\nu_{ij}\bar{\nu}_{Ri}\tilde{\Phi}^\dagger l_{Lj} + \text{h.c.}, \quad M^\nu_{ij} = \frac{1}{\sqrt{2}} y^\nu_{ij} v. \tag{2.40}$$

Similarly to the quark sector, the Yukawa couplings can have complex values and couple to different generations, which will introduce the Pontecorvo–Maki–Nakagawa–Sakata (PMNS) mixing matrix [38, 39, 40, 41]. While the quarks are known to be Dirac fermions, we do not know whether the neutrinos are Dirac or Majorana fermions. If the neutrinos are Majorana fermions, which means that the antineutrinos are the same fields as neutrinos, we would expect to observe the neutrinoless double beta ($0\nu2\beta$) decay, shown in Figure 2.3. However, we have not observed this phenomenon up to now, leaving us a puzzle to be resolved in the future.

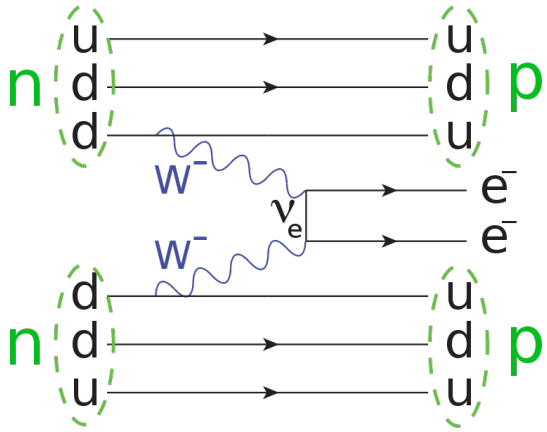

Figure 2.3: A representative Feynman diagram of neutrinoless double beta decay.

We can parameterize the PMNS mixing matrix similarly to the CKM one, with a slight difference:

$$
\begin{aligned}
U =& \begin{pmatrix} 1 & 0 & 0 \\ 0 & c_{23} & s_{23} \\ 0 & -s_{23} & c_{23} \end{pmatrix} \begin{pmatrix} c_{13} & 0 & s_{13}e^{-i\delta} \\ 0 & 1 & 0 \\ -s_{13}e^{-i\delta} & 0 & c_{13} \end{pmatrix} \begin{pmatrix} c_{12} & s_{12}\ 0 & \\ -s_{12} & c_{12} & 0 \\ 0 & 0 & 1 \end{pmatrix} \begin{pmatrix} e^{i\alpha_1/2} & 0 & 0 \\ 0 & e^{i\alpha_2/2} & 0 \\ 0 & 0 & 1 \end{pmatrix} \\
=& \begin{pmatrix} c_{12}c_{13} & s_{12}c_{13} & s_{13}e^{-i\delta} \\ -s_{12}c_{23} - c_{12}s_{23}s_{13}e^{i\delta} & c_{12}c_{23} - s_{12}s_{23}s_{13}e^{i\delta} & s_{23}c_{13} \\ s_{12}s_{23} - c_{12}c_{23}s_{13}e^{i\delta} & -c_{12}s_{23} - s_{12}c_{23}s_{13}e^{i\delta} & c_{23}c_{13} \end{pmatrix} \begin{pmatrix} e^{i\alpha_1/2} & 0 & 0 \\ 0 & e^{i\alpha_2/2} & 0 \\ 0 & 0 & 1 \end{pmatrix}.
\end{aligned}
\tag{2.41}
$$

Here we may have two phase factors $\alpha_{1,2}$ if neutrinos are Majorana fermions. If the neutrinos are Dirac fermions, we can absorb the phase factors into the redefinition of Dirac fields. Therefore, the $\alpha_{1,2}$ will disappear for the Dirac case. Instead, for the Majorana case, we can only absorb one phase into one generation of neutrino, while the relative phase difference $\alpha_{1,2}$ would remain. Therefore, there are 3 mass parameters $m_{1,2,3}$, three Euler angles $\theta_{12,13,23}$ and 1 CPV phase term δ for the Dirac neutrinos (and 2 more phase factors $\alpha_{1,2}$ for the Majorana case). Therefore, we have 7 (9 for Majorana case) more parameters to be added into the SM. In summary, the modified SM contains 26 (28) free parameters in total.

2.6 Determinations of SM parameters

Starting from the SM Lagrangian, we can obtain Feynman rules. The gauge-field coupling to the leptons can be written in terms of

$$
\begin{aligned}
\mathcal{L}_{g-l} =& \bar{l}_L\gamma^\mu(g_2\frac{\vec{\tau}}{2}\cdot\vec{W}'_\mu - g_1\frac{1}{2}B_\mu)l_L - \bar{e}_R g_1\gamma^\mu B'_\mu e_R \\
=& g_2(\frac{1}{2}\bar{l}_L\vec{\tau}\gamma^\mu l_L)\vec{W}'_\mu + \frac{1}{2}g_1(-\bar{l}_L\gamma^\mu l_L - 2\bar{e}_R\gamma^\mu e_R)B'_\mu \\
=& g_2(J_1^\mu W'_{1\mu} + J_2^\mu W'_{2\mu}) + (g_2 J_3^\mu W'_{3\mu} + \frac{1}{2}g_1 J_Y^\mu B'_\mu) \\
=& \mathcal{L}_{CC} + \mathcal{L}_{NC}.
\end{aligned}
\tag{2.42}
$$

We separate the $\mathcal{L}_{g-l}$ term into the charged and neutral current parts, $\mathcal{L}_{CC}$ and $\mathcal{L}_{NC}$. The charged current part can be written as

$$
\mathcal{L}_{CC} = g_2(J_1^\mu W'_{1\mu} + J_2^\mu W'_{2\mu}) = \frac{g_2}{2\sqrt{2}}(J^{-\mu}W_\mu^- + J^{+\mu}W_\mu^+),
\tag{2.43}
$$

where the charged current is defined as

$$
J^{-\mu} = 2(J^{1\mu} - iJ^{2\mu}) = \bar{l}_L(\tau^1 - i\tau^2)\gamma^\mu l_L = 2\bar{l}_L\tau^-\gamma^\mu l_L = \bar{e}\gamma^\mu(1-\gamma_5)\nu.
\tag{2.44}
$$

Similarly, we have $J^{+\mu} = 2(J^{1\mu} + iJ^{2\mu})$. The Feynman rules for the respective coupling factors are drawn in Figure 2.4. When scattering energies are much lower than $M_{W,Z}$, we

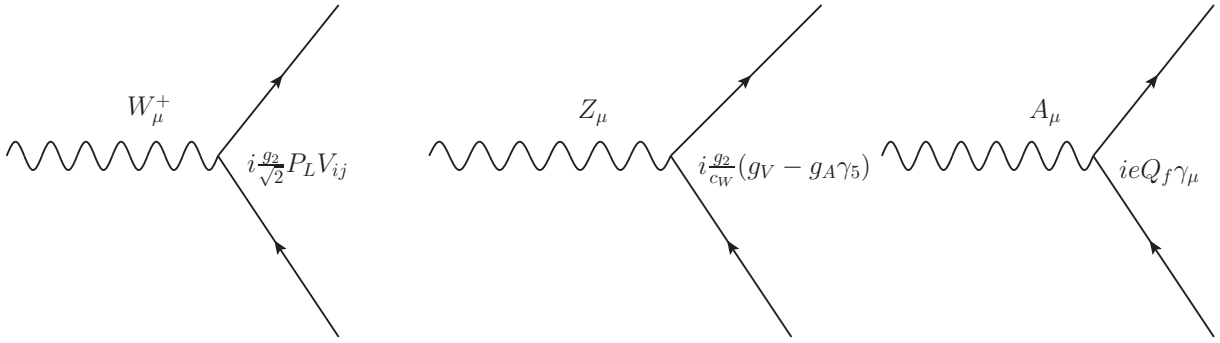

Figure 2.4: Feynman rules for EW gauge boson couplings to fermions.

can replace a subgraph containing W or Z propagators between $q\bar{q}W$ or $q\bar{q}Z$ vertices by an effective four-fermion coupling, shown in Figure 2.5. Therefore, we have

$$\mathcal{L}^{CC}_{\text{eff}} = \lim_{q^2\to 0}\left(\frac{g_2}{2\sqrt{2}}\right) J^{-\mu}\frac{g_{\mu\nu}}{q^2 - m_W^2}\left(\frac{g_2}{2\sqrt{2}}\right) J^{+\nu} = \frac{-g_2^2}{8m_W^2} J^-_\mu J^{+\mu}. \tag{2.45}$$

By comparing with the effective Lagrangian $\mathcal{L}_{\text{eff}} = -\frac{G_F}{\sqrt{2}} J^\dagger_\mu J^\mu$ [42, 43] of the V-A current-

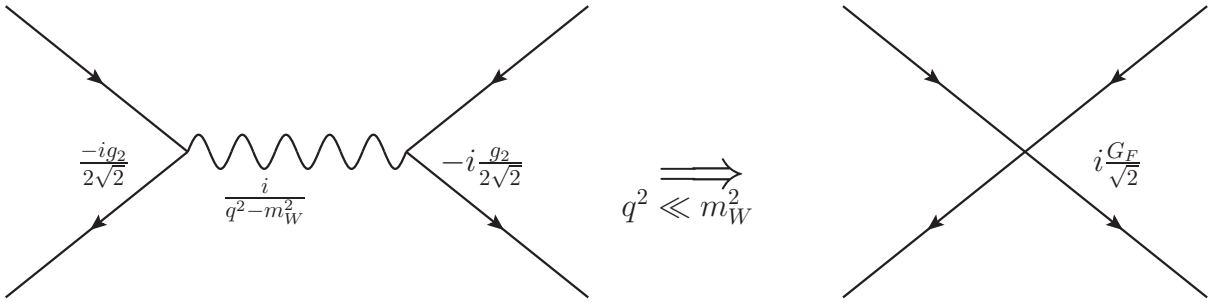

Figure 2.5: The Feynman diagram for the low-energy four-fermion interaction.

current theory, we can obtain

$$\frac{G_F}{\sqrt{2}} \equiv \frac{g_2^2}{8M_W^2} = \frac{1}{2v^2} \implies v = (\sqrt{2}G_F)^{-1/2} = 246.22\,\text{GeV}. \tag{2.46}$$

Here $G_F = 1.1663787 \times 10^{-5}\,\text{GeV}^{-2}$ is taken from the latest Review of Particle Physics [23].

Considering the neutral current, we have

$$\begin{aligned}\mathcal{L}_{NC} &= g_2 J_3^\mu W'_{3\mu} + \frac{1}{2} g_1 J_Y^\mu B'_\mu \\ &= g J_3^\mu (c_W Z_\mu + s_W A_\mu) + g_1 t_W (J_Q^\mu - J_3^\mu)(-s_W Z_\mu + c_W A_\mu) \\ &= g s_W J_Q^\mu A_\mu + \frac{g}{c_W} J_0^\mu Z_\mu.\end{aligned} \tag{2.47}$$

Here we introduce the notation $t_W \equiv \tan\theta_W$. We can define

$$\begin{aligned} e &\equiv g s_W, \\ J_0^\mu &\equiv J_3^\mu - s_W^2 J_Q^\mu = \bar{l}\gamma^\mu (g_V - g_A \gamma^5) l, \\ g_V &\equiv T_L^3 - 2 Q_f s_W^2, \quad g_A \equiv T_L^3, \end{aligned} \tag{2.48}$$

where $T_L^3 = \tau^3/2$. As a consequence, we have the neutral currents for the neutrino and electron respectively as

$$\begin{aligned} &J_{0\nu}^\mu = \bar{\nu}_L \gamma^\mu (\frac{1}{2} - \frac{1}{2}\gamma^5)\nu_L = \frac{1}{2}\bar{\nu}\gamma^\mu(1-\gamma_5)\nu \text{ and} \\ &J_{0e}^\mu = \bar{e}_L \gamma^\mu (-\frac{1}{2} + 2s_W^2 + \frac{1}{2}\gamma^5) e_L + \bar{e}_R \gamma^\mu (+2s_W^2) e_R = -\frac{1}{2} e\gamma^\mu (1 - 4s_W^2 + \gamma^5) e. \end{aligned} \tag{2.49}$$

Similarly to the charged current, we can also have effective 4-fermion interactions for the neutral current as

$$\mathcal{L}_{\text{eff}}^{NC} = \lim_{q^2 \to 0} \frac{g_2^2}{4c_W^2} J_{0\nu}^{\mu\dagger} \frac{g_{\mu\nu}}{q^2 - m_Z^2} J_{0e}^\mu = \frac{-g_2^2}{16 m_Z^2 c_W^2} [\bar{\nu}\gamma_\mu(1-\gamma_5)\nu][e\gamma^\mu(1 - 4s_W^2 + \gamma^5)e]. \tag{2.50}$$

Afterwards, we can define one dimensionless measure of the relative strength of neutral and charged-current interactions in the 4-fermion interactions as [44, 45]

$$\rho \equiv \frac{m_W^2}{m_Z^2 c_W^2} = \frac{\frac{1}{4} g_2^2 v^2}{\frac{1}{4}(g_1^2 + g_2^2) v^2 \frac{g_2^2}{g_1^2 + g_2^2}} = 1. \tag{2.51}$$

If we use the tree-level relation between the W and Z boson mass, we obtain $\rho = 1$.

The electric couplings can be determined in terms of the fine-structure constant,

$$\alpha \equiv \frac{e^2}{4\pi} \approx \frac{1}{137}, \quad e = \sqrt{4\pi\alpha} \approx 0.3028. \tag{2.52}$$

Many other EW parameters were measured very precisely, such as

$$s_W^2 = 0.23126, \quad m_W = 80.385\,\text{GeV}, \quad m_Z = 91.1876\,\text{GeV}. \tag{2.53}$$

Together with the VEV $v = 246.22$ GeV, we can fix the gauge couplings $g_{1,2}$. The fermion (quark and lepton) mass and CKM matrix elements are all measured precisely in various experiments. The specific values can be found in the latest Review of Particle Physics [23]. The last parameter to discuss is the quartic coupling λ or the μ parameter in the Higgs sector, which have also been determined by the Higgs mass [14, 15],

$$m_H = \sqrt{2}\mu = 125\ \text{GeV}, \quad \lambda = \frac{m_H^2}{2v^2} = 0.129. \tag{2.54}$$

Chapter 3

Electroweak symmetry breaking beyond the Standard Model

In the last chapter, we reviewed the EW theory of the SM. We also mentioned that neutrinos have nonzero masses, as indicated by the neutrino oscillation experiments. It is a hint suggesting that the SM is not complete. In this chapter, we will start with the seesaw mechanism to solve the neutrino mass problem, and then move to discuss the scalar triplet models.

3.1 Seesaw mechanism

As discussed in Chapter 2, the neutrino must be massless in the original version of the SM written down by Steven Weinberg [3], which contradicts the neutrino oscillation experiments [34, 35, 36, 37]. We have also proposed to solve this problem, by adding right-handed neutrinos.

However, experiments also tell us the neutrino must be superlight. The most stringent upper bound on the $\bar{\nu}_e$ mass from scattering experiment is

$$m_{\bar{\nu}_e} < 2.05\,\text{eV at } 95\%\text{ CL}, \tag{3.1}$$

obtained in the Troitsk experiment [46, 47]. A similar result is obtained by the Mainz experiment [48]: $m_{\bar{\nu}_e} < 2.3$ eV at 95% CL. The Cosmic Microwave Background (CMB) data of WMAP and PLANCK indicate $\sum_j m_j \lesssim 0.3 - 1.3$ eV [49]. The latest combined analysis of the Planck CMB temperature spectrum and Baryon Acoustic Oscillations (BAO) lowers the limit to [50]

$$\sum_j m_j < 0.170\,\text{eV at } 95\%\text{ CL}. \tag{3.2}$$

As a result, we obtain a large hierarchy between the mass of neutrinos and charged leptons or quarks. More specifically, the lightest charged lepton is the electron, whose mass is $m_e = 0.511$ MeV. We obtain at least an order of 10^6 difference between masses of the charged and neutral leptons. As we know, the electron and neutrino both acquire mass

through Yukawa interactions; so the mass hierarchy means the Yukawa couplings also differ by many orders of magnitude.

One straightforward way to generate such small neutrino masses is the well-known **Seesaw Mechanism**. In an effective field theory (EFT), we can write down a lepton-number violating interaction,

$$\mathcal{L}_{\text{eff}} = \frac{c}{\Lambda}(\bar{L^c}\tilde{\Phi}^*)(\tilde{\Phi}^\dagger L). \tag{3.3}$$

This is the only one mass dimension-5 operator that we may have, originally written down by Steven Weinberg [51]. After the Higgs develops a VEV, $\langle 0|\tilde{\Phi}|0\rangle = (v,0)^T/\sqrt{2}$, the neutrino would acquire mass as

$$m_\nu = \frac{c}{\Lambda}\frac{v^2}{2}, \tag{3.4}$$

where $v = 246$ GeV. We can easily see how the seesaw mechanism works: when $\Lambda \gg v$, $m_\nu \ll v$.

3.1.1 Type-I seesaw mechanism

There are several ways to obtain this seesaw mechanism. In Chapter 2, we have already added right-handed neutrinos into the SM, and also discussed the possibility of Majorana neutrinos. Therefore, we can add a Majorana mass term together with the Yukawa coupling in the Lagrangian,

$$\mathcal{L}_\nu = y^\nu \bar{\nu}_R \tilde{\Phi}^\dagger l_L + \frac{1}{2} M \nu_R^T C \nu_R + \text{h.c.} \tag{3.5}$$

If we separate the left-handed and right-handed neutrinos,

$$\nu = \nu_L + C\bar{\nu}_L^T, \quad N = \nu_R + C\bar{\nu}_R^T, \tag{3.6}$$

we get the mass mass matrix for the ν and N,

$$\begin{pmatrix} 0 & m_D \\ m_D^T & M \end{pmatrix}, \quad m_D = y^\nu \frac{v}{\sqrt{2}}. \tag{3.7}$$

Here the Dirac mass term proportional to m_D comes from the Yukawa coupling. Diagonalizing this matrix would give us the mass value as

$$m_{\nu,N} = \frac{M}{2}\left(1 \mp \sqrt{1 - \frac{4m_D^2}{M^2}}\right) \xrightarrow{M \gg m_D} \frac{m_D^2}{M}, M. \tag{3.8}$$

Therefore, we have the light neutrino mass,

$$m_\nu = \frac{m_D^2}{M} = \frac{y^2 v^2}{2M}. \tag{3.9}$$

This can be also understood in an EFT way. The Feynman diagram for the scattering process is shown in the left panel of Figure 3.1. After integrating out the heavy particle N, we get the mass term for the $\frac{y^2v^2}{M}\bar{\nu}\nu$.

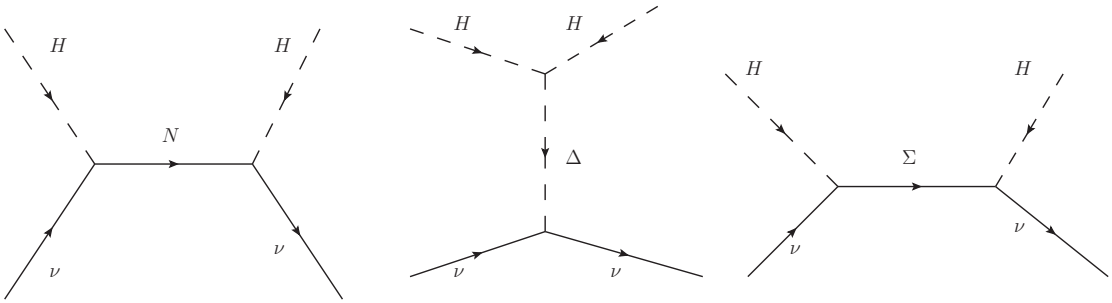

Figure 3.1: Three basic seesaw mechanisms to give neutrino small mass.

If we require the Yukawa coupling to be order of one, $y \sim O(1)$, we can estimate the heavy neutrino mass to be

$$M = \frac{yv^2}{2m_\nu} \sim \frac{1^2(100\text{GeV})^2}{1\text{eV}} \sim 10^{13}\ \text{GeV}. \tag{3.10}$$

3.1.2 Type-II seesaw

The heavy right-handed neutrino is not the only solution for getting a small neutrino mass. In an alternative approach, we can introduce a scalar isospin $SU(2)_L$ triplet $\Delta = (\delta^{++}, \delta^+, \delta^0)^T$ with hypercharge $Y = 2$ in addition to the SM scalar doublet. The electric charge is assigned by $Q = T_L^3 + Y/2$, where $T_L^3 = \text{diag}(1, 0, -1)$ is the third component of the triplet representation of the $SU(2)_L$ group. We can convert this triplet into a 2×2 matrix representation as

$$\Delta = \begin{pmatrix} \delta^+/\sqrt{2} & \delta^{++} \\ \delta^0 & -\delta^+/\sqrt{2} \end{pmatrix}. \tag{3.11}$$

Using this notation, we can write down the following new Lagrangian:

$$\mathcal{L} = \text{Tr}[(D_\mu\Delta)^\dagger(D^\mu\Delta)] - M_\Delta^2\text{Tr}(\Delta^\dagger\Delta) - \mu\tilde{\Phi}^T i\tau_2\Delta\tilde{\Phi} + y l_L^T C i\tau_2\Delta_L l_L + \text{h.c.} \tag{3.12}$$

The triplet will develop a VEV after the Spontaneous Symmetry Breaking (SSB),

$$\langle\Delta\rangle = \begin{pmatrix} 0 & 0 \\ v_\Delta & 0 \end{pmatrix},\ v_\Delta \simeq \frac{\mu v^2}{2M_\Delta^2}. \tag{3.13}$$

The value of the triplet VEV v_Δ in Equation (3.13) is approximate, and its exact value depends on the specific structure of the full scalar potential for both doublet and triplet scalar fields. As a result, the neutrino will obtain mass through the triplet Yukawa interactions,

$$m_\nu = 2yv_\Delta = y\frac{\mu v^2}{M_\Delta^2}. \tag{3.14}$$

The Feynman diagram that generates this mass can be viewed in the middle panel of Figure 3.1.

Performing a simple estimation, we have

$$O(y) \sim 1, m_\nu \sim 1 \text{ eV}, v \sim 100 \text{ GeV}, M_\Delta \sim 1 \text{ TeV}, \mu \sim 1 \text{ keV}. \tag{3.15}$$

We can see a big advantage in this mechanism: every scale is within the experimentally accessible range, which means we can test this idea at current and future colliders.

3.1.3 Type-III seesaw

Finally, let us take a glimpse at the Type III seesaw mechanisms. Instead of the scalar triplet, we can add a fermion (isospin) triplet with hypercharge $Y = 0$ into the SM and write it in the 2×2 matrix representation as

$$\Sigma = \begin{pmatrix} \Sigma^0/\sqrt{2} & \Sigma^+ \\ \Sigma^- & -\Sigma^0/\sqrt{2} \end{pmatrix}. \tag{3.16}$$

Therefore, we can write the following additional Lagrangian:

$$\mathcal{L} = \text{Tr}[\bar{\Sigma} \not{D} \Sigma] + \frac{1}{2}\text{Tr}\bar{\Sigma} m_\Sigma \Sigma^c + \sqrt{2} Y \tilde{\Phi}^\dagger \bar{\Sigma} l_L + \text{h.c.} \tag{3.17}$$

After the doublet Higgs develops a VEV, we can integrate out the heavy-fermion triplet and obtain the neutrino mass term as

$$m_\nu = \frac{v^2}{2} y^T \frac{1}{m_\Sigma} y, \tag{3.18}$$

as shown in the right diagram of Figure 3.1. When $m_\Sigma \gg v$, we obtain a small neutrino mass, $m_\nu \ll v$. Similarly to the Type-I seesaw, the heavy fermion mass can be estimated as $m_\Sigma \sim 10^{13}$ GeV when $y \sim O(1)$.

3.2 Scalar Triplets

In the last section, we mentioned that the scalar triplet VEV depends on the specific scalar potential in the Type-II seesaw mechanism. We will explore the general properties of the scalar triplet and some related issues in this section.

3.2.1 ρ parameter

Among the 3 types of seesaw mechanisms, we see that only the Type-II seesaw can bring the mass of the heavy particle down to EW scale, which opens the possibility to test this mechanism at colliders. However, this model is not free of problems. For example, to get the neutrino mass $m_\nu = 2yv_\Delta \sim 1$ eV $\ll v$, we need either to fine-tune the Yukawa coupling $y \ll 1$ or to take the limit $v_\Delta \ll v$. As pointed out already in Chapter 1, the triplet Yukawa operator $yl_L^T Ci\tau_2 \Delta_L l_L$ violates the lepton number. We have not observed lepton number violation processes in experiments yet, which means the associated Yukawa couplings must be very small. Therefore, we will accept that these Yukawa couplings are small and even set them to zero. We will refer to this choice as *fermiophobic*. On the other hand, the triplet VEV v_Δ will quantify its contribution to the electroweak symmetry breaking (EWSB) in the following way:

$$\rho = \frac{\sum_i [I_i(I_i+1) - (I_i^3)^2] v_i^2}{2\sum_i (I_i^3)^2 v_i^2}. \tag{3.19}$$

Here I_i is the $SU(2)_L$ isospin, and I_i^3 is the third component for the scalar field i which develops VEV v_i. For the SM doublet Higgs Φ, the isospin is $I = 1/2$, while $I^3 = \pm 1/2$, and we naturally have $\rho = 1$, i.e.

$$\Delta\rho = \rho - 1 = \frac{[I(I+1) - 3(I^3)^2]v^2}{2(I^3)^2 v^2} = 0. \tag{3.20}$$

The experiments strongly constrain this parameter to be small at a very high precision [23],

$$\Delta\rho = (0.39 \pm 0.19) \times 10^{-3}. \tag{3.21}$$

For the isospin triplet $I = 1$, the third component can be $I^3 = -1, 0, +1$. In a Higgs model only involving triplet scalars (no doublets or other representations), such as Georgi-Glashow $SO(3)$ Model [52] generalized by T. D. Lee [53, 54], we would have

$$\Delta\rho = \frac{-v_+^2 + 2v_0^2 - v_-^2}{2(v_+^2 + v_-^2)}. \tag{3.22}$$

We can very easily get a non-zero contribution to this ρ-parameter if the triplet model is not carefully constructed, which would be easily excluded by the experimental data. One straightforward way to escape this constraint is to add a triplet together with the Standard Model doublet H, and to take the triplet VEV to be small $v_\Delta \ll v_H$. For example,

$$\Delta\rho = \frac{-v_+^2 + 2v_0^2 - v_-^2}{2(\frac{1}{4}v_H^2 + v_+^2 + v_-^2)}, \quad |\Delta\rho| < \frac{2v_{\max}^2}{\frac{1}{2}v^2} < 10^{-3} \implies v_{\max} < 4 \text{ GeV}. \tag{3.23}$$

Here we have used the total EWSB $v_H^2 + 4(v_+^2 + v_-^2) = v^2 = 246$ GeV.

However, this small triplet VEV bears a disadvantage when embedded into the Standard Model. It behaves almost the same way as in the Standard Model, which makes it almost impossible for the triplet signals to be observed above the Standard Model backgrounds. For example, the doubly charged Higgs coupling to vector bosons,

$$g_{H^{\pm\pm}W_\mu^\mp W_\nu^\mp} = ig^2 v_\Delta g^{\mu\nu}, \tag{3.24}$$

proportional to v_Δ, will disappear in the $v_\Delta \to 0$ limit. Therefore, we need to come up with a technique to increase the v_Δ value, without violating the ρ-parameter constraint. When looking at the form of $\Delta\rho$ in Equation (3.23), we see that the $\Delta\rho = 0$ implies $v_\pm = v_0$, which is a natural consequence of a global symmetry called **custodial symmetry** [55]. Starting with the Standard Model, we need at least 2 more triplets: a real scalar giving triplet the VEV v_0 with isospin 0, and a complex one giving $v_\pm$ with isospin ± 1. This is the well-known **Georgi-Machacek** (GM) model [24].

3.2.2 The Georgi-Machacek Model

In the GM model, we have one SM doublet Higgs H ($Y = 1$), one real triplet Higgs with hypercharge η, and one complex Higgs χ with hyper-charge $Y = 2$. We can write these fields in a matrix form as

$$\Phi = \begin{pmatrix} \phi^{0*} & \phi^+ \\ \phi^-, & \phi^0 \end{pmatrix}, \quad \Delta = \begin{pmatrix} \chi^{0*} & \eta^+ & \chi^{++} \\ \chi^- & \eta^0 & \chi^+ \\ \chi^{--} & \eta^- & \chi^0 \end{pmatrix}. \tag{3.25}$$

Sometimes, we also use $(H^+, H^0)^T$ to denote the doublet Higgs. The matrix form transforms under the global $SU(2)_L \otimes SU(2)_R$ symmetry as

$$\Phi \to U_L \Phi U_R^\dagger, \quad \Delta \to U_L \Delta U_R^\dagger. \tag{3.26}$$

Therefore, we can construct the scalar potential in a global $SU(2)_L \otimes SU(2)_R$ invariant way,

$$\begin{aligned} V(\Phi, \Delta) = {} & \frac{\mu_2^2}{2}\mathrm{Tr}(\Phi^\dagger\Phi) + \frac{\mu_3^2}{2}\mathrm{Tr}(\Delta^\dagger\Delta) + \lambda_1\big[\mathrm{Tr}(\Phi^\dagger\Phi)\big]^2 + \lambda_2\mathrm{Tr}(\Phi^\dagger\Phi)\mathrm{Tr}(\Delta^\dagger\Delta) \\ & + \lambda_3\mathrm{Tr}(\Delta^\dagger\Delta\Delta^\dagger\Delta) + \lambda_4\big[\mathrm{Tr}(\Delta^\dagger\Delta)\big]^2 - \lambda_5\mathrm{Tr}(\Phi^\dagger\tau^a\Phi\tau^b)\mathrm{Tr}(\Delta^\dagger t^a \Delta t^b). \end{aligned} \tag{3.27}$$

Here, the $\tau^{a,b}$ and $t^{a,b}$ are generators for the $SU(2)$ group in the 2×2 and 3×3 matrix representations, respectively, and $a, b = 1, 2, 3$. The original version of the GM model does not contains the cubic term, as it violates a Z_2 symmetry. However, if we relax this Z_2

symmetry, we would allow 2 cubic terms as

$$\Delta V = -M_1 \mathrm{Tr}(\Phi^\dagger \tau^a \Phi \tau^b)(U \Delta U^\dagger)_{ab} - M_2 \mathrm{Tr}(\Delta^\dagger t^a \Delta t^b)(U \Delta U^\dagger)_{ab}, \tag{3.28}$$

where the matrix U is

$$U = \begin{pmatrix} -1/\sqrt{2} & i/\sqrt{2} & 0 \\ 0 & 0 & 1 \\ 1/\sqrt{2} & i/\sqrt{2} & 0 \end{pmatrix}. \tag{3.29}$$

We will see these 2 cubic terms are necessary when we supersymmetrize this model in Section 5.

After the spontaneous symmetry breaking (SSB), both doublet and triplet scalars will develop vacuum expectation values. As a result, the global $SU(2)_L \times SU(2)_R$ will break into a subgroup. Since the vacuum conserve charge, only neutral components can allow VEVs,

$$\langle \phi^0 \rangle = \frac{v_H}{\sqrt{2}}, \quad \langle \chi^0 \rangle = v_\chi, \quad \langle \eta^0 \rangle = v_\eta. \tag{3.30}$$

Other charged fields' VEVs are zero. Therefore, we would get the scalar potential in terms of the VEVs as

$$V(v_H, v_\chi, v_\eta). \tag{3.31}$$

As the VEV minimize this scalar potential, we can obtain the tadpole equations

$$0 = \frac{\partial V}{\partial v_H}, \quad 0 = \frac{\partial V}{\partial v_\chi}, \quad 0 = \frac{\partial V}{\partial v_\eta}, \tag{3.32}$$

which will give us the VEVs. Similar to the treatment in the SM, we could also use these 3 tadpole equations to substitute 3 Lagrangian parameters with these 3 VEVs.

We have 9 free parameters in total in the scalar potential, which leaves us a enough degree of freedom to impose a global **custodial symmetry**,

$$\langle \Phi \rangle \xrightarrow{SU(2)_C} U_V \langle \Phi \rangle U_V^\dagger = \langle \Phi \rangle, \quad \langle \Delta \rangle \xrightarrow{SU(2)_C} U_V \langle \Delta \rangle U_V^\dagger = \langle \Delta \rangle. \tag{3.33}$$

That is, we require the left and right unitary matrix to be the same, $U_L = U_R = U_V$, in the $SU(2)_L \otimes SU(2)_R$ transformation. Under this symmetry, the VEVs must take the alignment form as

$$\langle \Phi \rangle = \frac{1}{\sqrt{2}} \begin{pmatrix} v_H & 0 \\ 0 & v_H \end{pmatrix}, \quad \langle \Delta \rangle = \begin{pmatrix} v_\Delta & 0 & 0 \\ 0 & v_\Delta & 0 \\ 0 & 0 & v_\Delta \end{pmatrix}. \tag{3.34}$$

That is to say, the custodial symmetry is equivalent to the VEV alignment condition $v_\chi = v_\eta = v_\Delta$. We would like to remind that, the custodial symmetry is not a unique solution to the tadpole equations, but a prior assumption to be imposed.

As we indicated before, this custodial symmetry will ensure the alignment of the triplet VEV $v_\pm = v_0$. As a result, it naturally satisfies $\Delta\rho = 0$ at tree level. Both the doublet and triplet VEVs will contribute to the EWSB,

$$v_H^2 + 8v_\Delta^2 = v^2 = (246\text{ GeV})^2. \tag{3.35}$$

The EWSB will be associated with the global symmetry breaking $SU(2)_L \otimes SU(2)_R \to SU(2)_C$. In terms of the Goldstone theorem, we would expect to obtain 3 massless bosons to be eaten by the gauge bosons $W^\pm, Z$ to acquire mass.

We can shift the scalar field in terms of the the VEV as

$$\phi^0 = \frac{v_H}{\sqrt{2}} + \frac{\phi_R^0 + i\phi_I^0}{\sqrt{2}}, \quad \chi^0 = v_\Delta + \frac{\chi_R^0 + i\chi_I^0}{\sqrt{2}}, \quad \eta^0 = v_\Delta + \frac{\eta_R^0 + i\eta_I^0}{\sqrt{2}} \tag{3.36}$$

Then, the matrix form of the gauge eigenstates can be decomposed into the custodial basis. In terms of the $2 \otimes 2 = 1 \oplus 3$ and $3 \otimes 3 = 1 \oplus 3 \oplus 5$ decompositions, we will get 2 singlets, 2 triplets, and 1 quintuplet. The quintuplet is fully composed of the isospin triplet

$$H_5^{\pm\pm} = \chi^{\pm\pm}, \quad H_5^\pm = \frac{\chi^\pm - \eta^\pm}{\sqrt{2}}, \quad H_5^0 = -\sqrt{\frac{1}{3}}\chi_R^0 + \sqrt{\frac{2}{3}}\eta^0, \tag{3.37}$$

with the squared mass

$$m_5^2 = \frac{M_1}{4v_\Delta} + 12M_2 v_\Delta + \frac{3}{2}\lambda_5 v_\phi^2 + 8\lambda_3 v_\Delta^2. \tag{3.38}$$

The physical [1] triplets come from the mixing between the isospin doublet and triplet. In the custodial basis, we can define the custodial triplet as

$$\delta_3^\pm = \frac{\chi^\pm + \eta^\pm}{\sqrt{2}}, \quad \delta_3^0 = \chi_I^0; \quad \phi_3^\pm = \phi^\pm, \quad \phi_3^0 = \phi_I^0. \tag{3.39}$$

The squared mass matrix is diagonalized into one zero eigenvalue, while another one as

$$m_3^2 = \frac{M_1}{4v_\Delta}(v_H^2 + 8v_\Delta^2) + \frac{\lambda_5}{2}(v_H^2 + 8v_\Delta^2) = (\frac{M_1}{4v_\Delta} + \frac{\lambda_5}{2})v^2, \tag{3.40}$$

which corresponds to one massless Goldstone boson and another massive triplet as

$$\begin{aligned} G_3^\pm &= c_H\phi_3^\pm + s_H\delta_3^\pm, \qquad G_3^0 = c_H\phi_I^0 + s_H\chi_I^0, \\ H_3^\pm &= -s_H\phi_3^\pm + c_H\delta_3^\pm, \qquad H_3^0 = -s_H\phi_I^0 + c_H\chi_I^0. \end{aligned} \tag{3.41}$$

Here we have defined

$$c_H \equiv \cos\theta_H = \frac{v_H}{v}, \quad s_H \equiv \sin\theta_H = \frac{2\sqrt{2}v_\Delta}{v}. \tag{3.42}$$

[1] Here the physical state means the mass eigenstate.

Degeneracy	GM	
	scalar	pseudoscalar
singlet	h, H	
triplet		G_3, H_3
quintuplet	H_5	

Table 3.1: The mass spectrum of the GM model

Similarly, we have the custodial singlets as

$$\delta_1^0 = \frac{\sqrt{2}\chi_R^0 + \eta_0}{\sqrt{3}}, \quad \phi_1^0 = \phi_R^0. \tag{3.43}$$

The squared mass matrix is

$$\mathcal{M}^2 = \begin{pmatrix} \mathcal{M}_{11}^2 & \mathcal{M}_{12}^2 \\ \mathcal{M}_{21}^2 & \mathcal{M}_{22}^2 \end{pmatrix}, \tag{3.44}$$

where

$$\begin{aligned} \mathcal{M}_{11}^2 &= 8\lambda_1 v_H^2, \\ \mathcal{M}_{12}^2 &= \frac{\sqrt{3}}{2} v_H[-M_1 + 4(2\lambda_2 - \lambda_5)v_\Delta], \\ \mathcal{M}_{22}^2 &= \frac{M_1 v_H^2}{4v_\Delta} - 6M_2 v_\Delta + 8(\lambda_3 + 3\lambda_4)v_\Delta^2. \end{aligned} \tag{3.45}$$

Diagonalizing this squared mass matrix will give us the squared mass of the physical singlets,

$$h = c_\alpha \phi_1^0 - s_\alpha \delta_1^0, \quad H = s_\alpha \phi_1^0 + c_\alpha \delta_1^0, \tag{3.46}$$

where the $c_\alpha \equiv \cos\alpha$, $s_\alpha \equiv \sin\alpha$ and the angle α is defined in terms of

$$\sin 2\alpha = \frac{2\mathcal{M}_{12}^2}{m_H^2 - m_h^2}, \quad \cos 2\alpha = \frac{\mathcal{M}_{22}^2 - \mathcal{M}_{11}^2}{m_H^2 - m_h^2}, \tag{3.47}$$

and

$$m_{h,H}^2 = \frac{1}{2}\left[\mathcal{M}_{11}^2 + \mathcal{M}_{22}^2 \mp \sqrt{(\mathcal{M}_{11}^2 - \mathcal{M}_{22}^2)^2 + 4(\mathcal{M}_{12})^2}\right]. \tag{3.48}$$

We summarize the physical spectrum of the GM model in Table 3.1. One of the singlets in h, H can be interpreted as the SM-like 125 GeV Higgs, which can be either the lighter one h or the heavier one H. We can count the parameters in this model. Starting from the Standard Model, adding the isospin triplets, and writing the scalar potential, we have quadratic terms $\mu_{2,3}^2$, cubic terms $M_{1,2}$ and the quartic terms $\lambda_{1,2,3,4,5}$. With the tadpole equations, we can replace two of them with the VEVs of the doublet v_H and triplet v_Δ, and we choose to replace $\mu_{2,3}^2$. The EWSB and the Higgs mass will fix two of these parameters

as

$$v_H^2 + 8v_\Delta^2 = v^2 = (246\text{ GeV})^2, \quad m_{h,H} = 125\text{ GeV}. \tag{3.49}$$

As a result, we will have 7 free parameters in this model.

3.2.3 Bounds on the GM parameters

The parameters in the GM model are not totally free. For example, the quartic couplings have to satisfy the perturbative unitary bounds on the $2 \to 2$ scalar scattering amplitudes,

$$|a_0| \leq 1, \quad \text{or} \quad |\operatorname{Re} a_0| \leq \frac{1}{2}. \tag{3.50}$$

Here a_0 is the zeroth partial wave amplitude, which is related to the matrix element $\mathcal{M}$ of the $2 \to 2$ process by

$$\mathcal{M} = 16\pi \sum_{J=0}^{\infty} (2J+1) P_J(\cos\theta) a_J. \tag{3.51}$$

Here J is the orbital angular momentum, and $P_J(\cos\theta)$ are the Legendre polynomials. This unitary bound will constrain the magnitudes of the scalar quartic terms λ_i. Here we directly take the results from Reference [56],

$$\begin{aligned} &-\frac{1}{3}\pi < \lambda_1 < \frac{\pi}{3}, \qquad -\frac{2}{3}\pi < \lambda_2 < \frac{2}{3}\pi, \qquad -\frac{1}{2}\pi < \lambda_3 < \frac{3}{5}\pi, \\ &-\frac{1}{5}\pi < \lambda_4 < \frac{1}{2}\pi, \qquad -\frac{8}{3}\pi < \lambda_5 < \frac{8}{3}\pi. \end{aligned} \tag{3.52}$$

The Georgi-Machacek (GM) model can provide us with a lot of benefits. As mentioned in Section 3.2.2, the custodial symmetry will give us naturally $\Delta\rho = 0$ at tree level, which allow sizable contributions to the EWSB from the triplet sectors. Therefore, we can relax the constraint of $v_\Delta < 4$ GeV in Equation (3.23) to get the following bound:

$$v_\Delta < \sqrt{\frac{v^2 - v_H^2}{8}} \leq \sqrt{\frac{v^2}{8}} = 87\text{ GeV}. \tag{3.53}$$

This large triplet VEV v_Δ will give us large triplet signals, such as the $H^{\pm\pm}W^\mp W^\mp$ vertex mentioned above. In another example, the singlet Higgs h, H coupling to W boson can be written as

$$g_{hW^+W^-} = g_0 \left(c_\alpha c_H - \sqrt{\frac{8}{3}} s_\alpha s_H \right), \; g_{HW^+W^-} = g_0 \left(s_\alpha c_H + \sqrt{\frac{8}{3}} c_\alpha s_H \right), \tag{3.54}$$

where $g_0 = i g_2^2 v/2$ is the SM value. In the large v_Δ limit, i.e. $s_H \to 1$, we could even get a larger $h(H)W^+W^-$ coupling than the SM one, which can be easily measured at colliders.

Upon a more careful consideration, we find that the upper bound of the triplet VEV $v_\Delta \leq 87$ GeV corresponds to the doublet VEV $v_H \geq 0$. However, same as in the Standard

Model, the doublet VEV is responsible for giving nonzero masses to fermions through Yukawa couplings. There is another perturbative unitary bound which constrains the fermion-fermion scattering $f\bar{f} \to f\bar{f}$, shown in Figure 3.2. The amplitude is

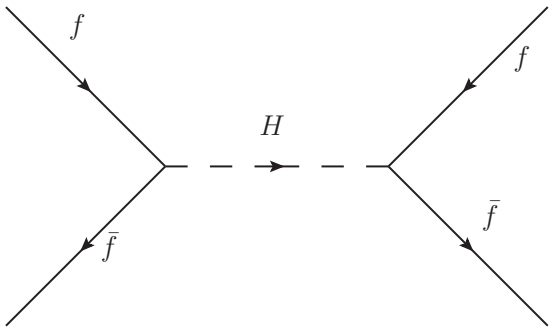

Figure 3.2: The fermion-fermion scattering through the intermediate Higgs boson.

$$\mathcal{M} = \bar{v}_2 iy u_1 \frac{1}{s - m_H^2} \bar{u}_3 iy v_4. \tag{3.55}$$

The Mandelstam variable is defined as $s = (p_1 + p_2)^2 = 4E^2$. In the high-energy limit $s \gg m_H^2$, we have

$$\bar{v}_2 u_1 = 2E, \quad \bar{u}_3 v_4 = 2E \implies \mathcal{M} = -y^2. \tag{3.56}$$

Then, we have a unitary bound

$$|a_0| = \frac{y^2}{16\pi} \leq 1, \quad y \leq \sqrt{16\pi}. \tag{3.57}$$

If we include both up- and down-type quarks in the scattering, we would get the zeroth partial wave amplitude as [57, 58],

$$|a_0|_{\max} = \frac{G_F}{8\sqrt{2}\pi} \left[3(m_1^2 + m_2^2) + \sqrt{9(m_1^2 - m_2^2)^2 + 4m_1^2 m_2^2 (2 + s_C^2)^2} \right]. \tag{3.58}$$

Here $m_{1,2}$ are the masses for the up- and down-type quarks, respectively, and $s_C = \sin\theta_C \leq 1$ is a Cabibbo-like angle. When taking the degeneracy limit $m_1 = m_2 = m$, we would get

$$|a_0|_{\max} = \frac{5G_F}{4\sqrt{2}\pi} m^2 = \frac{5y^2}{16\pi}. \tag{3.59}$$

If we have a pronounced mass hierarchy, such as $m_t \gg m_b$, we would have

$$|a_0| = \frac{3y_t^2}{16\pi} \leq 1 \implies y_t \leq \sqrt{16\pi/3}. \tag{3.60}$$

The top-quark mass will give us a lower bound on the doublet VEV (v_H):

$$m_t = \frac{y_t v_H}{\sqrt{2}} = 175 \text{ GeV} \implies v_H = \frac{\sqrt{2} m_t}{y_t} \geq \frac{\sqrt{2} \times 175}{\sqrt{16\pi/3}} = 60\,\text{GeV}. \tag{3.61}$$

From this condition, we can get a more exact upper bound to the triplet VEV,

$$v_\Delta = \sqrt{\frac{v^2 - v_H^2}{8}} \leq 84\,\text{GeV}. \tag{3.62}$$

Chapter 4

Supersymmetry in the electroweak sector

In the previous chapter, we showed that the custodial symmetry existing in the Higgs triplet model of the Georgi-Machacek type enforces the condition $\rho = 1$ at tree level, thus circumventing an important constraint on new physics models imposed by experimental measurements. In this chapter, we will discuss 1-loop electroweak corrections to the GM model. We will show that a quadratic divergence that arises in the 1-loop correction to the ρ parameter can be eliminated by introducing supersymmetry.

4.1 Quadratic divergence

As we discussed in section 3.2.2, the custodial symmetry in the Georgi-Machacek Model will give us a sizable contribution to the EWSB without violating the ρ-parameter constraint. The $\rho = 1$ condition (i.e., $\Delta\rho = 0$) is only held at tree level, as a natural result of the custodial symmetry. When including higher-oder contributions, we would receive corrections to $\Delta\rho$. As defined in Ref. [59], the ρ parameter is no longer directly related to vector boson masses. Instead, it directly probes the gauge boson two-point functions at small p^2 as

$$\Delta\rho = \frac{\Pi_{WW}(0)}{m_W^2} - \frac{\Pi_{ZZ}(0)}{m_Z^2}, \tag{4.1}$$

where $\Pi_{VV}(V = W, Z)$ is the coefficient of $-ig^{\mu\nu}$ in the vacuum-polarization amplitude of the gauge boson,

$$\Pi_{VV}^{\mu\nu}(p^2) = -ig^{\mu\nu}\Pi_{VV}(p^2), \tag{4.2}$$

which corresponds to the quantum correction to the transversal component of gauge-boson self-energy. The scalar contributions to the self-energy of a gauge boson are depicted in Figure 4.1. The left diagram can be removed by the tadpole equations that shift VEVs. With the power counting rules, the bubble diagram in the middle gives a logarithm divergence ($\ln\Lambda^2$), and the right one has a quadratic divergence (Λ^2). The divergent behavior is systematically investigated in Reference [60]. The respective contribution to $\Delta\rho$ is

$$\Delta\rho = \frac{g_1^2 s_H^2}{4\pi m_5^2}\Lambda^2. \tag{4.3}$$

This is an explicit example of the custodial symmetry violation caused by hypercharge gauge interaction $U(1)_Y$. The quadratic divergence comes from the scalars running in the right loop diagram of Figure 4.1, and also from the fermions running in the middle loop diagram of Figure 4.1.

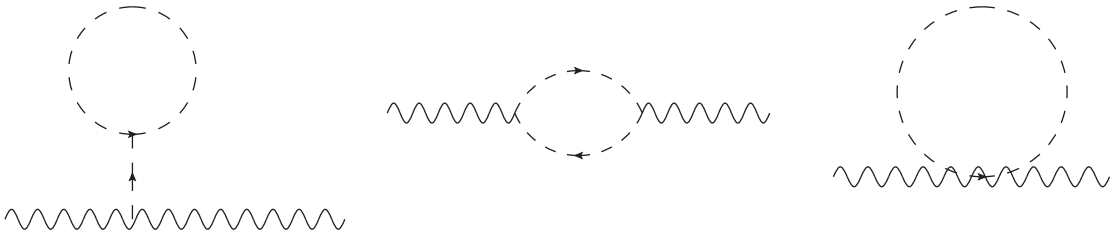

Figure 4.1: The self-energy of a vector boson contributed from scalars.

4.1.1 Quadratic divergence in the Higgs self-energy

Actually, the quadratic divergence emerging in ρ parameter is not a new characteristic. It is well-known for a long time and arises from the corrections to the Higgs mass. In the Standard Model, we have two kinds of quadratic divergences contributing to the Higgs self energy, shown in Figure 4.2. Let us briefly review the SM Yukawa interaction for the

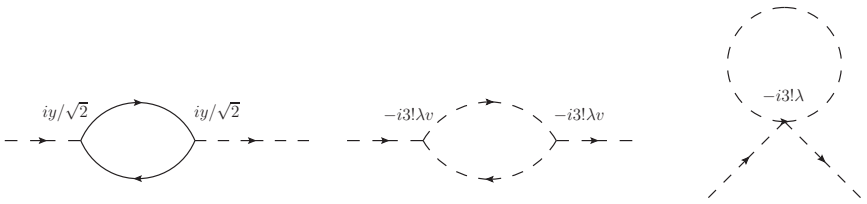

Figure 4.2: The quadratic divergence contributing to the Higgs self-energy.

contribution of one fermion flavor f. After the SSB, the shifted Higgs field in the unitary gauge can be written as $\Phi = (0, \phi)^T = (0, \frac{v+h}{\sqrt{2}})^T$. The Yukawa interaction Lagrangian is

$$\mathcal{L}_Y = y\bar{f}_L f_R \phi + \text{h.c.} = \frac{y}{\sqrt{2}} h\bar{f}f + \frac{yv}{\sqrt{2}}\bar{f}f. \tag{4.4}$$

This interaction renders the fermion mass as $m_f = yv/\sqrt{2}$ after the SSB, and the fermion-scalar coupling as $iy/\sqrt{2}$. Therefore, the fermion loop integral in the first diagram of Figure

4.2 can be written as

$$\begin{aligned}\Pi^f_{hh}(0) &= -N_c \int \frac{\mathrm{d}^4k}{(2\pi)^4} \mathrm{Tr} \frac{iy}{\sqrt{2}} \frac{i}{\not{k} - m_f} \frac{iy}{\sqrt{2}} \frac{i}{\not{k} - m_f} \\ &= -2y^2 N_c \int \frac{\mathrm{d}^4k}{(2\pi)^4} \frac{k^2 + m_f^2}{(k^2 - m_f^2)^2} = -2y^2 N_c \int \frac{\mathrm{d}^4k}{(2\pi)^2} \left[\frac{1}{k^2 - m_f^2} + \frac{2m_f^2}{(k^2 - m_f^2)^2} \right].\end{aligned} \tag{4.5}$$

Here the minus sign is due to the antisymmetry of the fermion loop, and N_c is the color factor whose value is 1 for leptons and 3 for quarks. We perform the **Wick rotation** to the Euclidean space,

$$k_0 \to ik_0, \ k^2 \to -k_0^2 - \vec{k}^2 = -k_E^2, \tag{4.6}$$

and compute the first integral as

$$\begin{aligned}&\int \frac{\mathrm{d}^4k}{(2\pi)^4} \frac{1}{k^2 - m_f^2} = i \int \frac{\mathrm{d}^4k_E}{(2\pi)^4} \frac{1}{-k_E^2 - m_f^2} \\ =&\frac{-i}{(2\pi)^4} \int k_E^3 \mathrm{d}k_E \mathrm{d}\Omega_4 \frac{1}{k_E^2 + m_f^2} = \frac{-i}{16\pi^2} \int_0^{\Lambda^2} \frac{k_E^2 \mathrm{d}k_E^2}{k_E^2 + m_f^2} \\ =&\frac{-i}{16\pi^2} \left(\Lambda^2 - m_f^2 \log \frac{\Lambda^2 + m_f^2}{m_f^2} \right),\end{aligned} \tag{4.7}$$

where we have used the surface area of a Euclidean unit 4-sphere: $\int \mathrm{d}\Omega_4 = 2\pi^2$. This exercise tells us explicitly that the quadratic divergence emerges in the loop integrals of $1/(k^2 - m^2)$ type, which is a simple example of the **power counting** [61, 62]. The Higgs propagator can be written as the summation of series as

$$\begin{aligned}G_{hh} &= \frac{i}{p^2 - m_h^2} + \frac{i}{p^2 - m_h^2} \Pi_{hh} \frac{i}{p^2 - m_h^2} + \cdots \\ &= \frac{i}{p^2 - m_h^2} \frac{1}{1 - \Pi_{hh} \frac{i}{p^2 - m_h^2}} = \frac{i}{p^2 - m_h^2 - i\Pi_{hh}}.\end{aligned} \tag{4.8}$$

We obtain the quadratic divergence in the corrections to the Higgs squared mass as

$$\Delta m_h^2 = i\Pi_{hh} \sim \frac{-2y^2 N_c}{16\pi^2} \Lambda^2. \tag{4.9}$$

At the same time, we can get the Higgs self-energy through the self-interaction (quartic coupling λ) shown in the second and third diagrams of Figure 4.2. In the unitary gauge, the Higgs potential terms are

$$\mathcal{L}_h = -\mu^2 h^2 - \lambda v h^3 - \frac{\lambda}{4} h^4. \tag{4.10}$$

The Higgs mass is $m_h = \sqrt{2}\mu = \sqrt{2\lambda} v$. The Feynman rules for Higgs self-couplings should be

$$V_{hhh} = -i3!\lambda v, \quad V_{hhhh} = -i4! \frac{\lambda}{4} = -i3!\lambda. \tag{4.11}$$

where $3! = 6$ and $4! = 24$ are symmetric factors. Therefore, the self-energy contributed by the two scalar loops is

$$\begin{aligned}\Pi^S_{hh}(0) &= \int \frac{\mathrm{d}^4k}{(2\pi)^4}(-i3!\lambda v)\frac{i}{k^2-m_h^2}(-i3!\lambda v)\frac{i}{k^2-m_h^2} + \int \frac{\mathrm{d}^4k}{(2\pi)^4}(-i3!\lambda)\frac{i}{k^2-m_h^2} \\ &= 6\lambda \int \frac{\mathrm{d}^4k}{(2\pi)^4}\left[\frac{1}{k^2-m_h^2} + \frac{6\lambda v^2}{(k^2-m_h^2)^2}\right].\end{aligned} \tag{4.12}$$

When summing over the scalar and fermion contributions to the self energy $\Pi^f_{hh}(0)+\Pi^S_{hh}(0)$, we would expect a cancellation of the quadratic divergence, if the scalar quartic coupling and the Yukawa coupling are fixed by a specific relation, such as $6\lambda - 2N_c y^2 = 0$. That is exactly the condition predicted by the supersymmetry (SUSY).

4.1.2 Cancellation of the quadratic divergence in supersymmetry

Let us play with a toy model to demonstrate how the quadratic divergence is canceled exactly. Under the SUSY, we will have the scalar superpartners $\tilde{f}_L$ and $\tilde{f}_R$ that accompany the chiral fermion f_L and f_R. The corresponding interaction can be written as

$$\mathcal{L}_{\tilde{f}\tilde{f}h} = \lambda|\phi|^2(|\tilde{f}_L|^2 + |\tilde{f}_R|^2) = \frac{1}{2}\lambda h^2(|\tilde{f}_L|^2 + |\tilde{f}_R|^2) + v\lambda h(|\tilde{f}_L|^2 + |\tilde{f}_R|^2). \tag{4.13}$$

Therefore, we obtain the scalar's contribution to the Higgs self-energy as

$$\begin{aligned}\Pi^{\tilde{f}}_{hh}(0) =& -N_c\lambda \int \frac{\mathrm{d}^4k}{(2\pi)^4}\left(\frac{1}{k^2-m^2_{\tilde{f}_L}} + \frac{1}{k^2-m^2_{\tilde{f}_R}}\right) \\ &+ N_c(\lambda v)^2 \int \frac{\mathrm{d}^4k}{(2\pi)^2}\left[\frac{1}{(k^2-m^2_{\tilde{f}_L})^2} + \frac{1}{(k^2-m^2_{\tilde{f}_R})^2}\right].\end{aligned} \tag{4.14}$$

Here $m_{\tilde{f}_{L,R}}$ are the mass for the scalars $\tilde{f}_{L,R}$. If the SUSY is unbroken, we have

$$m_f = m_{\tilde{f}_L} = m_{\tilde{f}_R},\ \lambda = -y^2. \tag{4.15}$$

Therefore, when summing over the contributions from fermion and scalar (superpartner), we get the Higgs self-energy as

$$\Pi^f_{hh}(0) + \Pi^{\tilde{f}}_{hh}(0) = 0. \tag{4.16}$$

Therefore, we explicitly verify the **non-renormalization theorem** [63]. Generally, in a supersymmetric model, each spin-0 (scalar) or spin-1 (vector) particle has a spin-1/2 superpartner, and each spin-1/2 (fermion) particle has a spin-0 (sfermion) superpartner. In such a way, every divergence is canceled systematically. If the SUSY is broken softly, the coupling relation $\lambda = -y^2$ is still valid, but the mass of superpartners are not degenerate anymore,

i.e. $m_f \neq m_{\tilde{f}_{L,R}}$. As a consequence, the quadratic divergence will be removed, while the logarithm divergence remains.

4.2 The Minimal Supersymmetric Standard Model

We leave the details of the supersymmetry algebra and superfields to the textbook of Quantum Field Theory (QFT) such as [64, 65], and move directly to the Minimal Supersymmetric Standard Model (MSSM).

4.2.1 The superpotential

In order to supersymmetrize the SM, we need to introduce superfields for each field in the SM, which will result in a superpartner for every particle. As a result, we would have spin-0 sfermions, such as sleptons and squarks, that accompany spin-1/2 leptons and quarks. We would also have Majorana fermions called gauginos associated with the gauge boson. For the scalar Higgs, we will have fermionic higgsinos, such as neutralinos and charginos. All the superfields are listed in Table 4.1. Just one reminder here: in the Standard Model, we can have only one scalar Higgs doublet, which gives the mass origins to both up-type and down-type fermion. The down-type fermions (down-type quarks and electron) couple to Φ, while the up-type fermions (up-type quarks) couple to the charge conjugate $\tilde{\Phi} = i\tau^2\Phi^*$. When supersymmetrizing the SM, we would need to double the number of the scalar fields, both for the up-type H_u and down-type H_d [1], and couple them separately to the up-type and down-type superfields in the superpotential. It is required by the holomorphic principle [63], which means that the superpotential can be only written as a function in terms of the chiral superfields, but not their complex conjugates. Therefore, we need to introduce another superfield H_u to take the place of $\tilde{\Phi}$ to couple to the up-type fermions. A non-holomorphic superpotential would lead to holomorphic anomalies that break the non-renormalization theorem [66, 67].

Furthermore, the non-renormalization theorem also requires the superpotential to be at most cubic. Therefore, we can only write down the following terms in the MSSM superpotential to satisfy the gauge symmetry $SU(3)_c \otimes SU(2)_L \otimes U(1)_Y$,

$$W = \mu H_d \cdot H_u + \lambda^e H_d \cdot L\bar{E} + \lambda^d H_d \cdot Q\bar{D} + \lambda^u Q \cdot H_u \bar{U}. \tag{4.17}$$

[1] In the following, we will denote $H_{d,u}$ as $H_{1,2}$.

Superfield	$SU(3)_c$	$SU(2)_L$	$U(1)_Y$
$L = \begin{pmatrix} L_\nu \\ L_e \end{pmatrix}$	1	2	-1
$\bar{E}$	1	1	2
$Q = \begin{pmatrix} Q_u \\ Q_d \end{pmatrix}$	3	2	$1/3$
$\bar{U}$	$\bar{3}$	1	$-4/3$
$\bar{D}$	$\bar{3}$	1	$2/3$
$H_d = \begin{pmatrix} H_d^0 \\ H_d^- \end{pmatrix}$	1	2	-1
$H_u = \begin{pmatrix} H_u^+ \\ H_u^0 \end{pmatrix}$	1	2	1

Table 4.1: The superfields of the MSSM.

The λ terms give us the Yukawa couplings, while only the μ-term is allowed for the Higgs potential. Integrating out the anti-communicating coordinates $\{\theta^\alpha, \bar{\theta}_{\dot{\alpha}}\}$ of the superpotential, we get the F-term potential as

$$\int \mathrm{d}^2\theta W + \text{h.c.} \rightarrow \ V_F = F_i^* F_i. = \left|\frac{\partial W}{\partial \Phi_i}\right|^2. \tag{4.18}$$

In such a way, we get the MSSM F-term potential for the Higgs fields

$$V_F = \mu^2(|h_1|^2 + |h_2|^2). \tag{4.19}$$

Similarly, integrating the Kahler potential, we get the D-term potential as

$$\int \mathrm{d}^4\theta \Phi^\dagger e^{qV} \Phi \rightarrow \ V_D = \frac{1}{2}\big[D_Y^2 + \vec{D}^2 + D^a D^a\big]. \tag{4.20}$$

Here $D_Y, \vec{D}, D^a$ correspond to the groups $U(1)_Y, SU(2)_L, SU(3)_c$, respectively:

$$D_Y = -g_1 \phi^\dagger \frac{Y}{2}\phi, \quad \vec{D} = -g_2 \phi^\dagger \frac{\vec{\tau}}{2}\phi, \quad D^a = -g_3 \phi^\dagger \frac{\lambda^a}{2}\phi, \tag{4.21}$$

where $\lambda^a/2$ are the generators for the $SU(3)_c$ group, and λ^a are the Gell-man matrices. The Higgs field does not participate in the color group, and as a result, only $D_Y = -g_1(-h_d^\dagger \frac{1}{2} h_d + h_u^\dagger \frac{1}{2} h_u)$ and $\vec{D} = -g_2(h_d^\dagger \frac{\vec{\tau}}{2} h_d + h_u \frac{\vec{\tau}}{2} h_u)$ contribute to the Higgs D-term potential as

$$V_D = \frac{G^2}{8}(|h_1|^2 - |h_2|^2|)^2 + \frac{g_2^2}{2}|h_1^\dagger h_2|^2, \tag{4.22}$$

where we define

$$G^2 \equiv g_1^2 + g_2^2, \quad g_1 = G \sin\theta_W, \quad g_2 = G\cos\theta_W. \tag{4.23}$$

4.2.2 Soft SUSY breaking

Under supersymmetry, the particle and its superpartner must share the same mass values. However, we have not yet found any superpartners of the Standard Model particles, meaning that the SUSY is broken by some unknown mechanism. From the phenomenological point of view, we can add an effective Lagrangian to break SUSY explicitly, which is called **soft SUSY breaking**. In the MSSM, we can have the following soft breaking terms in the Higgs sector,

$$V_{\text{soft}} = m_1^2|h_1|^2 + m_2|h_2|^2 + (B_\mu h_1 \cdot h_2 + \text{h.c.}). \tag{4.24}$$

Here $m_{1,2}$ is the soft mass term, and B_μ is the B-term corresponding to the μ-term in the superpotential.

By now, we have obtained all the pieces of the Higgs potential for the MSSM,

$$\begin{aligned} V_H =& V_F + V_D + V_{\text{soft}} \\ =& \frac{G^2}{8}(|h_1|^2 - |h_2|^2)^2 + \frac{g_2^2}{2}|h_1^\dagger h_2|^2 + m_{1h}|h_1|^2 + m_{2h}|h_2|^2 + (B_\mu h_1 \cdot h_2 + \text{h.c.}), \end{aligned} \tag{4.25}$$

where we redefine the mass parameters as $m_{1,2h}^2 = m_{1,2}^2 + |\mu|^2$.

The Spontaneous Symmetry Breaking will induce the VEVs as

$$\langle h_1 \rangle = \frac{1}{\sqrt{2}} \begin{pmatrix} v_1 \\ 0 \end{pmatrix}, \quad \langle h_2 \rangle = \frac{1}{\sqrt{2}} \begin{pmatrix} 0 \\ v_2 \end{pmatrix}, \tag{4.26}$$

which minimize the Higgs potential,

$$V(v_1, v_2) = \frac{1}{32}G^2(v_1^2 - v_2^2)^2 + \frac{1}{2}m_{1h}^2 v_1^2 + \frac{1}{2}m_{2h}^2 v_2^2 - B_\mu v_1 v_2. \tag{4.27}$$

The tadpole equations will allow us to replace two parameters with the VEVs. Thus, we choose $m_{1,2h}^2$ as

$$\begin{cases} \frac{\partial V}{\partial v_1} = 0 \\ \frac{\partial V}{\partial v_2} = 0 \end{cases} \implies \begin{cases} m_{1h}^2 = B_\mu \frac{v_2}{v_1} - \frac{1}{8}G^2(v_1^2 - v_2^2), \\ m_{2h}^2 = B_\mu \frac{v_1}{v_2} + \frac{1}{8}G^2(v_1^2 - v_2^2). \end{cases} \tag{4.28}$$

The kinematical terms of the Higgs fields will give the W and Z boson masses as

$$m_W = \frac{g_2}{2}v, \quad m_Z = \frac{G}{2}v, \quad v = \sqrt{v_1^2 + v_2^2} = 246 \text{ GeV}. \tag{4.29}$$

We can define a ratio of two VEVs as

$$t_\beta \equiv \tan\beta \equiv v_2/v_1, \quad v_2 = v\sin\beta, \quad v_1 = v\cos\beta. \tag{4.30}$$

In the following, we will often shorten the trigonometric functions as $s_\beta \equiv \sin\beta$ and $c_\beta \equiv \cos\beta$. We can rewrite the potential in terms of the shifted fields as

$$h_1 = \begin{pmatrix} \frac{v_1+h_1^R+ih_1^I}{\sqrt{2}} \\ h_1^- \end{pmatrix}, \quad \langle h_2 \rangle = \begin{pmatrix} h_2^+ \\ \frac{v_2+h_2^R+ih_2^I}{\sqrt{2}} \end{pmatrix}. \tag{4.31}$$

The quadratic terms will give us the mass spectrum of the Higgs scalars and their components. For the charged Higgs (h_1^+, h_2^+), we have

$$\begin{aligned} &(h_1^+, h_2^+) \begin{pmatrix} m_{1h}^2 + \frac{1}{8}G^2(v_1^2 - v_2^2) + \frac{1}{4}g_2^2 v_2^2 & B_\mu + \frac{1}{4}g_2^2 v_1 v_2 \\ B_\mu + \frac{1}{4}g_2^2 v_1 v_2 & m_{2h}^2 - \frac{1}{8}G^2(v_1^2 - v_2^2) + \frac{1}{4}g_2^2 v_1^2 \end{pmatrix} \begin{pmatrix} h_1^- \\ h_2^- \end{pmatrix} \\ =&\left(\frac{B_\mu}{v_1 v_2} + \frac{1}{4}g_2^2\right)(h_1^+, h_2^+) \begin{pmatrix} v_2^2 & v_1 v_2 \\ v_1 v_2 & v_1^2 \end{pmatrix} \begin{pmatrix} h_1^- \\ h_2^- \end{pmatrix}, \end{aligned} \tag{4.32}$$

where $m_{1,2h}^2$ are replaced by $v_{1,2}$. Diagonalizing this matrix, we will get the mass spectrum as

$$m_{G^\pm}^2 = 0, \quad m_{H^\pm}^2 = \left(\frac{B_\mu}{v_1 v_2} + \frac{1}{4}g_2^2\right)(v_1^2 + v_2^2) = \frac{g_2^2 v^2}{4} + \frac{B_\mu}{c_\beta s_\beta}. \tag{4.33}$$

The corresponding physical states are

$$G^\pm = c_\beta h_1^\pm - s_\beta h_2^\pm, \quad H^\pm = s_\beta h_1^\pm + c_\beta h_2^\pm. \tag{4.34}$$

The massless Goldstone boson $G^\pm$ will be absorbed by the $W^\pm$ bosons that will acquire mass.

Similarly, the squared mass matrix for the pseudoscalars (h_1^I, h_2^I) is

$$\begin{pmatrix} m_{1h}^2 + \frac{1}{8}G^2(v_1^2 - v_2^2) & B_\mu \\ B_\mu & m_{2h}^2 - \frac{1}{8}G^2(v_1^2 - v_2^2) \end{pmatrix} = B_\mu \begin{pmatrix} v_2/v_1 & 1 \\ 1 & v_{1/v_2} \end{pmatrix}. \tag{4.35}$$

Therefore, we have the mass spectrum

$$m_{G^0}^2 = 0, \quad m_A^2 = \frac{B_\mu}{c_\beta s_\beta}. \tag{4.36}$$

As expected, we have one massless Goldstone boson G^0, which is eaten by the Z boson. Surprisingly, we obtain the squared mass relation

$$m_{H^\pm}^2 = m_W^2 + m_A^2 \implies m_{H^\pm} > m_A. \tag{4.37}$$

Doing the same to the scalar fields (h_1^R, h_2^R), we get

$$\begin{aligned} \mathcal{M}^2 = \begin{pmatrix} \mathcal{M}_{11}^2 & \mathcal{M}_{12}^2 \\ \mathcal{M}_{12}^2 & \mathcal{M}_{22}^2 \end{pmatrix} &= \begin{pmatrix} B_\mu + \frac{1}{8}G^2(3v_1^2 - v_2^2) & -B - \frac{1}{4}G^2 v_1 v_2 \\ -B_\mu - \frac{1}{4}G^2 v_1 v_2 & B_\mu + \frac{1}{8}G^2(3v_2^2 - v_1^2) \end{pmatrix} \\ &= \begin{pmatrix} m_A^2 s_\beta^2 + m_Z^2 c_\beta^2 & -(m_A^2 + m_Z^2) s_\beta c_\beta \\ -(m_A^2 + m_Z^2) s_\beta c_\beta & m_A^2 c_\beta^2 + m_Z^2 s_\beta^2 \end{pmatrix}. \end{aligned} \tag{4.38}$$

The squared mass for this neutral scalars (CP-even) is

$$\begin{aligned} m^2_{h,H} &= \frac{1}{2}\left[\mathcal{M}^2_{11}+\mathcal{M}^2_{22} \mp \sqrt{(\mathcal{M}^2_{11}-\mathcal{M}^2_{22})^2+4(\mathcal{M}^2_{12})^2}\right] \\ &= \frac{1}{8}G^2v^2 + \frac{B}{\sin 2\beta} \mp \frac{1}{8\sin 2\beta}\sqrt{64B^2 - 16BG^2v^2\cos 4\beta \sin 2\beta + G^4v^4\sin^2 2\beta}. \end{aligned} \tag{4.39}$$

We also have the relation of the squared masses:

$$m^2_h + m^2_H = \frac{1}{4}G^2v^2 + \frac{B}{\sin\beta\cos\beta} = M^2_Z + m^2_A. \tag{4.40}$$

The mass eigenstates (h, H) can be expressed as a rotation of the gauge eigenstate (h^R_1, h^R_2):

$$\begin{pmatrix} H \\ h \end{pmatrix} = \begin{pmatrix} \cos\alpha & \sin\alpha \\ -\sin\alpha & \cos\alpha \end{pmatrix} \begin{pmatrix} h^R_1 \\ h^R_2 \end{pmatrix}. \tag{4.41}$$

The rotation angle is defined from

$$\begin{aligned} \sin 2\alpha &= \frac{2\mathcal{M}^2_{12}}{\sqrt{(\mathcal{M}^2_{11}-\mathcal{M}^2_{22})^2+4(\mathcal{M}^2_{12})^2}} = -\frac{(m^2_H+m^2_h)}{m^2_H-m^2_h}\sin 2\beta, \\ \cos 2\alpha &= \frac{\mathcal{M}^2_{11}-\mathcal{M}^2_{22}}{\sqrt{(\mathcal{M}^2_{11}-\mathcal{M}^2_{22})^2+4(\mathcal{M}^2_{12})^2}} = -\frac{(m^2_A-m^2_Z)}{m^2_H-m^2_h}\cos 2\beta, \\ \tan 2\alpha &= \frac{2\mathcal{M}^2_{12}}{\mathcal{M}^2_{11}-\mathcal{M}^2_{22}} = \frac{m^2_A+m^2_Z}{m^2_A-m^2_Z}\tan 2\beta = \frac{m^2_h+m^2_H}{m^2_A-m^2_Z}\tan 2\beta \end{aligned} \tag{4.42}$$

We have used the following relations:

$$\begin{aligned} \mathcal{M}^2_{12} &= -(m^2_A+m^2_Z)s_\beta c_\beta = (m^2_h+m^2_H)\frac{\sin 2\beta}{2}, \\ \mathcal{M}^2_{11}-\mathcal{M}^2_{22} &= -(m^2_A-m^2_Z)\cos 2\beta. \end{aligned} \tag{4.43}$$

One of the neutral scalars (h, H) will be interpreted as the SM-like 125 GeV Higgs [14, 15]. In terms of the squared mass relations (4.37) and (4.40), we get the following mass hierarchy:

$$\max(M^2_W, m^2_A) < m^2_{H^+}, \quad m^2_h < \min(m^2_A, M^2_Z) \le \max(m^2_A, M^2_Z) < m^2_H. \tag{4.44}$$

Let us count the parameters in the Higgs sector of the MSSM. The superpotential only contains 1 parameter μ, while the soft-breaking terms have 3 parameters: two soft masses $m^2_{1,2}$ and one B-term B_μ corresponding to μ in the superpotential. The tadpole equation will replace 2 parameters with the VEVs as $m^2_{1,2} \to v_{1,2}$. In addition, the EWSB $v = 246$ GeV and the SM-like Higgs mass $m_{h,H} = 125$ GeV will fix two parameters. As a result, we only have 2 free parameters in the Higgs sector of the MSSM. Usually, we choose them to be B_μ and $\tan\beta$.

Learning from the GM model, we may impose a custodial symmetry to obtain the aligned VEVs,

$$v_1 = v_2 = v/\sqrt{2} \implies \tan\beta = 1 \implies \beta = \frac{\pi}{4}. \tag{4.45}$$

Therefore, we have $c_\beta = s_\beta = 1/\sqrt{2}$, and the specific mass spectrum as

$$m^2_{H^\pm} = m^2_W + 2B_\mu, \quad m_A = 2B_\mu, \quad m_{h,H} = 0, m^2_Z + 2B_\mu. \tag{4.46}$$

We only have one free parameter B_μ in such a custodial limit. When inspecting the spectrum closely, we notice mild mass splitting in the approximate mass triplet $(H, H^\pm)$,

$$m^2_H - m^2_{H^\pm} = m^2_Z - m^2_W = \frac{1}{4} g_1^2 v^2. \tag{4.47}$$

It means that the custodial symmetry is slightly broken by the hypercharge interaction $U(1)_Y$. If we take the $g_1 \to 0$ limit, the custodial symmetry is restored. In such limit, the gauge bosons $W^\pm$ and Z share the same mass as $m_W = g_2 v/2$ and form a gauge triplet.

We can take another limit $B_\mu \to \infty$ (i.e., $B_\mu \gg G^2 v^2$), which gives

$$m^2_H \sim m^2_A \sim m^2_{H^\pm} \sim \frac{B}{s_\beta c_\beta} \to \infty. \tag{4.48}$$

That is $m^2_{H,A,H^\pm} \gg m^2_Z$. It means that all the non-SM scalar particles are decoupled from the SM ones. In this decoupling limit, we have

$$m^2_h = m^2_Z c^2_\beta, \quad \tan 2\alpha = \tan 2\beta \implies 2\alpha - 2\beta = \pm\pi, \quad \cos(\alpha - \beta) = 0. \tag{4.49}$$

That is, we have $|\alpha - \beta| \to \pi/2$, which is also called the **alignment limit** [68, 69, 70], since the Yukawa couplings $hf\bar{f}$ are exactly identical to the SM ones:

$$\begin{aligned} hf_d\bar{f}_d :\ \frac{s_\alpha}{c_\beta} = 1; \qquad & hf_u\bar{f}_u :\ \frac{c_\beta}{s_\beta} = 1; \\ Hf_d\bar{f}_d :\ \frac{c_\alpha}{c_\beta} = t_\beta; \qquad & Hf_u\bar{f}_u :\ \frac{s_\alpha}{s_\beta} = -1/t_\beta. \end{aligned} \tag{4.50}$$

4.2.3 Neutralinos and charginos

The MSSM particles in the Higgs sector and the corresponding superpartners are listed in Table 4.2. Starting with the Kahler potential $\Phi^\dagger e^V \Phi$, we can obtain the gaugino-higgsino-Higgs coupling term as

$$-\sqrt{2} g T^a \lambda^a \xi \phi^* + \text{h.c.} \tag{4.51}$$

where λ^a is the gaugino for the gauge group generator T^a, while ξ and ϕ are the fermionic and bosonic component of a Higgs chiral superfield, respectively. After the ϕ develop a VEV, we get the mass matrix mixing between the gaugino and the higgsino. We can write down

boson		fermion	
Higgs	$H_1 = \begin{pmatrix} h_1^0 \\ h_1^- \end{pmatrix}$ $H_2 = \begin{pmatrix} h_2^+ \\ h_2^0 \end{pmatrix}$	higgsino	$\tilde{H}_1 = \begin{pmatrix} \tilde{h}_1^0 \\ \tilde{h}_1^- \end{pmatrix}$ $\tilde{H}_2 = \begin{pmatrix} \tilde{h}_2^+ \\ \tilde{h}_2^0 \end{pmatrix}$
B boson	B	bino	$\tilde{B}$
W boson	W^i	wino	$\tilde{W}^i$

Table 4.2: Particles and the corresponding super-partners in the MSSM Higgs sector.

the charged gaugino filed (such as the wino) in the same form as the corresponding charged gauge boson (such as $W^\pm$),

$$\tilde{W}^\pm = \frac{1}{\sqrt{2}}(\tilde{W}_1 \mp i\tilde{W}_2). \tag{4.52}$$

In the soft-breaking Lagrangian, we have the Majorana mass term to account for heavy undiscovered gauginos,

$$\mathcal{L} = -\frac{1}{2}M_1\tilde{B}\tilde{B} - \frac{1}{2}M_2\tilde{W}^i\tilde{W}^i. \tag{4.53}$$

Therefore, we can write down the mass terms of the charged fermionic superpartner of the Higgs sector as

$$\mathcal{L}_c = -\frac{g_2}{\sqrt{2}}(v_1\tilde{W}^+\tilde{h}_1^- + v_2\tilde{W}^-\tilde{h}_2^+ + \text{h.c.}) - (M_2\tilde{W}^+\tilde{W}^- + \mu\tilde{h}_1^-\tilde{h}_2^+ + \text{h.c.}). \tag{4.54}$$

With the definition of four-component chargino field as

$$\psi^+ = \begin{pmatrix} \tilde{W}^+ \\ \tilde{h}_2^+ \end{pmatrix}, \quad \psi^- = \begin{pmatrix} \tilde{W}^- \\ \tilde{h}_1^- \end{pmatrix}. \tag{4.55}$$

The mass term can be written as

$$-\mathcal{L}_c = (\psi^-)^T X\psi^+ + \text{h.c.}, \quad X = \begin{pmatrix} M_2 & \sqrt{2}m_W s_\beta \\ \sqrt{2}m_W c_\beta & \mu \end{pmatrix}. \tag{4.56}$$

When taking the custodial limit,

$$v_1 = v_2 \implies s_\beta = c_\beta = \frac{1}{\sqrt{2}} \implies X = \begin{pmatrix} M_2 & m_W \\ m_W & \mu \end{pmatrix}. \tag{4.57}$$

We can diagonalize this mass matrix for fermions with 2 unitary matrices U and V:

$$M_c^2 = VX^\dagger XV^\dagger = U^*XX^\dagger U^T = \begin{pmatrix} m_1^2 & 0 \\ 0 & m_2^2 \end{pmatrix}, \tag{4.58}$$

boson		fermion	
singlet	$h_1^0 = -s_\beta h_d^0 + c_\beta h_u^0$		$\tilde{h}_1^0 = -s_\beta \tilde{h}_d^0 + c_\beta \tilde{h}_u^0$
triplet	$h_3^+ = h_u^+$ $h_3^0 = c_\beta h_d^0 + s_\beta h_u^0$ $h_3^- = h_d^-$		$\tilde{h}_3^+ = \tilde{h}_u^+$ $\tilde{h}_3^0 = c_\beta \tilde{h}_d^0 + s_\beta \tilde{h}_u^0$ $\tilde{h}_3^- = \tilde{h}_d^-$
W boson	$W^\pm = (W^1 \mp iW^2)/\sqrt{2}$	wino	$\tilde{W}^\pm = (\tilde{W}^1 \mp i\tilde{W}^2)/\sqrt{2}$
Z boson	$Z = c_W W^3 - s_W B$	zino	$\tilde{Z} = c_W \tilde{W}^3 - s_W \tilde{B}$
photon	$\gamma = s_W W^3 + c_W B$	photino	$\tilde{\gamma} = s_W \tilde{W}^3 + c_W \tilde{B}$

Table 4.3: The MSSM particles in rotation basis.

$$m_{1,2}^2 = \frac{1}{2}\left[|M_2|^2 + |\mu|^2 + 2m_W^2 \pm \sqrt{(|M_2|^2 + |\mu|^2 + 2m_W^2)^2 - 4|\mu M_2 - m_W^2 \sin 2\beta|^2}\right]. \quad (4.59)$$

In terms of the mass eigenstates of charginos

$$\chi^+ = \begin{pmatrix} \chi_1^+ \\ \chi_2^+ \end{pmatrix} = V \begin{pmatrix} \tilde{W}^+ \\ \tilde{h}_2^+ \end{pmatrix}, \quad \chi^- = \begin{pmatrix} \chi_1^- \\ \chi_2^- \end{pmatrix} = U \begin{pmatrix} \tilde{W}^- \\ \tilde{h}_1^- \end{pmatrix}, \quad (4.60)$$

the respective Lagrangian can be rewritten as

$$\begin{aligned} -\mathcal{L}_c &= (\psi^-)^T U^T U^* X V^- V \psi^+ + \text{h.c.} = (\chi^-)^T M_c \chi^+ + \text{h.c.}, \\ M_c &= U^* X V^- = \begin{pmatrix} m_1 & 0 \\ 0 & m_2 \end{pmatrix}. \end{aligned} \quad (4.61)$$

If taking the limit $M_2 \gg \mu \sim m_W$, we expect to get a wino-like χ_1^+ and and a higgsino-like χ_2^+ with masses

$$m_1 \sim M_2, \quad m_2 \sim |\mu|. \quad (4.62)$$

Similarly, we get the mass term of the neutralinos in the gauge eigenstate basis $\psi^0 = (\tilde{B}, \tilde{W}^0, \tilde{h}_1^0, \tilde{h}_2^0)$,

$$\mathcal{L}_n = -\frac{1}{2}(\psi^0)^T M \psi^0 + \text{h.c.}, \quad (4.63)$$

where

$$M = \begin{pmatrix} M_1 & 0 & -m_Z c_\beta s_W & m_Z s_\beta s_W \\ 0 & M_2 & m_Z c_\beta c_W & -m_Z s_\beta c_W \\ -m_Z c_\beta s_W & m_Z c_\beta c_W & 0 & -\mu \\ m_Z s_\beta s_W & -m_Z s_\beta c_W & -\mu & 0 \end{pmatrix}. \quad (4.64)$$

Next, we will express mass terms in the following rotation basis:

$$\begin{pmatrix}\tilde{\gamma}\\ \tilde{Z}\end{pmatrix}=\begin{pmatrix}c_W & -s_W\\ s_W & c_W\end{pmatrix}\begin{pmatrix}\tilde{B}\\ \tilde{W}^3\end{pmatrix},\quad \begin{pmatrix}\tilde{h}_3^0\\ \tilde{h}_1^0\end{pmatrix}=\begin{pmatrix}c_\beta & s_\beta\\ -s_\beta & c_\beta\end{pmatrix}\begin{pmatrix}\tilde{h}_d^0\\ \tilde{h}_u^0\end{pmatrix}. \tag{4.65}$$

We list all the MSSM particles in this rotation basis in Table 4.3. In this basis, the neutralino mass matrix becomes

$$\begin{pmatrix} M_1c_W^2+\ M_2s_W^2 & (M_2-M_1)c_Ws_W & 0 & 0\\ (M_2-M_1)c_Ws_W & M_2c_W^2+M_1s_W^2 & m_Z & 0\\ 0 & m_Z & -\mu\sin 2\beta & \mu\cos 2\beta\\ 0 & 0 & \mu\cos 2\beta & \mu\sin 2\beta \end{pmatrix} \xrightarrow{\tan\beta=1,t_W=0} \begin{pmatrix} M_1 & 0 & 0 & 0\\ 0 & M_2 & m_Z & 0\\ 0 & m_Z & -\mu & 0\\ 0 & 0 & 0 & \mu \end{pmatrix}. \tag{4.66}$$

Here the limit corresponds to the custodial $v_2 \to v_1$ and small hypercharge interaction $g_1 \to 0$,

$$\tan\beta=\frac{v_2}{v_1}=1,\quad t_W=\frac{g_1}{g_2}=0. \tag{4.67}$$

In such a limit, the zino $\tilde{Z}$ only mixes with the neutral component of triplet higgsino $\tilde{h}_3^0$. Another point we see is that the masses of the higgsinos $\tilde{h}_{1,3}^0$ remain of order of the mass parameter μ. In contrast, the masses of gauginos $\tilde{\gamma}, \tilde{Z}$ are of order the Majorana mass $M_{1,2}$.

The mass matrix is symmetric and can be diagonalized using a unitary matrix Z,

$$Z^*MZ^\dagger=M_n=\mathrm{diag}(m_1,m_2,m_3,m_4). \tag{4.68}$$

The neutralino mass eigenstate can be obtained as

$$\chi^0=Z\psi^0. \tag{4.69}$$

The lightest neutralino χ_1^0 is the **Lightest Supersymmetric Particle** (LSP), which is very stable and weakly interacting with the SM particles. Therefore, it can function as a WIMP-like (Weakly Interacting Massive Particle) dark matter candidate – the possibility that we explore as one of the future directions in the last chapter.

4.3 Two-Higgs-Doublet Model

Up to now, we have discussed the MSSM, which contains 2 doublet scalars. If we forget about the superpartner sector and only focus on the scalar Higgs sector, it becomes a specimen of the generic Two-Higgs-Doublet Model (2HDM). We can write down the most general scalar potential with 2 complex Higgs doublets $H_{1,2}$ as

$$\begin{aligned} V_H = & M_{11}^2 H_1^\dagger H_1 + M_{22}^2 H_2^\dagger H_2 \\ & + \lambda_1 (H_1^\dagger H_1)^2 + \lambda_2 (H_2^\dagger H_2)^2 + \lambda_3 H_1^\dagger H_1 H_2^\dagger H_2 + \lambda_4 H_1^\dagger H_2 H_2^\dagger H_1 \\ & + (M_{12}^2 H_1^\dagger H_2 + \frac{\lambda_5}{2} H_2^\dagger H_1 H_2^\dagger H_1 + \text{h.c.}). \end{aligned} \tag{4.70}$$

Using tadpole equations, we can replace M_{11}^2, M_{22}^2 with the vacuum expectation values $v_{1,2}$. Then, we can get the squared mass of pseudoscalar and the charged Higgs bosons as

$$m_A^2 = -(\lambda_5 + \frac{M_{12}}{v_1 v_2})(v_1^2 + v_2^2), \quad m_{H^+}^2 = -(\frac{\lambda_4 + \lambda_5}{2} + \frac{M_{12}}{v_1 v_2})(v_1^2 + v_2^2). \tag{4.71}$$

Here the VEVs satisfy $v^2 = v_1^2 + v_2^2 = 1/(\sqrt{2} G_f) = (246.22 \text{ GeV})^2$. Therefore, if fixing $\lambda_4 = \lambda_5$, we will get degenerate masses $m_A = m_{H^+}$.

The squared masses of the singlets are

$$m_{h,H}^2 = -M_{12}^2 + (\lambda_1 + \lambda_2) v_1^2 \pm \sqrt{(M_{12}^2 + (\lambda_3 + \lambda_4 + \lambda_5) v_1^2)^2 + (\lambda_1 - \lambda_2)^2 v_1^4}. \tag{4.72}$$

One of the (h, H) can be interpreted as the SM-like 125 GeV Higgs. The singlet Higgs couplings to the W boson are

$$g_{hW^+W^-} = g_0 \sin(\beta - \alpha), \ g_{HW^+W^-} = g_0 \cos(\beta - \alpha), \tag{4.73}$$

where $g_0 = i g_2^2 v/2$ is the SM value. We can see that these couplings are always smaller than the SM one, which is different from the GM (or other triplet) model. Similar observations apply to the $H(h)ZZ$ couplings.

Again we can choose the custodial basis $v_1 = v_2 = v/\sqrt{2}$. In addition, we can eliminate the mass dimensional parameter M_{12}^2 by imposing a Z_2 symmetry $H_1^+ \to -H_1^{-*}$. In such a case, the mass splitting for the singlets is

$$m_H^2 - m_h^2 = \sqrt{(\lambda_1 - \lambda_2)^2 + (\lambda_3 + 2\lambda_4)^2} v^2. \tag{4.74}$$

Therefore, we can choose a benchmark point $\lambda_1 = \lambda_2$, which gives $m_H^2 - m_h^2 = (\lambda_3 + 2\lambda_4) v^2$ by assuming $\lambda_3 + 2\lambda_4 > 0$. In such a case, all the Higgs squared masses are

$$m_h^2 = (\lambda_1 - \frac{\lambda_3}{2} - \lambda_4) v^2, \quad m_H^2 = (\lambda_1 + \frac{\lambda_3}{2} + \lambda_4) v^2, \quad m_A^2 = m_{H^+}^2 = -\lambda_4 v^2, \tag{4.75}$$

and the squared mass matrix of singlet is

$$\mathcal{M}^2 = \begin{pmatrix} \lambda_1 & \frac{\lambda_3}{2} + \lambda_4 \\ \frac{\lambda_3}{2} + \lambda_4 & \lambda_1 \end{pmatrix} v^2. \tag{4.76}$$

Therefore, we get the rotation angle as

$$\sin 2\alpha = \frac{2\mathcal{M}_{12}^2}{m_H^2 - m_h^2} = 1 \implies \alpha = \frac{\pi}{4}. \tag{4.77}$$

Chapter 5

The Supersymmetric Custodial Triplet Model

Now, equipped with the knowledge of supersymmetry and the two-Higgs-doublet electroweak sector in the MSSM, we will supersymmetrize the Georgi-Machacek model to obtain the Supersymmetric Custodial Triplet Model (SCTM) [71].

5.1 The Higgs scalar potential

As the MSSM case, the holomorphic principle will double the scalar particle contents in the GM model, as we are not allowed to write down the conjugate of a superfield in the superpotential. Therefore, besides the 2 MSSM electroweak doublets,

$$H_1 = \begin{pmatrix} H_1^0 \\ H_1^- \end{pmatrix}, \; H_2 = \begin{pmatrix} H_2^+ \\ H_2^0 \end{pmatrix}, \tag{5.1}$$

we need 3 triplets $\Sigma_-, \Sigma_0, \Sigma_+$ with hyperchargess as $Y = (-2, 0, 2)$ [71]. We write them down in a 2×2 matrix form,

$$\Sigma_- = \begin{pmatrix} \frac{\chi^-}{\sqrt{2}} & -\chi^0 \\ \chi^{--} & -\frac{\chi^-}{\sqrt{2}} \end{pmatrix}, \quad \Sigma_+ = \begin{pmatrix} \frac{\psi^+}{\sqrt{2}} & -\psi^{++} \\ \psi^0 & -\frac{\psi^+}{\sqrt{2}} \end{pmatrix}, \quad \Sigma_0 = \begin{pmatrix} \frac{\phi^0}{\sqrt{2}} & -\phi^+ \\ \phi^- & -\frac{\phi^0}{\sqrt{2}} \end{pmatrix}. \tag{5.2}$$

We can organize the fields into bi-doublet and bi-triplet representations of of $SU(2)_L \times SU(2)_R$,

$$\bar{H} = \begin{pmatrix} H_1 \\ H_2 \end{pmatrix}, \; \bar{\Delta} = \begin{pmatrix} -\frac{\Sigma^0}{\sqrt{2}} & \Sigma_- \\ -\Sigma_+ & \frac{\Sigma_0}{\sqrt{2}} \end{pmatrix}. \tag{5.3}$$

Here we put a bar above the fields to remind us that they are in the $SU(2)_L \otimes SU(2)_R$ basis. The superpotential can be written in terms of $\bar{H}$ and $\bar{\Delta}$ as

$$W = \lambda \bar{H} \cdot \bar{\Delta} \; \bar{H} + \frac{\lambda_\Delta}{3} \mathrm{Tr}\{\bar{\Delta}\bar{\Delta}\bar{\Delta}\} \; + \frac{\mu}{2} \bar{H} \cdot \bar{H} + \frac{\mu_\Delta}{2} \mathrm{Tr}\{\bar{\Delta}\bar{\Delta}\}, \tag{5.4}$$

and manifestly satisfies the $SU(2)_L \times SU(2)_R$ global symmetry. Here, the antisymmetric dot product is defined as

$$X \cdot Y = \epsilon^{ab} \epsilon_{ij} X_a^i X_b^j, \quad \epsilon^{12} = -\epsilon_{12} = 1, \tag{5.5}$$

where the upper a, b and lower i, j indices are acted upon by the $SU(2)_L$ and $SU(2)_R$ groups, respectively. We have dimensionless parameters λ, λ_Δ and mass dimension parameters μ, μ_Δ.

With $V_F = |\frac{\partial W}{\partial \Phi}|^2$, we obtain the F-term potential as

$$\begin{aligned} V_{\rm F} &= \mu^2\, \bar{H}^\dagger \bar{H} + \mu_\Delta^2\, {\rm Tr}\{\bar{\Delta}^\dagger \bar{\Delta}\} \ + 2\lambda\mu \left(\bar{H}^\dagger \bar{\Delta} \bar{H} + {\rm c.c.}\right) \\ &+ \lambda^2 \left(4\, {\rm Tr}\{(\bar{\Delta}\bar{H})^\dagger\, \bar{\Delta}\bar{H}\} + (\bar{H}^\dagger \bar{H})^2 - \frac{1}{4}\, |\bar{H}\cdot\bar{H}|^2 \right) \\ &+ \lambda_\Delta^2 \left({\rm Tr}\{\bar{\Delta}^\dagger \bar{\Delta}^\dagger \bar{\Delta}\bar{\Delta}\} - \frac{1}{4}\ {\rm Tr}\{\bar{\Delta}^\dagger \bar{\Delta}^\dagger\}\, {\rm Tr}\{\bar{\Delta}\bar{\Delta}\} \right) \\ &+ \lambda\lambda_\Delta \left(\bar{H}\cdot \bar{\Delta}^\dagger \bar{\Delta}^\dagger \bar{H} - \frac{1}{4} \bar{H}\cdot\bar{H}\ {\rm Tr}\{\bar{\Delta}^\dagger \bar{\Delta}^\dagger\} + {\rm h.c.} \right) \\ &+ \lambda\mu_\Delta \left(\bar{H}\cdot \bar{\Delta}^\dagger \bar{H} + {\rm c.c.} \right) + \lambda_\Delta \mu_\Delta \left({\rm Tr}\{\bar{\Delta}^\dagger \bar{\Delta}^\dagger \bar{\Delta}\} + {\rm h.c.} \right). \end{aligned} \tag{5.6}$$

Also the D-term is derived from Kahler potential with $V_D = \frac{1}{2} D^2$. The D-term for hypercharge gauge is

$$\begin{aligned} D_Y &= -\frac{g_1}{2} \left(\bar{H}^\dagger Y_H \bar{H} + {\rm Tr}\{\bar{\Delta} Y_\Delta \bar{\Delta}\} \right) \\ &= -\frac{g_1}{2} \left(-H_1^\dagger H_1 + H_2^\dagger H_2 + 2\, {\rm Tr}\Big\{ -\Sigma_-^\dagger \Sigma_- + \Sigma_+^\dagger \Sigma_+ \Big\} \right) \end{aligned} \tag{5.7}$$

where

$$Y_H = \begin{pmatrix} -1 & 0 \\ 0 & 1 \end{pmatrix}, \quad Y_\Delta = \begin{pmatrix} -2 & 0 \\ 0 & 2 \end{pmatrix}. \tag{5.8}$$

Similarly, we have a D-term for isospin weak gauge $SU(2)_L$,

$$\begin{aligned} \vec{D} &= -\frac{g_2}{2} \left(\bar{H}^\dagger \vec{T} \bar{H} + {\rm Tr}\Big\{ \bar{\Delta}^\dagger \vec{T} \bar{\Delta} \Big\} \right) \\ &= -\frac{g_2}{2} \left(H_1^\dagger \vec{\tau} H_1 + H_2^\dagger \vec{\tau} H_2 + {\rm Tr}\Big\{ \Sigma_-^\dagger \vec{\tau} \Sigma_- + \Sigma_0^\dagger \vec{\tau} \Sigma_0 + \Sigma_+^\dagger \vec{\tau} \Sigma_+ \Big\} \right), \end{aligned} \tag{5.9}$$

where generator $\vec{T} = {\rm diag}(\vec{\tau}, \vec{\tau})$ in the representations of $\bar{H}$ and $\bar{\Delta}$.

We can impose a G-parity condition:

$$\bar{H}^c = C \bar{H}^T = {\rm diag}(-i\tau_2, -i\tau_2) \bar{H}^*,\ \bar{\Delta}^c = C \bar{\Delta}^T C = \bar{\Delta}^\dagger,\ \text{where } C = \begin{pmatrix} 0 & 1 \\ -1 & 0 \end{pmatrix}. \tag{5.10}$$

In such circumstance, we have

$$H_2 = -i\tau_2 H_1^*, \quad \Sigma_- = -\Sigma_+^\dagger, \quad \Sigma_0 = \Sigma_0^\dagger. \tag{5.11}$$

More specifically, the component fields satisfy charge conjugate relations:

$$\begin{aligned} &h_1^{0*} = h_2^0, \qquad h_1^{-*} = -h_2^+, \\ &\chi^{0*} = \psi^0, \qquad \chi^{-*} = -\psi^+, \quad \chi^{--*} = \psi^{++}, \\ &\phi^{0*} = \phi^0, \qquad \phi^{-*} = -\phi^+. \end{aligned} \tag{5.12}$$

Therefore, we obtain $D_Y = 0$ and $\vec{D} = 0$ because of

$$\begin{aligned} &H_1^\dagger H_1 = H_2^\dagger H_2, \qquad H_1^\dagger \vec{\tau} H_1 + H_2^\dagger \vec{\tau} H_2 = 0, \\ &\Sigma_-^\dagger \Sigma_- = \Sigma_+^\dagger \Sigma_+, \qquad \Sigma_-^\dagger \vec{\tau} \Sigma_- + \Sigma_+^\dagger \vec{\tau} \Sigma_+ = 0, \quad \Sigma_0^\dagger \vec{\tau} \Sigma_0 = 0, \end{aligned} \tag{5.13}$$

which means that D-term potential is zero ($V_D = 0$) under the G-parity.

Next, we introduce soft supersymmetry breaking terms. They also respect the $SU(2)_L \otimes SU(2)_R$ global symmetry,

$$\begin{aligned} V_{\text{soft}} \ &= m_2^2 \bar{H}^\dagger \bar{H} + m_3^2 \,\mathrm{Tr}\big\{\bar{\Delta}^\dagger \bar{\Delta}\big\} \ + \Big(\frac{1}{2} B \bar{H} \cdot \bar{H} + \frac{1}{2} B_\Delta \,\mathrm{Tr}\big\{\bar{\Delta}\bar{\Delta}\big\} \\ &\quad + A_\lambda \bar{H} \cdot \bar{\Delta} \bar{H} + \ \frac{1}{3} A_\Delta \,\mathrm{Tr}\big\{\bar{\Delta}\bar{\Delta}\bar{\Delta}\big\} + \text{h.c.}\Big), \end{aligned} \tag{5.14}$$

Here $m_H^2, m_\Delta^2, B, B_\Delta$ have dimension of squared mass, while A, A_Δ have dimension of mass. We will see that B, B_Δ will help us to decouple the *non*-GM spectrum, similarly to the MSSM that decouples the SM particles.

After the SSB, the neutral scalars will develop VEVs:

$$\begin{aligned} &\langle H_1^0 \rangle = v_1/\sqrt{2}, \quad \langle H_2^0 \rangle = v_2/\sqrt{2}, \\ &\langle \chi^0 \rangle = v_\chi/\sqrt{2}, \quad \langle \psi^0 \rangle = v_\psi/\sqrt{2}, \quad \langle \phi^0 \rangle = v_\phi/\sqrt{2}. \end{aligned} \tag{5.15}$$

VEVs for other charged scalars must be zero, as the vacuum must be neutral to conserve charge. These VEVs minimize the scalar potential $V(v_1, v_2, v_\chi, v_\phi, v_\psi)$ and, therefore, we have the tadpole equations,

$$\frac{\partial V}{\partial v_1} = \frac{\partial V}{\partial v_2} = \frac{\partial V}{\partial v_\chi} = \frac{\partial V}{\partial v_\phi} = \frac{\partial V}{\partial \psi} = 0. \tag{5.16}$$

With these five tadpole equations, we can replace the Lagrangian parameters by the respective VEVs. As in the GM model, we can impose a custodial symmetry, which will require the VEVs to be aligned, that is,

$$v_d = v_u = v_2, \quad v_\chi = v_\psi = v_\phi = v_3. \tag{5.17}$$

The Higgs kinematical terms will give the gauge boson masses as

$$2v_2^2 + 8v_3^2 = v^2 = (246 \text{ GeV})^2, \quad m_W = \frac{g_2 v}{2}, \quad m_Z = \frac{\sqrt{g_1^2 + g_2^2}\, v^2}{2}. \tag{5.18}$$

Recalling that the EWSB in the GM model satisfies $v_H^2 + 8v_\Delta^2 = v^2$, we find from Equation (5.18) that the VEVs in the GM and SCTM models are related as

$$v_2 = v_H/\sqrt{2}, \quad v_3 = v_\Delta. \tag{5.19}$$

Similarly, we can define the VEV angle θ_H as

$$c_H = \cos\theta_H = \frac{\sqrt{2} v_2}{v}, \quad s_H = \sin\theta_H = \frac{2\sqrt{2} v_3}{v}. \tag{5.20}$$

Let us count the parameters in the Higgs sector of the SCTM model. The superpotential contains 2 cubic terms λ, λ_Δ and 2 quadratic terms μ, μ_Δ. Correspondingly, we have the 2 A-terms A, A_Δ and 2 B-terms B, B_Δ in the soft SUSY breaking terms. Furthermore, we have two soft-mass terms $m_{2,3}^2$ for the doublet and triplet, Consequently, we have 10 parameters

in total. Two of them can be replaced be the 2 VEVs $v_{2,3}$ – we choose to replace the soft masses $m^2_{2,3}$,

$$\begin{aligned} m_2^2 =& \frac{1}{2}\left[-3\lambda^2 v_2^2 - 3\lambda v_3^2(3\lambda+\lambda_3) - 2\mu^2 + 3\sqrt{2}\lambda v_3(2\mu+\mu_\Delta) - 2B + 3\sqrt{2}Av_3\right], \\ m_3^2 =& \frac{1}{2v_3}\Big[v_3(-2\lambda_3^2 v_3^2 + 3\sqrt{2}\lambda_3 v_3\mu_\Delta - 2\mu_\Delta^2) + \lambda v_2^2\left(-2v_3(3\lambda+\lambda_3) + \sqrt{2}(2\mu+\mu_\Delta)\right) \\ & - 2v_3 B_\Delta + \sqrt{2}v_2^2 A + \sqrt{2}v_3^2 A_\Delta\Big]. \end{aligned} \tag{5.21}$$

5.2 The mass spectrum

We decompose the Higgs field representations as $2 \otimes 2 = 1 \oplus 3$ and $3 \otimes 3 = 1 \oplus 3 \oplus 5$:

$$\bar{H} = h_1 \oplus h_3, \quad \bar{\Delta} = \delta_1 \oplus \delta_3 \oplus \delta_5, \tag{5.22}$$

where the subscripts represent the dimensionality of the $SU(2)_V$ representations. Hence, we can write the isospin doublet $\bar{H}$ in the custodial basis,

$$\begin{aligned} h_1^0 &= \frac{1}{\sqrt{2}}(H_1^0 + H_2^0), \\ h_3^+ &= H_2^+,\ h_3^0 = \frac{1}{\sqrt{2}}(H_1^0 - H_2^0),\ h_3^- = H_1^-. \end{aligned} \tag{5.23}$$

Similarly, the isospin triplet $\bar{\Delta}$ can decomposed as

$$\begin{aligned} &\delta_1^0 = \frac{\phi^0 + \chi^0 + \psi^0}{\sqrt{3}}, \\ &\delta_3^+ = \frac{\psi^+ - \phi^+}{\sqrt{2}},\ \delta_3^0 = \frac{\chi^0 - \psi^0}{\sqrt{2}}, \delta_3^- = \frac{\phi^- - \chi^-}{\sqrt{2}}, \\ &\delta_5^{++} = \psi^{++},\ \delta_5^+ = \frac{\phi^+ + \psi^+}{\sqrt{2}},\ \delta_5^0 = \frac{-2\phi^0 + \psi^0 + \chi^0}{\sqrt{6}},\ \delta_5^- = \frac{\phi^- - \chi^-}{\sqrt{2}},\ \delta_5^{--} = \chi^{--}. \end{aligned} \tag{5.24}$$

All fields components are complex. After the EWSB, the global symmetry $SU(2)_L \otimes SU(2)_R$ will break into a subgroup $SU(2)_V$. We can shift the fields around the VEVs as

$$\begin{aligned} &h_1^0 = v_2 + \frac{h_{1R}^0 + i h_{1I}^0}{\sqrt{2}}, \quad \delta_1^0 = \sqrt{\frac{3}{2}}v_3 + \frac{\delta_{1R}^0 + i\delta_{1I}^0}{\sqrt{2}}, \\ &h_3^a = \frac{h_{3R}^a + i h_{3I}^a}{\sqrt{2}}, \quad \delta_3^a = \frac{\delta_{3R}^a + i\delta_{3I}}{\sqrt{2}}, \quad (a = +, 0, -), \\ &\delta_5^a = \frac{\delta_{5R}^a + i\delta_{5I}}{\sqrt{2}}, \quad (a = ++, +, 0, -, --). \end{aligned} \tag{5.25}$$

This custodial basis will help us to construct the physical mass eigenstates.

Let us start from the quintuplet. The quintuplet is fully composed of the isospin triplet, and we can easily decompose it as scalar (CP-even) F_s part and pseudoscalar part F_p, where

letter F stands for the fiveplet.

$$F_s = \begin{pmatrix} \frac{1}{\sqrt{2}}(\delta_5^{++} + \delta_5^{--*}) \\ \frac{1}{\sqrt{2}}(\delta_5^{+} + \delta_5^{-*}) \\ \delta_{5R}^0 \\ \frac{1}{\sqrt{2}}(\delta_5^{-} + \delta_5^{+*}) \\ \frac{1}{\sqrt{2}}(\delta_5^{--} + \delta_5^{++*}) \end{pmatrix}, \quad F_p = \begin{pmatrix} \frac{1}{\sqrt{2}}(\delta_5^{++} - \delta_5^{--*}) \\ \frac{1}{\sqrt{2}}(\delta_5^{+} - \delta_5^{-*}) \\ \delta_{5R}^0 \\ \frac{1}{\sqrt{2}}(\delta_5^{-} - \delta_5^{+*}) \\ \frac{1}{\sqrt{2}}(\delta_5^{--} - \delta_5^{++*}) \end{pmatrix}. \tag{5.26}$$

The squared masses are

$$\begin{aligned} m_5^2 &= \frac{v_H^2\left[\lambda(2\mu - \mu_\Delta) - A_\lambda\right]}{\sqrt{2}v_\Delta} + \frac{3}{2}\lambda v_H^2(\lambda_\Delta - 2\lambda)\ \sqrt{2}v_\Delta(3\lambda_\Delta\mu_\Delta + A_\Delta) - v_\Delta^2\lambda_\Delta^2 \\ M_5^2 &= \frac{v_2^2[\lambda(2\mu + \mu_\Delta) + A]}{\sqrt{2}v_3} - \frac{1}{2}v_2^2(6\lambda + \lambda_3) + 2\sqrt{2}\lambda_3 v_3\mu_\Delta - 2B_\Delta. \end{aligned} \tag{5.27}$$

Here F_s is the quintuplet that emerges in the GM model with squared mass m_5^2, while F_p is the *mirror* particle, with squared mass M_5^2. We want to emphasize that the squared mass M_5^2 (capital letter) for the pseudoscalar field F_p has contributions from the soft B-term, which will help us to decouple F_p from the low-energy scale particles. We have already seen how this works in the MSSM case. The mass eigenvalue can be expanded around $v_3 \approx 0$ as

$$M_5^2 \approx \frac{v_H^2[\lambda(2\mu - \mu_\Delta) - A_\lambda]}{\sqrt{2}v_\Delta} - 2B_\Delta\ + \frac{1}{2}\lambda\ v_H^2(\lambda_\Delta - 6\lambda) + \mathcal{O}(v_\Delta). \tag{5.28}$$

The physical [1] triplets also include two scalars and two pseudoscalars. The pseudoscalar triplets show up in the GM model, while the scalar triplets are the corresponding *mirror* particles. For the pseudoscalar triplets, we write down the mass term as

$$(h_{3I}^a, \delta_{3I}^a) \begin{pmatrix} \mathcal{M}_{11}^2 & \mathcal{M}_{12}^2 \\ \mathcal{M}_{21}^2 & \mathcal{M}_{22}^2 \end{pmatrix} \begin{pmatrix} h_{3I}^a \\ \delta_{3I}^a \end{pmatrix} = (G^a, A^a) \begin{pmatrix} 0 & 0 \\ 0 & m_3^2 \end{pmatrix} \begin{pmatrix} G^a \\ A^a \end{pmatrix}, \tag{5.29}$$

where $a = 0, \pm$, and the squared mass matrix elements are given by

$$\begin{aligned} \mathcal{M}_{11}^2 &= 2v_3[-\lambda v_3(2\lambda + \lambda_3) + \sqrt{2}\lambda(2\mu + \mu_\Delta) + \sqrt{2}A], \\ \mathcal{M}_{22}^2 &= \frac{v_2^2[-\lambda v_3(2\lambda + \lambda_3) + \sqrt{2}\lambda(2\mu + \mu_\Delta) + \sqrt{2}A]}{2v_3}, \\ \mathcal{M}_{12}^2 &= \mathcal{M}_{21}^2 = v_2[\lambda v_3(2\lambda + \lambda_3) - \sqrt{2}\lambda(2\mu + \mu_\Delta) - \sqrt{2}A]. \end{aligned} \tag{5.30}$$

Diagonalization of this matrix will give us one zero eigenvalue, which corresponds the Goldstone Boson $G^{0,\pm}$, while another eigenvalue is for the pseudoscalar $A^{0,\pm}$ with squared mass

$$m_3^2 = \frac{v_2^2 + 4v_3^2}{2v_3}[\lambda(2\mu - \mu_\Delta - (2\lambda - \lambda_3)v_3) - A]. \tag{5.31}$$

[1] As mentioned before, the physical means mass eigenstate.

The mass eigenstate can be expressed as the rotation of the custodial pseudo scalar triplet,

$$\begin{pmatrix} G^a \\ A^a \end{pmatrix} = \begin{pmatrix} c_H & s_H \\ -s_H & c_H \end{pmatrix} \begin{pmatrix} h^a_{3I} \\ \delta^a_{3I} \end{pmatrix}, \quad a = +, 0, -. \tag{5.32}$$

The rotation angle is defined as $c_H = \sqrt{2}v_2/v$ and $s_H = 2\sqrt{2}v_3/v$.

Similarly, we write down the squared mass term for the mirror triplet (h^a_{3R}, δ_{3R}) in the custodial basis

$$(h^a_{3R}, \delta^a_{3R}) \begin{pmatrix} \mathcal{M}^2_{11} & \mathcal{M}^2_{12} \\ \mathcal{M}^2_{21} & \mathcal{M}^2_{22} \end{pmatrix} \begin{pmatrix} h^a_{3R} \\ \delta^a_{3R} \end{pmatrix} = (T^a_1, T^a_2) \begin{pmatrix} M^2_3 & 0 \\ 0 & M^2_{3'} \end{pmatrix} \begin{pmatrix} T^a_1 \\ T^a_2 \end{pmatrix}, \tag{5.33}$$

where $a = 0, \pm$, and the elements are

$$\begin{aligned} \mathcal{M}^2_{11} &= Gv_2^2 + 2\lambda(-4\lambda v_\Delta^2 + \lambda v_2^2 + 4\mu v_3) + 2B - 2v_3[A + \lambda(\mu_\Delta - \lambda_3 v_\Delta)], \\ \mathcal{M}^2_{22} &= 4G^2 v_3 - [2B_\Delta - 3\lambda\lambda_3 v_2^2 + 2v_3(\lambda_3^3 v_\Delta - A_3)] \\ &\quad - \frac{1}{v_3}[2\lambda v_2^2(\lambda v_3 - \mu) - (\lambda v_2^2 - 2\lambda_3 v_3^2)\mu_\Delta - v_2^2 A], \\ \mathcal{M}^2_{12} &= \mathcal{M}^2_{21} = 2v_2[-A + v_3(G^2 - 4\lambda^2 - \lambda\lambda_3) + \lambda\mu_\Delta]. \end{aligned} \tag{5.34}$$

Here $G^2 = g_2^2$ for the charged scalars, while $G^2 = g_1^2 + g_2^2$ for the neutral components. This is an explicit example showing that the hypercharge group $U(1)_Y$ breaks the custodial $SU(2)_V$ symmetry, which will break the degeneracy among the neutral and charged triplets. When we take the conjugate condition $\bar{\Delta} = \Delta$ and $H_2 = -i\tau_2 H_1^*$, the D-term will vanish and make the total *mirror* sector disappear. The model will return to the GM case. Similarly, we see the B-terms in both diagonal elements $\mathcal{M}^2_{11}$ and $\mathcal{M}^2_{22}$. We can obtain the squared mass values by diagonalizing this matrix. We can expand the mass eigenvalues around the small $v_3 \approx 0$ limit as

$$\begin{aligned} M^2_{3'} &\approx \frac{v_H^2[\lambda(2\mu - \mu_\Delta) - A_\lambda]}{\sqrt{2}v_\Delta} - 2B_\Delta \ + \frac{1}{2}\lambda\, v_H^2(3\lambda_\Delta - 2\lambda) + \mathcal{O}(v_\Delta), \\ M^2_3 &\approx \frac{1}{2}v_H^2(G^2 + 2\lambda^2) + \ 2B + O(v_\Delta). \end{aligned} \tag{5.35}$$

The physical states are given by

$$\begin{pmatrix} T^a_1 \\ T^a_2 \end{pmatrix} = \begin{pmatrix} \cos\alpha_T & \sin\alpha_T \\ -\sin\alpha_T & \cos\alpha_T \end{pmatrix} \begin{pmatrix} h^a_{3R} \\ \delta^a_{3R} \end{pmatrix}, \quad a = +, 0, -, \tag{5.36}$$

where the mixing angle can be expressed as

$$\sin 2\alpha_T = \frac{2\mathcal{M}^2_{12}}{\sqrt{\mathrm{Tr}^2\,\mathcal{M}^2 - 4\det\mathcal{M}^2}}, \ \cos 2\alpha_T = \frac{\mathcal{M}^2_{22} - \mathcal{M}^2_{11}}{\sqrt{\mathrm{Tr}^2\,\mathcal{M}^2 - 4\det\mathcal{M}^2}}. \tag{5.37}$$

Finally, let's examine the singlets (h_1, δ_1). We now have real scalar singlets (CP-even) that appear in the GM model, and the corresponding pseudoscalar singlets (CP-odd) as

mirror particles. The squared mass matrix for the scalar singlet is written as

$$(h^0_{1R}, \delta^0_{1R}) \begin{pmatrix} \mathcal{M}^2_{11} & \mathcal{M}^2_{12} \\ \mathcal{M}^2_{21} & \mathcal{M}^2_{22} \end{pmatrix} \begin{pmatrix} h^0_{1R} \\ \delta^0_{1R} \end{pmatrix} = (S_1, S_2) \begin{pmatrix} m^2_h & 0 \\ 0 & m^2_H \end{pmatrix} \begin{pmatrix} S_1 \\ S_2 \end{pmatrix}, \tag{5.38}$$

where

$$\begin{aligned} \mathcal{M}^2_{11} &= 6\lambda^2 v_2^2, \\ \mathcal{M}^2_{22} &= \frac{v_2^2}{v_\Delta}[\lambda(2\mu - \mu_\Delta) - A] + v_\Delta[-A_3 + \lambda_\Delta(4\lambda_\Delta v_3 - 3\mu_\Delta)], \\ \mathcal{M}^2_{12} &= \mathcal{M}^2_{21} = \sqrt{6} v_2[A + \lambda(6\lambda v_3 - 2\lambda_3 v_\Delta - 2\mu + \mu_\Delta]. \end{aligned} \tag{5.39}$$

The eigenvalues of this matrix give us the physical masses $m^2_{h,H}$. The eigenvectors correspond to the mass eigenstates (h, H), given by rotating the custodial states as

$$\begin{pmatrix} S_1 \\ S_2 \end{pmatrix} = \begin{pmatrix} \sin\alpha_S & \sin\alpha_S \\ -\sin\alpha_S & \cos\alpha_S \end{pmatrix} \begin{pmatrix} h^0_{1R} \\ \delta^0_{1R} \end{pmatrix}, \tag{5.40}$$

with the rotation angle is defined analogously in Equation (5.37). We can expand the mass $m^2_{h,H}$ and angle $\sin\alpha_S$ around $v_3 \approx 0$ as

$$\begin{aligned} m^2_{S_1} &= 6\lambda^2 v_2^2 + O(v_3), \\ m^2_{S_2} &= \frac{\lambda(2\mu - \mu_\Delta) - A}{v_3} + O(v_3), \\ \sin\alpha_S &= -\sqrt{6}\frac{v_3}{v_2} + O(v_3^2), \end{aligned} \tag{5.41}$$

These 2 CP-even scalars match onto the singlets in the GM model, and one of them can be interpreted as the SM-like 125 GeV Higgs measured at the LHC [14, 15]. This boson can be either the lighter one h or the heavier H. We will explore the experiment constraints in both cases.

For the mirror pseudoscalar singlets $(h^0_{1I}, \delta^0_{1I})$, we have the mass term

$$(h^0_{1I}, \delta^0_{1I}) \begin{pmatrix} \mathcal{M}^2_{11} & \mathcal{M}^2_{12} \\ \mathcal{M}^2_{21} & \mathcal{M}^2_{22} \end{pmatrix} \begin{pmatrix} h^0_{1I} \\ \delta^0_{1I} \end{pmatrix} = (P_1, P_2) \begin{pmatrix} M^2_1 & 0 \\ 0 & M^2_{1'} \end{pmatrix} \begin{pmatrix} P_1 \\ P_2 \end{pmatrix}. \tag{5.42}$$

The mass eigenstates are expressed as

$$\begin{pmatrix} P_1 \\ P_2 \end{pmatrix} = \begin{pmatrix} \sin\alpha_P & \sin\alpha_P \\ -\sin\alpha_P & \cos\alpha_P \end{pmatrix} \begin{pmatrix} h^0_{1I} \\ \delta^0_{1I} \end{pmatrix}, \tag{5.43}$$

where the rotation angle is defined similarly to Equation (5.37). We expand the squared mass eigenvalues M^2_1 and $M^2_{1'}$ around $v_3 \approx 0$ as

$$\begin{aligned} M^2_{1'} &\approx \frac{v_H^2[\lambda(2\mu - \mu_\Delta) - A_\lambda]}{\sqrt{2} v_\Delta} - 2B_\Delta \ + 2\lambda\lambda_\Delta v_H^2 + \mathcal{O}(v_\Delta), \\ M^2_1 &\approx 2B. \end{aligned} \tag{5.44}$$

Degeneracy	GM		SCTM	
	scalar	pseudo scalar	scalar	pseudo scalar
singlet	h, H		$S_{1,2}$	$P_{1,2}$
triplet		G, H_3	$T_{1,2}$	G, A
quintuplet	H_5		F_s	F_p

Table 5.1: The mass spectrum of the SCTM compared with the GM model

Finally, let us summarize the spectrum in Table 5.1. As we mentioned, we need 2 complex isospin doublets and 3 complex isospin triplets. In terms of the $2 \otimes 2 = 1 \oplus 3$ and $3 \otimes 3 = 1 \oplus 3 \oplus 5$ decompositions, we have 1 complex quintuplet, with the real part (CP-even) matching on the scalar quintuplet H_5 in the GM model, and the imaginary part as its corresponding mirror particle F_p. We have 2 complex triplets, of which the imaginary parts show up already in the GM model as a Goldstone boson and physical triplet H_3, and the real parts as their mirror-GM particles $T_{1,2}$. Similarly, we have 2 complex singlets, and the real part matching onto the physical singlets (h, H) in the GM model, and with the corresponding pseudoscalar singlets $P_{1,2}$ being their mirror particles.

When looking at the squared mass of all the mirror-GM particles $M^2_{5,3,3',1,1'}$ in Equations (5.28,5.35,5.44), we realize that all of them contain the soft SUSU breaking B-terms B, B_Δ. We have already seen this behavior in the MSSM. Therefore, if we take the decoupling limit $|B| \sim |B_\Delta| \to \infty$, all the masses of the mirror particles become large, while the GM-like scalars remain light at the EW scale. Of course, we need to properly adjust the sign of the B, B_Δ in order to avoid tachyons (negative squared mass states), as those indicates an unstable vacuum. In short, in the large-B limit,

$$B \to \infty, \quad B_\Delta \to -\infty, \tag{5.45}$$

the SCTM behaves exactly the same as the GM model, and we dub this decoupling limit of the SCTM as the **Supersymmetric Georgi-Machacek** (SGM) model [72], which gives a weakly coupled origin for the GM model at the EW scale.

5.3 The Supersymmetric Georgi-Machacek Model

Let us count the free parameters in the Higgs sector of the SGM model. In the superpotential of the SCTM, we have 2 cubic terms λ, λ_Δ and 2 quadratic terms μ, μ_Δ. Correspond-

ingly, we have the soft SUSY breaking terms A, A_Δ corresponding to λ, λ_Δ, and the bilinear terms B, B_Δ corresponding to μ, μ_Δ. Furthermore, we have 2 soft mass terms $m^2_{2,3}$ for the isospin doublets and triplets, respectively. As a consequence, we have 10 parameters in the Higgs sector of the SCTM model. We have taken the decoupling limit $B = -B_\Delta \to \infty$ to get the SGM model, which eliminates 2 parameters. If we assume a **gauge-mediated supersymmetry breaking** (GMSB) scenario [25], the trilinear soft SUSY breaking terms are generated at two loops. Therefore, the A-parameters are much smaller than masses of the scalars and the gauginos. We can safely set them to be zero in our phenomenological applications,

$$A \to 0, \quad A_\Delta \to 0. \tag{5.46}$$

As a result, the SGM Higgs sector contains 6 parameters. The electroweak measurements of the Higgs and W boson mass [23] will provide us with

$$2v_2^2 + 8v_3^2 = v^2 = (246\ \text{GeV})^2, \quad m_h = 125\ \text{GeV}. \tag{5.47}$$

Here this SM-like 125 GeV Higgs can be interpreted as one of the scalar singlets $S_{1,2}$. As a result, we have only 4 free parameters in total for the SGM model.

5.3.1 Map the SGM onto the GM model

Going back to the GM model, we can construct the bi-doublet and bi-triplet fields in terms of

$$\bar{\Delta}^\dagger = \bar{\Delta}, \quad H_2 = -i\tau_2 H_1^*. \tag{5.48}$$

Then, we can rewrite the Higgs potential as

$$\begin{aligned} V_{\text{GM}} \ =& \frac{1}{2}\mu_2^2\, \bar{H}^\dagger \bar{H} + \ \frac{1}{2}\mu_3^2\ \text{Tr}\big\{\bar{\Delta}\bar{\Delta}\big\} + \lambda_1 (\bar{H}^\dagger \bar{H})^2 \ + \ (\lambda_2 + \frac{1}{4}\lambda_5)(\bar{H}^\dagger \bar{H})\ \ \text{Tr}\big\{\bar{\Delta}\bar{\Delta}\big\} \\ & - 2\,\lambda_3\,\text{Tr}\big\{(\bar{\Delta}\bar{\Delta})^2\big\} + (\frac{3}{2}\ \lambda_3 + \lambda_4)\ \text{Tr}\big\{\bar{\Delta}\bar{\Delta}\big\}^2 - \lambda_5\, \bar{H}^\dagger \bar{\Delta}\bar{\Delta}\bar{H} \\ & + \ \frac{M_1}{2}\bar{H}^\dagger \bar{\Delta}\bar{H} + 2M_2\ \text{Tr}\big\{\bar{\Delta}\bar{\Delta}\bar{\Delta}\big\}. \end{aligned} \tag{5.49}$$

When comparing it to the SCTM scalar potential $V_{\text{SCTM}} = V_F + V_D + V_{\text{soft}}$, we obtain the mapping between two models,

$$\begin{aligned} & \lambda_1 = \frac{3}{4}\lambda^2, \ \ \lambda_2 \ = \lambda^2, \ \ \lambda_3 = -\frac{1}{2}\lambda_\Delta^2, \ \lambda_4 = \frac{1}{2}\lambda_\Delta^2, \ \lambda_5 = 2\lambda(\lambda_\Delta - 2\lambda), \\ & M_1 = 4\big[\lambda(2\mu - \mu_\Delta) - A_\lambda\big], \ M_2 = \frac{1}{3}(3\lambda_\Delta \mu_\Delta + A_\Delta), \\ & \mu_2^2 = 2(\mu^2 + m_H^2) + B, \ \mu_3^2 = 2(\mu_\Delta^2 + m_\Delta^2) + B_\Delta. \end{aligned} \tag{5.50}$$

We will use these mapping conditions to define the SGM model Higgs potential in terms of the GM potential in Equations (3.27) and (3.28).

In one sense, we can treat the SGM model as a doubled version of the GM model. We can construct the SCTM in terms of $(2,\bar{2})$ and $(3,\bar{3})$ representations of the global $SU(2)_L \otimes SU(2)_R$ symmetry as

$$\Phi = \begin{pmatrix} H_1^0 & H_2^+ \\ H_1^- & H_2^0 \end{pmatrix} \ , \ X = \begin{pmatrix} \chi^0 & \phi^+ & \psi^{++} \\ \chi^- & \phi^0 & \psi^+ \\ \chi^{--} & \phi^- & \psi^0 \end{pmatrix}, \tag{5.51}$$

which transform like $\Phi \to U_L \Phi U_R^\dagger$ and $X \to U_L X U_R^\dagger$. The superpotential can be constructed like

$$\begin{aligned} W = 2\lambda \ \mathrm{Tr}\Big[\Phi_c \frac{\tau_i}{2} \Phi \frac{\tau_j}{2}\Big][UXU^\dagger]_{ij} \quad &- \ \frac{\lambda_\Delta}{6} \mathrm{Tr}[X_c t_i X t_j][UX \ U^\dagger]_{ij} \\ - \ \frac{\mu}{2} \mathrm{Tr}[\Phi_c \Phi] \ &+ \frac{\mu_\Delta}{2} \mathrm{Tr}[X_c X], \end{aligned} \tag{5.52}$$

where $\tau_i/2$ and t_i are the dimension-2 and dimension-3 representations of the $SU(2)$ generators,

$$t_1 = \frac{1}{\sqrt{2}} \begin{pmatrix} 0 & 1 & 0 \\ 1 & 0 & 1 \\ 0 & 1 & 0 \end{pmatrix} , \ t_2 = \frac{1}{\sqrt{2}} \begin{pmatrix} 0 & -i & 0 \\ i & 0 & -i \\ 0 & i & 0 \end{pmatrix} , \ t_3 = \begin{pmatrix} 1 & 0 & 0 \\ 0 & 0 & 0 \\ 0 & 0 & -1 \end{pmatrix} . \tag{5.53}$$

The matrix U is defined to rotate the matrix field X into the Cartesian basis,

$$U = \begin{pmatrix} -1/\sqrt{2} & i/\sqrt{2} & 0 \\ 0 & 0 & 1 \\ 1/\sqrt{2} & i/\sqrt{2} & 0 \end{pmatrix} . \tag{5.54}$$

The complex conjugate fields are defined as

$$\Phi_c = \tau_2 \Phi^T \tau_2, \quad X_c = C X^T C, \quad C = \begin{pmatrix} 0 & 0 & 1 \\ 0 & -1 & 0 \\ 1 & 0 & 0 \end{pmatrix} . \tag{5.55}$$

With these definitions, the fields X_c and Φ_c are transformed in the same way as fields $X^\dagger$ and $\Phi^\dagger$ under the global group $SU(2)_L \otimes SU(2)_R$. In terms of the fields (Φ, Φ_c, X, X_c), we

can write the F-term potential of the SCTM as

$$
\begin{aligned}
V_{\rm F} = {} & \mu^2\,{\rm Tr}\{\Phi^\dagger\Phi\} \;+\; \mu_\Delta^2\;{\rm Tr}\{X^\dagger X\} \;+\lambda^2\Big({\rm Tr}\{\Phi^\dagger\Phi\}^2 - \frac{1}{4}\,{\rm Tr}\{\Phi_c\Phi\}\;{\rm Tr}\{\Phi_c^\dagger\Phi^\dagger\} \\
& +\; {\rm Tr}\{X^\dagger t_i X t_j\}\;{\rm Tr}\{\Phi^\dagger\tau_i\Phi\tau_j\} + \;{\rm Tr}\{X^\dagger X\}\;{\rm Tr}\{\Phi^\dagger\Phi\} \;-\; {\rm Tr}\{X^\dagger t_i X\}\;{\rm Tr}\{\Phi^\dagger\tau_i\Phi\} \\
& - {\rm Tr}\{X_c^\dagger t_i X_c\}\;{\rm Tr}\{\Phi_c^\dagger\tau_i\Phi_c\}\;\Big) + \frac{\lambda\mu_\Delta}{2}\left({\rm Tr}\{\Phi_c\tau_i\Phi\tau_j\}\left[UX^\dagger U^\dagger\right]_{i,j} + {\rm h.c.}\right) \\
& -\;\frac{\lambda_3^2}{2}\;\Big({\rm Tr}\{X^\dagger X X^\dagger X\} - {\rm Tr}\{X^\dagger X\}^2\Big) \;-\; \frac{\lambda_3\lambda}{4}\;\left({\rm Tr}\{X^\dagger t_i X_c^\dagger t_j\}\;{\rm Tr}\{\Phi\tau_j\Phi_c\tau_i\} + {\rm h.c.}\right) \\
& -\;\frac{\lambda_3\mu_\Delta}{2}\left({\rm Tr}\{X^\dagger t_i X t_j\}\;\left[UXU^\dagger\right]_{i,j} + {\rm h.c.}\;\right) \;-\; \lambda\;\mu\;\left({\rm Tr}\{\Phi^\dagger\tau_i\Phi\tau_j\}\;\left[UXU^\dagger\right]_{i,j} + {\rm h.c.}\;\right),
\end{aligned}
\tag{5.56}
$$

The soft SUSY breaking terms can be constructed in a similar fashion,

$$
\begin{aligned}
V_{\rm soft} = {} & \;\; m_H^2\;{\rm Tr}\{\Phi^\dagger\Phi\} \;+ m_\Delta^2\;{\rm Tr}\{X^\dagger X\} \;\; + \;\left(\frac{B_\Delta}{2}\;{\rm Tr}\{X_c X\} - \frac{B}{2}\;{\rm Tr}\{\Phi_c\Phi\}\right. \\
& \left. +\;\frac{A_\lambda}{2}\;{\rm Tr}\{\Phi_c\;\tau_i\Phi\tau_j\}(UXU^\dagger)_{ij} - \frac{A_\Delta}{6}\;\;{\rm Tr}\{X_c t_i X t_j\}(UXU^\dagger)_{ij} \;+ {\rm h.c.}\right),
\end{aligned}
\tag{5.57}
$$

In light of the self-conjugation condition of the matrix fields,

$$
X_c = X^\dagger, \quad \Phi_c = \Phi^\dagger,
\tag{5.58}
$$

which indicates $V_D = 0$, the SCTM scalar potential $V_{\rm SCTM} = V_F + V_D + V_{\rm soft}$ can be totally reduced to the form of the GM one,

$$
\begin{aligned}
V_{\rm GM} = {} & \;\frac{\mu_2^2}{2}\,{\rm Tr}\{\Phi^\dagger\Phi\} \;+\frac{\mu_3^2}{2}\,{\rm Tr}\{X^\dagger X\} + \lambda_1\,{\rm Tr}\{\Phi^\dagger\Phi\;\}^2 \;+\lambda_2\,{\rm Tr}\{\Phi^\dagger\Phi\}\;{\rm Tr}\{X^\dagger X\} \\
& +\lambda_3\,{\rm Tr}\{X^\dagger X X^\dagger X\} \;+\; \lambda_4\;\;{\rm Tr}\{X^\dagger X\}^2 \;-\lambda_5\,{\rm Tr}\{\Phi^\dagger\tau^a\;\Phi\;\tau^b\}\;\;{\rm Tr}\{X^\dagger t^a X t^b\;\} \\
& -M_1\,{\rm Tr}\{\Phi^\dagger\tau^a\Phi\;\tau^b\}(UXU^\dagger)_{ab} \;-\;\; M_2\,{\rm Tr}\{X^\dagger t^a\;Xt^b\}(UXU^\dagger)_{ab},
\end{aligned}
\tag{5.59}
$$

by applying the mapping conditions of Equation (5.50). We can see the cubic terms $\lambda_{(3)}\mu_{(\Delta)}$ in Equation (5.56) and $A_{\lambda(\Delta)}$ in Equation (5.57) are mapped onto the cubic terms in Equation (3.28), which violate the discrete Z_2 symmetry.

If we take the SGM model to define a weakly coupled origin for the GM model at the electroweak scale, the mapping condition (5.50) implies the following constraints among the five quartic couplings in the Higgs potential of the GM model:

$$
\lambda_1 = \frac{3}{4}\lambda_2,\; \lambda_3 = -\lambda_4,\; \lambda_5 = -4\lambda_2 + 2\sqrt{2\lambda_2\lambda_4}.
\tag{5.60}
$$

Therefore, the 5 quartic couplings of the GM model can be written in terms of λ_2 and λ_4, henceforth defining a constrained GM model. Here we have made an implicit assumption that the dimensionless parameters λ and λ_Δ in the superpotential are real. If these 2 parameters

are complex, we would get the mapping conditions as

$$\lambda_1 = \frac{3}{4}|\lambda|^2, \;\; \lambda_2 \; = |\lambda|^2, \;\; \lambda_3 = -\frac{1}{2}|\lambda_\Delta|^2, \; \lambda_4 = \frac{1}{2}|\lambda_\Delta|^2, \; \lambda_5 = 2\lambda(\lambda_\Delta - 2\lambda). \tag{5.61}$$

Therefore, the holomorphic principle for the superpotential implies a bound $0 < \lambda_{2,4} \in \mathcal{R}$ on the couplings in a constrained GM model.

Once again, we will count the parameters, this time in the constrained GM model. We have 5 quartic coupling parameters $\lambda_{1\cdots5}$ which can be written in terms of two of them, $\lambda_{2,4}$. The mass terms μ_2^2, μ_3^2 are responsible for the isospin doublet and triplet respectively. In addition, we have 2 cubic terms $M_{1,2}$ which is necessary when mapping the SGM model onto the GM model. Therefore, we have 6 parameters in total for this constrained GM model, which can be one-to-one mapped to that of the SGM model,

$$(\lambda_2, \lambda_4, M_1, M_2, m_2^2, m_3^2) \leftrightarrow (\lambda, \lambda_\Delta, \mu, \mu_\Delta, m_2^2, m_3^2). \tag{5.62}$$

The mass terms m_2^2, m_3^2 can be replaced by the VEVs (v_2, v_3), and those can be fixed from the experimental measurements of the W and Higgs boson masses,

$$v = 246 \text{ GeV}, \;\; m_{h,H} = 125 \text{ GeV}. \tag{5.63}$$

Altogether, we have 4 parameters in both the GM and SGM models.

5.3.2 The fermionic superpartners

Now, we want to compare the GM vs SGM models in the above 4-dimensional parameter space. By the way of Equation (5.50), the spectrum and the couplings are exactly the same in both models, which makes the phenomenology at the LHC quite the same, too. However, the SGM model contains higgsinos and gauginos as the fermionic superpartners of the GM-like particles. We will see that the masses of these superpartners are also at the EW scale, which provides us the possibility to distinguish the SGM model from the GM model.

We list all the superpartners of the Higgs and gauge bosons in Table 5.2. We can write down the mass matrix for these higgsinos and gauginos, together called *electroweakinos* as well. Let us first look at the doubly charginos $f^{--} = \tilde{\chi}^{--}$ and $f^{++} = \psi^{++}$. Their mass is as simple as [2]

$$-\mathcal{L} = (f^{--})^T m f^{++} + \text{h.c.}, \;\; m = \mu_\Delta + \frac{\Lambda_3 v_3}{\sqrt{2}}. \tag{5.64}$$

[2] In this section, we replace symbols λ, λ_Δ as Λ, Λ_3 in order to distinguish from the quartic couplings $\lambda_{1\cdots5}$ in the GM model.

boson		fermion	
Higgs	$H_1 = \begin{pmatrix} h_1^0 \\ h_1^- \end{pmatrix}$ $H_2 = \begin{pmatrix} h_2^+ \\ h_2^0 \end{pmatrix}$ $\Sigma_- = \begin{pmatrix} \frac{\chi^-}{\sqrt{2}} & -\chi^0 \\ \chi^{--} & -\frac{\chi^-}{\sqrt{2}} \end{pmatrix}$ $\Sigma_0 = \begin{pmatrix} \frac{\phi^0}{\sqrt{2}} & -\phi^+ \\ \phi^- & -\frac{\phi^0}{\sqrt{2}} \end{pmatrix}$ $\Sigma_+ = \begin{pmatrix} \frac{\psi^+}{\sqrt{2}} & -\psi^{++} \\ \psi^0 & -\frac{\psi^+}{\sqrt{2}} \end{pmatrix}$	higgsino	$\tilde{H}_1 = \begin{pmatrix} \tilde{h}_1^0 \\ \tilde{h}_1^- \end{pmatrix}$ $\tilde{H}_2 = \begin{pmatrix} \tilde{h}_2^+ \\ \tilde{h}_2^0 \end{pmatrix}$ $\tilde{\Sigma}_- = \begin{pmatrix} \frac{\tilde{\chi}^-}{\sqrt{2}} & -\tilde{\chi}^0 \\ \tilde{\chi}^{--} & -\frac{\tilde{\chi}^-}{\sqrt{2}} \end{pmatrix}$ $\tilde{\Sigma}_0 = \begin{pmatrix} \frac{\tilde{\phi}^0}{\sqrt{2}} & -\tilde{\phi}^+ \\ \tilde{\phi}^- & -\frac{\tilde{\phi}^0}{\sqrt{2}} \end{pmatrix}$ $\tilde{\Sigma}_+ = \begin{pmatrix} \frac{\tilde{\psi}^+}{\sqrt{2}} & -\tilde{\psi}^{++} \\ \tilde{\psi}^0 & -\frac{\tilde{\psi}^+}{\sqrt{2}} \end{pmatrix}$
B boson W boson	B W^i	bino wino	$\tilde{B}$ $\tilde{W}^i$

Table 5.2: Particles and the corresponding super-partners in the SGM Higgs sector.

We can see that, for this doubly chargino, the gauge eigenstate is the same as the mass eigenstate, also the same as the custodial state that is shown in Table 5.3.

For the single-charged electroweakinos, we write down the mass term in the gauge basis

$$f^+ = (\tilde{W}^+, \tilde{h}_u^+, \tilde{\phi}^+, \tilde{\psi}^+),\ f^- = (\tilde{W}^-, \tilde{h}_d^-, \tilde{\phi}^-, \tilde{\chi}^-). \tag{5.65}$$

The mass term is

$$-\mathcal{L} = (f^-)^T M f^+ + \text{h.c.},\ M = \begin{pmatrix} M_2 & \frac{g_2 v_2}{\sqrt{2}} & -g_2 v_3 & g_2 v_3 \\ \frac{g_2 v_2}{\sqrt{2}} & -\frac{\Lambda v_3}{\sqrt{2}} - \mu & -\Lambda v_2 & \Lambda v_2 \\ -g_2 v_3 & -\Lambda v_2 & \frac{\Lambda_3 v_3}{\sqrt{2}} & \mu_\Delta \\ g_2 v_3 & \Lambda v_2 & \mu_\Delta & \frac{\Lambda_3 v_3}{\sqrt{2}} \end{pmatrix}. \tag{5.66}$$

Similarly to the scalar particles, we can construct the custodial multiplets of the electroweakinos as in Table 5.3. Then, we can rotate the single-charged electroweakino mass to the custodial basis

$$f^+ = (\tilde{W}^+, \tilde{h}_3^+, \tilde{\delta}_3^+, \tilde{\delta}_5^+),\ f^- = (\tilde{W}^-, \tilde{h}_3^-, \tilde{\delta}_3^-, \tilde{\delta}_5^-), \tag{5.67}$$

boson		fermion	
singlet	$h_1^0 = (h_d^0 + h_u^0)/\sqrt{2}$		$\tilde{h}_1^0 = (\tilde{h}_d^0 + \tilde{h}_u^0)/\sqrt{2}$
triplet	$h_3^+ = h_u^+$ $h_3^0 = (h_u^0 - h_d^0)/\sqrt{2}$ $h_3^- = h_d^-$		$\tilde{h}_3^+ = \tilde{h}_u^+$ $\tilde{h}_3^0 = (\tilde{h}_u^0 - \tilde{h}_d^0)/\sqrt{2}$ $\tilde{h}_3^- = \tilde{h}_d^-$
singlet	$\delta_1^0 = (\phi^0 + \chi^0 + \psi^0)/\sqrt{3}$		$\tilde{\delta}_1^0 = (\tilde{\phi}^0 + \tilde{\chi}^0 + \tilde{\psi}^0)/\sqrt{3}$
triplet	$\delta_3^+ = (\psi^+ - \phi^+)/\sqrt{2}$ $\delta_3^0 = (\chi^0 - \psi^0)/\sqrt{2}$ $\delta_3^- = (\phi^- - \chi^-)/\sqrt{2}$		$\tilde{\delta}_3^+ = (\tilde{\psi}^+ - \tilde{\phi}^+)/\sqrt{2}$ $\tilde{\delta}_3^0 = (\tilde{\chi}^0 - \tilde{\psi}^0)/\sqrt{2}$ $\tilde{\delta}_3^- = (\tilde{\phi}^- - \tilde{\chi}^-)/\sqrt{2}$
quintuplet	$\delta_5^{++} = \psi^{++}$ $\delta_5^+ = (\phi^+ + \psi^+)/\sqrt{2}$ $\delta_5^0 = (-2\phi^0 + \psi^0 + \chi^0)/\sqrt{6}$ $\delta_5^- = (\phi^- + \chi^-)/\sqrt{2}$ $\delta_5^{--} = \chi^{--}$		$\tilde{\delta}_5^{++} = \tilde{\psi}^{++}$ $\tilde{\delta}_5^+ = (\tilde{\phi}^+ + \tilde{\psi}^+)/\sqrt{2}$ $\tilde{\delta}_5^0 = (-2\tilde{\phi}^0 + \tilde{\psi}^0 + \tilde{\chi}^0)/\sqrt{6}$ $\tilde{\delta}_5^- = (\tilde{\phi}^- + \tilde{\chi}^-)/\sqrt{2}$ $\tilde{\delta}_5^{++} = \tilde{\chi}^{--}$
W boson	$W^\pm = (W^1 \mp iW^2)/\sqrt{2}$	wino	$\tilde{W}^\pm = (\tilde{W}^1 \mp i\tilde{W}^2)/\sqrt{2}$
Z boson	$Z = c_W W^3 - s_W B$	zino	$Z = c_W \tilde{W}^3 - s_W \tilde{B}$
photon γ	$\gamma = s_W W^3 + c_W B$	photino	$\tilde{\gamma} = s_W \tilde{W}^3 + c_W \tilde{B}$

Table 5.3: The SGM particles in custodial basis

and get the block-diagonal form,

$$\begin{pmatrix} M_2 & \frac{g_2 v_2}{\sqrt{2}} & -\sqrt{2} g_2 v_3 & 0 \\ \frac{g_2 v_2}{\sqrt{2}} & -\mu - \frac{\Lambda v_3}{\sqrt{2}} & -\sqrt{2}\Lambda v_2 & 0 \\ -\sqrt{2} g_2 v_3 & -\sqrt{2}\Lambda v_2 & -\mu_3 + \frac{\Lambda_3 v_3}{\sqrt{2}} & 0 \\ 0 & 0 & 0 & \mu_3 + \frac{\Lambda_3 v_3}{\sqrt{2}} \end{pmatrix}. \tag{5.68}$$

We separate the singly-charged quintuplet $\tilde{\delta}_5^\pm$ automatically in this basis. Similarly to the MSSM case, the charged triplet gaugino $\tilde{W}^\pm$ mixes with the charged triplet higgsinos $(\tilde{h}_3^\pm, \tilde{\delta}^\pm)$.

Finally, we go to the neutralino case. We first write down the mass term in the gauge basis

$$-\frac{1}{2}(f^0)^T M f^0, \;\; f^0 = (\tilde{B}, \tilde{W}_3, \tilde{H}_d^0, \tilde{H}_u^0, \tilde{\chi}^0, \tilde{\phi}^0, \tilde{\psi}^0), \tag{5.69}$$

where the mass matrix is

$$\begin{pmatrix} M_1 & 0 & -\frac{g_1 v_2}{2} & \frac{g_1 v_2}{2} & -g_1 v_3 & 0 & g_1 v_3 \\ 0 & M_2 & \frac{g v_2}{2} & -\frac{g_2 v_2}{2} & g_2 v_3 & 0 & -g_2 v_3 \\ -\frac{g_1 v_2}{2} & \frac{g_2 v_2}{2} & -\sqrt{2}\Lambda v_3 & -\frac{\Lambda v_3}{\sqrt{2}} + \mu & 0 & -\frac{\Lambda v_2}{\sqrt{2}} & -\sqrt{2}\Lambda v_2 \\ \frac{g_1 v_2}{2} & -\frac{g_2 v_2}{2} & -\frac{\Lambda v_3}{\sqrt{2}} + \mu & -\sqrt{2}\Lambda v_3 & -\sqrt{2}\Lambda v_2 & -\frac{\Lambda v_2}{\sqrt{2}} & 0 \\ -g_1 v_3 & g_2 v_3 & 0 & -\sqrt{2}\Lambda v_2 & 0 & -\frac{\Lambda_3 v_3}{\sqrt{2}} & -\frac{\Lambda_3 v_3}{\sqrt{2}} + \mu_\Delta \\ 0 & 0 & -\frac{\Lambda v_2}{\sqrt{2}} & -\frac{\Lambda v_2}{\sqrt{2}} & -\frac{\Lambda_3 v_3}{\sqrt{2}} & \mu_\Delta & -\frac{\Lambda_3 v_3}{\sqrt{2}} \\ g_1 v_3 & -g_2 v_3 & -\sqrt{2}\Lambda v_2 & 0 & -\frac{\Lambda_3 v_3}{\sqrt{2}} + \mu_\Delta & -\frac{\Lambda_3 v_3}{\sqrt{2}} & 0 \end{pmatrix}. \tag{5.70}$$

Rotating it to the custodial basis,

$$f^0 = (\tilde{h}_1^0, \tilde{\delta}_1^0, \tilde{\gamma}, \tilde{Z}, \tilde{h}_3^0, \tilde{\delta}_3^0, \tilde{\delta}_5^0), \tag{5.71}$$

we arrive at a block-diagonal mass matrix

$$\begin{pmatrix} \mu - \frac{3\Lambda v_3}{\sqrt{2}} & -\sqrt{3}\Lambda v_2 & 0 & 0 & 0 & 0 & 0 \\ -\sqrt{3}\Lambda v_2 & \mu_3 - \sqrt{2}\Lambda_3 v_3 & 0 & 0 & 0 & 0 & 0 \\ 0 & 0 & M_1 c_W^2 + M_2 s_W^2 & (M_2 - M_1) c_W s_W & 0 & 0 & 0 \\ 0 & 0 & (M_2 - M_1) c_W s_W & M_1 s_W^2 + M_2 c_W^2 & \frac{G v_2}{\sqrt{2}} & \sqrt{2} G v_3 & 0 \\ 0 & 0 & 0 & \frac{G v_2}{\sqrt{2}} & -\mu - \frac{\Lambda v_3}{\sqrt{2}} & \sqrt{2}\Lambda v_2 & 0 \\ 0 & 0 & 0 & \sqrt{2} G v_3 & \sqrt{2}\Lambda v_2 & -\mu_3 + \frac{\Lambda_3 v_3}{\sqrt{2}} & 0 \\ 0 & 0 & 0 & 0 & 0 & 0 & \mu_3 + \frac{\Lambda_3 v_3}{\sqrt{2}} \end{pmatrix}. \tag{5.72}$$

Here $G = \sqrt{g_1^2 + g_2^2}$ for the neutralinos, while $G = g_2$ for the charginos. We make an already familiar observation that the hypercharge interaction breaks the custodial symmetry. Also, the triplet higgsinos $(\tilde{h}_3^0, \tilde{\delta}_3^0)$ mix with zino $\tilde{Z}$, and zino $\tilde{Z}$ also mixes with photino $\tilde{\gamma}$, which also has been seen in the MSSM already. A new phenomenon emerges that the singlet higgsinos mix with each other, which does not happen in the MSSM, since it has one singlet higgsino (neutral). Diagonalizing the block matrix for the singlet higgsinos, we get the eigenvalues as

$$\mathcal{M}_{f_1^0} = \begin{pmatrix} \mu - \frac{3\Lambda v_3}{\sqrt{2}} & -\sqrt{3}\Lambda v_2 \\ -\sqrt{3}\Lambda v_2 & \mu_3 - \sqrt{2}\Lambda_3 v_3 \end{pmatrix} \implies$$

$$m_{f_1^0} = \frac{1}{4}\left[2(\mu + \mu_3) - \sqrt{2} v_3 (3\Lambda + 2\Lambda_3) \pm \sqrt{48\Lambda^2 v_2^2 + (2(\mu - \mu_3) - \sqrt{2} v_3 (3\Lambda - 2\Lambda_3))^2}\right]. \tag{5.73}$$

If we take the limit of a small hypercharge interaction,

$$g_1 = 0,\ s_W = 0,\ c_W = 1,\ G = g_2, \tag{5.74}$$

the mass matrix for neutralinos becomes

$$\begin{pmatrix} \mu - \frac{3\Lambda v_3}{\sqrt{2}} & -\sqrt{3}\Lambda v_2 & 0 & 0 & 0 & 0 & 0 \\ -\sqrt{3}\Lambda v_2 & \mu_3 - \sqrt{2}\Lambda_3 v_3 & 0 & 0 & 0 & 0 & 0 \\ 0 & 0 & M_1 & 0 & 0 & 0 & 0 \\ 0 & 0 & 0 & M_2 & \frac{g_2 v_2}{\sqrt{2}} & \sqrt{2} g_2 v_3 & 0 \\ 0 & 0 & 0 & \frac{g_2 v_2}{\sqrt{2}} & -\mu - \frac{\Lambda v_3}{\sqrt{2}} & \sqrt{2}\Lambda v_2 & 0 \\ 0 & 0 & 0 & \sqrt{2} g_2 v_3 & \sqrt{2}\Lambda v_2 & -\mu_3 + \frac{\Lambda_3 v_3}{\sqrt{2}} & 0 \\ 0 & 0 & 0 & 0 & 0 & 0 & \mu_3 + \frac{\Lambda_3 v_3}{\sqrt{2}} \end{pmatrix}. \quad (5.75)$$

We obtain a block matrix for the singly-charged electroweakinos, which means that the custodial symmetry gets recovered.

We can further assume the Majorana mass for the gaugino to be large, $M_2 \to \infty$, to decouple the winos $\tilde{W}^{\pm}, \tilde{Z}$ from the triplet higgsino:

$$\mathcal{M}_{f_3^0} = \begin{pmatrix} -\mu - \frac{\Lambda v_3}{\sqrt{2}} & \sqrt{2}\Lambda v_2 \\ \sqrt{2}\Lambda v_2 & -\mu_3 + \frac{\Lambda_3 v_3}{\sqrt{2}} \end{pmatrix} \Longrightarrow$$
$$m_{f_3^0} = \frac{1}{4}\Big[-2(\mu + \mu_3) + \sqrt{2} v_3(-\Lambda + \Lambda_3) \pm \sqrt{32\Lambda^2 v_2^2 + (2(\mu - \mu_3) - \sqrt{2} v_3(\Lambda + \Lambda_3))^2} \Big]. \quad (5.76)$$

Let's take the small triplet VEV limit $v_3 \to 0$, then the mass eigenvalues simplify as

$$\begin{aligned} m_{f_1^0} &= \frac{1}{2}(\mu + \mu_3 \pm \sqrt{12\Lambda^2 v_2^2 + (\mu - \mu_3)^2}), \\ m_{f_3^0} &= \frac{1}{2}(-\mu - \mu_3 \pm \sqrt{8\Lambda^2 v_2^2 + (\mu - \mu_3)^2}), \\ m_{f_5^0} &= \mu_3. \end{aligned} \quad (5.77)$$

By taking $\mu = \mu_3$, we will get

$$m_{f_1^0} = \mu \pm \sqrt{3}|\Lambda| v_2, \quad m_{f_3^0} = -\mu \pm \sqrt{2}|\Lambda| v_2, \quad m_{f_5^0} = \mu. \quad (5.78)$$

We can also take $\mu = -\mu_3$ to get

$$m_{f_1^0} = \pm\sqrt{3\Lambda^2 v_2^2 + \mu^2}, \quad m_{f_3^0} = \pm\sqrt{2\Lambda^2 v_2^2 + \mu^2}, \quad m_{f_5^0} = -\mu. \quad (5.79)$$

Now let us examine how the higgsino mass behaves. First, the unitary bound (3.52) of the GM model, associated with the map conditions (5.50), gives us the allowed parameter space:

$$\begin{aligned} &-\frac{1}{3}\pi < \lambda_1 = \frac{3}{16}\Lambda^2 < \frac{\pi}{3}, \ -\frac{2}{3}\pi < \lambda_2 = \frac{1}{4}\Lambda^2 < \frac{2}{3}\pi, \ -\frac{1}{2}\pi < \lambda_3 = -\frac{1}{8}\Lambda_3^2 < \frac{3}{5}\pi, \\ &-\frac{1}{5}\pi < \lambda_4 = \frac{1}{8}\Lambda_3^2 < \frac{1}{2}\pi, \quad -\frac{8}{3}\pi < \lambda_5 = -\Lambda(\Lambda + \frac{1}{2}\Lambda_3) < \frac{8}{3}\pi, \end{aligned} \quad (5.80)$$

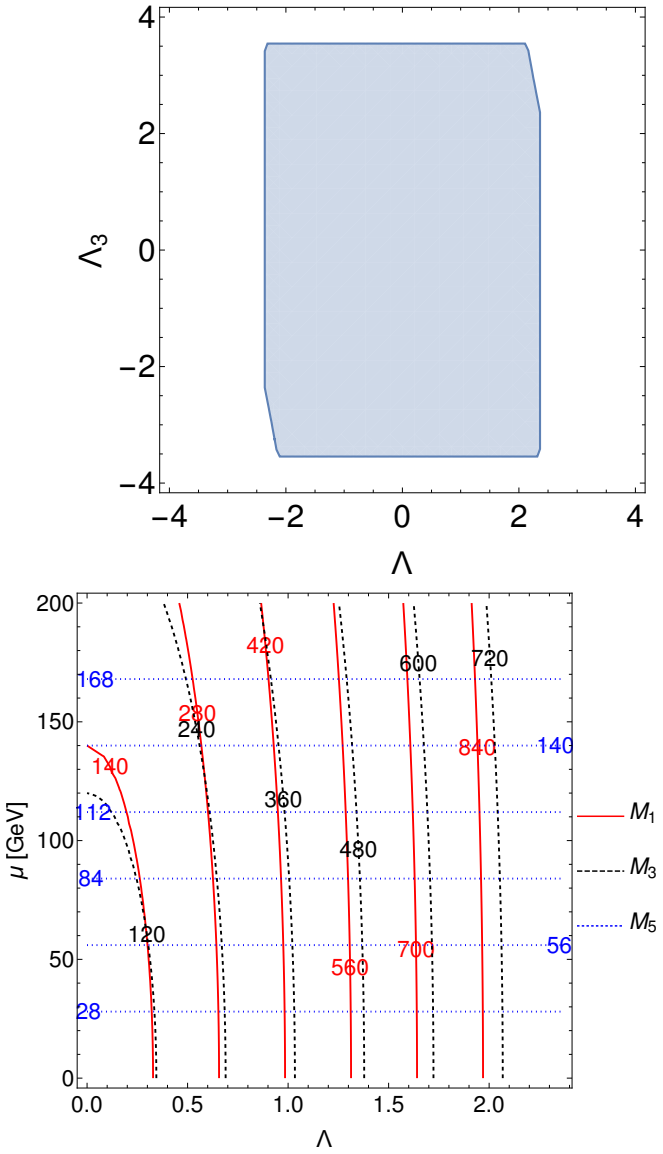

Figure 5.1: Left: The parameter space (Λ, Λ_3) allowed by pertubativity. The curved boundary results from the constraint $-\frac{8}{3}\pi < \lambda_5 = -\Lambda(\Lambda + \frac{1}{2}\Lambda_3) < \frac{8}{3}\pi$. Right: The higgsino masses $M_{1,3,5}$ [GeV] for singlet, triplet, and quintuplet in the 2-dimensional parameter space (Λ, μ), when taking $\mu = -\mu_3,\ v_3 = 0$.

With these conditions, we roughly have $|\Lambda| < 4\sqrt{\pi}/3 \approx 2.36327$ and $|\Lambda_3| < 2\sqrt{\pi} \approx 3.54491$, which is shown in Figure 5.1. For this allowed Λ space, the higgsino masses $m_{f_{1,3,5}}$ for the singlet, triplet, and quintuplet are shown in the right plot of Figure 5.1, with

$$\Lambda \in [0, \frac{4}{3}\sqrt{\pi}],\ \mu = -\mu_3 \in [0, 200]\ \text{GeV}, v_3 = 0. \tag{5.81}$$

We can see that the quintuplet higgsino mass follows the μ parameter, while the singlet and triplet higgsino mass roughly follows the Λ parameter. When $\Lambda v_2 \gg \mu$, we roughly have $m_{f_1,f_3} \propto \Lambda$, given that $v_2 \approx 246$ GeV is fixed by the W mass.

Chapter 6

Phenomenological applications

In the previous chapter, we have constructed the SCTM and obtained a decoupling limit called the SGM model, which in turn gives rise to the GM model at the EW scale. In this chapter, we will perform some phenomenological studies in these models.

6.1 Higgsino production at colliders

The first interesting question to explore is how we produce the new particles predicted by these models. In this regard, we wish to single out the doubly-charged electroweakino f^{++}. Since it possesses two units of electric charges, its production rate through electromagnetic interaction is enhanced by a factor of 2^4 compared to the singly-charged particles. Let us calculate its production rate at the LEP with collision energy $\sqrt{s} = 209$ GeV. For the electromagnetic interaction of $f^{\pm\pm}$, we have the coupling to photon as

$$g_{f^{++}f^{--}A^\mu} = i(g_1 c_W + g_2 s_W)\gamma_\mu = iG \sin 2\theta_W = 2ie\gamma_\mu, \tag{6.1}$$

where $g_2 = e/s_W$ and $g_1 = e/c_W$. Similarly for the Z-boson interaction, we have

$$g_{f^{++}f^{--}Z^\mu} = i(-g_1 s_W + g_2 c_W)\gamma_\mu = iG \cos 2\theta_W = 2i\frac{e}{\tan 2\theta_W}\gamma_\mu. \tag{6.2}$$

For the photon-mediated process $e^+e^- \to \gamma^* \to f^{++}f^{--}$ with the Feynman diagram depicted in Figure 6.1, the squared scattering amplitude is

$$|\mathcal{M}|^2 = \frac{1}{16}(g_1 c_W + g_2 s_W)^2(5g_1^2 c_W^2 + 2g_1 g_2 s_W c_W + g_2^2 s_W^2)\frac{2M^4 + T^2 + 2M^2(S - T - U) + U^2}{S^2}, \tag{6.3}$$

where M is the mass of $f^{\pm\pm}$ and S, T, U are the Mandelstam variables,

$$S = (p_1 + p_2)^2 = (p_3 + p_4)^2,\ T = (p_1 - p_3)^2 = (p_2 - p_4)^2,\ U = (p_1 - p_4)^2 = (p_3 - p_2)^2. \tag{6.4}$$

When we substitute the couplings $e = g_2 s_W = g_1 c_W$, we get

$$|\mathcal{M}|^2 = 2e^4\frac{2M^4 + 2M^2(S - T - U) + T^2 + U^2}{S^2}. \tag{6.5}$$

Parameterizing the S, T, U in the center-of-mass frame of e^+e^- pairs,

$$S = Q^2,\ T = -Q^2(1 + \beta^2 - 2\beta\cos\theta)/4,\ U = -Q^2(1 + \beta^2 + 2\beta\cos\theta)/4, \tag{6.6}$$

where Q is the collision energy, θ is the scattering angle, and the Lorentz factor $\beta = \sqrt{1-4M^2/Q^2}$, we have

$$|\mathcal{M}|^2 = e^4(2-\beta^2\sin^2\theta). \tag{6.7}$$

The cross section measured in the phase space $\mathrm{d}\Phi_2 = \frac{\beta}{32\pi^2}\mathrm{d}\Omega$ is

$$\mathrm{d}\sigma = \frac{1}{2S}\mathrm{d}\Phi_2\frac{1}{4}\sum_{\text{spin}}|\mathcal{M}|^2 = 4\mathrm{d}\Omega\frac{\alpha^2}{4S}\beta(2-\beta\sin^2\theta). \tag{6.8}$$

Here the prefactor $\frac{1}{4}$ arises from averaging over the spin of the initial states, while the sum runs over the spins of all final states. Integrating out the azimuthal angle, we get the total cross section as

$$\sigma = \frac{e^4\beta(3-\beta^2)}{6\pi Q^2} = e^4\sqrt{1-\frac{4M^2}{Q^2}}\frac{2M^2+Q^2}{3\pi Q^2}. \tag{6.9}$$

The cross section in the (Q, M) space is shown in Fig. 6.1. In the limit $Q \gg M$, we have

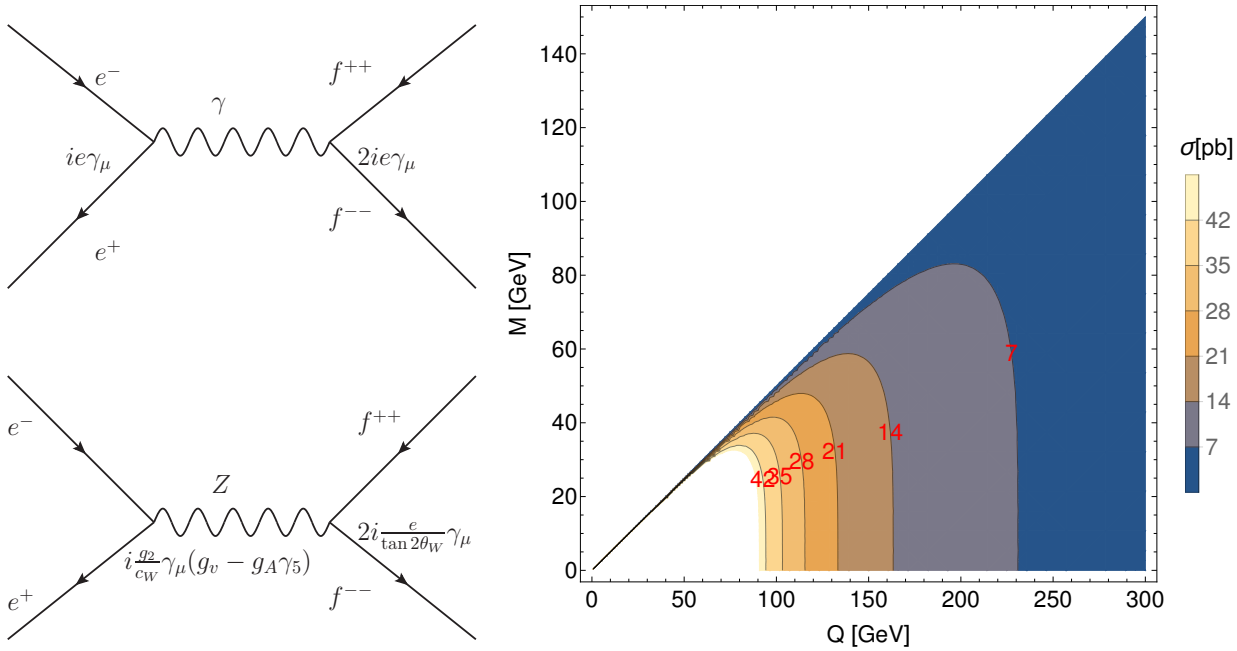

Figure 6.1: Left: The Feynman Diagrams for $e^+e^- \to \gamma^*/Z \to f^{++}f^{--}$, Right: The cross section $\sigma(e^+e^- \to \gamma^* \to f^{++}f^{--})$ [pb] in the parameter space (Q, M).

$\beta \approx 1$, and $\sigma \sim 1 + 2M^2/Q^2$, that is why we observe the behavior that the cross section decreases with the increase of collision energy in Figure 6.1.

In order to obtain large amounts of numerical calculations, we need to invoke widely used codes including `SPheno` [73, 74] and `MadGraph` [75]. In the following, we perform benchmark

calculations to make sure these codes work correctly. We take a numerical point,

$$\alpha = e^2/4\pi = 1/132.2, \quad M = 11.9 \text{ GeV}, \quad Q = \sqrt{S} = 209 \text{ GeV}, \tag{6.10}$$

as a trial. The analytical cross section (6.9) for this trial point turns out to be

$$\sigma(e^+e^- \to \gamma^* \to f^{++}f^{--}) = 8.57\,\text{pb}. \tag{6.11}$$

`MadGraph` gives us the numerical values

$$\sigma(e^+e^- \to \gamma^* \to f^{++}f^{--}) = 8.54 \text{ pb}. \tag{6.12}$$

which agrees with our analytical calculation satisfactorily. Furthermore, we can easily get the cross section

$$\sigma(e^+e^- \to \gamma^* \to f^+f^-) = 2.13 \text{ pb}, \tag{6.13}$$

from `Madgraph`, which verifies the ratio

$$\sigma(f^{++}f^{--})/\sigma(f^+f^-) = (Q_{f^{++}}/Q_{f^+})^2 = 4. \tag{6.14}$$

These cross sections does not depend on the mixing angle (rotation matrix) because the vertices $\gamma f_5 f_5$ are fully determined by the electric charges. If we include the γ^*/Z mixing, the numerical cross sections from `MadGraph` become

$$\sigma(e^+e^- \to \gamma^*/Z \to f^{++}f^{--}) = 11.6 \text{ pb}, \ \sigma(e^+e^- \to \gamma^*/Z \to f^+f^-) = 2.90 \text{ pb}. \tag{6.15}$$

Additionally, we can verify $\sigma(e^+e^- \to f^0 f^0) = 0$ in `Madgraph` to test $V_{f_5^0 f_5^0 \gamma^*(Z)} = 0$.

Next, let us explore the fermionic quintuplet couplings to charged vector boson,

$$V_{f_5^0 f_5^- W^+} = -i\frac{\sqrt{3}}{2} g_2 \gamma^\mu, \quad V_{f_5^+ f_5^{--} W^+} = i\frac{\sqrt{2}}{2} g_2 \gamma^\mu. \tag{6.16}$$

The Scalar-Scalar-Vector (SSV) coupling in the convention $V^\mu_{SSV} = i g_{SSV}(p_1 - p_2)^\mu$ is

$$g_{H_5^0 H_5^- W^+} = -i\frac{\sqrt{3}}{2} g_2, \quad g_{H_5^+ H_5^{--} W^+} = i\frac{\sqrt{2}}{2} g_2, \tag{6.17}$$

which is a result of supersymmetry. Similarly to $\gamma(Z) f_5 f_5$, the vertices $H_5 H_5 V$ are fully determined by the gauge couplings g_2, which is independent of the small v_3 suppression. Consequently, the processes $pp \to W^\pm \to H_5^0 H_5^\pm$ and $pp \to W^\pm \to f_5^0 f_5^\pm$ dominate the H_5^0 and f_5^0 hadroproduction rates. The production cross sections for the LHC 13 TeV, with NNPDF 3.1 NNLO QED PDF [76] and $\mu_R = \mu_F = M_W$, $M_{f_5} = 11.9$ GeV, are given by

$$\sigma(pp \to W^\pm \to f_5^0 f_5^\pm) = 5.14 \text{ pb}, \quad \sigma(pp \to W^\pm \to f_5^\pm f_5^{\mp\mp}) = 3.42 \text{ pb}. \tag{6.18}$$

The ratio satisfies

$$\frac{\sigma(pp \to W^\pm \to f_5^0 f_5^\pm)}{\sigma(pp \to W^\pm \to f_5^\pm f_5^{\mp\mp})} = \left(\frac{V_{f_5^0 f_5^- W^+}}{V_{f_5^+ f_5^{--} W^+}}\right)^2 = \frac{3}{2}. \tag{6.19}$$

6.2 Higgs decay

The SGM and GM models introduce so a large amount of new Higgs (pseudo)scalars. This subsection, we will examine the decays of these (pseudo)scalars, especially into the SM particles.

6.2.1 The SM Higgs

To familiarize ourselves with the calculations, we start with the decays and production of the Standard Model Higgs boson. First, let us calculate a simpler case for the process $H(k_1) \to b(k_2)\bar{b}(k_3)$ at tree level, Feynman diagram shown in Figure 6.2. The amplitude is

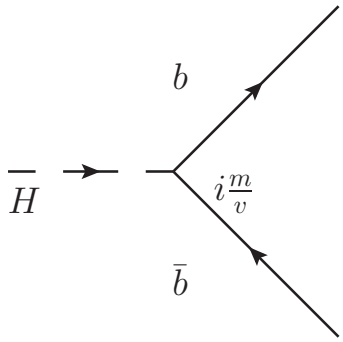

Figure 6.2: The Feynman diagram for $H \to b\bar{b}$ decay.

$$\mathcal{M} = \frac{m_b}{v}\bar{u}_2 v_3 = \frac{e m_b}{2 M_W s_W}\bar{u}_2 v_3. \tag{6.20}$$

We have substituted $M_W = gv/2$ and $e = g s_W$. Then the squared amplitude averaged over spins is given by

$$\begin{aligned}\sum_{s_2,s_3}|\mathcal{M}|^2 &= \sum_{s_2,s_3}\frac{3\alpha m_b^2\pi}{M_W^2 s_W^2}(\bar{u}_2 v_3)^*\bar{u}_2 v_3 = \frac{3\alpha m_b^2\pi}{M_W^2 s_W^2}\,\mathrm{Tr}(\not{k}_2 - m_b)(\not{k}_3 + m_b)\\ &= \frac{3\alpha m_b^2\pi}{M_W^2 s_W^2}[\mathrm{Tr}(\not{k}_2\not{k}_3) - 4m_b^2] = \frac{3\alpha m_b^2\pi}{M_W^2 s_W^2}(4k_2\cdot k_3 - 4m_b^2).\end{aligned} \tag{6.21}$$

We have used $\mathrm{Tr}(\gamma^\mu) = 0$ and $\mathrm{Tr}(\gamma^\mu\gamma^\nu) = 4g^{\mu\nu}$ (due to $\{\gamma^\mu, \gamma^\nu\} = 2g^{\mu\nu}\mathcal{I}$). We have the momentum conservation as

$$k_1 = k_2 + k_3 \Rightarrow M_H^2 = k_1^2 = (k_2 + k_3)^2 = m_b^2 + 2k_2\cdot k_3 + m_b^2. \tag{6.22}$$

Therefore, we get

$$\sum|\mathcal{M}|^2 = \frac{3\alpha m_b^2\pi}{M_W^2 s_W^2}\left[2(M_H^2 - 2m_b^2) - 4m_b^2\right] = \frac{3\alpha m_b^2\pi}{M_W^2 s_W^2}2M_H^2\beta^2. \tag{6.23}$$

We have defined the phase space suppression factor $\beta = \sqrt{1 - 4m_b^2/M_H^2}$.

The two-body phase space for system $A(P) \to B(p_1) + C(p_2)$ is very simple:

$$\begin{aligned}
\mathrm{d}\Phi_2 &= (2\pi)^4\delta^{(4)}(P - p_1 - p_2)\frac{\mathrm{d}^3p_1}{(2\pi)^3 2p_1^0}\frac{\mathrm{d}^3p_2}{(2\pi)^3 2p_2^0} \\
&= \frac{1}{(2\pi)^2}\delta(M - p_1^0 - p_2^0)\frac{\mathrm{d}^3p_1}{4p_1^0p_2^0} \\
&= \frac{1}{(2\pi)^2}\delta(M - \sqrt{m_1^2 + p^2} - \sqrt{m_2^2 + p^2})\frac{p^2\mathrm{d}p\mathrm{d}\Omega}{4p_1^0p_2^0} \\
&= \frac{1}{(2\pi)^2}\frac{\delta(p - p^*)}{\frac{p}{\sqrt{m_1^2+p^2}} + \frac{p}{\sqrt{m_2^2+p^2}}}\frac{p^2\mathrm{d}p\mathrm{d}\Omega}{4p_1^0p_2^0} \\
&= \frac{1}{(2\pi)^2}\frac{p}{4(p_1^0 + p_2^0)}\mathrm{d}\Omega = \frac{p}{(2\pi)^2 4M}\mathrm{d}\Omega.
\end{aligned} \tag{6.24}$$

The 3-momentum is obtained as

$$p = \frac{1}{2M}\sqrt{(M^2 - m_1^2 - m_2^2)^2 - 4m_1^2m_2^2} = \frac{\sqrt{\lambda(M^2, m_1^2, m_2^2)}}{2M}, \tag{6.25}$$

where $\lambda(a, b, c) = (a-b-c)^2 - 4bc$ is the Kallen function. Then, we obtain the partial width for the Higgs decay into $b\bar{b}$ pair,

$$\Gamma(H \to b\bar{b}) = \frac{1}{2M_H}\int \mathrm{d}\Phi_2|\mathcal{M}|^2 = \frac{1}{2M_H}\int \frac{p}{(2\pi)^2 4M_H}\mathrm{d}\Omega\frac{3\alpha m_b^2\pi}{M_W^2 s_W^2}2M_H^2\beta^2 = \frac{3\alpha M_H m_b^2}{8M_W^2 s_W^2}\beta^3, \tag{6.26}$$

where we have used

$$p = \frac{\sqrt{\lambda(M_H^2, m_b^2, m_b^2)}}{2M_H} = \frac{\sqrt{M_H^4 - 4M_H^2 m_b^2}}{2M_H} = \frac{M_H}{2}\beta. \tag{6.27}$$

Let us move on to the 1-loop induced decay $H \to \gamma\gamma$. In the Standard Model, all the charged particles can induce a Higgs decay into a photon pair. The fermion induced decay is dominated by the top quark loop, due to top's large Yukawa coupling, and is shown in Figure 6.3. With `FeynArts` [77] and `FormCalc` [78], we can get the amplitude of these

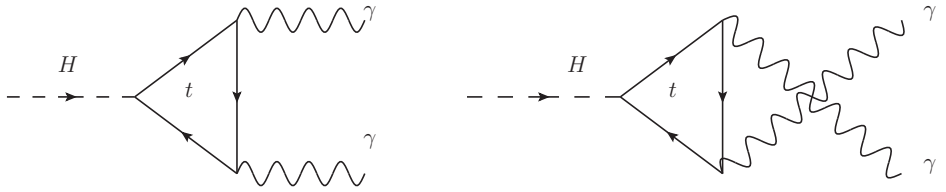

Figure 6.3: The Feynman diagram for top quark loop induced decay $H \to \gamma\gamma$ decay.

diagrams to be

$$\begin{aligned}
\mathcal{M} = \frac{2\alpha e m_t^2}{3M_W\pi s_W}\Big[&(2B_0 + M_H^2C_0 - 8C_{00} + 2M_H^2C_2)\epsilon_2^* \cdot \epsilon_3^* \\
&- 2(C_0 + 4C_{12} + 4C_2 + 4C_{22})\epsilon_2^* \cdot k_1\epsilon_3^* \cdot k_1\Big].
\end{aligned} \tag{6.28}$$

The loop integral functions are defined in Section A.1. Here we introduced B, C functions,

$$B(0, m_t^2, m_t^2),\ C(0, 0, M_H^2, m_t^2, m_t^2, m_t^2). \tag{6.29}$$

For a massless vector boson (photon), we have $k^\mu = (E, \vec{k})$, where $E = |\vec{k}|$. We define $\bar{k}^\mu = (E, -\vec{k})$. So the polarization sum in $|\mathcal{M}|^2$ is

$$\sum_{\lambda=\pm1} \epsilon_\mu \epsilon_\nu^* = -g_{\mu\nu} + \frac{k_\mu \bar{k}_\nu + k_\nu \bar{k}_\mu}{k \cdot \bar{k}} = \begin{cases} -g_{i,j} - \frac{k_i k_j}{|\vec{k}|^2} & (i, j = 1, 2, 3) \\ 0 & (\mu \,\text{and/or}\, \nu = 0) \end{cases} \tag{6.30}$$

to the amplitude square (matrix element) $|\mathcal{M}|^2$. For a massive vector boson, such as W/Z, the polarization sum is

$$\sum_{\lambda=0,\pm1} \epsilon_\mu \epsilon_\nu^* = -g_{\mu\nu} + \frac{k_\mu k_\nu}{m^2}. \tag{6.31}$$

We can work in the center-of-mass frame of the Higgs boson for $H(k_1) \to \gamma(k_2)\gamma(k_3)$. The 4-momentum for external particles are

$$k_1 = (M_H, 0, 0, 0), \quad k_2 = (M_H/2, 0, 0, M_H/2), \quad k_3 = (M_H/2, 0, 0, -M_H/2). \tag{6.32}$$

Therefore, we can get the squared amplitude as

$$\sum_{\lambda_2, \lambda_3} |\mathcal{M}|^2 = \frac{32\alpha^3 m_t^4}{9 M_W^2 \pi s_W^2} |2B_0 + M_H^2 C_0 - 8C_{00} + 2M_H^2 C_2|^2. \tag{6.33}$$

In our special case for $H(k_1) \to \gamma(k_2)\gamma(k_3)$, we have $M = M_H$ and $p = M_H/2$. The decay width is given by

$$\begin{aligned} \Gamma &= \frac{1}{2M_H} \int \mathrm{d}\Phi_2 \frac{1}{2} \sum_{\lambda_2, \lambda_3} |\mathcal{M}|^2 \\ &= \frac{1}{4M_H} \int \frac{M_H/2}{(2\pi)^2 4M_H} \mathrm{d}\Omega \frac{32\alpha^3 m_t^4}{9 M_W^2 \pi s_W^2} |2B_0 + M_H^2 C_0 - 8C_{00} + 2M_H^2 C_2|^2 \\ &= \frac{\alpha^3 m_t^4}{9\pi^2 M_H M_W^2 s_W^2} |2B_0 + M_H^2 C_0 - 8C_{00} + 2M_H^2 C_2|^2. \end{aligned} \tag{6.34}$$

Here we included a symmetric factor $\frac{1}{2}$ in the front, since photons in the final states are identical. Indistinguishability of identical particles restricts the integration to inequivalent configurations, i.e., to dividing the integral by a factor of $n!$ after integrating all the sets of momenta [1]. With the Standard Model parameter inputs [23], we have

$$\Gamma = 7.8 \times 10^{-7}\,\mathrm{GeV}. \tag{6.35}$$

Let us go to the W-loop induced $H \to \gamma\gamma$ decay, shown in Figure 6.4. With `FormCalc`,

[1] Please refer Page 108 of Michael Peskin's QFT textbook [61] or Page 316 of the book [79].

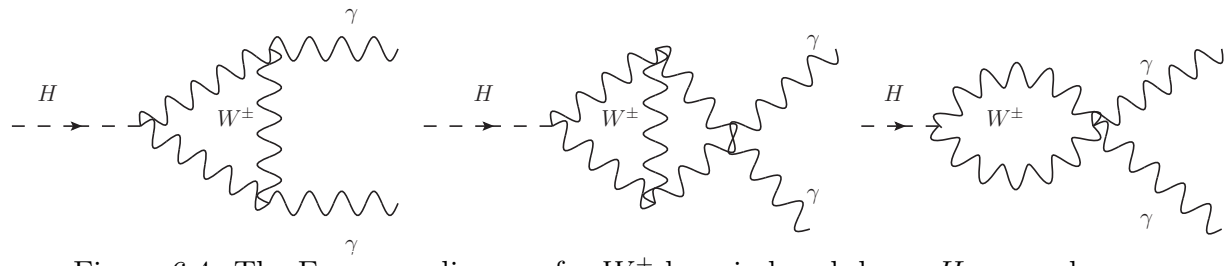

Figure 6.4: The Feynman diagram for $W^{\pm}$ loop induced decay $H \to \gamma\gamma$ decay.

we obtain

$$\Gamma(\tau_W) = \frac{\alpha^3 M_W^2}{32 M_H \pi^2 s_W^2} \Big| 4B_0 - 6B_0' + 4(-M_H^2 + M_W^2)C_0 + 20C_{00} + M_H^2 C_1 + 4M_H^2 C_2 \Big|^2. \quad (6.36)$$

Here the integral functions are

$$B_0(0, M_W^2, M_W^2),\ B_0' = B_0(M_H^2, M_W^2, M_W^2),\ C(0, 0, M_H^2, M_W^2, M_W^2, M_W^2), \quad (6.37)$$

respectively. After we plug in the SM parameters, we obtain

$$\Gamma(\tau_W) = \begin{cases} 1.55 \times 10^{-5}\,\text{GeV} & (\mu = M_H), \\ 5.97 \times 10^{-6}\,\text{GeV} & (\mu = M_W). \end{cases} \quad (6.38)$$

Here, the results strongly depend on the scale choice, which is mainly comes from the B function generated by the third diagram in Figure 6.4. So we choose $\mu = M_H(M_W)$ as benchmarks. The analytical formula for Higgs decay into diphoton can be found in literature [80]:

$$\begin{aligned} \Gamma(H \to \gamma\gamma) &= \frac{G_F \alpha^2 M_H^3}{128\sqrt{2}\pi^3} \Big| \sum_f N_c Q_f^2 A_{1/2}^H(\tau_f) + A_1^H(\tau_W) \Big|^2, \\ A_{1/2}^H(\tau) &= 2[\tau + (\tau - 1) f(\tau)]\tau^{-2}, \\ A_1^H(\tau) &= -[2\tau^2 + 3\tau + 3(2\tau - 1) f(\tau)]\tau^{-2}, \\ f(\tau) &= \begin{cases} \arcsin^2 \sqrt{\tau} & (\tau \le 1), \\ -\frac{1}{4}\Big[\log \frac{1 + \sqrt{1 - \tau^{-1}}}{1 - \sqrt{1 - \tau^{-1}}} - i\pi \Big] & (\tau > 1). \end{cases} \end{aligned} \quad (6.39)$$

where the parameters $\tau_i = M_H^2/4M_i^2$ for $i = f, W$ for the heavy-loop particles. For the top quark running in the loop, we have $\tau_t = M_H^2/4m_t^2 < 1$. In turn,

$$\Gamma(H \to \gamma\gamma) = \frac{G_F \alpha^2 M_H^3}{128\sqrt{2}\pi^3} \Big| 3\left(\frac{2}{3}\right)^2 2\big[\tau + (\tau - 1)\arcsin^2 \sqrt{\tau}\big]\tau^{-2} \Big|^2 = 7.84 \times 10^{-7}\,\text{GeV}, \quad (6.40)$$

which agrees with our calculation very well. For the W-induced part, we have

$$\Gamma(\tau_W) = \frac{G_F \alpha^2 M_H^3}{128\sqrt{2}\pi^3} \Big| -\big[2\tau^2 + 3\tau + 3(2\tau - 1)\arcsin^2 \sqrt{\tau}\big]\tau^{-2} \Big|^2 = 1.62 \times 10^{-5}\,\text{GeV}, \quad (6.41)$$

which agrees with our calculation with the choice of $\mu = M_H$. With these calculations, we arrive at a conclusion that most of the $H \to \gamma\gamma$ decay rate is contributed by the diagrams with $W^{\pm}$ bosons running in the triangle and bubble loops.

Similarly, we can have a 1-loop top-quark induced decay $H \to gg$, with the same diagram as Figure 6.3, but with the photon replaced by a gluon. Then we repeat the 1-loop calculation and get the decay width as

$$\Gamma(H \to gg) = \frac{1}{2}\frac{\alpha\alpha_s^2 m_t^4}{4M_H M_W^2 \pi^2 s_W^2}\left|2B_0 + M_H^2 C_0 - 8C_{00} + 2M_H^2 C_2\right|^2 = 2.14 \times 10^{-4}\,\text{GeV}. \quad (6.42)$$

This result agrees well with Ref. [80],

$$\Gamma(H \to gg) = \frac{G_F \alpha_s^2 M_H^3}{36\sqrt{2}\pi^3}\left|\frac{3}{4}A_{1/2}^H(\tau)\right|^2 = 2.16 \times 10^{-4}\,\text{GeV}. \quad (6.43)$$

We obtain a slight difference from our value estimated in Equation (6.42) because of the choice of the renormalization scale in our calculation. In the limit $\tau = M_H^2/4m_t^2 = 0.13 \ll 1$, we have $A_{1/2}^H(\tau) \to 4/3$, which gives $\Gamma = \frac{G_F \alpha_s^2 M_H^3}{36\sqrt{2}\pi^3} = 2.03 \times 10^{-4}$ GeV. At the next-to-leading order (NLO), the digluon partial width of Higgs boson can be found in Ref. [81] as

$$\begin{aligned} \Gamma^{N_F}[H \to gg(g), q\bar{q}g] &= \Gamma_{LO}[\alpha_s^{(N_F)}(\mu)](1 + E^{N_F}\frac{\alpha_s^{(N_F)(\mu)}}{\pi}), \\ E^{N_F} &= \frac{95}{4} - \frac{7}{6}N_F + \frac{33 - 2N_F}{6}\log\frac{\mu^2}{M_H^2} \end{aligned} \quad (6.44)$$

Taking the scale $\mu = M_H$ and $N_F = 5$, we get the NLO corrections to the Higgs' digluon decay as a ratio

$$K = \Gamma_{NLO}/\Gamma_{LO} \approx 1.68. \quad (6.45)$$

6.2.2 The Higgs decay in the GM and SGM models

Equipped with the tree-level and 1-loop induced decay of the SM Higgs boson, we are able to apply the same calculations to the Higgs bosons in the GM and SGM models. Firstly, let us reorganize the mass terms for neutral scalar (CP-even) and pseudoscalar (CP-odd) in the gauge basis,

$$\begin{aligned} \mathcal{L}_0 &= -\frac{1}{2}(H_g^0)^T \mathcal{M}_{H,g}^2 H_g^0 - \frac{1}{2}A_g^0 \mathcal{M}_{A,g}^2 A_g^0 \\ H_g^0 &= (h_{1R}^0, h_{2R}^0, \chi_R^0, \phi_R^0, \psi_R^0)^T,\ A_g = (h_{1I}^0, h_{2I}^0, \chi_I^0, \phi_I^0, \psi_I^0)^T. \end{aligned} \quad (6.46)$$

We can rotate this gauge basis into the mass basis in one step, by jumping over the intermediate custodial basis,

$$\begin{aligned}\mathcal{L}_0 &= -\frac{1}{2}(H_g^0)^T(Z^H)^\dagger Z^H \mathcal{M}^2_{H,g}(Z^H)^\dagger Z^H H_g^0 - \frac{1}{2}(A_g^0)^T(Z^A)^\dagger Z^A \mathcal{M}^2_{A,g}(Z^A)^\dagger Z^A A_g^0 \\ &= -\frac{1}{2}(H_m^0)^T \mathcal{M}^2_{H,m} H_m^0 - \frac{1}{2}(A_m^0)^T \mathcal{M}^2_{A,m} A_m^0\end{aligned} \tag{6.47}$$

With the rotation matrices $Z^{H,A}$, we get the diagonalized squared-mass matrices as

$$\begin{aligned}\mathcal{M}^2_{H,m} &= Z^H \mathcal{M}^2_{H,g}(Z^H)^\dagger = \text{diag}(m^2_{H_1}, m^2_{H_2}, m^2_{H_3}, m^2_{H_4}, m^2_{H_5}), \\ \mathcal{M}^2_{A,m} &= Z^A \mathcal{M}^2_{A,g}(Z^A)^\dagger = \text{diag}(m^2_{A_1}, m^2_{A_2}, m^2_{A_3}, m^2_{A_4}, m^2_{A_5}),\end{aligned} \tag{6.48}$$

The physical states in the mass basis can be obtained by rotating the gauge eigenstates as

$$H_m^0 = Z^H H_g^0,\ A_m^0 \ = Z^A A_g^0, \tag{6.49}$$

Similarly, the mass term for singly-charged Higgs in the gauge basis is

$$\mathcal{L}_\pm = -(H_g^+)^\dagger \mathcal{M}^2_{\pm,g} H_g^+,\ H_g^+ = (h_1^{-*}, h_2^+, \chi^{-*}, \phi^{-*}, \phi^+, \psi^+)^T, \tag{6.50}$$

Diagonalizing this squared mass matrix, we get spectrum for the singly-charged Higgs boson,

$$\mathcal{L}_\pm = -(H_g^+)^\dagger (Z^\pm)^\dagger Z^\pm \mathcal{M}^2_{\pm,m}(Z^\pm)^\dagger Z^\pm H_g^+ = -(H_m^+)\mathcal{M}^2_{\pm,g} H_m^+, \tag{6.51}$$

The corresponding eigenvalues and eigenvectors for the squared mass matrix are

$$\mathcal{M}^2_{\pm,m} = \text{diag}(m^2_{H_1^\pm}, m^2_{H_2^\pm}, m^2_{H_3^\pm}, m^2_{H_4^\pm}, m^2_{H_5^\pm}, m^2_{H_6^\pm}),\ H_m^+ = Z^\pm H_g^\pm. \tag{6.52}$$

Numerically, we have $m^2_{H_1^\pm} = m^2_{A_1} = 0$, which correspond to the Goldstone bosons. The doubly-charged Higgs mass term in the gauge basis is much simpler,

$$\mathcal{L}_{\pm\pm} = -(H_g^{++})\mathcal{M}^2_{\pm\pm,g} H_g^{++}, \quad H_g^{++} = (\chi^{--*}, \psi^{++})^T. \tag{6.53}$$

After diagonalizing the squared mass matrix, we rewrite the mass term in the mass basis as

$$\mathcal{L}_{\pm\pm} = -(H_g^+)^\dagger (Z^{\pm\pm})^\dagger Z^{\pm\pm} \mathcal{M}_{\pm\pm,m}(Z^{\pm\pm})^\dagger Z H_g^{++} = -(H_m^{++})\mathcal{M}^2_{\pm\pm,g} H_m^{++}. \tag{6.54}$$

The eigenvalues, eigenvectors and the rotation matrix are

$$\mathcal{M}_{\pm\pm} = \text{diag}(m^2_{H_1^{\pm\pm}}, m^2_{H_2^{\pm\pm}}),\ H_m^{++} = Z^{\pm\pm} H_g^{++},\ Z^{\pm\pm} = \begin{pmatrix} 1/\sqrt{2} & 1/\sqrt{2} \\ -1/\sqrt{2} & 1/\sqrt{2} \end{pmatrix}. \tag{6.55}$$

These mass eigenstates are the same as that in custodial basis (5.26), with the masses are the same as that in Equation (5.27).

So far, we have obtained all the numerical squared masses of the physical states, and we can compare the specific values to pick out singlets, triplets, and quintuplets. Just a reminder here: in the *mirror*-GM sector, the masses of the triplet neutral components $T^0_{1,2}$ are a little different from that of charged one $T^\pm_{1,2}$, which is the consequence of the custodial symmetry violation due to the hypercharge gauge. However, in the decoupling limit, all the

mirror-GM particles become very heavy, which leaves that the small difference in the triplet mass spectrum does not impact the GM-like particles at the EW scale.

Let us perform a benchmark study. As we mentioned before, we have totally 4 free parameters in the SGM model. In addition, we can choose relations $\lambda = \lambda_\Delta$ and $\mu = -\mu_\Delta$ to fix 2 degrees of freedom. In such a case, we only have 2 free parameters, and we set them to be GM-like triplet and quintuplet masses,

$$m_3 = 750 \text{ GeV}, \quad m_5 = 500 \text{ GeV}. \tag{6.56}$$

We list all other numerical inputs here,

$$\begin{aligned} &A = A_3 = 0 \text{ GeV}, && B = -B_3 = -(10^3 \text{ GeV})^2, \\ &\Lambda = \Lambda_3, \ \mu = -\mu_3, && M_{\tilde{B}} = M_{\tilde{W}} = 1000 \text{ GeV}, \\ &m_h = 125 \text{ GeV}, && 2v_2^2 + 8v_3^2 = v^2 = (246.22 \text{ GeV})^2. \end{aligned} \tag{6.57}$$

We can solve the spectrum equations to get the SGM parameters,

$$\mu = 896 \text{ GeV}, \quad \Lambda = 1.08, \quad v_3 = 33.6 \text{ GeV}. \tag{6.58}$$

The mapping conditions (5.50) between the GM and SGM models can help us to determine all the GM Lagrangian parameters as

$$\begin{aligned} &v_X = 33.6 \text{ GeV}, && \lambda_1 = 0.217, && \lambda_2 = 0.290, \\ &\lambda_3 = -0.145, && \lambda_4 = 0.145, && \lambda_5 = -1.74, \\ &M_1 = 1365 \text{ GeV}, && M_2 = -341 \text{ GeV}. \end{aligned} \tag{6.59}$$

At this stage, we are able to calculate all the spectrum in both the GM and SGM models, and we list the results in Table 6.1. We see a slight difference in the masses of the

	GM		SCTM		
	scalar	pseudo	scalar	pseudo	fermion
singlet	125, 818		125, 818	1320, 1599	869, 997, 1000
triplet		0, 750	1432, 1588	0, 750	926(931), 956, 1030(1025)
quintuplet	500		500	1525	871

Table 6.1: Benchmark of mass spectrum [GeV] calculated with `SARAH` [82, 83] and confirmed by `SPheno` [73, 74]). The numbers in the parentheses denote the charged component of the triplet fermions, which quantify the custodial symmetry violation.

neutral and charged (numbers in the parentheses) fermionic triplet, which results from the custodial symmetry violation. Here we have fixed the Majorana masses of gauginos to be $M_{\tilde{B}} = M_{\tilde{W}} = 1$ TeV. As a result, we obtain the masses for photino, zino-like and wino-like

fermions as

$$m_{\tilde{\gamma}} = 1000 \text{ GeV},\ m_{\tilde{Z}} = 1030 \text{ GeV},\ m_{\tilde{W}} = 1025 \text{ GeV}. \tag{6.60}$$

The zino-like and wino-like fermions get small contributions from the gauge-doublet VEV as $Gv_2/\sqrt{2}$ and gauge-triplet VEV as $\sqrt{2}Gv_3$, where $G = g_2, \sqrt{g_1^2 + g_2^2}$ for the wino-,zino-like charginos. The lightest supersymmetric particle (LSP) is a singlet fermion with mass as $m_{f_1} = 868.9$ GeV, and next-to-LSP is a neutral quintet fermion f_5^0, whose mass can be determined analytically as

$$m_{f_5} = \frac{\Lambda_3 v_3}{\sqrt{2}} - \mu_\Delta = -871 \text{ GeV}. \tag{6.61}$$

We have discovered the Standard Model (or SM-like) Higgs [14, 15], whose mass is less than twice of that of W, Z bosons. It means tree-level decays $H \to W^\pm W^\mp$ and $H \to ZZ$ are threshold forbidden. The Higgs boson can only decay in this channel to an off-shell state, such as $H \to ZZ^*, Z^* \to l^+ l^-$. However, in the GM and SGM models, the Higgs masses can be larger than twice of W, Z boson masses. Under such a circumstance, we can obtain the Higgs' di-Boson decay at the tree-level, which may dominate the Higgs branching ratio. With the rotation matrix Z^H, we obtain the vertices $g_{H_i^0 VV}$ $(V = W^\pm Z)$ as in Figure 6.5, where the index i indicates the mass ordering from the lowest to the highest.

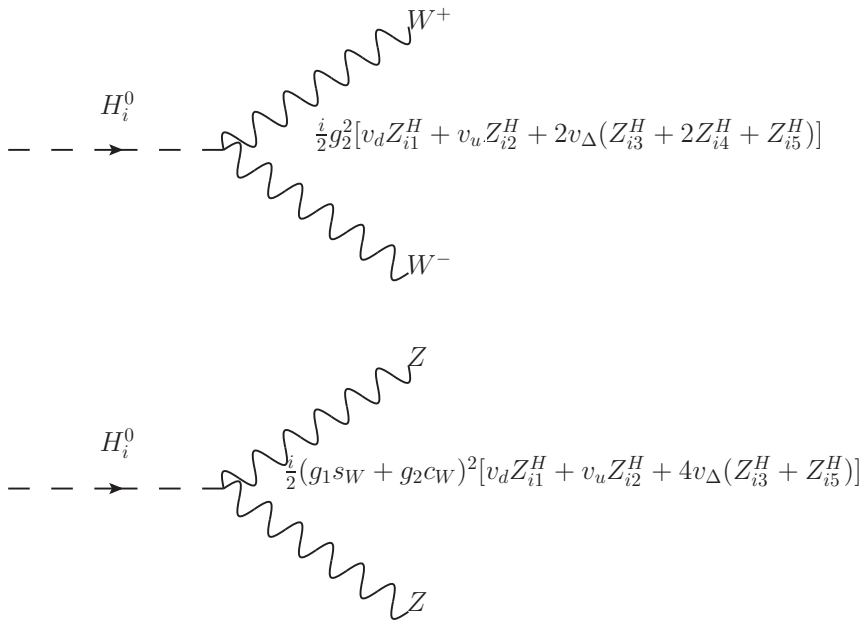

Figure 6.5: The Feynman diagrams for decays $H_i^0 \to W^+W^-$ and $H_i^0 \to ZZ$.

Here, we choose the quintuplet $H_5(F_s)$ with mass $m_5 = 500$ GeV in our benchmark example, with index $i = 2$ from Table 6.1. With `FeynArts` [77] and `FormCalc` [78], we obtain the squared amplitudes as

$$|\mathcal{M}(F_s \to W^+W^-)|^2 = \frac{1}{16}g_2^4\left(12 - \frac{4m_5^2}{M_W^2} + \frac{m_5^4}{M_W^4}\right)\left[v_2(Z_{21}^H + Z_{22}^H) + 2v_3(Z_{23}^H + 2Z_{24}^H + Z_{25}^H)\right]^2,$$
$$|\mathcal{M}(F_s \to ZZ)|^2 = \frac{1}{16}(c_W g_2 + s_W g_1)^4\left(12 - \frac{4m_5^2}{M_Z^2} + \frac{m_5^4}{M_Z^4}\right)\left[v_2(Z_{21}^H + Z_{22}^H) + 4v_3(Z_{23}^H + Z_{25}^H)\right]^2. \tag{6.62}$$

Considering the fact that quintuplets are totally composed of the gauge triplets, we determine the corresponding rotation matrix elements as

$$Z_{2,1\cdots5}^H = 0, 0, -1/\sqrt{6}, 2/\sqrt{6}, -1/\sqrt{6}, \quad \sum_{i=1}^{5}(Z_{2,i}^H)^2 = 1, \tag{6.63}$$

which simplifies the squared amplitudes as

$$\begin{aligned}|\mathcal{M}(F_s \to W^+W^-)|^2 &= \frac{1}{16}g_2^4\left(12 - \frac{4m_5^2}{M_W^2} + \frac{m_5^4}{M_W^4}\right)\left[2v_3(2/\sqrt{6})\right]^2,\\ |\mathcal{M}(F_s \to ZZ)|^2 &= \frac{1}{16}(c_W g_2 + s_W g_1)^4\left(12 - \frac{4m_5^2}{M_Z^2} + \frac{m_5^4}{M_Z^4}\right)\left[4v_3(-2/\sqrt{6})\right]^2.\end{aligned} \tag{6.64}$$

In the small hypercharge coupling limit, we have

$$g_1 \approx 0 \implies s_W \approx 0,\ M_W \approx M_Z \implies |\mathcal{M}(F_s \to W^+W^-)|^2 \approx \frac{1}{4}\mathcal{M}(F_s \to ZZ)|^2. \tag{6.65}$$

Integrating out the phase space, we obtain

$$\Gamma(F_s \to W^+W^-) \approx \frac{1}{2}\Gamma(F_s \to Z^+Z^-). \tag{6.66}$$

We want to remind that for the $F_s \to ZZ$ case, we have a symmetry factor $1/2$ due to the identical particles in the final states. Inputing the numerical values, we get the results from `FormCalc` as

$$\Gamma(F_s \to W^+W^-) = 3.47 \text{ GeV}, \quad \Gamma(F_s \to Z^+Z^-) = 6.65 \text{ GeV}. \tag{6.67}$$

We implement the SGM and GM models in `SPheno` [73, 74], which gives us the total width and branching ratios as

$$\Gamma_{\text{tot}}(F_s) = 17.03 \text{ GeV} \quad Br(F_s \to W^+W^-) = 0.204, \quad Br(F_s \to ZZ) = 0.403. \tag{6.68}$$

Therefore, we have

$$\Gamma(F_s \to W^+W^-) = 3.47\,\text{GeV}, \quad \Gamma(F_s \to ZZ) = 6.86\,\text{GeV}. \tag{6.69}$$

In such a way, we get an excellent agreement with the results of `FormCalc`. In such a way, we validate our numerical calculations in `SPheno`.

In Table 6.2, we list the total decay widths and the dominated branching ratios of GM-like particles in both the GM and the SGM models. We can see that the SGM model reproduces

States	Channel	GM	SGM
h	$\Gamma_{\rm tot}$	3.71E-03	3.65E-03
	W^+W^{-*}	2.46E-01	2.50E-01
	$b\bar{b}$	5.41E-01	5.49E-01
H	$\Gamma_{\rm tot}$	2.62E+01	2.62E+01
	$t\bar{t}$	1.90E-01	1.90E-01
	W^+W^-	5.41E-01	5.41E-01
	ZZ	2.67E-01	2.67E-01
$A(H_3)$	$\Gamma_{\rm tot}$	6.63E+01	6.63E+01
	$t\bar{t}$	1.05E-01	1.05E-01
	F_sZ	3.32E-01	3.32E-01
	$F_s^+W^-$	2.62E-01	2.62E-01
	$F_s^-W^+$	2.62E-01	2.62E-01
$F_s(H_5)$	$\Gamma_{\rm tot}$	5.26E+00	5.26E+00
	W^+W^-	3.42E-01	3.42E-01
	ZZ	6.58E-01	6.58E-01

Table 6.2: The total decay width $\Gamma_{\rm tot}$ [GeV] of the GM-like particles and the corresponding dominant branching ratios.

the GM model very well in our benchmark case, which can be understood in terms of the decoupling of non-GM particles. As shown in Table 6.1, the masses of non-GM scalars are around $m^S_{\not{\rm GM}} \approx 1500$ GeV and the masses of the electroweakinos are around $m_f \approx 1000$ GeV. The mapping conditions (5.50) ensure the spectrum and the coupling vertices of the GM-like particles are exactly the same in both models. The non-GM particles in the SGM model are decoupled at high scale, and do not affect the low-energy EW scale physics, which behaves the same as the GM model.

6.2.3 How to distinguish the SGM model from the GM model

By now, we have calculated the decay of the GM-like particles in both the GM and SGM models. As a benchmark study in Section 6.2.2, we obtained the same spectrum, decay width and branching ratios in both models. The next question for us is whether we can distinguish the SGM model from the GM model. To answer this question, we need to perform a systematic analysis in the full parameter space. In the ten parameters of the SGM model, two $B, B_\Delta \to \infty$ are taken to be large in order to obtain the decoupling limit. Furthermore, we have adopted the gauge mediated supersymmetry breaking scenario [25], which fixes $A = A_\Delta = 0$. With tadpole equations, we can replace two of the Lagrangian (or

superpotential) parameters by the VEVs of the gauge doublet v_H and gauge triplet v_Δ. In some cases, we use $v_{2,3}$ to denote the VEVs, as well. With the mapping conditions (5.50), we have the one-to-one correspondence relationship between the SGM and GM models,

$$(\lambda, \lambda_\Delta, \mu, \mu_\Delta, v_2, v_3) \leftrightarrow (\lambda_2, \lambda_4, M_1, M_2, v_H, v_\Delta). \tag{6.70}$$

We remind readers that the $A = A_\Delta = 0$ is not strictly necessary in other SUSY breaking mechanisms, such as supergravity [84] or anomaly mediated supersymmetry breaking (AMSB) [85]. We take this condition only for simplification while without qualitatively changing the results. We may consider relaxing this constraint in a more comprehensive analysis in the future.

Furthermore, we take the experimental measurements of the Higgs and W boson mass [23], which would fix 2 degree of freedom in the parameter space,

$$v = 246 \text{ GeV}, \ m_h = 125 \text{ GeV}. \tag{6.71}$$

These two inputs will allow us to eliminate the isospin doublet and triplet VEVs in both the SGM and GM models. As a result, the six-dimensional (6D) parameter space in Equation (6.70) is reduced to a four-dimensional (4D) one, and we choose the free parameters to be

$$(\lambda, \lambda_\Delta, \mu, \mu_\Delta) \leftrightarrow (\lambda_2, \lambda_4, M_1, M_2). \tag{6.72}$$

As we used in Equation (6.57) before, we furtherly reduce this 4D parameter space down to a 2D one by imposing the conditions $\lambda = \pm\lambda_\Delta$ and $\mu = \pm\mu_\Delta$. We have to carefully choose the signs in order to avoid the negative eigenvalues of the squared mass matrices for scalars, which represent the unstable vacuum. Finally, we obtain 2 benchmark scenarios which provide us with a safe scalar spectrum,

$$\begin{aligned} &\textbf{Point 1} : \lambda = \lambda_\Delta, \mu = -\mu_\Delta; \\ &\textbf{Point 2} : \lambda = -\lambda_\Delta, \mu = \mu_\Delta. \end{aligned} \tag{6.73}$$

Thus, we have 2 degrees of freedom in our systematical analysis, and we choose them to be the GM-like triplet and quintuplet masses $m_{3,5}$. All other parameters are determined self-consistently.

We remind the reader that the (m_3, m_5) parameter space is not totally free. We have to confront several constraints. The first one is the perturbative unitarity of the $2 \to 2$ scalar field scattering amplitudes, which requires the quartic couplings in the GM model to satisfy the conditions (3.52). Combining these with the mapping conditions (5.50), we get

the constraints on the coefficients of the cubic terms in the superpotential, as in Equation (5.80). The allowed $(\lambda, \lambda_\Delta)$ parameter space is depicted in Figure 5.1. The second set of constraints is coming from the unitarity bounds on the Yukawa couplings, as in Equation (3.60). Together with the top quark mass $m_t = 175$ GeV, we get a lower bound on the isospin doublet VEV to be $v_H \geq 60$ GeV as in Equation (3.61), and the upper bound on the isospin triplet VEV to be $v_\Delta \leq 84$ GeV as in Equation (3.62). The last set of constraints is from the non-negativity of the eigenvalues of all the scalar squared mass matrices, which constrains the combinations of all the Lagrangian parameters. We summarize these three constraints as follows.

- Perturbative unitarity of scattering $hh \to hh$ constraints on quartic couplings λ's requires
$$\begin{aligned} &-\frac{1}{3}\pi < \lambda_1 = \frac{3}{16}\Lambda^2 < \frac{\pi}{3}, \quad -\frac{2}{3}\pi < \lambda_2 = \frac{1}{4}\Lambda^2 < \frac{2}{3}\pi, \quad -\frac{1}{2}\pi < \lambda_3 = -\frac{1}{8}\Lambda_3^2 < \frac{3}{5}\pi, \\ &-\frac{1}{5}\pi < \lambda_4 = \frac{1}{8}\Lambda_3^2 < \frac{1}{2}\pi, \quad -\frac{8}{3}\pi < \lambda_5 = -\Lambda(\Lambda + \frac{1}{2}\Lambda_3) < \frac{8}{3}\pi, \end{aligned} \tag{6.74}$$
- Perturbative unitarity of $f\bar{f} \to h \to f\bar{f}$ constraints on Yukawa couplings requires
$$y_t \leq \sqrt{\frac{16\pi}{3}} \implies v_H \geq 60 \text{ GeV}, \ v_\Delta \leq 84 \text{ GeV}. \tag{6.75}$$
- Non-negativity of the eigenvalues of scalar squared mass matrices requires
$$m_S^2 \geq 0, \ S = H^0_{1\cdots5}, A^0_{1\cdots5}, (H^\pm_{1\cdots6}, H^{\pm\pm}_{1,2}). \tag{6.76}$$
Here, due to the mass degeneracy, the $H^\pm_{1\cdots6}$ must share the same masses as three H^0_i and three A^0_i. $H^{\pm\pm}_{1,2}$ must share the same masses as two $H^\pm_i$, one H^0_i, and one A^0_i in order to form one scalar quintuplet F_s and one pseudoscalar quintuplet F_p.

First, lets us take a glimpse at the approximate mass hierarchy structure. Starting with the GM-like triplet and quintuplet, we have
$$m_3^2 - m_5^2 = \Lambda^2(\frac{3}{2}v^2 - 17v_3^2) + 5\sqrt{2}\Lambda v_3 \mu. \tag{6.77}$$
Here we have already used the relation $2v_2^2 + 8v_3^2 = v^2 = (246 \text{ GeV})^2$. Therefore, if $\Lambda > 0$ and $\mu > 0$, we roughly have $m_3^2 > m_5^2$ when $v_3 < v\sqrt{3/34} = 73$ GeV. We do not consider about the negative triplet VEV case $v_3 < 0$, as the negative sign can be rotated away with a phase factor $e^{i\pi}$. For GM-like singlets, we interpret the lighter one as the SM-like $m_h = 125$ GeV Higgs. The heavier singlet Higgs mass m_H is derived from the eigenvalue of squared mass matrix $\mathcal{M}^2_{S_{1,2}}$, which involves the square root when solving the quadratic equations.

We take the small gauge triplet VEV limit $v_3 \to 0$ to expand these square roots, and get the value referred to the quintuplet mass as

$$m_H^2 - m_5^2 = \frac{9v^2\Lambda^2}{4} + \frac{15\Lambda\mu v_3}{\sqrt{2}} - 45\Lambda^2 v_3^2. \tag{6.78}$$

Therefore, we roughly get $m_H > m_5$ if $v_3 < v/\sqrt{20} = 55$ GeV. Similarly, we get the relation of the SM-like Higgs h when compared with the scalar quintet,

$$m_h^2 - m_5^2 = -\frac{\Lambda v^2 \mu}{2\sqrt{2}v_3} + \frac{15\Lambda^2 v^2}{4} + 2\sqrt{2}\Lambda\mu v_3 + \Lambda^2 v_3^2. \tag{6.79}$$

We will see that the sign of this difference is uncertain, as it can flip in our numerical scan. We also estimate the difference of the squared mass of the heavier singlet and the triplet as

$$m_H^2 - m_3^2 = \frac{3\Lambda^2 v^2}{4} + \frac{5\Lambda\mu v_3}{\sqrt{2}} - 28\Lambda^2 v_3^2, \tag{6.80}$$

and we get $m_H > m_3$ when $v_3 < v\sqrt{3/112} = 40$ GeV. To summarize, the mass hierarchy approximately goes as

$$m_5, m_h \lesssim m_3 \lesssim m_H. \tag{6.81}$$

The sign of the squared mass difference between the quintet m_5^2 and SM-like Higgs singlet m_h^2 is unknown. All the mirror-GM particles are very heavy in our SGM model, when we take the decoupling limit $B = -B_\Delta \to \infty$.

Now, to perform the numerical calculations, and we will choose the mass parameter range $0 < m_{3,5} < 2m_h = 250$ GeV. We focus on the mass range below $2m_h$ for two reasons. First, we limit ourselves to be within the threshold forbidden region for the $S \to 2h$ decay. The partial widths $\Gamma(S \to hh)$ are related by the triple Higgs couplings V_{hhh} [86], and we reserve it for a future study. Second, a new Higgs scalar with mass below 250 GeV can be well-probed at the current and future Large Hadron Collider (LHC), which can provide us powerful and robust data for direct search of the Higgs bosons in this range [87, 88].

Let us first take a look at the physical parameters for our two benchmark points in Equation (6.73), which are shown in Figure 6.6. Here we plot the masses for the heavier singlet Higgs m_H and the Lightest Supersymmetric Particle $m_{\rm LSP}$, and the gauge triplet VEV v_3. As we discussed before, the upper boundary of the allowed parameter space (m_3, m_5) indicates the approximate hierarchy $m_5 \lesssim m_3$, and the blue lines representing the heavier singlet mass indicate that $m_3 \lesssim m_H$. In the left figure corresponding to **Point 1**, the LSP mass is roughly within the same range of the GM-like scalar masses. In contrast, the right

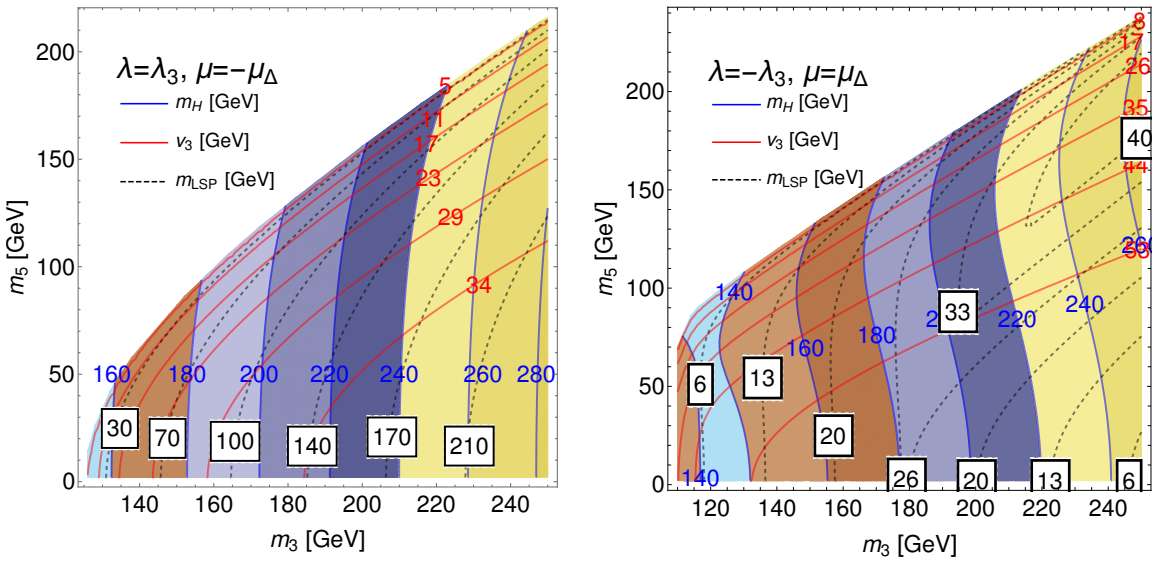

Figure 6.6: The heavier Higgs mass m_H, LSP mass $m_{\rm LSP}$ and isospin triplet VEV v_3 for **Point 1** (left) and **Point 2** (right).

figure (**Point 2**) shows the LSP mass is much smaller when compared to the GM-like scalar masses $m_{3,5,H}$. Also, we obtain a different trends about the $m_{\rm LSP}$ when (m_3, m_5) goes from the left-upper corner to the right-lower direction, which indicates a phase transition. We will see this phase transition will have an effect on the cross-section of LSP-nucleon scattering in the Dark Matter direct detection (DD) experiments in Chapter 11.

Even though we have not found any new particles beyond the Standard Model yet, they are still allowed within the current experimental uncertainties. The smoking gun to discover the GM-like particles is to observe the doubly-charged Higgs through same-sign W boson pair decay $H^{\pm\pm} \to W^{\pm}W^{\pm}$. The doubly-charged Higgs is one component of the mass quintuplet, which has the neutral partners H_5^0. Let us look at this neutral component of the quintuplet H_5^0 first. We have calculated the total and partial decay width for one benchmark point in Section 6.2.2 already. Now, we can perform a systemically scan in the parameter space $0 < m_{3,5} < 250$ GeV for **Point 1** and **Point 2**. The total decay width is shown in Figure 6.7. We can see for the **Point 1** case, we have roughly the same decay width for the neutral quintuplet H_5^0 in both the GM and SGM models, in spite of that the decay width of the SGM H_5^0 is slightly larger. In contrast, the H_5^0 decay width for the **Point 2** in the SGM model is significantly larger than the GM one. The $\Gamma^{\rm SGM}_{H_5^0}$ can even be a few order higher

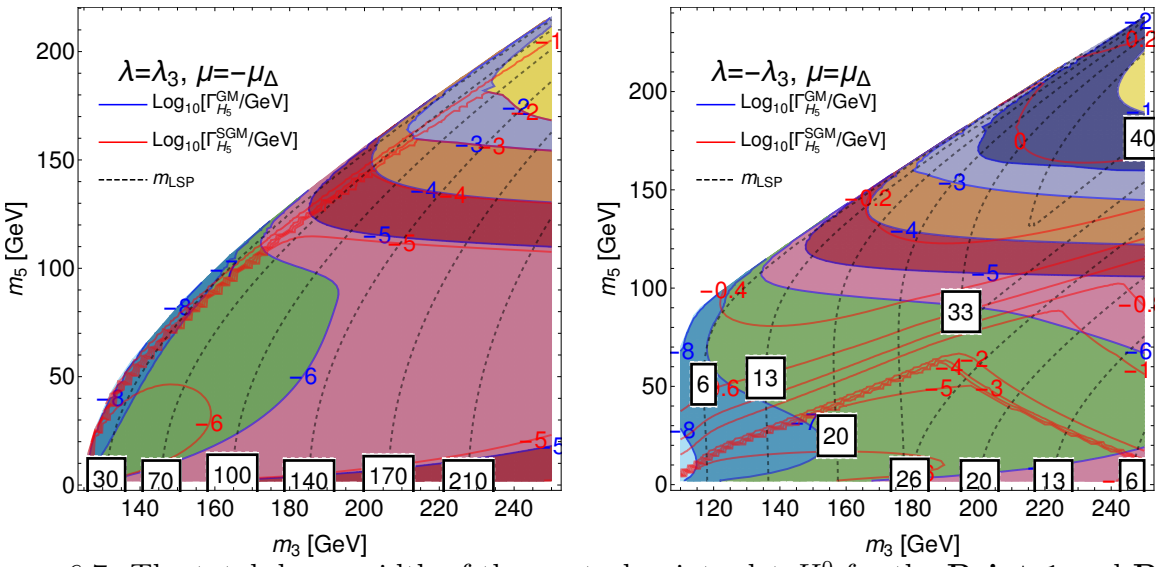

Figure 6.7: The total decay width of the neutral quintuplet H_5^0 for the **Point 1** and **Point 2**.

than $\Gamma^{\rm GM}_{H_5^0}$, i.e., $\Gamma^{\rm SGM}_{H_5^0} \gg \Gamma^{\rm GM}_{H_5^0}$. It is because of the light LSP mass for this point, which opens up the new decay channels, $H_5^0 \to f_i \bar{f}_j$. These channels do not exist in the GM model. As a result, we would expect the branch fractions for the standard decay channels, such as $H_5^0 \to \gamma\gamma, W^+W^-, ZZ$, should be lower down significantly.

Let us look at the quintuplet decays to the $\gamma\gamma$ and ZZ pairs. We are interested in di-photon decay because it is a very powerful direct search for the new particles, which have been proved to be very successful in the SM-like Higgs discovery [14, 15]. Meanwhile, the LHC has produced robust diphoton data up to now and will generate more in the future runs. It provides us a very good battlefield to pursue the BSM particles predicted by various new physics models, such as H_5^0 in the GM and SGM models. The branching fractions [2] of $H_5 \to \gamma\gamma$ for **Point 1** and **Point 2** in the GM and SGM models are displayed in Figure 6.8.

As we expected, for **Point 1**, we have roughly similar branching fractions of $\mathrm{Br}(H_5^0 \to \gamma\gamma)$ in both the GM and SGM models, while totally different ones for the **Point 2**. For the **Point 2**, $\mathrm{Br}^{\rm SGM}_{H_5 \to \gamma\gamma} \ll \mathrm{Br}^{\rm GM}_{H_5^0 \to \gamma\gamma}$ can be understood easily. We have very low LSP mass in this case of

[2]The branching fraction, also be called as branching ratio, is defined as the fraction of a partial width Γ_i in the total width $\Gamma_{\rm tot}$, while the total width sums over the partial width of all the possible decay channels,

$$\mathrm{Br}_i = \frac{\Gamma_i}{\Gamma_{\rm tot}} = \frac{\Gamma_i}{\sum_j \Gamma_j}. \tag{6.82}$$

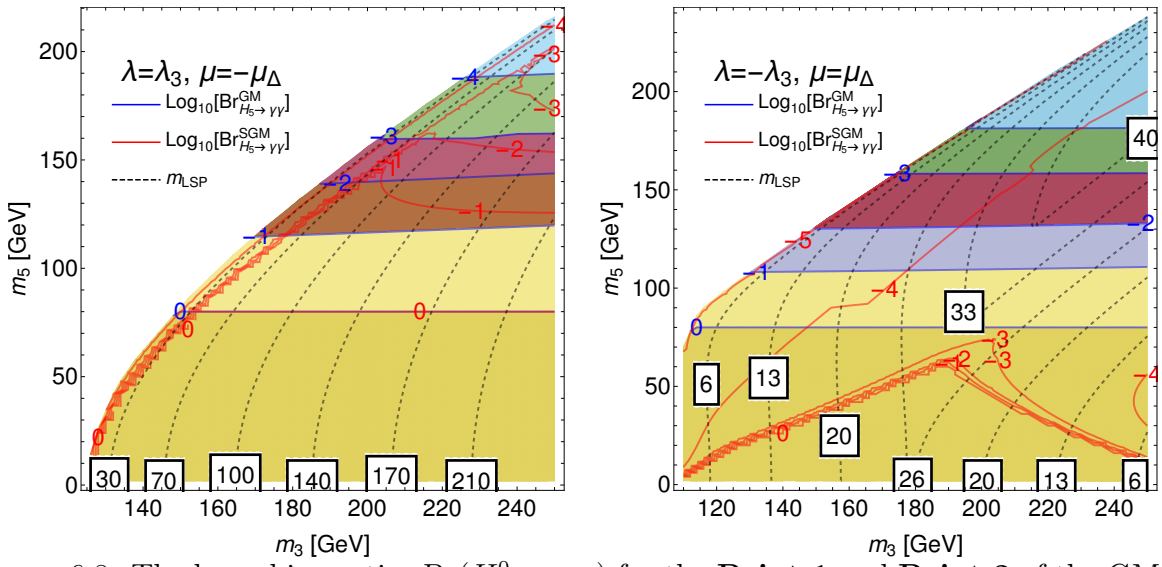

Figure 6.8: The branching ratios $\mathrm{Br}(H_5^0 \to \gamma\gamma)$ for the **Point 1** and **Point 2** of the GM and SGM models.

the SGM model, which opens the channels of H_5^0 decay into the fermionic superpartners of the GM and mirror-GM scalars. These new decay channels enter into the total decay width of H_5^0 and lower down the branching fractions of $H_5^0 \to \gamma\gamma$ in the SGM model. However, the LSP is much heavier in the **Point 1** case, which forbids the H_5^0 on-shell decay into the fermionic electroweakinos. Remind that we have taken the gaugino mass to be large as $M_1 = M_2 = 1$ TeV. Here we want to point it out that in the upper-right coroner of Figure 6.8 left plot, the $\mathrm{Br}^{\mathrm{SGM}}_{H_5^0\to\gamma\gamma} \gtrsim \mathrm{Br}^{\mathrm{GM}}_{H_5^0\to\gamma\gamma}$, which contradicts to the new decay channels open in the **Point 2** case. This can be understood as new charged particles (chargios and doubly charginos) enter into the triangle loops in Figure 6.3 to induced the $H_5^0 \to \gamma\gamma$ decay. As a result, we expect the effective couplings $C_{H_5^0\gamma\gamma}$ get an enhancement from the constructive contributions of these new charged particles, especially the doubly charginos. Therefore, the partial decay width $\Gamma(H_5^0 \to \gamma\gamma)$ increases, which is confirmed by Figure 6.9. In the next Chapter, we will use this effective coupling method to explore the new particles' constructive and destructive contributions to the diphoton decays of light exotic Higgs.

Let us move on to $H_5^0 \to ZZ$ decay. The ZZ pair production attracts a lot of experimental interests, as the $ZZ \to 4l$ mode provides very clean final state signature, which can be used to fully reconstruct the Higgs mass with excellent detector resolution, including both electron and muon channels. It is one of the main channels contributing to the Higgs discovery in

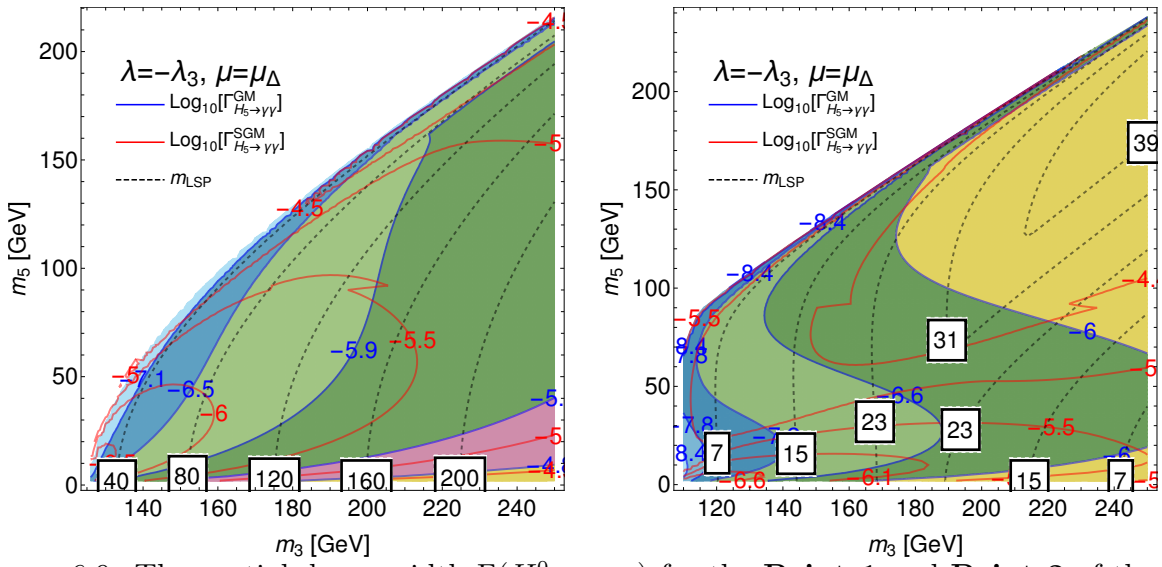

Figure 6.9: The partial decay width $\Gamma(H_5^0 \to \gamma\gamma)$ for the **Point 1** and **Point 2** of the GM and SGM models.

both ATLAS [14] and CMS [15] experiments. Furthermore, this channel is an excellent instrument to study the spin and parity of new resonance, since the full decay chain and intrinsic property can be reconstructed from the angular and invariant mass distribution of the final states [89]. The branching fractions for $H_5 \to ZZ^*$ in both the GM and SGM models for **Point 1** and **Point 2** are shown in Figure 6.10. We expect that the branching ratio for $H_5^0 \to ZZ^*$ behaves pretty much the same for **Point 1** of the GM and SGM models, while for **Point 2**, the SGM $\mathrm{Br}(H_5^0 \to ZZ^*)$ is much smaller than that of the GM model, as the low LSP mass in the SGM model open new decay channels. However, the $H_5^0 \to ZZ^*$ decay happens at the tree level, shown in Figure 6.5. The mapping conditions (5.50) ensure that the vertex of $g_{H_5^0 ZZ}$ is exactly the same in the GM and the SGM models. We would expect the partial width of $\Gamma(H_5^0 \to ZZ^*)$ is the same in the GM and SGM models, even though the branching fractions can be very different.

The experimental searches for this neutral quintuplet suffer a lot from large uncertainties, including the luminosity and the backgrounds. However, we can come up with some ratio or double ratio observables which cancel a lot of systematic uncertainties, including experimental and theoretical ones (such as renormalization and factorization uncertainties).

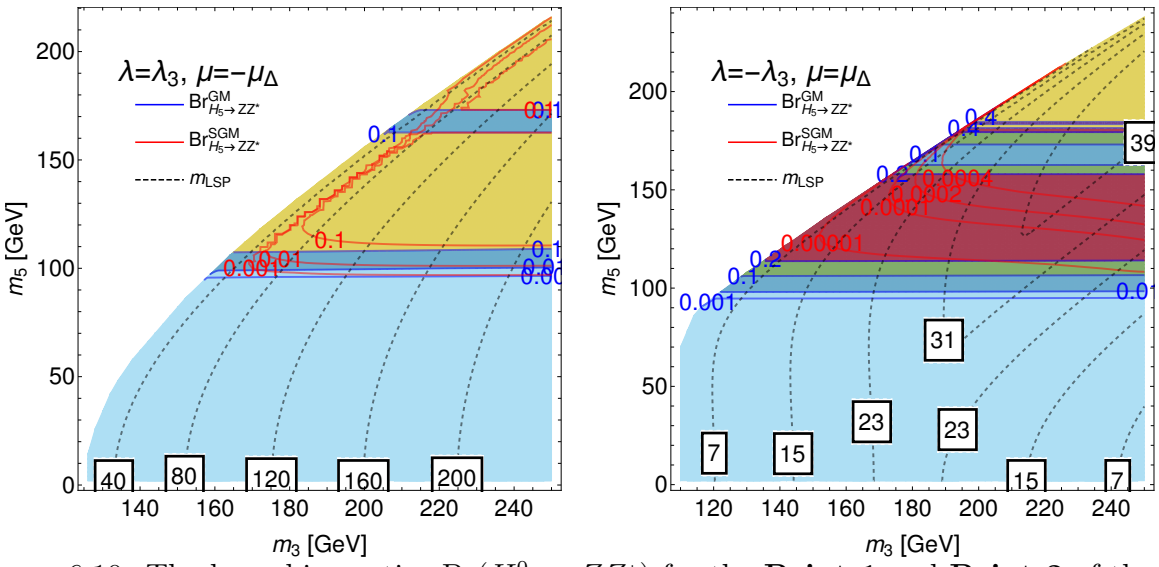

Figure 6.10: The branching ratios $\mathrm{Br}(H_5^0 \to ZZ^*)$ for the **Point 1** and **Point 2** of the GM and SGM models.

The Higgs golden ratio is such an observable defined as [90]

$$\mathcal{D}_{\gamma\gamma}^{\mathrm{BSM}} = \frac{\mathrm{Br}_{h\to\gamma\gamma}^{\mathrm{BSM}}/\mathrm{Br}_{h\to ZZ}^{\mathrm{BSM}}}{\mathrm{Br}_{h\to\gamma\gamma}^{\mathrm{SM}}/\mathrm{Br}_{h\to ZZ}^{\mathrm{SM}}}, \tag{6.83}$$

where we use $\mathrm{Br}_{h\to\gamma\gamma}^{\mathrm{SM}} = 0.228\%$ and $\mathrm{Br}_{h\to ZZ}^{\mathrm{SM}} = 2.64\%$ [23]. This observable can be measured very precisely as many uncertainties from the production side cancel. We would expect the experimental measurements of $\mathcal{D}_{\gamma\gamma}$ to reach $\mathcal{O}(1\%)$ precision in the future colliders, such as high luminosity LHC. We show the contours of this Golden Ratio $\mathcal{D}_{\gamma\gamma}$ in the 2D space (m_3, m_5) in both the GM and SGM models in Figure 6.11. Same result as before, we obtain similar contours in both models for the **Point 1** case, while totally different for the **Point 2**. Good to see that in both cases, we got large parameters space close to the Standard Model value $\mathcal{D}_{\gamma\gamma}^{\mathrm{SM}} = 1$, while large deviations from this value may be excluded when the measurements become more precise.

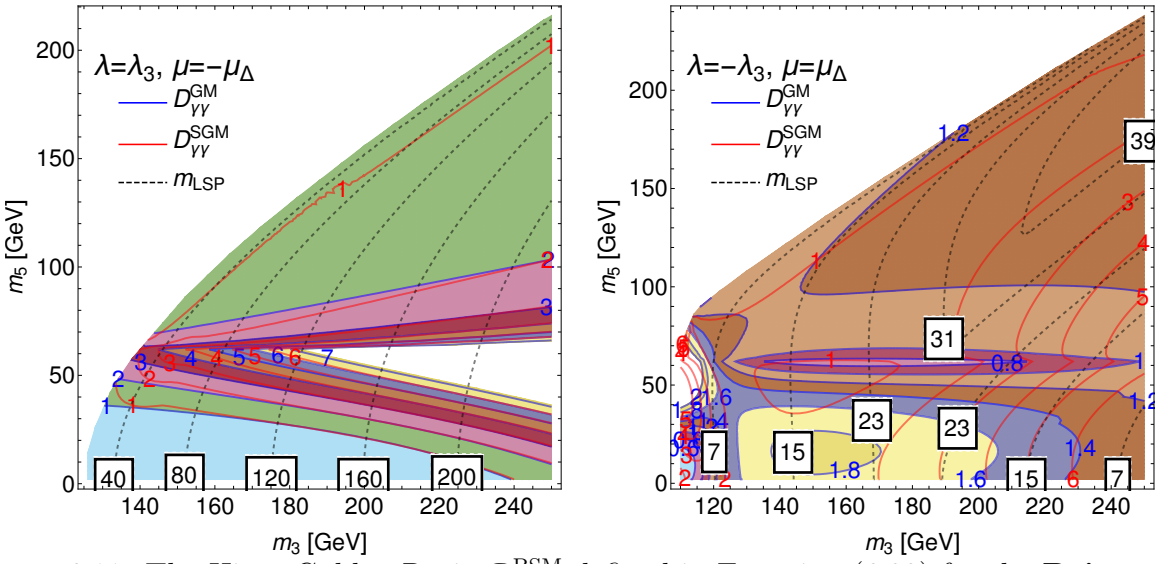

Figure 6.11: The Higgs Golden Ratio $\mathcal{D}_{\gamma\gamma}^{\mathrm{BSM}}$ defined in Equation (6.83) for the **Point 1** and **Point 2** of the GM and SGM models.

Chapter 7

Light Exotic Higgs

We have talked about the Georgi-Macachek (GM) and Supersymmetric Georgi-Macachek (SGM) Models as examples of isospin triplet extensions of the Standard Model Higgs sector. As discussed in Section 3.1.2, this triplet VEV can provide the neutrino mass through the Type II seesaw mechanism,

$$m_\nu = 2yv_\Delta. \tag{7.1}$$

As we know, the neutrino mass is constrained by $m_\nu \lesssim 1$ eV [46, 47, 48, 49, 50], which means either the Yukawa coupling is very small, or the triplet VEV is small. We manually impose the Custodial Symmetry in the GM and SGM models, which allows us to obtain triplet VEV to be large as long as $v_\Delta < 84$ GeV in Equation (3.62). Under these conditions, the Yukawa couplings must be bounded as tiny as $y \lesssim 10^{-10}$. It means the isospin triplet scalars' couplings to the Standard Model fermions are extremely suppressed or even vanish. As a result, these models give us exotic fermiophobic scalars, which cannot be produced via gluon-gluon fusion mechanism [87, 88]. In this chapter, we take the GM and SGM models as examples to talk about a more general exotic Higgs.

7.1 Exotic Higgs production channels

The current Higgs searches strongly depend on the vector boson fusion (VBF) and Higgs associated with vector boson production (VH) mechanisms, shown in Figure 7.1. The cross sections for both types production of the exotic Higgs are proportional to the square of coupling g_{VVh}, which is proportional to the exotic Higgs VEV v_{ex}. Similarly to our previous definition of the triplet VEV angle θ_H in Equation (3.42) and (5.20), we can define a SM doublet-exotic Higgs VEV mixing angle as

$$c_\theta \equiv \cos\theta = \frac{v_H}{v}, \quad s_\theta \equiv \sin\theta = \frac{v_{\text{ex}}}{v}, \quad v_H^2 + v_{\text{ex}}^2 = v^2 = (246\text{ GeV})^2. \tag{7.2}$$

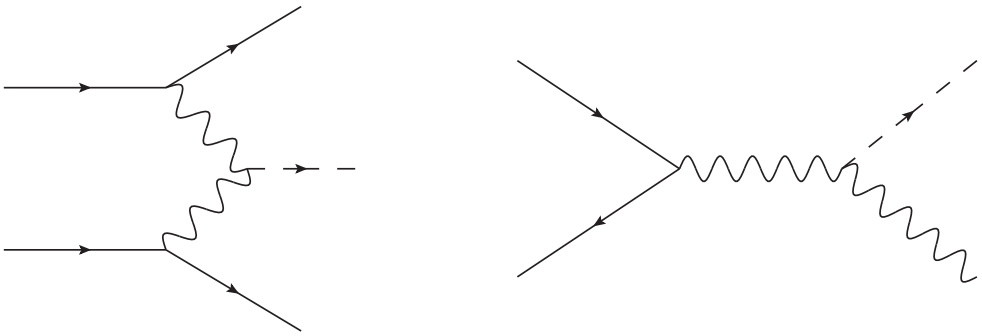

Figure 7.1: The. Feynman diagrams for VBF and VH production.

If this VEV angle s_θ is small, both VBF and VH production quickly become highly suppressed. In such scenario, both VBF and VH searches become obsolete.

However, in comparison with VBF and VH production, we have a new production mechanism through Drell-Yan (DY) Higgs pair production, shown in Figure 7.2, which is not present in the Standard Model because of no charged Higgs [87, 91]. The cross section of this channel is determined by the Higgs-Higgs-Vector boson couplings, which can be parameterized as

$$g_{VHH} = -ig_2 C_{VHH}(p_1 - p_2)_\mu, \tag{7.3}$$

where the coefficient C_{VHH} is fixed by $SU(2)_V$ custodial representations $(N, \bar{N})$. For example, in the GM model, we have the mass triplet $H_3^{0,\pm}$ and quintuplet $H_5^{0,\pm,\pm\pm}$, with the couplings to $W^\pm$ boson as

$$C_{W^\pm H_3^\mp H_3^0} = \frac{1}{2},\ C_{W^\pm H_5^\mp H_5^0} = \frac{\sqrt{3}}{2},\ C_{W^\pm H_5^\pm H_5^{\mp\mp}} = \frac{1}{\sqrt{2}}. \tag{7.4}$$

The mixing representations $C_{WHH'}$, such as $C_{W^+H_3^- h}$, is proportional to s_H defined in Equation (7.2). Similarly, Z boson mediated neutral Higgs pair production channel also mixes different custodial representations, with $C_{ZHH'}$ (such as $C_{ZhH_3^0}$) proportional to s_θ as well.

Although experimental measurements of the SM-like 125 GeV Higgs couplings [92] still allow exotic Higgs VEV contributions to the EWSB, they constrain $v_{\rm ex}$ well enough at low masses. As a result, the DY Higgs pair production dominates when compared with the single Higgs production channels such as VBF or VH, which is suppressed by the small $v_{\rm ex}$. We take $H_5^0 H_5^\pm$ as an example of DY Higgs pair production and compare its Leading Order

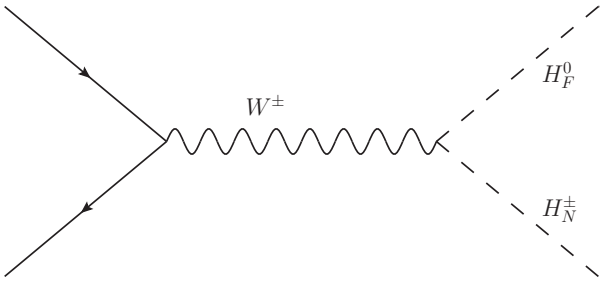

Figure 7.2: The Feynman diagrams for Drell-Yan Higgs pair production.

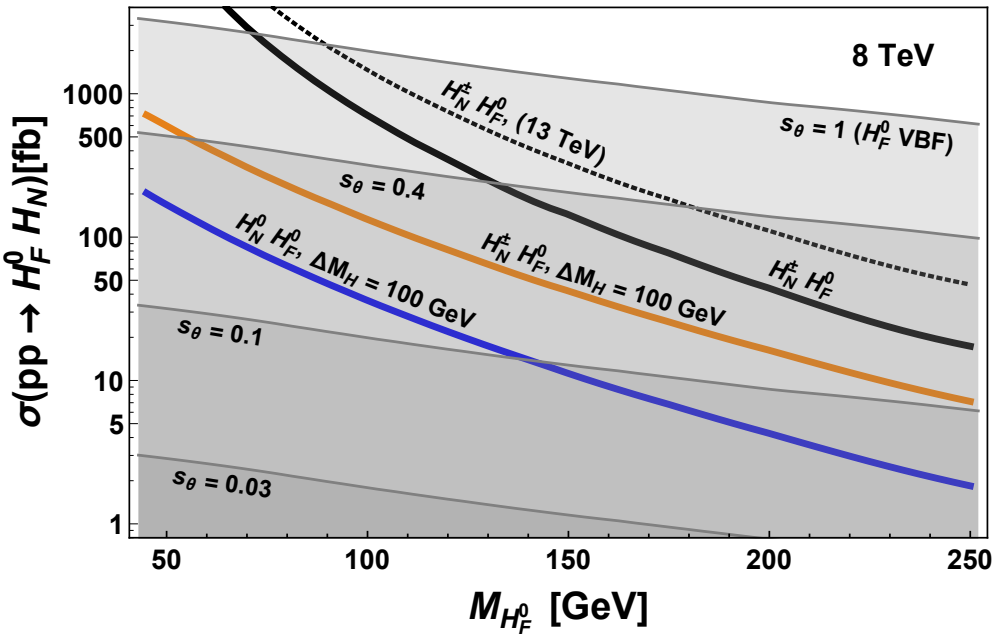

Figure 7.3: The cross section for Drell-Yan Higgs Higgs production [87].

cross-section with VBF at various s_θ in Figure 7.3. Furthermore, we also include the cross-section with assuming a 100 GeV mass splitting between the neutral and charged scalars $M_{H_N^{\pm}} > M_{H_F^0}$ (solid orange curve) to account for some custodial symmetry violation effects. The cross section of Z boson mediated $H_F^0 H_N^0$ production (solid blue curve) with the same mass splitting is significantly smaller than the W mediated channels. We see clearly when $s_\theta \ll 1$, the cross-section for VBF production channel quickly become highly suppressed relative the DY Higgs pair production. Similar behavior occurs to the VH production channels, whose cross sections are typically smaller than the VBF ones expect at very low masses [93, 94, 95].

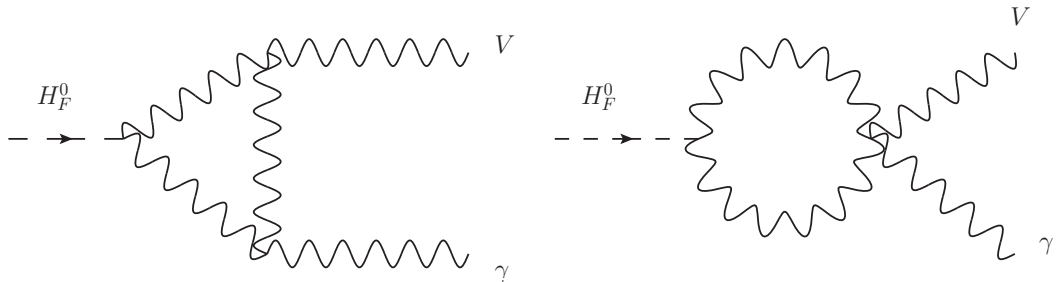

Figure 7.4: One-loop contributions from $W^\pm$ loops to the $H_F^0 V\gamma (V = Z, \gamma)$ effective couplings defined in Equation (7.9).

7.2 Fermiophobic Higgs Diboson Decays

In addition to VHH couplings, the neutral fermiophobic Higgs H_F^0 couplings to the WW and ZZ boson pairs, which are generated through EWSB and proportional to the exotic Higgs VEV v_{ex}. We can parametrize these couplings with the VEV angle s_θ as

$$\mathcal{L} \supset s_\theta \frac{H_F^0}{v}(g_Z m_Z^2 Z^\mu Z_\mu + g_W m_W^2 W^{+\mu} W_\mu^-), \tag{7.5}$$

where g_Z and g_W are fixed by $SU(2)_V$ custodial representations of H_F^0. For example, in the GM and SGM models, we have the mass quintuplet H_5^0,

$$g_Z = \frac{4}{\sqrt{3}},\ g_W = \frac{2}{\sqrt{3}}. \tag{7.6}$$

The mass triplet couplings are zero as it is CP-odd property, while the couplings to the singlet H, h involve the rotation angles α. We can define a ratio of the couplings

$$\lambda_{W/Z} = g_W / g_Z, \tag{7.7}$$

which is fixed the custodial symmetry at tree level to be

$$\lambda_{W/Z} = \begin{cases} 1, & H_F^0 = H, h, \\ 1/2, & H_F^0 = H_5^0. \end{cases} \tag{7.8}$$

The factor of s_θ is implicitly canceled in this coupling ratio.

Starting at one-loop level, the charged particles will generate the effective couplings to photon, shown in Figure 7.4. As a result, we would expect the following effective operators

$$\mathcal{L} \supset \frac{H_F^0}{v}(\frac{c_{\gamma\gamma}}{4} F^{\mu\nu} F_{\mu\nu} + \frac{c_{Z\gamma}}{2} Z^{\mu\nu} F_{\mu\nu}), \tag{7.9}$$

where field tensor is defined as $V_{\mu\nu} = \partial_\mu V_\nu - \partial_\nu V_\mu$. Again, we can define coupling ratios

$$\lambda_{V\gamma} = c_{V\gamma} / g_Z,\ V = Z, \gamma, \tag{7.10}$$

to absorb the implicit factor s_θ. Any charged particles will contribute to the effective couplings in Equation (7.9), including the $W^\pm$ boson, charged scalars and also charged fermions

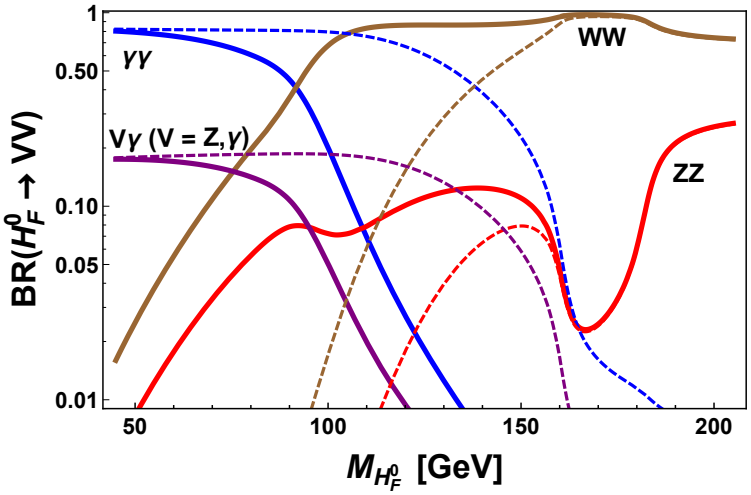

Figure 7.5: The Branching ratios of H_F^0 as a function of its mass by assuming $\lambda_{W/Z} = 1$. The solid curves corresponds to effective couplings $c_{V\gamma}$ only generated by $W^{\pm}$ loop, while dashed curves is calculated by taking effective couplings as $\lambda_{\gamma\gamma} = \lambda_{Z\gamma} = 0.05$ in Equation (7.10) [87].

as well. In such case, the effective couplings can be enhanced when the charged particles in the loop carry large chargers such as $H^{\pm\pm}, f^{\pm\pm}$ and interface constructively with other loop contributions. However, these effects are in principle expected to cannel to lead small $c_{V\gamma}$ effective couplings [96, 97].

We illustrate effect of these effective couplings with the branching ratios of the fermiophobic Higgs in two scenarios in Figure 7.5. The solid curves correspond to the effective couplings $c_{V\gamma}$ generated only by $W^{\pm}$ loops, in which $\lambda_{V\gamma} \sim 0.005 - 0.01$ depending on the Higgs mass. In the second scenario, we take the effective couplings $c_{V\gamma}$ as free parameters and set $c_{Z\gamma} = c_{\gamma\gamma} = 0.05$ to plot the branching ratios as dashed curves in Figure 7.5. Under the threshold of $(2)M_{W,Z}$, the branching ratios are obtained with the 3 or 4 body decays in $H_F^0 \to V\gamma \to 2l\gamma$ and $H_F^0 \to VV \to 4l$.

7.3 Diboson and diphoton searches at the LHC

Combining the fermiophobic Higgs boson production and decays, we can examine the possibility to search for fermiophobic Higgs bosons with diphoton and diboson searches at the LHC. As we discussed the before, no gluon fusion channels are available for the fermiophobic Higgs production, and single Higgs production channels such as VBF and VH associated

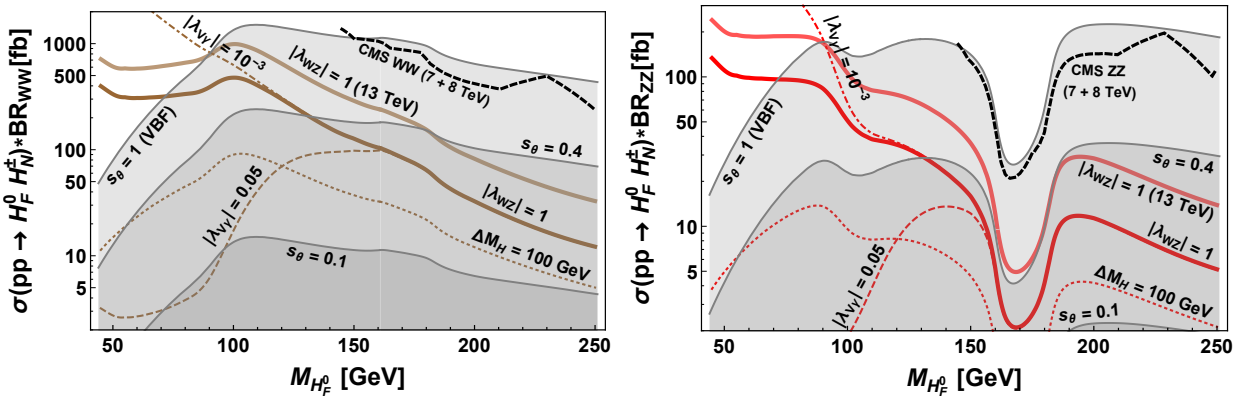

Figure 7.6: The products of the cross section $\sigma(pp \to W^{\pm} \to H_F^0 H_N^{\pm})$ times the branching ratios $BR(H_F^0 \to WW, ZZ)$, compared with the 95% exclusion limits from CMS diboson searches [98].

production are suppressed by the small VEV angle s_θ. We only consider the DY Higgs pair production mechanism $pp \to W^{\pm} \to H_N^{\pm} H_F^0$, where H_F^0 and $H_N^{\pm}$ can have a degenerated mass or large mass splitting. The cross sections for VBF and VH production are suppressed through a small angle of s_θ, which can be seen in Figure 7.3.

7.3.1 Diboson probing intermediate masses

Recently, the CMS collaboration has published the search results for a heavy boson in the $H \to WW$ and $H \to ZZ$ decay channels based on $\sqrt{s} = 7$ and 8 TeV data [98]. No significant signal of new Higgs boson has been found yet, but the upper exclusion limits at 95% confidence level on the production cross section times the branching ratios have been obtained, shown as dashed lines in Figure 7.6. The data only constrain the Higgs in mass range $145 < M_H < 1000$ GeV. When compared with the DY Higgs pair production cross section $\sigma(pp \to W^{\pm} \to H_N^{\pm} H_F^0)$ and the branching ratios $BR(H_F^0 \to WW, ZZ)$, we see the CMS 7+8 TeV exclusion limits are not quite sensitive to constrain our fermiophobic Higgs H_F^0. However, if the 13 and 14 TeV data can improve the current limits by an order of magnitude, these two channels will become quickly sensitive to probe fermiophobic Higgs boson in the intermediate mass range ($\gtrsim 2M_{W,Z}$) and up to ~ 250 GeV.

7.3.2 Diphoton to probe light masses

In contrast to the diboson WW, ZZ channels, the diphoton can probe very light mass range as no threshold effect at all in this channel. The ATLAS collaboration has performed

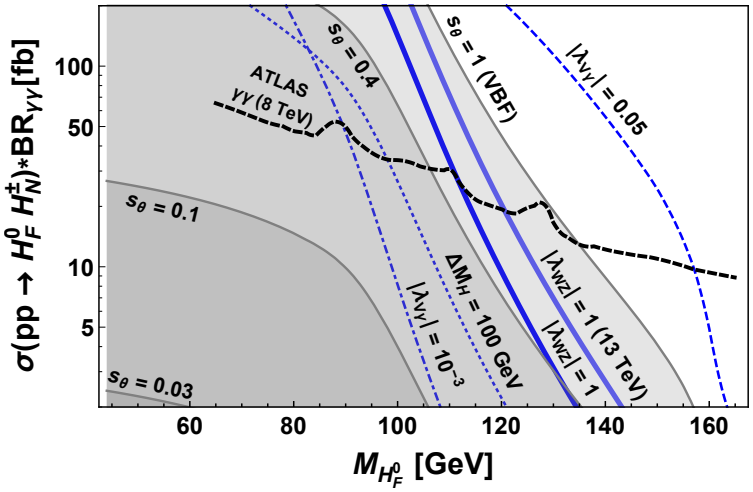

Figure 7.7: The production cross section of $\sigma(pp \to W^{\pm} \to H_F^0 H_N^{\pm})$ at 8 TeV times the branching ratio $BR(H_F^0 \to \gamma\gamma)$, compared with the ATLAS 95% exclusion limits [99].

the analysis of the 8 TeV data of possible scalar particles decaying into two photons in the mass range 65-600 GeV [99]. Similarly, no significant signal for new scalars has been observed, and the results are presented as 95% exclusion limit of the cross section times branching ratios, shown in Figure 7.7. When comparing with DY Higgs pair production $pp \to W^{\pm} \to H_N^{\pm} H_F^0$ times the branching ratios $BR(H_F^0 \to \gamma\gamma)$ by assuming only $W^{\pm}$ loop contributing to the effective couplings $c_{V\gamma}$, we realize the fermiophobic Higgs masses below ~ 115 GeV is ruled out by this ATLAS 8 TeV data. Recently, the latest 13 TeV data from both CMS [100] and ATLAS [101] have come out, but both groups only analyzed data up to 110 GeV diphoton invariant mass. In the future, we would expect the 13 TeV data could push the bound up to 125 GeV when all the diphoton data are released.

However, the exclusion limit $m_{H_F^0} \gtrsim 115$ GeV relies on various assumptions. The first one is that the neutral Higgs H_F^0 has a degenerate mass with charged Higgs $H_N^{\pm}$. If we allow the charged scalar to be heavier than the neutral one $M_{H_N^{\pm}} > M_{H_F^0}$, which quantifies the custodial symmetry breaking effects, the cross-section of the DY Higgs pair production $\sigma(pp \to W^{\pm} \to H_N^{\pm} H_F^0)$ will decrease, shown as the blue dashed curves in Figure 7.7. As a result, the bound on the neutral fermiophobic Higgs mass can be lowered down. Another assumption is that we only include the $W^{\pm}$ boson in the loop contributing to the effective couplings $c_{V\gamma}$. If other charged particles such as charged scalars $H_N^{\pm}$ or charged fermion $f^{\pm}$ enters into the loops in Figure 7.4, we would expect constructive or destructive interfaces

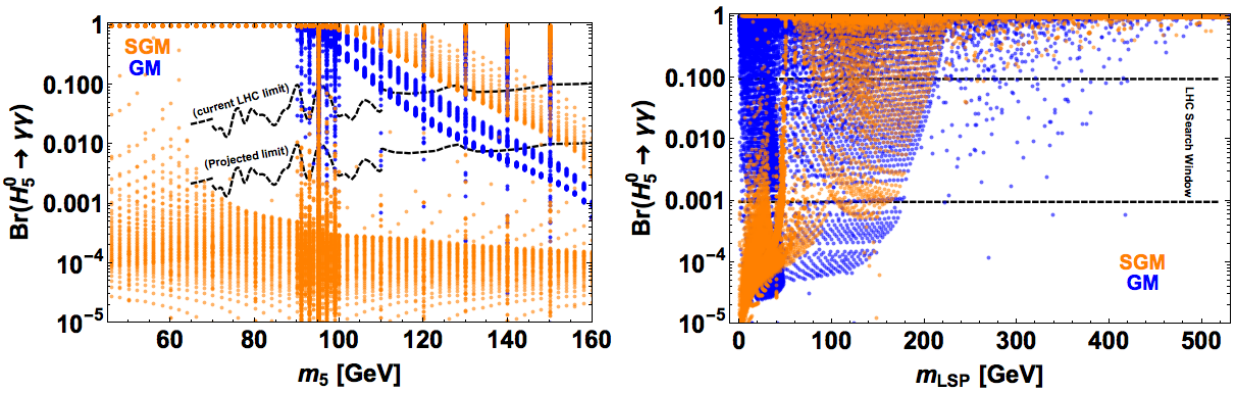

Figure 7.8: The allowed custodial quintuplet branching ratio into photons in the GM (blue) and SGM (orange) models [102].

with the $W^\pm$ loops. By taking $\lambda_{V\gamma} = 10^{-3}$ to quantify the destructive effect, we would lower down the bounds to $M_{H_F^0} \gtrsim 90$ GeV, shown in Figure 7.7. On the contrary, if we allow large charged particles such as doubly charged scalars $H^{\pm\pm}$ or fermions $f^{\pm\pm}$ to run in the $c_{V\gamma}$ loops, or the new charged particles contribute to $c_{V\gamma}$ constructively by the interface with $W^\pm$ loops, we would expect to get large effective couplings $c_{V\gamma}$. For example, with $\lambda_{V\gamma} = 0.05$ shown in Figure 7.7, the bounds on the neutral fermiophobic Higgs mass can be as large as $M_{H_F^0} \gtrsim 160$ GeV. We want to mention that VBF production mode by assuming $s_\theta \approx 1$, this ATLAS 8 TeV diphoton searches would rule out the SM-like scalar with masses below ~ 140 GeV. But this production mode becomes less sensitive when $s_\theta \lesssim 0.1$, which is constrained by the measurements of the exotic contributions to the EWSB.

Besides the mass splitting from the custodial symmetry violation and new charged particles' contribution to $c_{V\gamma}$ loops, there is another possibility which can help us to lower down the exclusion limit of the fermiophobic Higgs mass, which is the invisible decay into the dark sector. Taking the SGM model as an example, we have a whole sector of fermionic superpartners accompanying with the scalars in the GM model. If these fermionic superpartners are light, which is quantified by the LSP mass, we would expect the GM-like scalars to decay into the fermion higgsinos, which would lower down the branching ratios of the neutral scalars H_F^0 decay into photons. As a result, we could allow very low mass neutral fermiophobic scalars as long as the invisible LSP mass is even lower than the neutral H_F^0. Here in Figure 7.8, we show the allowed branching ratios of the quintuplet emerging in the GM and SGM

models, by dividing the latest CMS 8+13 TeV 95% exclusion limit of $\sigma \times BR(H \to \gamma\gamma)$ [100] with DY Higgs pair production cross section $\sigma(pp \to W^{\pm} \to H_5^0 H_5^{\pm})$. We can see a lot of points with low quintuplet mass m_5 are stilled allowed by the current LHC limit, which corresponds to the LSP mass in the SGM model. Furthermore, we have projected the current LHC limit to the future by assuming two orders of magnitude improvement in sensitivity, which is beyond the future LHC diphoton searches, but achievable at future high energy colliders, such as CLIC, ILC, HL-LHC, etc [103].

Part II

Massive quarks in perturbative Quantum Chromodynamics

Chapter 8

QCD factorization theorem

In the first part, we explored Higgs triplet models as a window to the physics beyond the Standard Model, and we used them to predict a large number of new particles, including the Higgs scalars and the superpartners. A remaining fundamental question is how we can directly detect these BSM particles in laboratories. The most powerful experimental machine is the hadron collider, offering the most efficient way to push the energy up to the highest frontier. The physics at hadron colliders strongly relies on our understanding of the proton structure in the framework of quantum chromodynamics (QCD), which is the main subject of this part.

8.1 Factorization theorem

In the last chapter of Part I, we have discussed Higgs production through vector-boson fusion (VBF), associated with vector boson production (VH), and the Drell-Yan (DY) Higgs pair production, see Figures 7.1 and 7.2. However, the primary production mechanism for the SM-like Higgs boson at hadron colliders is gluon fusion $gg \to H$, shown in Figure 8.1. In this section, we will take the gluon fusion as a starting example to demonstrate the QCD factorization theorem.

8.1.1 Higgs production through gluon fusion

With the notation

$$k_1^2 = 0,\ k_2^2 = 0,\ (k_1 + k_2)^2 = p^2 = \hat{s} = M_H^2, \tag{8.1}$$

the partonic cross section can be expressed as

$$\hat{\sigma}(gg \to H) = \frac{1}{2\hat{s}} \int \frac{\mathrm{d}^3 p}{(2\pi)^3 2E_p} (2\pi)^4 \delta^4(k_1 + k_2 - p) |\mathcal{M}|^2. \tag{8.2}$$

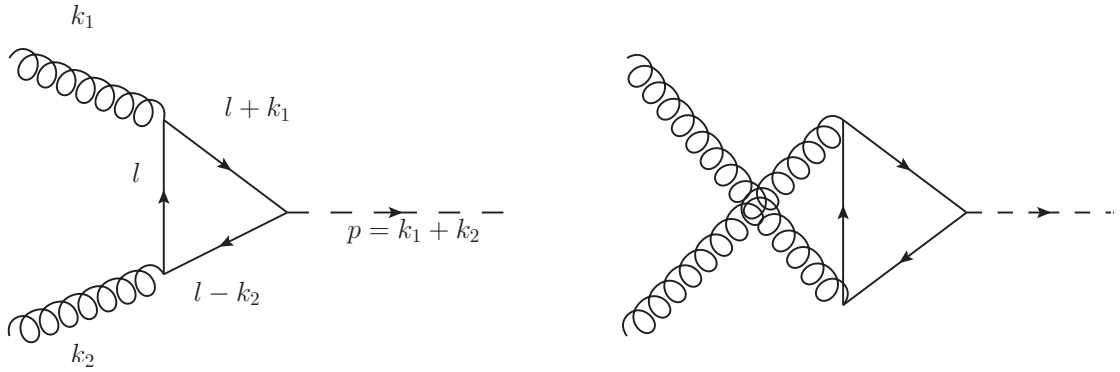

Figure 8.1: The Feynman diagrams for Higgs production through gluon fusion at the lowest order.

The amplitude square $|\mathcal{M}|^2$ already shows up in Equation (6.42). Therefore, we can express the LO partonic cross section in terms of the partial decay width as

$$\begin{aligned}\hat{\sigma}(gg \to H) &= \frac{8\pi^2}{N_g^2 M_H}\Gamma(H \to gg)\int \frac{\mathrm{d}^4 p}{E}\delta^4(k_1 + k_2 - p) \\ &= \frac{\pi^2}{8M_H}\Gamma(H \to gg)\delta(\hat{s} - M_H^2) = \sigma_0 \delta(\hat{s} - M_H^2),\end{aligned} \tag{8.3}$$

where the partial width is

$$\Gamma(H \to gg) = \frac{G_F \alpha_s^2 M_H^3}{36\sqrt{2}\pi^3}\left|\frac{3}{4}A_{1/2}(\tau)\right|^2, \tag{8.4}$$

and

$$\begin{aligned}A_{1/2}(\tau) &= 2[\tau + (\tau - 1)f(\tau)]\tau^{-2}, \\ f(\tau) &= \begin{cases}\arcsin^2\sqrt{\tau} & (\tau \leq 1) \\ -\frac{1}{4}\left[\log\frac{1+\sqrt{1-\tau^{-1}}}{1-\sqrt{1-\tau^{-1}}} - i\pi\right] & (\tau > 1).\end{cases}\end{aligned} \tag{8.5}$$

The τ parameter is defined as $\tau = M_H^2/4m^2$, where m denotes the quark mass running in the triangle loops. The main contribution is from top quark, due to its large Yukawa coupling. Hence, we can safely ignore other SM quarks and only focus on top quark. In turn, we have the final partonic cross section of gluon fusion as

$$\hat{\sigma}(gg \to H) = \frac{G_F \alpha_s^2 M_H^2}{288\sqrt{2}\pi}\left|\frac{3}{4}A_{1/2}(\tau_t)\right|^2 \delta(\hat{s} - M_H^2) = \hat{\sigma}_0 M_H^2 \delta(\hat{s} - M_H^2), \tag{8.6}$$

where the prefactor is defined as $\hat{\sigma}_0 = \frac{G_F \alpha_s^2}{288\sqrt{2}\pi}\left|\frac{3}{4}A_{1/2}(\tau_t)\right|^2$. In the large top quark mass limit $m_t \to \infty$, i.e., $\tau_t \to 0$, we have

$$f(\tau_t) = 0 \implies A_{1/2}(\tau_t) = \frac{4}{3} \implies \hat{\sigma}_0 = \frac{G_F \alpha_s^2}{288\sqrt{2}\pi}. \tag{8.7}$$

The gluons come from the initial hadrons (e.g. protons), shown in Figure 8.2. In

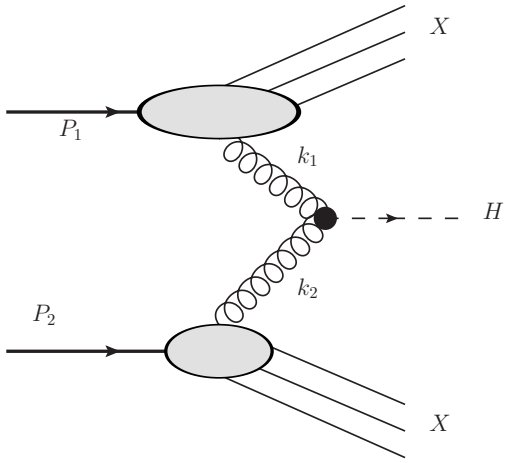

Figure 8.2: The gluon fusion $pp \to H$ in proton-proton collision.

the picture of the parton model or its QCD improved version, the gluon momenta can be parameterized as

$$k_1 = x_1 P_1,\ k_2 = x_2 P_2, \tag{8.8}$$

where

$$P_1 = \frac{\sqrt{s}}{2}(1,0,0,1),\ P_2 = \frac{\sqrt{s}}{2}(1,0,0,-1),\ s = (P_1 + P_2)^2, \tag{8.9}$$

where we neglect the proton mass and work in the center-of-mass frame of the initial-state protons. Here we only consider at the LO to demonstrate the QCD factorization. At a higher order, the gluon can come from splitting of initial-state gluons or quarks. The δ function in Equation (8.6) gives us

$$M_H^2 = p^2 = \hat{s} = (k_1 + k_2)^2 = x_1 x_2 s. \tag{8.10}$$

In the QCD improved parton model, the hadronic cross section can be obtained by weighting the partonic cross section $\hat{\sigma}(gg \to H)$ with the parton distribution functions (PDFs) $f_{g/p}(x)$,

$$\sigma(pp \to H) = \int \mathrm{d}x_1 \mathrm{d}x_2 f_{g/p}(x_1) f_{g/p}(x_2) \hat{\sigma}(gg \to H) = \hat{\sigma}_0 M_H^2 L_{gg}(M_H^2), \tag{8.11}$$

where we define the partonic luminosity as [104]

$$L_{gg}(M_H^2) = \int \mathrm{d}x_1 \mathrm{d}x_2 f_{g/p}(x_1) f_{g/p}(x_2) \delta(\hat{s} - M_H^2) = \frac{1}{s} \int \frac{\mathrm{d}x_1}{x_1} f_{g/p}(x_1) f_{g/p}(\frac{\tau}{x_1}), \tag{8.12}$$

with $\tau = x_1 x_2 = M_H^2/s$ at the LO. In many cases, we shorten the gluon PDF as $g(x) = f_{g/p}(x)$.

8.1.2 The factorization formalism

The hadronic cross section in Equation (8.11) reflects the factorization theorem of Quantum Chromodynamics (QCD). It was first pointed out by Drell and Yan that Bjorken scaling [105] and Feynman's parton model [106, 107], which was developed for deep inelastic scattering (DIS), can be extended to hadron-hadron collision processes [108]. As an example, a massive lepton pair production through quark-antiquark annihilation, or Drell-Yan (DY) process $q\bar{q} \to l^+ l^-$ can be formulated as

$$\sigma(AB) = \sum_{a,b} \int \mathrm{d}x_a \mathrm{d}x_b f_{a/A}(x_a) f_{b/B}(x_b) \hat{\sigma}_{ab}, \tag{8.13}$$

where $f_{a/A}(x)$ is the parton distribution function that in early 1970s was extracted from the structure functions in DIS, and is now extracted from the global analysis of QCD processes.

However, problems arise when perturbative corrections to Equation (8.13) from real and virtual gluon emissions are included. Large logarithms from the collinear gluon emission spoil the perturbation convergence. It was quickly realized that these large logarithms should be absorbed into the redefinition of the parton distribution functions via DGLAP evolution equations [109, 110, 111, 112], which explains the phenomenon of the scaling violation of the structure functions. The magic is that all the logarithms appearing in the collinear parton emission in the corrections to the DY process can be absorbed into renormalized PDFs.

It has been rigorously proved that inclusive scattering cross section of the DIS and DY processes dependent on one typical energy scale $Q \gg 1$ GeV can be systematically factorized into the short-distance and long-distance parts [113, 114]. The short-distance part absorbs hard interactions of partons that can be calculated as a perturbative series in the QCD coupling strength. In contrast, the long-distance part absorbs the nonperturbative effects. It is parameterized by functions describing the distribution of partons in the hadron. For other single-scale QCD observables, we have no rigorous proof of the factorization theorem yet.

Beyond the leading order (LO), we expect the perturbative corrections to the hadronic cross section of Equation (8.13) to be schematically written in the form

$$\sigma = \sum_{a,b} \int \mathrm{d}x_a \mathrm{d}x_b f_{a/A}(x_a, \mu_F) f_{b/B}(x_b, \mu_F)[\hat{\sigma}_0 + \alpha_s(\mu_R)\hat{\sigma}_1 + \cdots] + O(\Lambda_{QCD}/Q). \quad (8.14)$$

Here μ_F is called a factorization scale, symbolizing the scale to separate the long- and short-distance effects, and μ_R is the renormalization scale for renormalization group equation (RGE) running of the strong coupling α_s. Formally, the all-order cross-section, which is a physical observable, does not depend on the choice of the factorization and renormalization scales. That is to say, the cross section calculated to all orders in Equation (8.14) is invariant when varying the artificial parameters μ_F and μ_R. However, obtaining the complete set of higher-order corrections is impractical, which forces us to make a reasonable choice of the two scales to ensure the predictivity of our theoretical calculations. The standard choice is to set the two scales equal to the physical energy scale Q of the hard scattering process[1], to avoid large logarithms, such as $\mu_F = \mu_R = Q = M_{ll}$ for the DY process. Varying these scales yields the scale uncertainty, which can be used as an estimator of the unknown higher-order corrections.

8.1.3 Drell-Yan process

As we mentioned above, the Drell-Yan process corresponds to the lepton pair (e^+e^- or $\mu^+\mu^-$) production in a hadron-hadron collision. In the basic process, a quark and an antiquark annihilate to produce a massive virtual photon, which decays into a lepton pair, $q\bar{q} \to \gamma^* \to l^+l^-$, as shown in Figure 8.3. The total partonic cross section for the DY process at the LO can be obtained from $e^+e^- \to \mu^+\mu^-$ in QED by inserting the appropriate color and electric charge factors,

$$\hat{\sigma}(q\bar{q} \to \gamma^* \to l^+l^-) = \hat{\sigma}_0 \frac{e_q^2}{N_c}, \ \hat{\sigma}_0 = \frac{4\pi\alpha^2}{3\hat{s}}. \quad (8.15)$$

Here e_q is the fractional electric charge of quarks: $e_u = 2/3$ and $e_d = -1/3$, and $N_c = 3$ is the color factor.

As in Equation (8.8), the momenta of the initial partons in the lab frame can be parametrized as

$$k_1 = \frac{\sqrt{s}}{2}(x_1, 0, 0, x_1), \ k_2 = \frac{\sqrt{s}}{2}(x_2, 0, 0, -x_2). \quad (8.16)$$

[1]Sometimes, we multiply by a factor of order unity. That is, $\mu_{F,R} = \xi Q$, where $\xi \sim O(1)$.

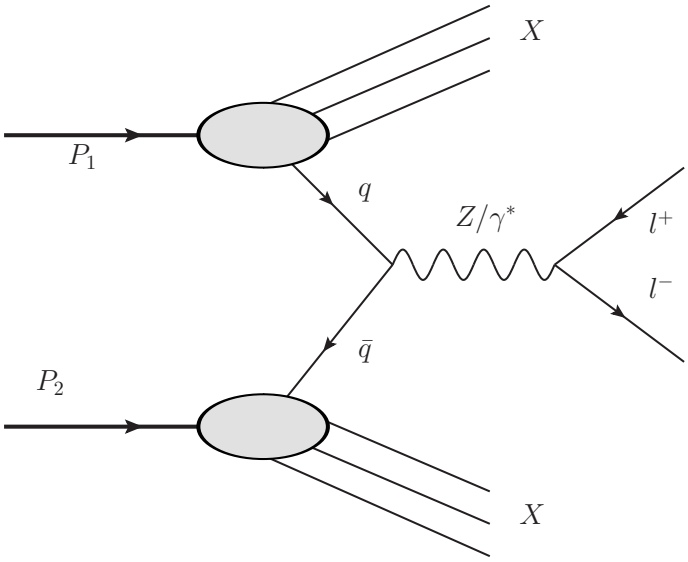

Figure 8.3: The Feynman diagram for the DY process.

At the LO, the momentum conservation gives us the invariant mass of the final-state lepton pair as

$$\hat{s} = M_{ll}^2 = p_{ll}^2 = (k_1 + k_2) = x_1 x_2 s. \tag{8.17}$$

With the definition of rapidity of the lepton pair as

$$y \equiv \frac{1}{2} \log \frac{p_{ll}^0 + p_{ll}^3}{p_{ll}^0 - p_{ll}^3} = \frac{1}{2} \log \frac{x_1}{x_2}, \tag{8.18}$$

we have

$$x_1 = \frac{M_{ll}}{\sqrt{s}} e^y, \; x_2 = \frac{M_{ll}}{\sqrt{s}} e^{-y}. \tag{8.19}$$

In terms of the factorization formalism (8.13), the LO hadronic cross section takes the form

$$\sigma = \int \mathrm{d}x_1 \mathrm{d}x_2 \sum_k \left[q_k(x_1, M_{ll}) \bar{q}_k(x_2, M_{ll}) + \bar{q}_k(x_1, M_{ll}) q_k(x_2, M_{ll}) \right] \hat{\sigma}_0 \frac{e_k^2}{N_c}. \tag{8.20}$$

where we choose the factorization scale to be the invariant mass of the lepton pair, $\mu_F = M_{ll}$. Substituting the integration variables as

$$\mathrm{d}x_1 \mathrm{d}x_2 = \left| \frac{\partial(x_1, x_2)}{\partial(M_{ll}^2, y)} \right| \mathrm{d}M_{ll}^2 \mathrm{d}y = \frac{1}{s} \mathrm{d}M_{ll}^2 \mathrm{d}y, \tag{8.21}$$

we can get the double-differential cross section as

$$\frac{\mathrm{d}\sigma}{\mathrm{d}M_{ll}^2 \mathrm{d}y} = \frac{\hat{\sigma}_0}{N_c s} \sum_k e_k^2 \left[q_k(x_1, M) \bar{q}_k(x_2, M) + \bar{q}_k(x_1, M) q_k(x_2, M) \right]. \tag{8.22}$$

8.2 Deep inelastic scattering

As we mentioned above, deep inelastic scattering (DIS) is another process in which the factorization theorem has been proved rigorously. Because of its relatively simple structure, it has been extensively studied since the SLAC experiment [115, 116, 117], both experimentally and theoretically. DIS is very important for the QCD factorization in two aspects. First, it was the first experiment to see partons as point-like particles inside the hadron, which stimulated the formulation of the parton model [106, 107] and Quantum Chromodynamics (QCD). Second, DIS experiments provide the most precise data to determine the parton distribution functions, which will play a key role in searches for new physics beyond the Standard Model in the future.

8.2.1 Kinematics

The Feynman diagram for deep inelastic scattering at the Born level is illustrated in

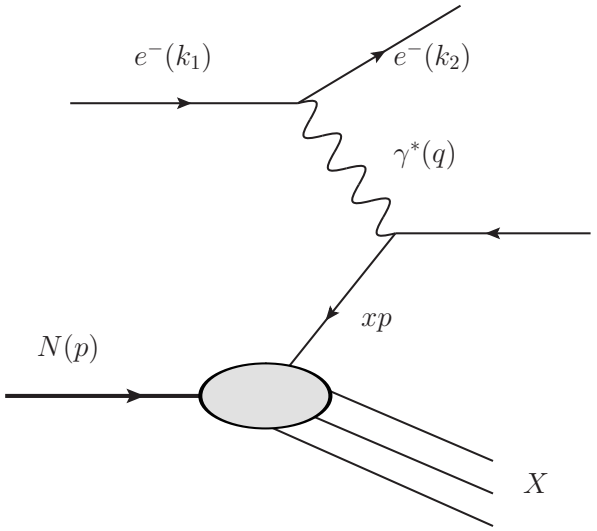

Figure 8.4: The Feynman diagram for deep inelastic scattering $e^-(k_1)N(p) \to e^-(k_2)X$

Figure 8.4. The particle momenta defined in the rest frame of the proton are

$$p = (m_p, 0), \quad k_1 = (E_1, \vec{k}_1), \quad k_2 = (E_2, \vec{k}_2). \tag{8.23}$$

We can define the Lorentz-invariant variables as

$$\begin{aligned} S &= (p+k_1)^2 = p^2 + 2p\cdot k_1 = m_p^2 + 2m_p E_1, \\ \nu &= p\cdot q/m_p = E_1 - E_2, \\ Q^2 &= -q^2 = 2k_1\cdot k_2 = 2E_1E_2(1-\cos\theta), \end{aligned} \tag{8.24}$$

where we have used the zero-mass approximation for lepton $k_1^2 = k_2^2 = 0$. We can introduce the dimensionless variables

$$x = \frac{Q^2}{2p\cdot q} = \frac{Q^2}{2m_p\nu}, \quad y = \frac{q\cdot p}{k_1\cdot p} = \frac{\nu}{E_1} = 1 - \frac{E_2}{E_1}, \tag{8.25}$$

which satisfies

$$0 \le x \le 1, \quad 0 \le y \le 1. \tag{8.26}$$

Hence, all the Lorentz variables can be expressed in terms of S, x and y.

$$\begin{aligned} p\cdot q &= M(E_1 - E_2) = ME_1(1 - E_2/E_1) = Sy/2, \\ Q^2 &= 2xp\cdot q = Sxy, \\ \frac{p\cdot q}{q^2} &= \frac{Sy/2}{-Sxy} = -\frac{1}{2x}. \end{aligned} \tag{8.27}$$

Then, we can integrate the phase space

$$\begin{aligned} \mathrm{d}\Phi &= \frac{\mathrm{d}^3k_2}{(2\pi)^3 2E_2} = \frac{1}{(2\pi)^3 2E_2} 2\pi \mathrm{d}\cos\theta E_2^2 \mathrm{d}E_2 \\ &= \frac{yS}{(4\pi)^2}\mathrm{d}x\mathrm{d}y = \frac{y}{x(4\pi)^2}\mathrm{d}Q^2\mathrm{d}x, \end{aligned} \tag{8.28}$$

where we have integrated out the azimuthal angle $\int \mathrm{d}\phi = 2\pi$. The differential cross section for DIS is

$$\begin{aligned} \mathrm{d}\sigma &= \frac{1}{F}\frac{\mathrm{d}^3k_2}{(2\pi)^3 2E_2}\sum_X (2\pi)^4\delta^4(q - p - p_X)\frac{1}{2}\sum_{s_e}|\mathcal{M}|^2 \\ &= \frac{1}{2S}\mathrm{d}\Phi L_{\mu\nu}\frac{e^4}{q^4}W^{\mu\nu}. \end{aligned} \tag{8.29}$$

Here $F = 4E_1M = 2S$ is the flux factor in the hadron rest frame. The matrix element

$$\frac{1}{2}\sum_{s_e}|\mathcal{M}|^2 = \frac{e^4}{q^4}L_{\mu\nu}\langle H(p)|J_h^\mu|X\rangle\langle X|J_h^\nu|H(p)\rangle \tag{8.30}$$

contains the leptonic tensor $L_{\mu\nu}$ that for $m_e = 0$ takes the form

$$\begin{aligned} L_{\mu\nu} &= \frac{1}{2}\sum_{s_e}\Big[\bar{u}(k_1\gamma_\mu u(k_2)\bar{u}(k_2)\gamma_\nu u(k))\Big] \\ &= \frac{1}{2}\,\mathrm{Tr}[\not{k}_1\gamma_\mu\not{k}_2\gamma_\nu] = 2(k_{1,\mu}k_{2,\nu} + k_{1,\nu}k_{2,\mu} - g_{\mu\nu}k_1\cdot k_2). \end{aligned} \tag{8.31}$$

We define a structure function of the hadron as

$$\begin{aligned} W_H^{\mu\nu}(q,p) &= \sum_X (2\pi)^4 \delta^4(q+p-p_X)\langle H(p)|J_h^\mu|X\rangle\langle X|J_h^\nu|H(p)\rangle \\ &= (-g^{\mu\nu}+\frac{q^\mu q^\nu}{q^2})W_1 + (p^\mu - \frac{p\cdot q}{q^2}q^\mu)(p^\nu - \frac{p\cdot q}{q^2}q^\nu)W_2 \\ &= (g^{\mu\nu}Q^2 + q^\mu q^\nu)\frac{W_1}{-Q^2} + (p^\mu + \frac{q^\mu}{2x})(p^\nu+\frac{q^\nu}{2x})W_2 \\ &= (g^{\mu\nu}Sxy + q^\mu q^\nu)\frac{W_1}{-Sxy} + (2xp^\mu + q^\mu)(2xp^\nu+q^\nu)\frac{W_2}{4x^2}, \end{aligned} \tag{8.32}$$

where we have used the identity $(p_X - p)_\mu \langle X|J_h^\mu|J(p)\rangle = 0$, and in turn $q_\mu W_H^{\mu\nu}(q,p) = q_\nu W_H^{\mu\nu}(q,p) = 0$ because of the $U(1)_{\rm EM}$ Ward identity. Since $q^\mu L_{\mu\nu} = q^\nu L_{\mu\nu} = 0$, we have

$$L_{\nu\mu}W_H^{\nu\mu}(q,p) = 2Sxy W_1 + S^2(1-y)W_2. \tag{8.33}$$

So, we have the fully differential cross section,

$$\frac{{\rm d}\sigma}{{\rm d}x{\rm d}y} = \frac{y\alpha^2}{2Q^4}S[2xyW_1 + S(1-y)W_2], \tag{8.34}$$

which can be also written in terms of (x, Q^2),

$$\frac{{\rm d}\sigma}{{\rm d}x{\rm d}Q^2} = \frac{y\alpha^2}{2Q^2}\left[2yW_1 + S\frac{1-y}{x}W_2\right] = \frac{4\pi\alpha^2}{Q^2}\left[y^2F_1 + F_2\frac{1-y}{x}\right], \tag{8.35}$$

Equation (8.35) contains the structure functions $F_i(x,Q^2)$ that are commonly introduced in modern DIS calculations:

$$F_1(x,Q^2) = W_1/4\pi, \quad F_2(x,Q^2) = SyW_2/8\pi. \tag{8.36}$$

For the charged-current neutrino DIS process,

$$\nu_\mu(k_1) + H(p) \to \mu^-(k_2) + X, \quad \text{or} \quad \bar\nu_\mu(k_1) + H(p) \to \mu^+(k_2) + X. \tag{8.37}$$

we derive the cross sections by following Ref. [118]. We just need to change the propagator and EW couplings in the amplitude,

$$-\frac{e^2}{q^2} \to \frac{1}{8}\frac{g^2}{m_W^2 - q^2} = \frac{G_F}{\sqrt{2}}\frac{m_W^2}{m_W^2+Q^2}. \tag{8.38}$$

If $Q^2 \ll m_W^2$, we can write the differential cross section as

$$\frac{{\rm d}\sigma_{\nu H,\bar\nu H}}{{\rm d}x{\rm d}y} = \frac{G_F^2}{2\pi}2ME\Big[(1-y)F_2^\pm(x,Q^2) + xy^2F_1^\pm(x,Q^2) \pm xy(1-\frac{1}{2}y)F_3^\pm(x,Q^2)\Big]. \tag{8.39}$$

8.2.2 The parton model

Similarly to the hadronic cross section defend in Equation (8.13) at the lowest order in QCD coupling α_s, we can obtain the hadronic tensor by weighting the partonic tensor with the parton distribution function as

$$W^{\mu\nu}(x,Q^2) = \sum_a \int \frac{{\rm d}x}{x} f_a(x) w^{\mu\nu}(x,Q^2), \tag{8.40}$$

where $w^{\mu\nu}$ denotes the partonic tensor:

$$w^{\mu\nu}(x,Q^2) = \langle q|J^\mu|X\rangle\langle X|J^\nu|q\rangle = \sum_X \int \mathrm{d}\Phi_X |\mathcal{M}(\gamma q \to X)|^2 = 2\,\mathrm{Im}\,\mathcal{M}(\gamma q \to \gamma q), \quad (8.41)$$

where we have applied the optical theorem. Therefore, inserting the amplitude of "deeply virtual Compton scattering", we obtain the hadronic tensor as

$$\begin{aligned} W^{\mu\nu}(x,Q^2) =& 2\,\mathrm{Im}\int \frac{\mathrm{d}x}{x} f(x)(-\frac{1}{2})\,\mathrm{Tr}\left[\gamma^\mu \frac{x\not{p}+\not{q}}{(xp+q)^2+i\epsilon}\gamma^\nu x\not{p}\right] \\ =& 2\,\mathrm{Im}\int \frac{\mathrm{d}x}{x} f(x)\frac{1}{2}(-4)\frac{2xp^\mu xp^\nu + xp^\mu q^\nu + xp^\nu q^\mu - g^{\mu\nu}xp\cdot q}{2xp\cdot q - Q^2 + i\epsilon}. \end{aligned} \quad (8.42)$$

Using the imaginary part of the expression,

$$\mathrm{Im}\,\frac{-1}{2xp\cdot q - Q^2 + i\epsilon} = \pi\delta(2xp\cdot q - Q^2) = \frac{\pi}{yS}\delta(x - \frac{Q^2}{2p\cdot q}), \quad (8.43)$$

we obtain

$$\begin{aligned} W^{\mu\nu} &= f(x)\frac{2\pi}{xyS}(2xp^\mu 2xp^\nu + 2xp^\mu q^\nu + 2xp^\nu q^\nu - g^{\mu\nu}xys) \\ &= f(x)\frac{2\pi}{xyS}\Big[-(g^{\mu\nu}Sxy + q^\mu q^\nu) + (2xp^\mu + q^\mu)(2xp^\nu + q^\nu)\Big]. \end{aligned} \quad (8.44)$$

By comparing to the Equation (8.32), we get the structure functions as

$$\begin{aligned} W_1 &= \frac{f(x)}{x}\frac{2\pi}{yS}Q^2 = \frac{f(x)}{x}\frac{2\pi}{yS}Sxy = f(x)2\pi, \\ W_2 &= \frac{f(x)}{x}\frac{2\pi}{yS}4x^2 = 8f(x)x\frac{\pi}{yS}. \end{aligned} \quad (8.45)$$

Substituting $W_{1,2}$ into the Equation (8.34), we get the fully differential cross section for DIS as

$$\begin{aligned} \frac{\mathrm{d}\sigma}{\mathrm{d}x\mathrm{d}y} &= \frac{\alpha^2 y}{2Q^4}S\left[2xyf(x)2\pi + S(1-y)8f(x)x\frac{\pi}{yS}\right] \\ &= \frac{2\pi\alpha^2 S}{Q^4}f(x)x\Big[y^2 + 2(1-y)\Big] = \frac{2\pi\alpha^2 S}{Q^4}f(x)x\Big[1+(1-y)^2\Big]. \end{aligned} \quad (8.46)$$

With the definitions of the structure functions in Equation (8.35), we have

$$\begin{aligned} F_1(x,Q^2) &= \frac{W_1}{4\pi} = \frac{1}{2}\sum_k e_k^2\big[q_k(x) + \bar{q}_k(x)\big], \\ F_2(x,Q^2) &= \frac{SyW_2}{8\pi} = 2xF_1(x,Q^2) = x\sum_k e_k^2\big[q_k(x) + \bar{q}_k(x)\big]. \end{aligned} \quad (8.47)$$

We can define the longitudinal component with the combination of F_1 and F_2 as

$$F_L \equiv F_2 - 2xF_1. \quad (8.48)$$

At the leading order $O(\alpha\alpha_s^0)$ that we are working, we have $F_L = 0$.

We can express the structure functions in terms of PDFs for individual flavors:

$$F_2^{ep}(x,Q^2) = x\left\{\frac{4}{9}\big[u(x) + \bar{u}(x)\big] + \frac{1}{9}\big[d(x) + \bar{d}(x)\big]\right\} + \cdots, \quad (8.49)$$

where the dots represent the contributions from heavy flavors. Partons inside of the proton include both valence and sea quarks,

$$f_u(x) = u(x) = u_v(x) + u_{sea}(x),\ f_{\bar{u}} = \bar{u}(x) = u_{sea}(x), \cdots \tag{8.50}$$

Considering that a proton is made up of three valence quarks, sea (anti)quarks, and gluons, the PDFs in the proton satisfy three sum rules reflecting the quantum numbers of the proton:

- isospin

$$\frac{1}{2}\int \mathrm{d}x(u - \bar{u} - d + \bar{d}) = \frac{1}{2}; \tag{8.51}$$

- strangeness

$$\int \mathrm{d}x(s - \bar{s}) = 0; \tag{8.52}$$

- electric charge

$$\frac{2}{3}\int \mathrm{d}x(u - \bar{u}) - \frac{1}{3}\int \mathrm{d}x(d - \bar{d}) - \frac{1}{3}\int \mathrm{d}x(s - \bar{s}) = 1. \tag{8.53}$$

Consequently, we can obtain the flavor sum rules

$$\int \mathrm{d}x\,(u - \bar{u}) = \int \mathrm{d}x\,u_v = 2,\ \int \mathrm{d}x\,(d - \bar{d}) = \int \mathrm{d}x\,d_v = 1. \tag{8.54}$$

For the charged current (CC) DIS, the basic scattering subprocesses are

$$\begin{aligned} W^+ :&\ \ \nu d \to \mu^- u,\ \nu\bar{u} \to \mu^- \bar{d}, \\ W^- :&\ \ \bar{\nu}u \to \mu^+ d,\ \bar{\nu}d \to \mu^+ u. \end{aligned} \tag{8.55}$$

Following the same derivation, we get the structure function for CC DIS at LO as

$$F_2^{\nu p} = 2x\,(u + \bar{d}),\ F_2^{\bar{\nu}p} = 2x\,(d + \bar{u}). \tag{8.56}$$

Therefore, we obtain the Adler sum rule [119]

$$\int \frac{\mathrm{d}x}{x}(F_2^{\nu p} - F_2^{\bar{\nu}p}) = 2\int \mathrm{d}x\,(u - \bar{u} - d + \bar{d}) = 2. \tag{8.57}$$

Similarly, we can derive the Gross-Llewellyn Smith (GLS) sum rule [120] as

$$\int \mathrm{d}x(u + d + s - \bar{u} - \bar{d} - \bar{s}) = N(q) - N(\bar{q}) = 3, \tag{8.58}$$

which is also referred to as the baryon number sum rule. With the isospin symmetry between the proton and neutron, we would expect the structure function of neutron to be

$$F_2^{en} = x\left[\frac{1}{9}(u + \bar{u}) + \frac{4}{9}(d + \bar{d})\right]. \tag{8.59}$$

Comparing with the proton structure function in Equation (8.49), we obtain the Gottfried sum rule [121]

$$S_G = \int \frac{\mathrm{d}x}{x}(F_2^{ep} - F_2^{en}) = \frac{1}{3}\int \mathrm{d}x(u + \bar{u} - d - \bar{d}) = \frac{1}{3} + \frac{2}{3}\int \mathrm{d}x(\bar{u} - \bar{d}). \tag{8.60}$$

If the quark sea were $SU(2)_{\text{flavor}}$ symmetric, we would have $\bar{u} = \bar{d}$, and $S_G = 1/3$. However, the NMC experiment measured the value $S_G = 0.2281 \pm 0.0065$ at $Q = 4$ GeV for the integration interval $0.004 \leq x \leq 0.8$ [122, 123, 124], which implies a flavor-asymmetric sea.

Finally, the total momentum carried by quarks is given by

$$\langle x \rangle_q = \int \mathrm{d}x x \sum_q (q + \bar{q}) = 1 - \epsilon, \tag{8.61}$$

where the $\epsilon = \int x g \mathrm{d}x = \langle x \rangle_g$ indicates the gluon momentum. Experiment measurements tell us that $\langle x \rangle_q = 0.465 \pm 0.023$ at $Q = 15$ GeV [125], indicating that a large fraction of the proton's momentum is carried by gluons.

8.2.3 QCD corrections

From the quantum field theory point of view, the quark fields in the electric charge currents $J^\mu = \sum \bar{q} \gamma^\mu q$ were effectively free, which is justified by the asymptotic freedom of QCD. However, the radiation of hard gluons from quarks or gluons splitting into quark pairs breaks the naive picture of the parton model, leading to logarithmic violation of the Bjorken scaling. For example, in Figure 8.5, an approximate scaling is observed in the DIS data at $x \approx 0.1$, but apparent scaling violation happens for the lower and higher x. This scaling violation can be systematically explained by including the higher-order QCD corrections. The diagrams of next-to leading order (NLO) correction are shown in Figure 8.6.

Starting at NLO, the DIS structure function is generalized as the convolution of the coefficient functions and the corresponding PDFs,

$$F(x, Q^2) = \sum_i C_i \otimes f_i = \sum_i \int_x^1 \frac{\mathrm{d}y}{y} C_i(\frac{x}{y}, \frac{Q^2}{\mu_F^2}) f_i(y, \mu_F), \tag{8.62}$$

where $\otimes$ denotes the convolution integral, and μ_F is the factorization scale. The structure function, which is a physical observable, should be independent of the choice of factorization scale μ_F when computing to all orders in α_s. That is to say, $F(x, Q^2)$ is invariant when varying μ_F,

$$0 = \frac{\mathrm{d}F}{\mathrm{d}\ln \mu_F^2} = \frac{\mathrm{d}C_i}{\mathrm{d}\ln \mu_F^2} \otimes f_i + C_i \otimes \frac{\mathrm{d}f_i}{\mathrm{d}\ln \mu_F^2}. \tag{8.63}$$

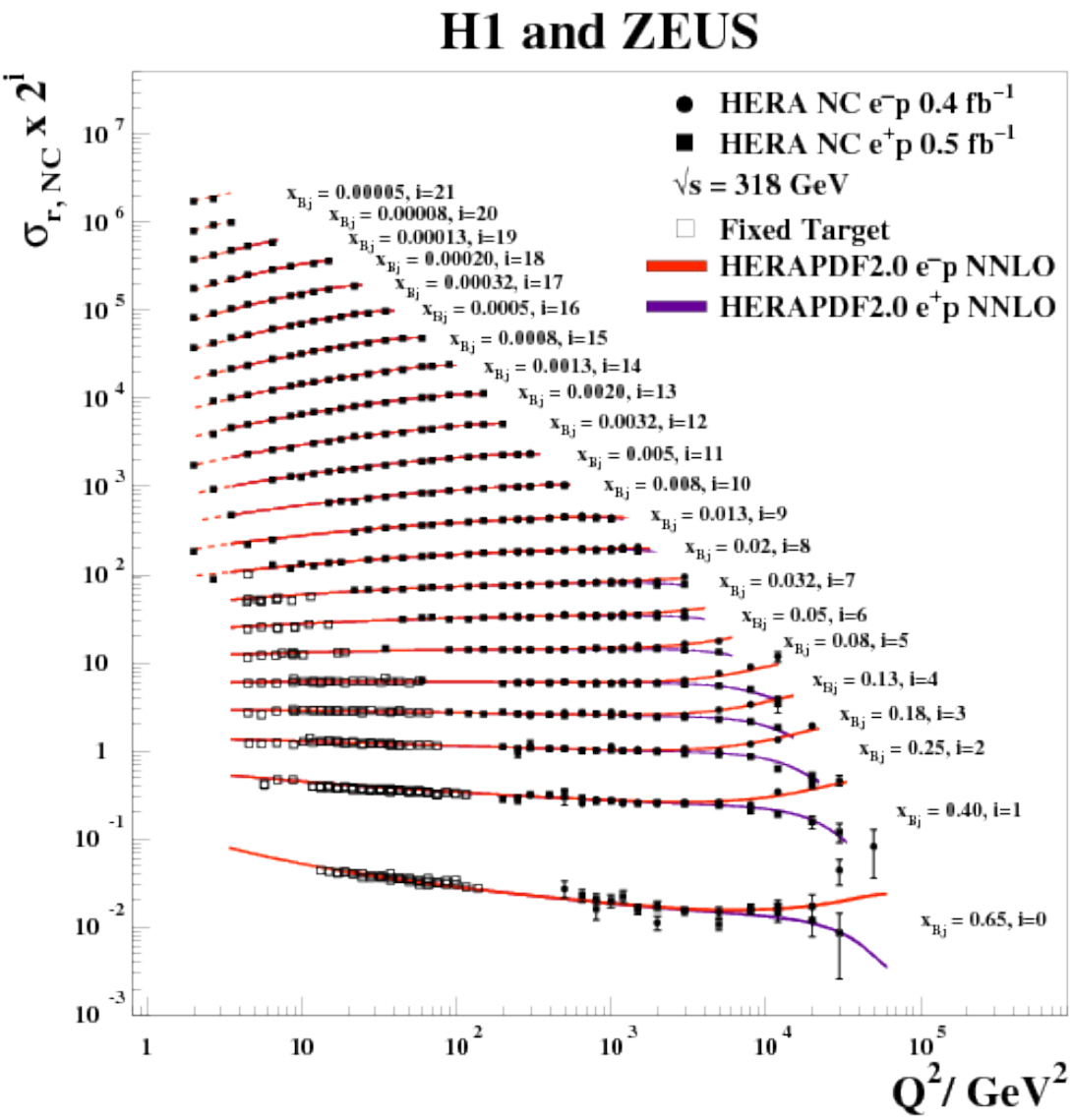

Figure 8.5: The inclusive NC e^+p and e^-p cross section together with fixed-target experiments, BCDMS [126, 127] and NMC [128], compared with the predictions of HERAPDF 2.0 NNLO [129].

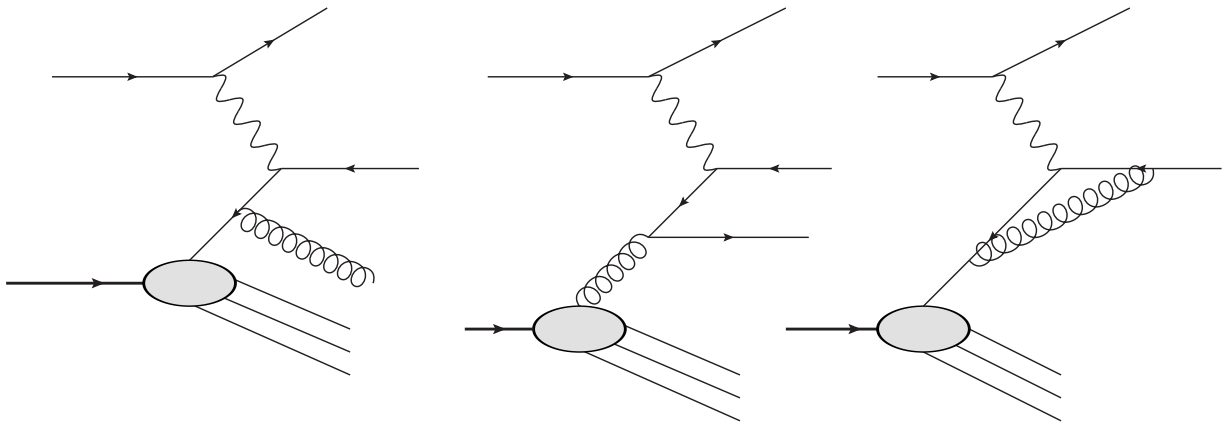

Figure 8.6: The next-to leading order (NLO) corrections to the DIS $e^-(k_1)N(p) \to e^-(k_2)X$.

We implicitly sum over the repeated index $i = q, \bar{q}, g$. The factorization scale dependence of PDFs is governed by the DGLAP evolution equations [109, 110, 111, 112],

$$\frac{\mathrm{d}f_i}{\mathrm{d}\ln\mu_F^2} = \frac{\alpha_s(\mu_R^2)}{2\pi} P_{ij} \otimes f_j. \tag{8.64}$$

Here we evaluate the QCD coupling strength α_s at another "renormalization" scale μ_R that is generally different from the factorization scale μ_F. When solving the DGLAP equations numerically, we normally set the two scales to be the same, $\mu_R = \mu_F$. In the Wilson coefficient function, both scales μ_F and μ_R are normally chosen to be of order of the hard scale Q, even though they don't need to be equal. The strong coupling α_s evolves with the renormalization scale according to the renormalization group equation (RGE),

$$\frac{\mathrm{d}\alpha_s/4\pi}{\mathrm{d}\ln\mu^2} = \beta(\alpha_s) = -\beta_0 \left(\frac{\alpha_s}{4\pi}\right)^2 + \cdots, \tag{8.65}$$

where $\beta_0 = 11 - 2N_f/3$.

If we use a shorthand notation,

$$L \equiv \ln\frac{Q^2}{\mu^2},\ a(\mu^2) \equiv \frac{\alpha_s(\mu^2)}{4\pi},\ a_0 = a(Q^2), \tag{8.66}$$

we can expand the running strong coupling a, PDF f, splitting functions P and coefficient functions in terms of strong couplings a_0. Let us start with the running strong coupling a:

$$a = a_0 + A_1 a_0^2 + A_2 a_0^3 + \cdots. \tag{8.67}$$

The RGE for α_s can be rewritten as

$$\frac{\mathrm{d}a}{\mathrm{d}L} = a(\beta_0 a + \beta_1 a^2 + \cdots). \tag{8.68}$$

Substituting Equation (8.67) into Equation (8.68), we could determine the expansion coefficients $A_{1,2\cdots}$. Therefore, we obtain the perturbative expansion for the scale-dependent coupling as

$$a = a_0 + \beta_0 L a_0^2 + (\beta_0^2 + \beta_1) a_0^3 + \cdots . \tag{8.69}$$

Similarly, we can expand the splitting function P and the PDF f in terms of a_0,

$$\begin{aligned} f_i &= f_i^{(0)} + f_i^{(1)} a_0 + f_i^{(2)} a_0^2 + \cdots , \\ P_{ij} &= P_{ij}^{(0)} a + P_{ij}^{(1)} a + P_{ij}^{(2)} a^2 + \cdots \\ &= P_{ij}^{(0)} a_0 + (\beta_0 L P_{ij}^{(0)} + P_{ij}^{(1)}) a_0^2 + \left[(\beta_0^2 L^2 + \beta_1 L) P_{ij}^{(0)} + 2\beta_0 L P_{ij}^{(1)} + P_{ij}^{(2)} \right] a_0^3 + \cdots , \end{aligned} \tag{8.70}$$

where we have substituted the result of Equation (8.69). Please be careful, the expansion coefficients of splitting functions $P_{ij}^{(0,1,\cdots)}$ are defined in terms of a, not a_0. The DGLAP equation can be written as

$$\frac{\mathrm{d}f_i}{\mathrm{d}L} = -2aP_{ij} \otimes f_j. \tag{8.71}$$

Plugging in the expansion (8.70), we get the perturbative coefficients as

$$\begin{aligned} f_i^{(0)} &= f_{i,0}^{(0)}, \\ f_i^{(1)} &= -L P_{ij}^{(0)} \otimes f_{j,0}^{(0)} + f_{i,0}^{(1)}, \\ f_i^{(2)} &= \frac{1}{2}(L^2 P_{ij}^{(0)} \otimes P_{jk}^{(0)} - 2L P_{ik}^{(1)} - \beta_0 L^2 P_{ik}^{(0)}) \otimes f_{k,0}^{(0)} - L P_{ij}^{(0)} \otimes f_{j,0}^{(1)} + f_{i,0}^{(2)}. \end{aligned} \tag{8.72}$$

Please note, $f_{i,0}^{(k)}$ is the PDF expansion coefficients at the initial scale $\mu_0^2 = Q^2$, while $f_i^{(k)}$ is the coefficients at any scale μ. In our practical PDF parameterization, we have the freedom to choose the initial conditions for DGLAP equation as $f_{i,0}^{(0)} = f_{i,0}$, and set $f_{i,0}^{(k>0)} = 0$.

Now, with the scale invariance condition (8.63), we obtain the structure function at any scale as

$$F(\mu^2) = F(\mu_0^2), \text{ i.e. } C(\mu^2) \otimes f(\mu^2) = C(\mu_0^2) \otimes f(\mu_0^2). \tag{8.73}$$

We can expand the coefficient function at any scale as

$$C_i(x, \alpha_s(\mu^2), L) = \sum_{k=0} a^k \left(c_i^{(k)} + \sum_m^k c_i^{(k,m)} L^m \right). \tag{8.74}$$

The $c_i^{(k)}$ can be calculated perturbatively, such as $c_q^{(0)} = \delta(1-x)$, while $c_g^{(0)} = 0$. The first order corrections $c_i^{(1)}$ are calculated in Ref. [130]. The coefficients of L^m are

$$\begin{aligned} c_i^{(1,1)} &= c_j^{(0)} \otimes P_{ji}^{(0)}, \\ c_i^{(2,1)} &= c_j^{(0)} \otimes P_{ji}^{(1)} \quad + c_j^{(1)} \otimes (P_{ji}^{(0)} - \beta_0 \delta_{ji}), \\ c_i^{(2,2)} &= \frac{1}{2} c_j^{(1,1)} \otimes \quad (P_{ji}^{(0)} - \beta_0 \delta_{ji}), \end{aligned} \tag{8.75}$$

This way, we can get the coefficients at each α_s order recursively. In the next chapter, we will apply this recursive relation to the coefficient functions for heavy-flavor production in the framework of the intermediate mass (IM) scheme up to N3LO.

Chapter 9

Heavy-flavor production in deep inelastic scattering

As we mentioned before, DIS data play a crucial part in probing the parton structure, which is described by parton distribution functions (PDFs). In the next two chapters, we will focus on a practically important question of QCD theory: computation of radiative contributions with massive quarks in deep-inelastic scattering, heavy-flavor hadroproduction, and other such processes. The quark masses arise in perturbative QCD expressions as additional mass scales: modern precise calculations must be based on a QCD factorization formalism that properly accounts for relevant mass effects in the whole range of accessible energies. In the **asymptotic region** where the physical energy scale Q (such as photon virtuality) is much larger than the heavy-quark mass, $Q \gg m_q (q = c, b, t)$, the heavy quark behaves effectively like a massless parton. The large logarithms $\alpha_s^m \log^n(Q^2/m_q^2)$ spoil the convergence of the perturbative expansion and, therefore, need to be resummed into heavy-flavor PDFs. In the **threshold region**, $Q \sim m_q$, quark masses may be non-negligible both in the phase space factor and scattering amplitudes. For instance, DIS at the ep collider HERA has successfully probed the proton structure function at as low as $x \sim 10^{-5}$ [129]. Contribution from charm quark scattering can be as much as 20% of the total DIS cross section, especially at small x. HERA collaborations have published combined measurements of semi-inclusive charm production in DIS, $ep \to eCX$, where C is a charmed meson such as D_0 [131]. For these processes, we have to correctly deal with the heavy-quark mass terms in the DIS structure functions.

9.1 Fixed-flavor number scheme

When the mass of a heavy quark m_q is of the same order or larger than the hard scale Q, its radiative contributions may be included only in the hard cross section, in which the heavy-quark mass is retained; but not in the running QCD coupling, $\overline{\text{MS}}$ masses, or PDFs. That is to say, at such Q values, the heavy quark is included solely in the short-distance cross

section, and does not contribute as an **active parton flavor** [1]. This common theoretical approach is referred to as the **fixed-flavor number** (FFN) scheme. When such a scheme is applied to DIS, heavy quarks can be only produced through virtual photon-gluon fusion into heavy-quark pairs ($\gamma^* g \to c\bar{c}$), which is also called **flavor-creation** (FC) process. The active flavors are renormalized by $\overline{\rm MS}$ subtraction, and inactive flavors by zero-momentum subtraction. In the **decoupling limit** when masses of heavy quarks are much larger than the physical scale of the process, $m_q \gg Q$, graphs involving heavy quarks are suppressed by a power of Q/m_q, which can be safely dropped. The PQCD computations presented in the previous chapters were done for particles whose masses were much smaller than the physical energy, $Q^2 \gg m^2$, so that we could neglect the quark masses by introducing errors of order $\mathcal{O}(m^2/Q^2)$, which corresponded to the **zero-mass** (ZM) Scheme.

However, neither the zero-mass nor the FFN scheme works perfectly in the region when the physical energy is about the same as the quark mass, $Q^2 \sim m_q^2$. In such a case, we need a composite scheme composed of a sequence of subschemes, which transits from the decoupling region, $Q^2 \ll m_q^2$ to the asymptotic region $Q^2 \gg m_q^2$ smoothly. A heavy-quark scheme proposed by Collins, Wilczek, and Zee (CWZ) [132] realizes this idea. In the CWZ scheme, heavy quarks are inactive when $Q^2 \ll m_q^2$, and become active when $Q^2 \gg m_q^2$. In the threshold region $Q^2 \sim m_q^2$, heavy quarks switch from inactive to active flavors when the physical energy scale crosses the transition point $Q^2 = m_q^2$. In such a way, the CWZ scheme realizes a smooth transition from the N_F subscheme to the $N_F + 1$ subscheme. Therefore, it is a **variable flavor number** (VFN) scheme. This scheme has become a standard [133, 134] and was extended to deal with the PDFs for massive quarks under the name of the ACOT scheme [135, 136, 137, 138, 139]. In the subsequent subsection, we will take the charm-flavor production in DIS to demonstrate the idea of the ACOT scheme explicitly.

9.1.1 Massive $N_F = 3$ scheme vs. massless $N_F = 4$ scheme

$Q^2 \gg m_c^2$. When the photon virtuality is much larger than the charm quark mass, we can safely take the charm quark to be active, both in PDFs of proton and also

[1] Active flavors refer to the quarks that contribute as partons to scale dependence of the QCD coupling, particle masses, and the parton distributions inside the hadrons. Light quarks with $m \ll Q$ can be safely treated as active, and heavy quarks with $m \gg Q$ are inactive. Quarks with mass $m \sim Q$ can be treated either active or inactive, depending on the specific scheme.

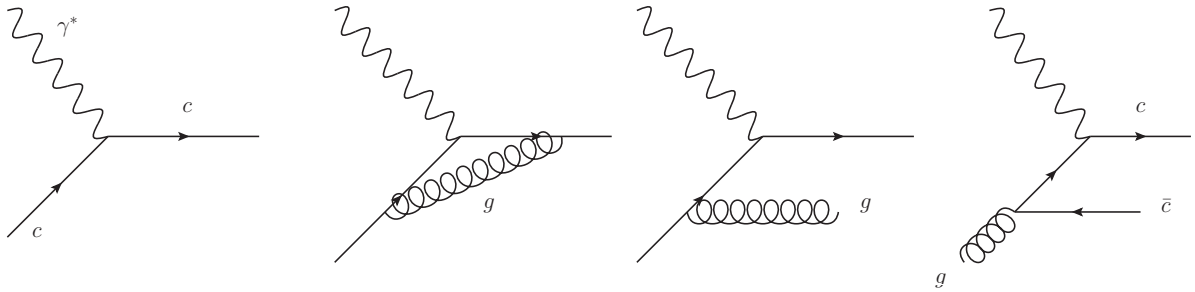

Figure 9.1: The Feynman diagrams contribute to charm production in the massless 4 flavor scheme.

in the running of α_s (i.e., the α_s and PDFs are evaluated with $N_F = 4$ active flavors). The leading order (LO) process comes from **flavor excitation** (FE) of the initial charm parton. The next-to-leading order (NLO) corrections involve virtual loops and the real radiation of an extra gluon, and also the flavor creation (FC) of $c\bar{c}$ pairs. We show the representative Feynman diagrams of the LO and NLO charm production mechanisms in Figure 9.1. Furthermore, we can work in the massless $N_F = 4$ approximation by setting $m_c = 0$, which simplifies our calculations significantly. However, when the energy scale Q goes down towards the threshold region $Q \sim m_c$, the zero-mass approximation becomes unreliable, because the missing higher-order terms $\mathcal{O}(m_c^2/Q^2)$ are no longer negligible. The qualitative behavior of the applicability and uncertainty of structure-function $F_2^c(x, Q)$ as a function of Q, for moderate x, is illustrated in the left panel of Figure 9.2.

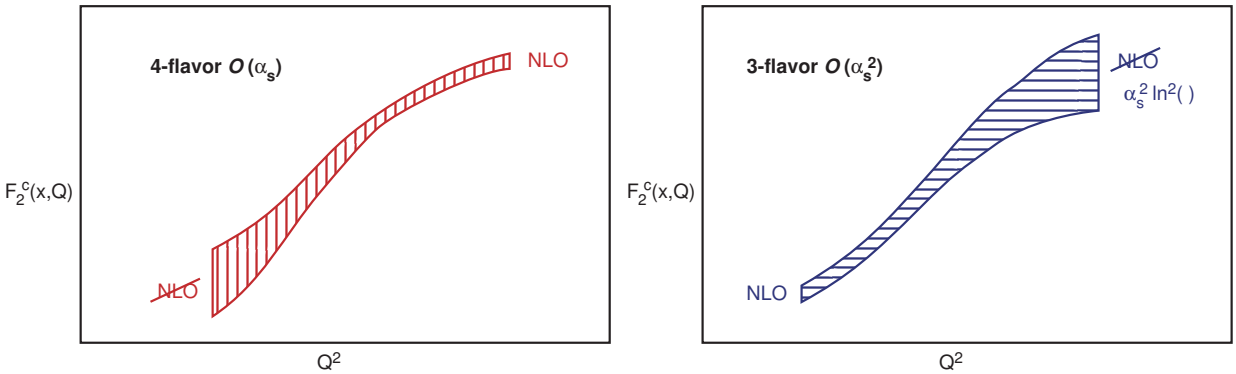

Figure 9.2: The expected reliable regions of the 4-flavor (left) and 3-flavor (right) schemes (taken from Ref. [140]).

$\boldsymbol{Q^2 \sim m_c^2}$. When the physical energy scale is of the same order as the charm quark mass, the charm quark must be treated as a massive particle. As the charm PDF that resums collinear logarithms $\ln(Q^2/m_c^2)$ in the limit of $Q^2 \gg m_c^2$ does not carry real physics near the charm production threshold, the hadronic cross section is best computed in the massive $N_F = 3$ scheme. The leading order of charm production comes from the **flavor creation** (FC) of a $c\bar{c}$ pair shown in the first diagram of Figure 9.3. In this massive $N_F = 3$ scheme, we have to keep the charm mass m_c explicitly through all the calculations, and we use thick lines to denote propagators and external legs for particles with non-zero masses in the Feynman diagrams. In comparison, the thin lines refer to the partons which are treated as massless (i.e., quark masses are neglected in the respective quark wave functions and propagators). The gluon is always massless. In the $N_F = 3$ FFN scheme, the LO Feynman diagram is order of $\alpha\alpha_s$, and the NLO diagrams corresponds to $O(\alpha\alpha_s^2)$ (shown in Figure 9.3 as well). They are much more complicated due to charm mass, m_c, dependence, as we will see in following sections. We would expect this FFN scheme to apply when $Q^2 \sim m_c^2$. However, when the physical energy goes much larger than charm mass $Q \gg m_c$, FFN calculation becomes invalid because the omitted terms $\mathcal{O}(\alpha_s^m \log^n \frac{m_c^2}{Q^2})$ become large and ruin the convergence of perturbative expansions for the Wilson coefficient function. In the limit $m_c \to 0$ or $Q \to \infty$, these logarithmic terms are no longer infrared safe. As a result, we would expect that the uncertainty expands in the $N_F = 3$ scheme when the physical energy increases to $Q \gg m_c$, as demonstrated in the right panel of Figure 9.2.

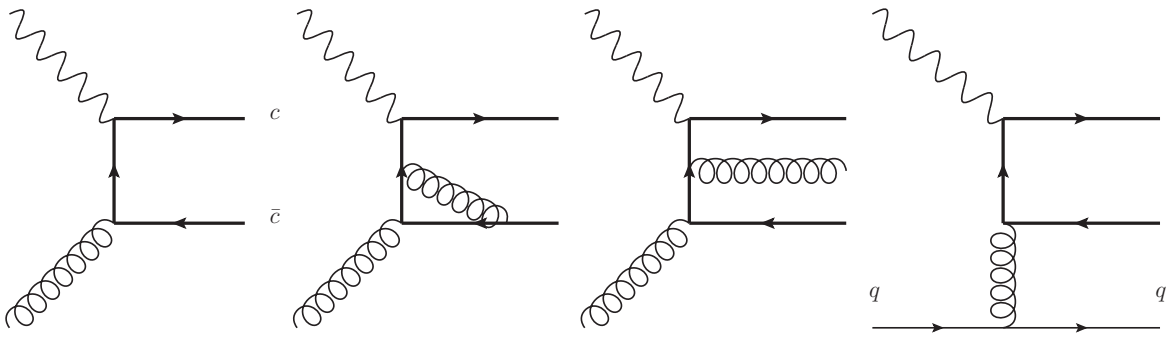

Figure 9.3: The representative Feynman diagrams contribute to charm production in 3 flavor scheme.

9.2 Variable Flavor Number scheme

As we discussed above, neither the zero-mass $N_F = 4$ scheme (mainly FE) nor the massive $N_F = 3$ scheme (mainly FC) works perfectly across the full energy range. But either of them individually works well in its own region of validity. Therefore, it is very natural to come up with a composite scheme that reproduces the advantages of each scheme in its respective kinematic limit. In this new scheme, the active flavor number varies when the energy goes from low $Q(\sim m_c)$ up to high $Q(\gg m_c)$, and therefore, it is a **variable flavor number** (VFN) scheme. A naive idea is to implement a hard switch from the massive $N_F = 3$ scheme to the massless $N_F = 4$ scheme at some intermediate "switching scale", Q, above m_c. But perturbative QCD does not predict the switch point Q_0, and also this approach will create a discontinuity in the hadronic cross section at the switching point.

In order to overcome this discontinuity of the "hard switch" approach, we need to come up with asymptotic **subtraction** terms in order to get the massive $N_F = 4$ scheme of the ACOT family [135, 136, 137, 138, 139], which naturally switches from the massive $N_F = 3$ scheme (mainly FC) to the massless $N_F = 4$ scheme (mainly FE) when Q increases, in the following way:

$$\text{ACOT} = \text{FE} - \text{Subtraction} + \text{FC}. \tag{9.1}$$

Ideally, the subtraction terms will get close to the FE terms asymptotically in the low energy limit ($Q \sim m_c$), and approach to the FC terms in the high-energy limit ($Q \gg m_c$). In such a way, we can realize the switching smoothly as

- $Q \sim m_c$, Subtraction $\simeq$ FE, ACOT $\simeq$ FC, massive $N_F = 3$ scheme;
- $Q \gg m_c$, Subtraction $\simeq$ FC, ACOT $\simeq$ FE, massless $N_F = 4$ scheme.

This idea in Equation (9.1) is depicted in Figure 9.4. The first diagram represents the FE terms, which are the main contribution in $N_F = 4$ scheme. The third diagram stands for the FC terms, in which we have to keep charm quark mass. The middle diagram represents the subtraction terms, which come from the convolution of the gluon splitting function with the Wilson coefficient functions of flavor-excitation terms.

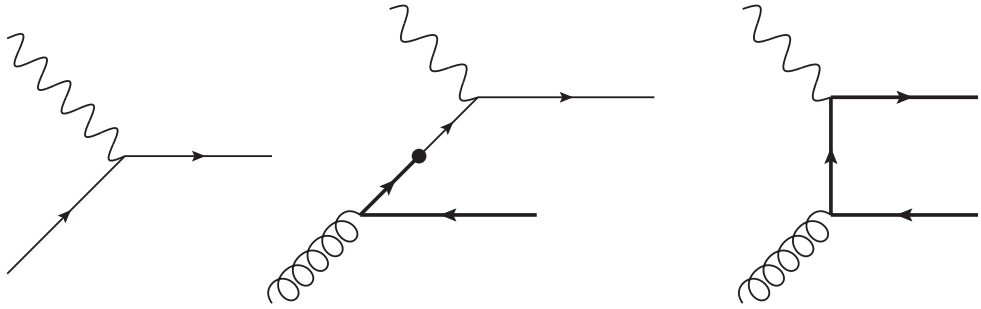

Figure 9.4: The realization of subtraction in VFN scheme. The thick lines indicate the m_c dependence, while think lines represent massless quark. The black point means the convolution in ACOT scheme.

Note that all three terms on the right-hand side of Eq. (9.1) are evaluated by assuming $N_F = 4$, so that the scheme presented in Equation (9.1) is a general-mass $N_F = 4$ scheme. By its construction, its prediction reduces to the massive $N_F = 3$ at $Q \sim m_c$.

To accommodate bottom quarks and even heavier flavors, the practical ACOT scheme increments the number N_F of active flavors as 3, 4, 5,... when Q crosses heavy-quark masses $m_c,\ m_b, ...$ [2] Therefore, the complete ACOT scheme is a **general-mass variable-flavor-number** (GM-VFN) factorization scheme that consists of a series of subschemes with incremented N_F, and with the FE and Subtraction terms introduced like in Equation (9.1).

In the original version of ACOT scheme [135, 136, 137, 138, 139], the heavy quarks are treated as massive in both the FE and the FC terms. Soon, it is realized that we can treat the heavy quark as massless in the FE terms, which simplifies the calculation significantly but without losing the accuracy, which is called Simplified-ACOT scheme [141, 142]. In such a scheme, the FE terms in Equation (9.1) exactly correspond to the massless $N_F = 4$ scheme.

Since the ACOT scheme was proposed as the first realization of GM-VFN scheme, many other similar implementations have been developed for photo-[143], lepto-[144, 145, 146, 147, 148, 149] and hadroproduction [150] of charm as a heavy flavor. Different VFN implementations adopt different subtraction scheme, but the key underlying ideas are the same as Equation (9.1).

[2] The switching from $N_F = i - 1$ to $N_F = i$ need not to happen exactly when $Q = m_i$.

9.2.1 Subtraction term

Let us examine the the inclusive structure function for charm production in DIS to demonstrate explicitly how the subtraction works in the (Simplified-)ACOT scheme. In terms of the factorization theorem, we can write down the structure function as

$$F(x,Q) = \int \frac{\mathrm{d}z}{z} C_a(\frac{x}{z}, \frac{Q^2}{\mu^2}, \frac{m_c^2}{\mu^2}, \alpha_s) f_a(x,\mu) + \mathcal{O}(\alpha_s^{n+1}, \frac{\Lambda^2}{Q^2}, \frac{\Lambda^2}{m_c^2}). \tag{9.2}$$

Here f_a is the parton distribution function, and C_a is the corresponding coefficient function which can be calculated perturbatively up to some order (such as n) of α_s. For charm production, we can write the leading order expression explicitly as

$$\begin{aligned} F_c(x,Q) = C_c^{(0)} c(x,Q) - \alpha_s \log\frac{\mu^2}{m_c^2} \int_x^1 \frac{\mathrm{d}z}{z} C_c^{(0)} P_{c\leftarrow g}\left(\frac{x}{z}\right) g(z,\mu) \\ + \alpha_s \int_x^1 C_g^{(1)}\left(\frac{x}{z}, \frac{m_c}{Q}\right) g(z,\mu), \end{aligned} \tag{9.3}$$

where we have neglected the power suppressed terms proportional to $\Lambda^2 \sim 1\mathrm{GeV}^2$, and the convolution is defined as

$$C \otimes f = \int_x^1 \frac{\mathrm{d}z}{z} C\left(\frac{x}{z}\right) f(z). \tag{9.4}$$

We can shorten Equation (9.3) as

$$F_c = C_c^{(0)} \otimes c - \alpha_s \log\frac{\mu^2}{m_c^2} C_c^{(0)} \otimes P_{c\leftarrow g} \otimes g + \alpha_s C_g^{(1)} \otimes g. \tag{9.5}$$

The first term is the FE term. In the lowest order, its coefficient function can be written as $C_{2,c}^{(0)}(x) = e_c^2 \delta(1-x)$. The third term indicates the lowest order of the FC term, which is the gluon fusion shown in the right panel of Figure 9.4. The second term corresponds to the gluon splitting into the charm, which is counted twice both in the resummed charm PDF and the hard cross section of $c\bar{c}$ production shown in the right panel of Figure 9.4. Therefore, we have to subtract it in order to avoid double-counting, which is the key point of the (Simplified-)ACOT scheme.

In the Simplified-ACOT scheme, we have neglected the quark mass in the FE terms, which destabilizes the numerical cancelation between the FE and the subtraction terms in the threshold region, due to the divergence behavior of $\log(Q^2/m_c^2)$ when $m_c \to 0$. In order to amend this numerical problem, Tung *et. al.* proposed a rescaling $\chi = x(1+4m_c^2/Q^2)$ variable [140], which captures the threshold effect, enforces the momentum-energy conservation in production of the heavy final states, and, therefore, improves the perturbative convergence of the ACOT scheme in the region close to the threshold, $Q \sim m_c$. It can be understood in

terms of the DGLAP equation for the heavy-flavor PDF. In the first-order approximation, we have $P^{(1)}_{c\leftarrow q}(x) = 0$. Together with the initial conditions $c(x, m_c) = 0$, the DGLAP equation for charm PDF reduces to

$$\frac{\mathrm{d}c}{\mathrm{d}\ln\mu^2} = \frac{\alpha_s}{2\pi} P_{c\leftarrow g} \otimes g \implies c \sim \alpha_s \log\frac{\mu^2}{m_c^2} P_{c\leftarrow g} \otimes g. \tag{9.6}$$

In the region $\mu \sim m_c$, we would naively expect the cancellation between flavor-excitation and subtraction terms. However, in the small-x region, the gluon PDF diverges as x^{-p} due to the parameterization guided by Regge theory or $\ln(1/x)$ from BFKL resummation effect. It spoils the cancelation between $c(x, \mu_F)$ and $P_{c\leftarrow g} \otimes g$, because of the mismatch in the higher-order collinear logarithms that they contain. The rescaling variable $\chi = x(1 + 4m_c^2/Q^2)$ pushes the small x up to the kinematic allowed region, which improves the perturbative convergence.

9.2.2 Cancellation between the flavor-creation and subtraction terms

We have introduced a rescaling variable $\chi = x(1+4m_c^2/Q^2)$ in the previous subsection. In the large Q limit, this rescaling variable reduces to the Bjorken x variable, $\chi \to x(Q \to \infty)$. Meanwhile, we would expect that the flavor-creation term is dominated by the subtraction term asymptotically, since $m_c \to 0$. Let us demonstrate this behavior explicitly.

We follow the notations used in Ref. [151]. We consider the hadronic part of the DIS cross section (i.e., the cross section for scattering of the virtual photon scattering on the nucleon). So, for the heavy-quark production in DIS, we have

$$\gamma^*(q) + g(k_1) \to Q(p_1) + \bar{Q}(p_2). \tag{9.7}$$

The corresponding Feynman diagram is shown in the right panel of Fig. 9.4. With $k_1^2 = 0$ and $p_1^2 = p_2^2 = m^2$, we can define the Mandelstam-like variables,

$$\begin{aligned} s' &= s - q^2 = (q + k_1)^2 - q^2 = 2q \cdot k_1, \\ t_1 &= t - m^2 = (k_1 - p_2)^2 - m^2 = -2k_1 \cdot p_2, \\ u_1 &= u - m^2 = (q - p_2)^2 - m^2 = -2q \cdot p_2 + q^2, \end{aligned} \tag{9.8}$$

which satisfy $s' + t_1 + u_1 = 0$. In $D = 4 + \epsilon$ spacetime dimensions, the two-body phase space is

$$\mathrm{d}\Phi_2 = \frac{\mathrm{d}^{D-1}p_1}{(2\pi)^{D-1}2p_1^0} \frac{\mathrm{d}^{D-1}p_2}{(2\pi)^{D-1}2p_2^0} (2\pi)^D \delta^{(D)}(q + k_1 - p_1 - p_2). \tag{9.9}$$

Repeating what we have done before, we work in the center-of-mass frame of $\gamma^* g$ system,

$$q + k_1 = (M, 0) = (p_1^0, \vec{p}_1) + (p_2^0, \vec{p}_2) = (\sqrt{m^2 + p^2}, \vec{p}) + (\sqrt{m^2 + p^2}, -\vec{p}). \tag{9.10}$$

So, we have

$$p_1^0 = p_2^0 = \frac{M}{2}, \quad p = \frac{\sqrt{\lambda(M^2, m^2, m^2)}}{2M} = \frac{M}{2}\sqrt{1 - \frac{4m^2}{M^2}} = \frac{M}{2}\beta. \tag{9.11}$$

The 2-body phase space is

$$\begin{aligned} \mathrm{d}\Phi_2 &= \frac{1}{(2\pi)^{D-2}} \frac{p_1^{D-2} \mathrm{d}p_1 \mathrm{d}\Omega_{D-1}}{2p_1^0 2p_2^0} \delta(q^0 + k_1^0 - p_1^0 - p_2^0) \\ &= \frac{1}{(2\pi)^{D-2}} \frac{p^{D-2}\mathrm{d}p}{4p_1^0 p_2^0} \frac{\delta(p - p^*)}{\frac{p}{p_1^0} + \frac{p}{p_2^0}} \mathrm{d}\Omega_{D-1} \\ &= \frac{1}{(2\pi)^{D-2}} \frac{p^{D-3}}{4(p_1^0 + p_2^0)} \mathrm{d}\Omega_{D-1} \\ &= \frac{1}{(2\pi)^{D-2}} \frac{1}{4M} \Big(\frac{M}{2}\beta\Big)^{D-3} \mathrm{d}\Omega_{D-1}. \end{aligned} \tag{9.12}$$

We can integrate it out to get the volume,

$$V_2^D = \int \mathrm{d}\Phi_2 = \frac{1}{(2\pi)^{D-2}} \frac{1}{4M} \Big(\frac{M}{2}\beta\Big)^{D-3} \Omega_{D-1} \xrightarrow{D=4} \frac{1}{(2\pi)^2} \frac{\pi}{2}\beta. \tag{9.13}$$

Here $\mathrm{d}\Omega_{D-1} = \mathrm{d}\phi \sin^{D-3}\theta \mathrm{d}\theta$, where θ is the angle between $\vec{p}_1$ and $\vec{q}$ in the $\gamma^* g$ center-of-mass frame. We have

$$\begin{aligned} q &= (q^0, 0, 0, \vec{q}), & k_1 &= (k_1^0, 0, 0, -\vec{q}) = |\vec{q}|(1, 0, 0, -1), \\ p_1 &= \frac{M}{2}(1, 0, \beta\sin\theta, \beta\cos\theta), & p_2 &= \frac{M}{2}(1, 0, -\beta\sin\theta, -\beta\cos\theta), \end{aligned} \tag{9.14}$$

where we have used $k_1^2 = (k_1^0)^2 - |\vec{q}|^2 = 0$. Therefore, we have

$$s = M^2 = (q + k_1)^2 = (q^0 + |\vec{q}|)^2, \quad q^2 = (q^0)^2 - |\vec{q}|^2 = -Q^2. \tag{9.15}$$

Solving these equations, we get

$$q^0 = \frac{M^2 - Q^2}{2M}, \quad |\vec{q}| = \frac{M^2 + Q^2}{2M}. \tag{9.16}$$

Previously, we obtained $p = M\beta/2$. Then, the Mandelstam-like variables take the form

$$\begin{aligned} s' &= 2q \cdot k_1 = 2|\vec{q}|(q^0 + |\vec{q}|) = 2|\vec{q}|M = M^2 + Q^2, \\ t_1 &= -2k_1 \cdot p_2 = -2\frac{M}{2}|\vec{q}|(1 - \beta\cos\theta) = -\frac{s'}{2}(1 - \beta\cos\theta), \\ u_1 &= -2q \cdot p_2 + q^2 = -2\frac{M}{2}(q^0 + |\vec{q}|\beta\cos\theta) + (q^0)^2 - |\vec{q}|^2 \\ &= -M|\vec{q}|(1 + \beta\cos\theta) = -\frac{s'}{2}(1 + \beta\cos\theta); \end{aligned} \tag{9.17}$$

and we can verify the relation $s' + t_1 + u_2 = 0$.

In order to explore the infrared-divergent phase-space integral, we go back to Fig. 9.4. We wish to demonstrate the collinear divergence only appear when $m \to 0$, which can be

also regulated by a finite quark mass m. First, let us consider the propagator

$$\frac{\mathrm{i}}{\not{k}_1 - \not{p}_2 - m + \mathrm{i}\epsilon} = \frac{\mathrm{i}(\not{k}_1 - \not{p}_2 + m)}{(k_1 - p_2) - m^2 + \mathrm{i}\epsilon} = \frac{\mathrm{i}(\not{k}_1 - \not{p}_2 + m)}{-2k_1 \cdot p_2 + \mathrm{i}\epsilon} \sim \frac{1}{t_1 + \mathrm{i}\epsilon}. \tag{9.18}$$

Here, we used on-shell condition $k_1^2 = 0$ and $p_2^2 = m^2$. We have the phase space factor

$$\begin{aligned}\int \mathrm{d}\Phi_2 |\mathcal{M}|^2 &\sim \int \frac{1}{(2\pi)^{D-2}} \frac{1}{4M} \Big(\frac{M}{2}\beta\Big)^{D-3} \mathrm{d}\Omega_{D-1} \frac{1}{(2k_1 \cdot p_2)^2} \\ &= \int \frac{1}{(2\pi)^{D-2}} \frac{1}{4M} \Big(\frac{M}{2}\beta\Big)^{D-3} \mathrm{d}\phi \sin^{D-3}\theta \mathrm{d}\theta \frac{1}{(\frac{s'}{2})^2 (1-\beta\cos\theta)^2} \\ &= \frac{1}{(2\pi)^{D-2}} \frac{1}{4M} \Big(\frac{M}{2}\beta\Big)^{D-3} 2\pi \Big(\frac{2}{s'}\Big)^2 \mathcal{I}(D,\beta),\end{aligned} \tag{9.19}$$

where we define the factor $\mathcal{I}(D,\beta)$ as

$$\begin{aligned}\mathcal{I}(D,\beta) &= \int_0^\pi \sin^{D-3}\theta \mathrm{d}\theta \frac{1}{(1-\beta\cos\theta)^2} \\ &= \frac{\sqrt{\pi}\Gamma(\frac{D}{2}-1)\Big[(D-4)\,{}_2F_1(1,\frac{D-2}{2};D-2;\frac{2\beta}{\beta+1}) - (\beta+1)(D-3)\Big]}{(\beta-1)(\beta+1)^2\Gamma(\frac{D-1}{2})}\end{aligned} \tag{9.20}$$

The hypergeometric function is defined as

$${}_2F_1(a,b;c;z) = \sum_{n=0}^{\infty} \frac{(a)_n (b)_n}{(c)_n} \frac{z^n}{n!}, \quad \text{where} \quad (q)_n = \begin{cases} 1, & n = 0; \\ q(q+1)\cdots(q+n-1) & n > 0. \end{cases} \tag{9.21}$$

We expand this integral $\mathcal{I}(D,\beta)$ around $D = 4$,

$$\mathcal{I}(D,\beta) = -\frac{2}{\beta^2-1} + \frac{(D-4)\Big[\beta(-2+\gamma+\psi^{(0)}(\frac{3}{2})) - \ln\big(1-\frac{2\beta}{\beta+1}\big)\Big]}{\beta(\beta^2-1)} + O\Big((D-4)^2\Big), \tag{9.22}$$

where $\psi^{(0)}(z) = \Gamma'(z)/\Gamma(z)$. We can easily to see that, when $D = 4$, the integral becomes

$$\mathcal{I}(4,\beta) = -\frac{2}{\beta^2-1} = \frac{1}{1-\beta} + \frac{1}{2} + \frac{1-\beta}{4} + \cdots. \tag{9.23}$$

For the massless particle $m = 0$, we have the threshold function $\beta = 1$, which results in infrared (IR) divergence. In contrast, if we assign a small mass to the massless particles, such as m_γ for photon, which will serve as an infrared cutoff to regulate the IR divergence. Similarly, if we impose a cutoff for the transverse momentum (p_T) of this massless particle, which serves as an effective mass, and regulate the IR divergence in turn.

With the assumption $m = 0$, the integration becomes

$$\begin{aligned}\mathcal{I}(D,1) &= \int_0^\pi \sin^{D-3}\theta \mathrm{d}\theta \frac{1}{(1-\cos\theta)^2} = \int_0^\pi \sin^{D-4}\theta \mathrm{d}\cos\theta \frac{1}{(1-\cos\theta)^2} \\ &= \int_{-1}^1 (1-x^2)^\epsilon \mathrm{d}x \frac{1}{(1-x)^2} = \frac{\sqrt{\pi}\Gamma(\epsilon+1)}{(\epsilon-1)\Gamma(\epsilon+1/2)}, \quad (\mathrm{Re}\,\epsilon > 1)\end{aligned} \tag{9.24}$$

where we have set $D = 4 + 2\epsilon$. The condition $\mathrm{Re}\,\epsilon > 1$ means this integral only converges when $D > 6$.

Equipped with these results, we can write down the partonic structure tensor for $\gamma^*(q) + g(k_1) \to c(p_1) + \bar{c}(p_2)$ as

$$W_{\mu\nu} = \frac{1}{2s'} \frac{1}{2(1+\epsilon)} \frac{1}{N_c^2 - 1} M_\mu M_\nu^* \mathrm{d}\Phi_2. \tag{9.25}$$

We can decompose this structure tensor as

$$\begin{aligned} W_{\mu\nu} =& \mathrm{d}\sigma_T \left(-g_{\mu\nu} + \frac{q_\mu q_\nu}{q^2} \right) + \\ & \left(k_{1\mu} - \frac{k_1 \cdot q}{q^2} q_\mu \right) \left(k_{1\nu} - \frac{k_1 \cdot q}{q^2} q_\nu \right) \frac{-4q^2}{s'^2} (\mathrm{d}\sigma_T + \mathrm{d}\sigma_L). \end{aligned} \tag{9.26}$$

With projection operators $g^{\mu\nu}$ and $k_1^\mu k_1^\nu$, we can decompose the partonic cross section as

$$\mathrm{d}\sigma_G = -\frac{1}{2(1+\epsilon)} g^{\mu\nu} W_{\mu\nu}, \quad \mathrm{d}\sigma_L = -\frac{4q^2}{s'^2} k_1^\mu k_1^\nu W_{\mu\nu}. \tag{9.27}$$

The transverse partonic cross section can be obtained via

$$\mathrm{d}\sigma_T = \mathrm{d}\sigma_G + \frac{1}{2(1+\epsilon)} \mathrm{d}\sigma_L. \tag{9.28}$$

In the following, we write a universal expression for the cross section

$$\mathrm{d}\sigma_i = C_i |M|^2 \mathrm{d}\Phi_2, \tag{9.29}$$

where $i = G, L$. The squared matrix elements are written in terms of

$$\begin{aligned} |M_G|^2 &= -g^{\mu\nu} M_\mu(\gamma^* g \to c\bar{c}) M_\nu^*(\gamma^* g \to c\bar{c}), \\ |M_L|^2 &= -\frac{4q^2}{s'^2} k_1^\mu k_1^\nu M_\mu(\gamma^* g \to c\bar{c}) M_\nu^*(\gamma^* g \to c\bar{c}). \end{aligned} \tag{9.30}$$

The constant prefactor is

$$C_i = \frac{1}{2(1+\epsilon)} a_i \frac{1}{2s'} \frac{1}{2(1+\epsilon)} \frac{1}{N_c^2 - 1}, \ a_G = 1, \ a_L = 2(1+\epsilon). \tag{9.31}$$

With the the algebraic calculations in `FormCalc` [78], we obtain the squared amplitudes as

$$|M_i|^2 = 8g^2 (e_c e)^2 N_c C_F B_i, \tag{9.32}$$

where

$$\begin{aligned} B_G =& \frac{u_1}{t_1} + \frac{t_1}{u_1} + \frac{2q^2 s}{t_1 u_1} + \frac{4m^2 s'}{t_1 u_1} \left(1 - \frac{m^2 s'}{t_1 u_1} \right) + \frac{2m^2 q^2}{t_1 u_1} \left(2 - \frac{s'^2}{t_1 u_1} \right) \\ & + \epsilon \left(-1 + \frac{s'^2}{t_1 u_1} + \frac{s' q^2}{t_1 u_1} + \frac{q^4}{t_1 u_1} - \frac{m^2 q^2 s'^2}{t_1^2 u_1^2} \right) + \epsilon^2 \frac{s'^2}{4 t_1 u_1} \\ B_L =& -\frac{4q^2}{s'^2} \left(s - \frac{m^2 s'^2}{t_1 u_1} \right), \end{aligned} \tag{9.33}$$

with $e_c = 2/3$, and $C_F = (N_c^2 - 1)/2N_c = 4/3$. Comparing the structure tensor (9.26) with our old definitions for the structure functions in Equations (8.32) and (8.36), we can obtain the structure functions written as

$$F_k = \frac{Q^2}{4\pi^2 \alpha} \sigma_k (k = 2, L), \ \sigma_2 = \sigma_G + 3\sigma_L/2. \tag{9.34}$$

We remind readers that the longitudinal structure function is defined as $F_L = F_2 - 2xF_1$.

At the lowest order, we have

$$F_k = \frac{Q^2\alpha_s}{4\pi^2 m^2}\int_\chi^1 \frac{\mathrm{d}z}{z} e_c^2 C_{k,g}^{(1)}(\frac{x}{z},\frac{Q^2}{m^2}) g(z,\mu^2),\ \chi = x(1+4m^2/Q^2), \tag{9.35}$$

where the lower boundary χ arises from the threshold effect. In the asymptotic limit $Q^2 \gg m^2$, we have $\chi \to x$, and the coefficient functions become very simple,

$$\begin{aligned} C_{L,g}^{(1)}(z,\frac{Q^2}{m^2}) &= T_F[16z(1-z)], \\ C_{2,g}^{(1)}(z,\frac{Q^2}{m^2}) &= T_F\left[4(1-2z+2z^2)\left(\ln\frac{Q^2}{m^2}+\ln(1-z)-\ln z\right)-4+32z-32z^2\right], \end{aligned} \tag{9.36}$$

where $T_F = 1/2$. We know that the splitting function is $P_{c\leftarrow g}(x) = T_F(1+2x-2x^2)$, and the leading order coefficient functions are

$$C_{L,c}^{(0)} = 0,\ C_{2,c}^{(0)}(x) = \delta(1-x). \tag{9.37}$$

Therefore, in the large Q limit, the subtraction term in Equation (9.1) can be written as

$$\begin{aligned} \text{Subtraction} &= -\alpha_s \ln\frac{Q^2}{m^2}\int_x^1 \frac{\mathrm{d}y}{y}\delta(1-\frac{x}{y})\int_y^1 \frac{\mathrm{d}z}{z} T_F\left[1+2\frac{y}{z}-2\left(\frac{y}{z}\right)^2\right] g(z,\mu) \\ &= -\alpha_s \ln\frac{Q^2}{m^2}\int_x^1 \frac{\mathrm{d}z}{z} T_F\left[1+2\frac{x}{z}-2\left(\frac{x}{z}\right)^2\right] g(z,\mu), \end{aligned} \tag{9.38}$$

which exactly cancels the large logarithm term in Equations (9.35) and (9.36).

9.2.3 The Intermediate-mass scheme

From the last subsection, we learn two lessons. First, we have demonstrated the complexity of treatment of the mass-dependent coefficient functions of the flavor-creation terms. Second, the threshold effect in the exact FC terms like Equation (9.35) inspires us to introduce the rescaling variable in the S-ACOT-χ scheme [140] in the flavor-excitation and subtraction terms as well. When the higher-order corrections to DIS with full mass dependence are not available, we can combine the rescaling variable χ and the massless coefficient functions as an intermediate step to approximate the full mass dependence that would be predicted in the general mass (GM) scheme. This idea was first introduced as an intermediate-mass (IM) scheme in Ref. [152], which employs the zero-mass coefficients and the rescaling variable to approximate the quark mass dependence due to phase space in DIS at NLO and beyond.

Furthermore, we can generalize the rescaling χ to a more flexible variable $\zeta(\lambda)$ defined as the solution of

$$x = \frac{\zeta}{1+\zeta^\lambda 4m_c^2/Q^2}. \tag{9.39}$$

Factorization schemes	Mass dependence in the FC terms	Mass dependence of the FE and subtraction terms	Introduce heavy-quark PDFs at large Q
FFN	Exact	N/A	no
ZM	None	None	yes
IM	Approximate	Approximate	yes
GM	Exact	Approximate	yes

Table 9.1: Treatment of mass dependence in various heavy-quark factorization schemes.

As the purpose of the rescaling variable is to *approximately* reproduce in the FE and subtraction terms the kinematic constraint from integration over mass-dependent phase space in the FE term, we introduce a new parameter λ, which allows us to tune this approximate mass effect better, depending on the specific values of Bjorken x and Q. In the limit $\lambda = 0$, the new variable becomes the traditional rescaling variable, $\chi = \zeta(0)$. In the opposite limit $\lambda \to \infty$, we have $\zeta(\infty) = x$, which corresponds to no rescaling in the plain S-ACOT scheme [141, 142]. The practical numerical value of the λ parameter can be obtained by fitting the full mass dependence in the general mass cross section, if available. Usually, the exact FE and FC terms are very difficult to calculate, especially at high orders of α_s. In the IM scheme, we can extract the λ value from a lower-order calculation and apply it to approximate higher-order coefficient functions using the zero-mass coefficients. Treatment of heavy-quark mass dependence in the FFN, ZM, IM and GM factorization schemes is compared in Table 9.1.

9.3 Structure functions at N3LO in the IM scheme

The ACOT scheme was applied to compute inclusive and semi-inclusive DIS cross section with massive quarks at NLO in Refs. [135, 136, 137]. Its simplified version [141, 142] that uses the rescaling variable [140] was extended to compute these DIS cross sections at the NNLO level [153]. Equipped with the techniques of the intermediate-mass scheme, we are able to extend this calculation up to N3LO level $O(\alpha\alpha_s^3)$. Here we summarize the N3LO calculation for DIS in the IM scheme performed together with Bowen Wang and previously reported in [154].

9.3.1 The flavor structure

Let us start with the solution to the DGLAP equations that govern the evolution of PDFs with the factorization scale μ:

$$\frac{\partial f_i(x,\mu^2)}{\partial \ln \mu^2} = \sum_{j=q,\bar{q},g} \int_x^1 \frac{\mathrm{d}z}{z} P_{ij}\left(\frac{x}{z},\mu^2\right) f_j(z,\mu^2). \tag{9.40}$$

With the following definition of convolution,

$$[f\otimes g](x) = \int_x^1 \frac{\mathrm{d}z}{z} f\left(\frac{x}{z}\right) g(z) = \int_x^1 \frac{\mathrm{d}z}{z} f(z) g\left(\frac{x}{z}\right), \tag{9.41}$$

we can write down the DGLAP equations as

$$\frac{\partial f_i}{\partial \ln \mu^2} = \sum_{j=q,\bar{q},g} P_{ij}\otimes f_j. \tag{9.42}$$

The splitting functions have the following symmetry properties [155],

$$\begin{aligned} P_{gq_i} &= P_{g\bar{q}_i} = P_{gq}, & P_{q_iq_k} &= P_{\bar{q}_i\bar{q}_k} = \delta_{ik}P^v_{qq} + P^s_{qq}, \\ P_{q_ig} &= P_{\bar{q}_ig} = \frac{1}{2N_F}P_{qg}, & P_{q_i\bar{q}_k} &= P_{\bar{q}_iq_k} = \delta_{ik}P^v_{q\bar{q}} + P^s_{q\bar{q}}. \end{aligned} \tag{9.43}$$

Therefore, we can decompose the DGLAP equations (9.42) in terms of the singlet quark PDF q_s and the non-singlet quark PDFs $q_v, q^\pm_{ij}$,

$$q_s = \sum_{i=1}^{N_F}(q_i+\bar{q}_i),\ q_v = \sum_{i=1}^{N_F}(q_i-\bar{q}_i),\ q^\pm_{ij} = (q_i\pm\bar{q}_i) - (q_j\pm\bar{q}_j). \tag{9.44}$$

Equation (9.42) becomes

$$\frac{\partial}{\partial\ln\mu^2}\begin{pmatrix} q_s \\ g\end{pmatrix} = \begin{pmatrix} P_{qq} & P_{qg} \\ P_{gq} & P_{gg}\end{pmatrix}\otimes\begin{pmatrix} q_s \\ g\end{pmatrix},\ \frac{\partial q_v}{\partial\ln\mu^2} = P_v\otimes q_v,\ \ \frac{\partial q^\pm_{ij}}{\partial\ln\mu^2} = P_\pm\otimes q^\pm_{ij}, \tag{9.45}$$

with the combination of splitting functions as

$$P_{qq} = P^v_{qq} + P_{q\bar{q}} + N_F(P^s_{qq}+P^s_{q\bar{q}}),\ P_v = P^v_{qq} - P^v_{q\bar{q}} + N_F(P^s_{qq}-P^s_{q\bar{q}}),\ P_\pm = P^v_{qq}\pm P^v_{q\bar{q}}. \tag{9.46}$$

As a result, we get the non-singlet PDFs $q^\pm_{ij}$ and q_V evolve independently, and the singlet PDF evolves together with the gluon PDF. For a specific flavor, we can introduce the linear combinations as

$$q^\pm_i = q_i\pm\bar{q}_i,\ q^+_{i,ns} = q^+_i - \frac{1}{N_F}q_s. \tag{9.47}$$

Then Equation (9.45) becomes

$$\frac{\partial q^+_{i,ns}}{\partial\ln\mu^2} = P^+_{ns}\otimes q^+_{i,ns},\ \frac{\partial q^-_i}{\partial\ln\mu^2} = P^-_{ns}\otimes q^-_i. \tag{9.48}$$

We do not consider the minus component q^-_i here, because it only arise in cross sections that are asymmetric with respect to crossing symmetry, such as $F_3^{\nu N+\bar{\nu}N}$ in neutrino scattering through W-boson change. Therefore, we leave out the + sign in the non-singlet PDF and denote them as $q_{i,ns}$ without causing any confusion.

In this singlet and non-singlet basis, the structure functions need to be decomposed accordingly as

$$F_k(x,Q^2) = x\left\{\sum_i^{N_F} e_i^2 c_{k,ns}\otimes q_{i,ns} + \frac{1}{N_F}\sum_i^{N_F} e_i^2\left[c_{k,s}\otimes q_s + c_{k,g}\otimes g\right]\right\},\ k=2,L. \tag{9.49}$$

The e_i is the electric charge of a quark flavor, i.e. +2/3 for up-type quarks, and -1/3 for down-type quarks. With the definition of $q_{i,ns} = q_i^+ - \frac{q_s}{N_F}$, we have

$$F_k(x,Q^2(x) = x\left\{\sum_i^{N_F} e_i^2 c_{k,ns}\otimes q_i^+ + \frac{1}{N_F}\sum_i^{N_F} e_i^2\left[(c_{k,s}-c_{k,ns})\otimes q_s + c_{k,g}\otimes g\right]\right\}. \tag{9.50}$$

Therefore, we can define the pure singlet [156, 157], with the coefficient functions as

$$c_{k,ps} = c_{k,s} - c_{k,ns},\ k=2,L. \tag{9.51}$$

9.3.2 Flavor classes

In Equation (9.49), scattering contributions for quarks of different flavors in DIS at N3LO will be associated with Feynman diagrams of several topologies. Let us review the topological classes of Feynman diagrams that will arise. We follow Refs. [156, 157] to category the Feynman diagrams into 5 groups, and show the representative 3-loop diagrams in Figure 9.5. Here, the handbag diagrams are the cut ones, corresponding to the terms in squared amplitude $\mathcal{M}^\mu\mathcal{M}^{\nu *}$.

We first define the electric charge matrix as

$$\hat{Q} = \mathrm{diag}(-\frac{1}{3},\frac{2}{3},-\frac{1}{3},\cdots),\ \ \mathrm{Tr}\,\hat{Q} = \sum_i e_i,\ \ \mathrm{Tr}\,\hat{Q}^2 = \sum_i e_i^2. \tag{9.52}$$

The charge matrix $\hat{Q}$ consists of vertex factors e_i for the photon couplings $e_i e A_\mu \bar{q}_i\gamma^\mu q_i$ to quark flavors i. $\hat{Q}$ arises in squared amplitudes with virtual quark loops. An internal quark loop, with one or two external photon attached to it, runs over N_F active quark flavors, and therefore contributes with a factor $\mathrm{Tr}\,\hat{Q}$ or $\mathrm{Tr}\,\hat{Q}^2$. If a virtual loop with a quark propagator is attached only to the gluons, as in the gluon polarization diagram, all active contributes equally, given rise to a prefactor N_F in the contribution of this loop to $|\mathcal{M}|^2$.

With the help of charge matrix $\hat{Q}$, we are able to classify all the Feynman diagrams with massless quarks and up to three loops into 5 groups or flavor classes (FC). The first flavor class, FC_2, represents diagrams with both external photons attached to the same external quark line, as shown in Figure 9.5a. After summation over all quark and antiquark flavors, they contribute with an overall prefactor $\hat{Q}^2$. Classes FC_{02} contains Feynman diagrams in

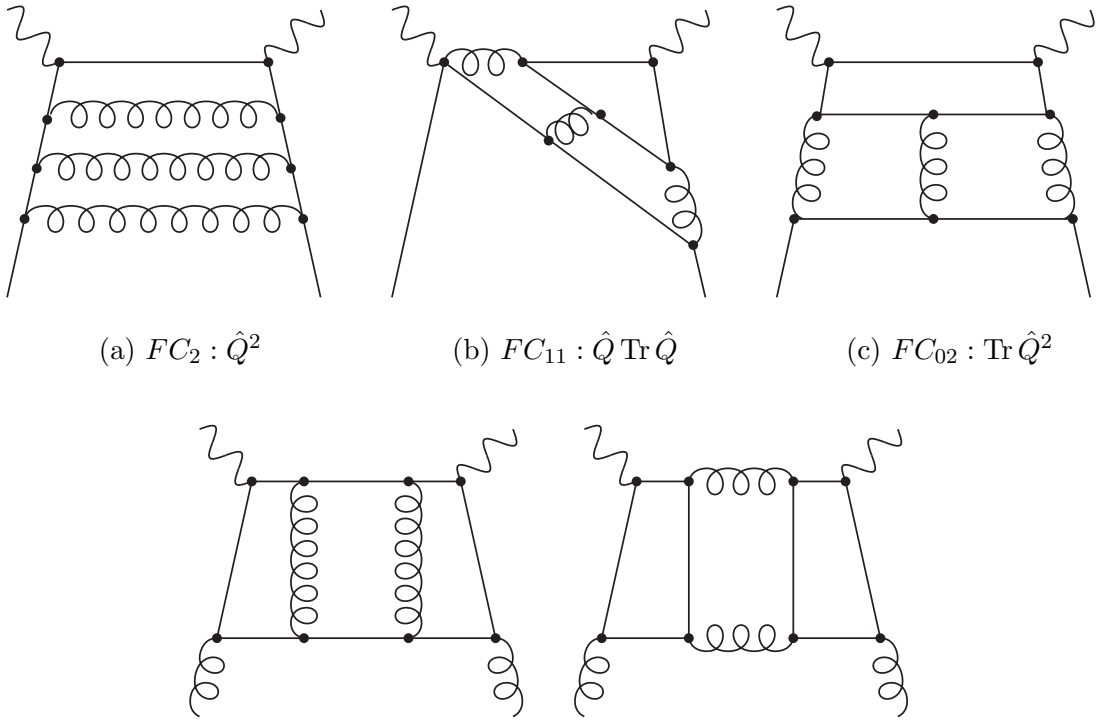

(a) $FC_2 : \hat{Q}^2$ (b) $FC_{11} : \hat{Q}\,\mathrm{Tr}\,\hat{Q}$ (c) $FC_{02} : \mathrm{Tr}\,\hat{Q}^2$

(d) $FC_2^g : \mathrm{Tr}\,\hat{Q}^2$ (e) $FC_{11}^g : (\mathrm{Tr}\,\hat{Q})^2$

Figure 9.5: Representative 3-loop diagrams for different flavor classes. The expressions after the colon signs indicate the corresponding flavor factors.

which both photons couple to one quark loop, as shown in Figure 9.5c. Their sum contributes with a flavor prefactor $\mathrm{Tr}\,\hat{Q}^2$. The FC_{11} flavor class contains Feynman diagrams in which one photon is coupled to a closed quark loop while another photon is attached to the external quark line. The corresponding flavor factor is $\hat{Q}\,\mathrm{Tr}\,\hat{Q}$. The diagrams that have initial-state gluon legs must contain a gluon splitting into quarks. The quark flavors in these gluon diagrams are summed over. If both external photons are attached to the same quark loop, as shown in Figure 9.5d, the flavor factor is $\mathrm{Tr}\,\hat{Q}^2$, the respective flavor class is called as FC_2^g. In contrast, the FC_{11}^g class stands for diagrams in which photons are attached to different quark loops, and quarks need to be summed separately in each loop, as $(\mathrm{Tr}\,\hat{Q})^2$.

The non-singlet PDFs were defined as

$$q_{i,ns} = (q_i + \bar{q}_i) - \frac{1}{N_F} q_s = (q_i + \bar{q}_i) - \frac{1}{N_F} \sum_j (q_j + \bar{q}_j). \tag{9.53}$$

In terms of the vector $\vec{q} = (q_1 + \bar{q}_1, \cdots q_i + \bar{q}_i, \cdots q_{N_F} + \bar{q}_{N_F})^T$, we can express the i-th component of non-singlet PDF as

$$q_{i,ns} = \lambda^i \cdot \vec{q}, \text{ where } \lambda^i = \mathrm{diag}(-\frac{1}{N_F}, \cdots, \frac{N_F - 1}{N_F}, \cdots, -\frac{1}{N_F}). \tag{9.54}$$

That is, the i-th diagonal element of diagonal matrix λ^i is $(N_F - 1)/N_F$, while other diagonal elements are $-1/N_F$. When performing the sum over quark flavors (i.e. taking the trace of the operators), the non-singlet coefficient function for FC_{02} class does not contribute to the cross section, because its contribution is proportional to

$$\sum_i q_{i,ns} = \sum_i \left[(q_i + \bar{q}_i) - \frac{1}{N_F} q_s \right] = q_s - q_s = 0, \text{ i.e. } \mathrm{Tr}\,\lambda^i = 0. \tag{9.55}$$

Therefore, the nonzero non-singlet contributions are only from flavor classes FC_2 and FC_{11}. The traces of the FC_2 and FC_{11} classes are, respectively,

$$\mathrm{Tr}\Big(\hat{Q}^2 \lambda^i\Big), \;\; \mathrm{Tr}\Big(\hat{Q}\lambda^i\Big)\,\mathrm{Tr}\,\hat{Q}. \tag{9.56}$$

A simple calculation shows that

$$\mathrm{Tr}\Big(\hat{Q}\lambda^i\Big) = 3\,\mathrm{Tr}\Big(\hat{Q}^2\lambda^i\Big). \tag{9.57}$$

Therefore, we can normalize all the flavor factors in terms of a reference factor $\mathrm{Tr}\Big(\hat{Q}^2\lambda^i\Big)$ as

$$\begin{aligned} \sum_i e_i^2 C_{k,ns}^i \otimes q_{ns}^i &= \left[c_{k,ns}(FC_2) + \frac{\mathrm{Tr}\Big(\hat{Q}\lambda^j\Big)\,\mathrm{Tr}\,\hat{Q}}{\mathrm{Tr}\Big(\hat{Q}^2\lambda^j\Big)} C_{k,ns}(FC_{11}) \right] \otimes \sum_i \mathrm{Tr}\Big(\hat{Q}^2\lambda^i\Big) q_{ns}^i \\ &= c_{k,ns} \otimes \tilde{q}_{ns}, \end{aligned} \tag{9.58}$$

Flavor class	FC_2	FC_{11}	FC_{02}	FC_2^g	FC_{11}^g
Flavor factor	fl_2	fl_{11}	fl_{02}	fl_2^g	fl_{11}^g
Flavor structure	$\hat{Q}^2$	$\hat{Q}\,\mathrm{Tr}\,\hat{Q}$	$\hat{I}\,\mathrm{Tr}\,\hat{Q}^2$	$\mathrm{Tr}\,\hat{Q}^2$	$(\mathrm{Tr}\,\hat{Q})^2$
Non-Singlet	1	$3\langle e\rangle$	0	–	–
Singlet	1	$\langle e\rangle^2/\langle e^2\rangle$	1	1	$\langle e\rangle^2/\langle e^2\rangle$

Table 9.2: The flavor factor values for 5 flavor classes.

Here we redefine the coefficient $c_{k,ns}$ which does not depend on the flavor index i, and modified non-singlet PDF is $\tilde{q}_{ns} = \sum_i \mathrm{Tr}\Big(\hat{Q}^2\lambda^i\Big)q^i_{ns}$. With the standard normalization, we have perturbative expansion $C_k = 1 + \sum c_p a_s^p$. We denote the prefactor as

$$fl_{11} = \frac{\mathrm{Tr}\Big(\hat{Q}\lambda^j\Big)\,\mathrm{Tr}\,\hat{Q}}{\mathrm{Tr}\Big(\hat{Q}^2\lambda^j\Big)} = \frac{3}{N_F}\sum e_i = 3\langle e\rangle. \tag{9.59}$$

For the convolutions with the singlet PDF $q_S = \sum_i (q_i + \bar{q}_i)$, we also extract the overall normalization prefactor from the FC_2 class. Summation of the flavor structure $\hat{Q}^2$ gives $\sum_i e_i^2 = N_F\langle e^2\rangle$. It is very easy to obtain all the corresponding flavor factors $fl_2, fl_{02}, fl_{11}, fl_2^g, fl_{11}^g$ (respectively corresponding to flavor classes $FC_2, FC_{02}, FC_{11}, FC_2^g, FC_{11}^g$), listed in Table 9.2. We have normalized two of these factors to unity, $fl_2^g = fl_2 = 1$. We choose this convention of flavor factors in order to reduce the singlet flavor factor to unity when replacing $\hat{Q}$ matrix by the identity matrix $\mathrm{diag}(1, 1, \cdots)$.

9.3.3 Further classifications and rescaling variables

As we mentioned before, apart from the quark-photon couplings, we have another flavor structure involving the quark-gluon vertex. In the cut diagrams $\mathcal{M}\mathcal{M}^*$, a virtual quark loop in the gluon polarization diagrams will contribute a factor N_F. If the loop is cut into final states corresponding to the gluon splitting into a real $q\bar{q}$ pair, we may end up with flavor-dependent threshold effects in this subgraph. Specifically, the gluon splitting into heavy quarks requires more threshold energy than that for light quarks. In the general mass scheme, the light- and heavy-quark contributions are intrinsically different, as the coefficients are fully mass-dependent. However, as we know, the mass-dependent coefficient functions are very difficult to calculate, and we only have the 2-loop massive calculations up to now. In contrast, we have the massless N3LO coefficients functions, obtained from Ref. [156, 157, 158].

In terms of the N_F dependence, we can classify each flavor class into several different types. The 3-loop component $c_{2,ns}^{(3)}$ of the non-singlet massless coefficient function can be written as

$$c_{2,ns}^{(3)} = c_{2,ns}^{(3)}(FC_2, T_1) + N_F c_{2,ns}^{(3)}(FC_2, T_2) + N_F^2 c_{2,ns}^{(3)}(FC_2, T_3) + fl_{11,ns} c_{2,ns}^{(3)}(FC_{11}). \quad (9.60)$$

Representative Feynman diagrams for $T_{1,2,3}$ of the FC_2 class are shown in Figure 9.6. The coefficients for each type can be extracted from [156, 157, 158], and are explicitly tabulated in Ref. [154].

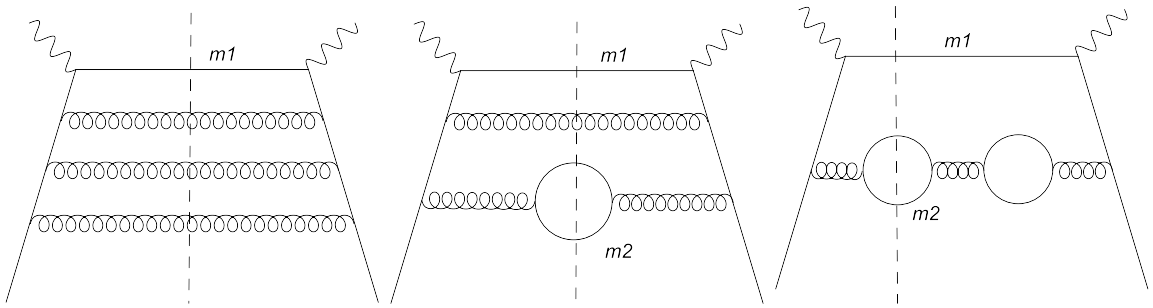

(a) T_1 (b) T_2 (c) T_3

Figure 9.6: Representative diagrams from FC_2 class.

The DIS subprocesses of order $\mathcal{O}(\alpha_s^3)$ may produce up to two distinct quark flavors in the final state, as can be seen in the diagrams of 9.6 and subsequent figures. We denote the masses of two types of quarks as m_1 and m_2. The presence of two distinct masses at this order modifies the kinematic dependence of key diagrams at N3LO, as compared to (N)NLO, and it modifies the form of the rescaling variable $\chi = x(1 + 4m^2/Q^2)$ that was introduced in the S-ACOT-χ scheme at (N)NLO [140, 153]. in order to capture the threshold effect in phase space integration. A more general form than χ can be used for the rescaling variable, which is denoted by ζ and is implicitly determined from the condition $x = \zeta/(1 + \zeta^\lambda 4m^2/Q^2)$. We will now construct approximate flavor-creation and flavor-excitation coefficients for neutral-current DIS up to N3LO using the approach of the intermediate-mass scheme [152] and the individual 3-loop *massless* coefficient functions for five flavor classes that we identified in the previous section.

To approximately reproduce the unknown mass effects, we estimate zero-mass coefficient functions in the diagrams with heavy-quark lines using the appropriate kinematic variable as the input. For the flavor class FC_2, we have diagrams of 3 different types, corresponding

to different final states, shown in Figure 9.6. We can see that in these cut diagrams, the kinematic behavior varies with the quark's mass, so that it depends on the quark's flavor. For example, for the T_1-type diagrams, the threshold constraints give us the rescaling variable as $\chi = x(1 + 4m^2/Q^2)$, while for $T_{2,3}$-type diagrams, phase space integration is constrained by

$$\chi(\sum_{fs} m_i) = x\left(1 + \frac{(2m_1 + 2m_2)^2}{Q^2}\right) = x\left(1 + \frac{(\sum_{fs} m_i)^2}{Q^2}\right), \tag{9.61}$$

where fs indicates to sum over all the final states. Accordingly, the generalized rescaling variable ζ should be written in an arbitrary scattering channel as

$$x = \frac{\zeta}{1 + \zeta^\lambda \left(\sum_{fs} m_i\right)^2 / Q^2}. \tag{9.62}$$

We have introduced a parameter λ to tune the magnitude of the mass effect. The value of λ can be fitted to reproduce kinematic dependence of the exact (massive) lower-order calculations. When the parameter λ varies in the interval $0 < \lambda < \infty$, ζ changes smoothly from x to χ. We set the sum of a final state masses as a parameter to denote the generalized rescaling variable in any channel by $\zeta(\sum_{fs} m_i)$.

By approximating the mass effects using generalized rescaling variables, we can obtain the intermediate-mass coefficient functions as

$$\begin{aligned} C^{(3)}_{2,ns}(FC_2, T_1) &= c^{(3)}_{2,ns}(FC_2, T_1, \zeta(2m_1)), \\ C^{(3)}_{2,ns}(FC_2, T_2) &= c^{(3)}_{2,ns}(FC_2, T_2, \zeta(2m_1 + 2m_2)), \\ C^{(3)}_{2,ns}(FC_2, T_3) &= N'_F c^{(3)}_{2,ns}(FC_2, T_3, \zeta(2m_1 + 2m_2)). \end{aligned} \tag{9.63}$$

Here, we use the capital letters to denote the coefficient functions with mass effects from the generalized rescaling variable, and the N'_F is the number of the quark flavors in the uncut quark loop in Figure 9.6c. The IM coefficient functions in this subsection, including Equation (9.63) and subsequent equations, corresponding to the factorization scale $\mu = Q$. In the next subsection, we will show how to include the scale dependence in the IM coefficient functions.

The FC_{11} class is shown in Figure 9.7, The rescaling variable in this channel is of the form $\zeta(2m_1 + 2m_2)$.

Returning to the singlet-quark coefficient function, we have to decompose it into a non-singlet and a pure singlet parts, i.e. $c_{k,s} = c_{k,ns} + c_{k,ps}$ [156, 157]. Similarly to the non-singlet

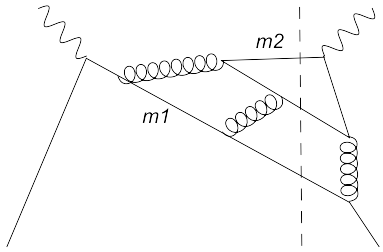

Figure 9.7: The representative diagram for FC_{11} class.

case, we can decompose the massless pure singlet functions as follows:

$$c_{2,ps} = N_F c^{(3)}_{2,ps}(FC_{02}, T_1) + N_F^2 c^{(3)}_{2,ps}(FC_{02}, T_2) + fl_{11,ps} N_F c^{(3)}_{2,ps}(FC_{11}). \tag{9.64}$$

Two topologies of the Feynman graphs of the FC_{02} class are illustrated in Figure 9.8. The IM coefficient functions can be written as

$$\begin{aligned} C^{(3)}_{2,ps}(FC_{02}, T_1) &= c^{(3)}_{2,ps}(FC_{02}, T_1, \zeta(2m_1 + 2m_2)), \\ C^{(3)}_{2,ps}(FC_{02}, T_2) &= c^{(3)}_{2,ps}(FC_{02}, T_2, \zeta(2m_1 + 2m_2)). \end{aligned} \tag{9.65}$$

Their full expressions are presented in Ref. [154].

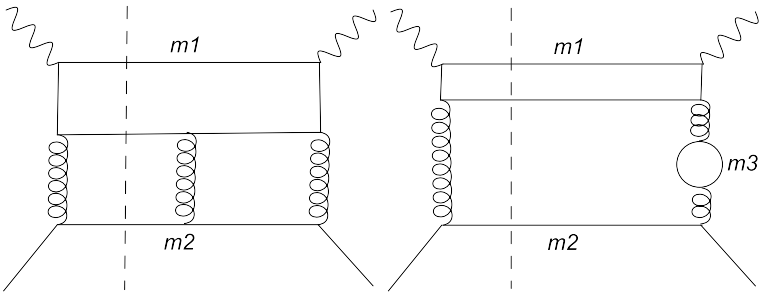

(a) T_1 (b) T_2

Figure 9.8: Representative diagrams from FC_{02} class.

The massless gluon coefficient function is

$$c^{(3)}_{2,g} = N_F c^{(3)}_{2,g}(FC^g_2, T_1) + N_F^2 c^{(3)}_{2,g}(FC^g_2, T_2) + fl^g_{11} N_F^2 c^{(3)}_{2,g}(FC^g_{11}). \tag{9.66}$$

The 3 types of Feynman diagrams of the FC^g_2 class are depicted in Figure 9.9. The corresponding generalized rescaling variables are $\zeta(2m_1), \zeta(2m_1 + 2m_2), \zeta(2m_1 + 2m_2)$. A representative FC^g_{11} diagram is are illustrated in Figure 9.10, and its respective rescaling variable is $\zeta(2m_1 + 2m_2)$.

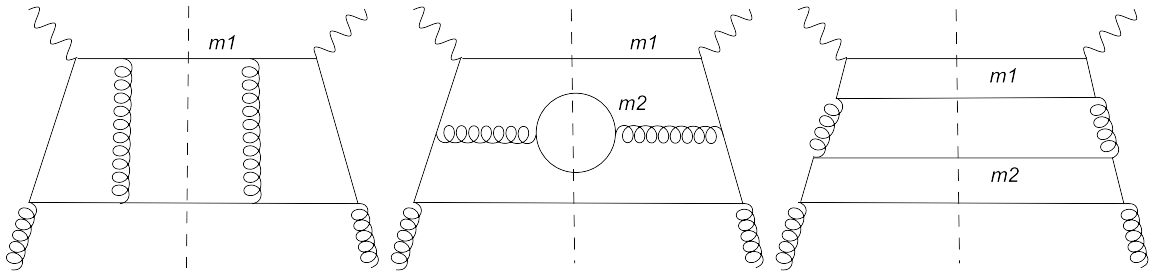

(a) T_1 (b) T_2 (c) T_3

Figure 9.9: Representative diagrams from FC_2^g class.

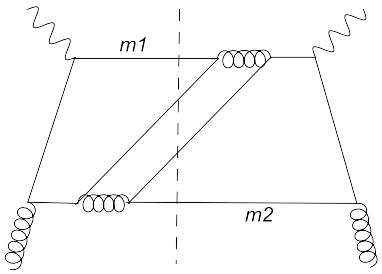

Figure 9.10: The representative diagram for FC_{11}^g class.

We can repeat the same calculations for the structure function, F_L. Decompositions of its 3-loop coefficient functions is in the massless case are listed as follows:

$$
\begin{aligned}
c_{L,ns}^{(3)} &= c_{L,ns}^{(3)}(FC_2, T_1) + N_F c_{L,ns}^{(3)}(FC_2, T_2) + N_F^2 C_{L,ns}^{(3)}(FC_2, T_3) + fl_{11}^{ns} N_F c_{L,ns}^{(3)}(FC_{11}).\\
c_{L,ps}^{(3)} &= N_F c_{L,ps}^{(3)}(FC_{02}, T_1) + N_F^2 c_{L,ps}^{(3)}(FC_{02}, T_2) + fl_{11}^{ps} N_F c_{L,ps}^{(3)}(FC_{11}),\\
c_{L,g}^{(3)} &= N_F c_{L,g}^{(3)}(FC_2^g, T_1) + N_F^2 c_{L,g}^{(3)}(FC_2^g, T_2) + fl_{11}^{g} N_F^2 c_{L,g}^{(3)}(FC_{11}^g).
\end{aligned}
\tag{9.67}
$$

The representative Feynman diagrams and the rescaling variables for $F_L(x, Q^2)$ are that for $F_2(x, Q^2)$. We summarize the subtypes of different flavor classes and the corresponding generalized rescaling variables in Table 9.3.

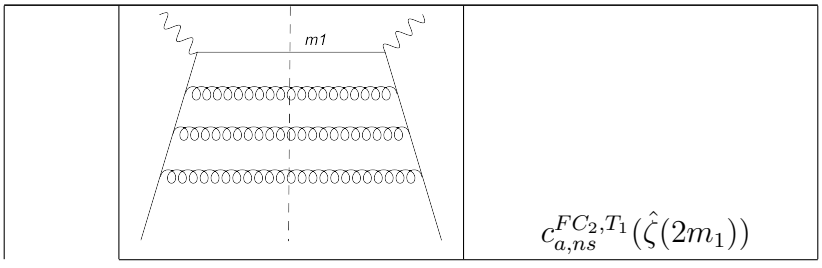

FC_2

	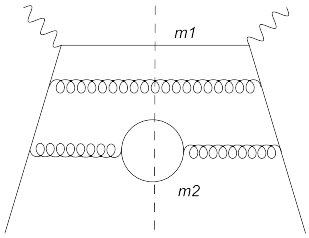	$c_{a,ns}^{FC_2,T_2}(\hat{\zeta}2((m_1+m_2)))$
	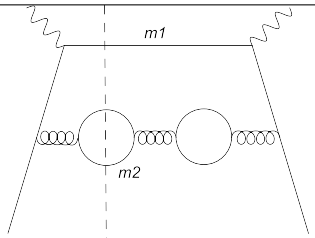	$c_{a,ns}^{FC_2,T_3}(\hat{\zeta}2((m_1+m_2)))$
FC_{02}	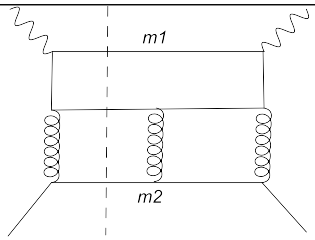	$c_{a,ps}^{FC_{02},T_1}(\hat{\zeta}(2(m_1+m_2)))$
	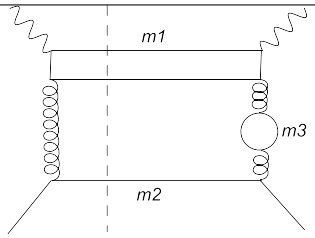	$c_{a,ps}^{FC_{02},T_2}(\hat{\zeta}(2(m_1+m_2)))$
FC_{11}	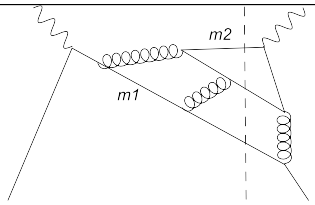	$c_{a,ns(ps)}^{FC_{11},T_1}(\hat{\zeta}(2(m_1+m_2)))$
FC_2^g	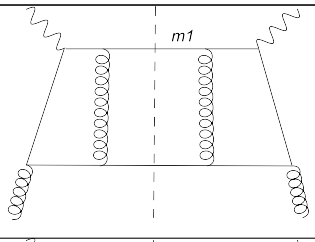	$c_{a,g}^{FC_2^g,T_1}(\hat{\zeta}(2m_1))$
	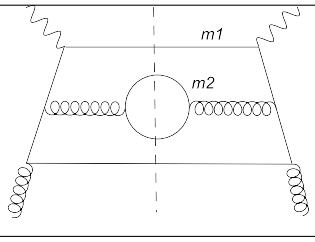	$c_{a,g}^{FC_2^g,T_2}(\hat{\zeta}(2(m_1+m_2)))$

	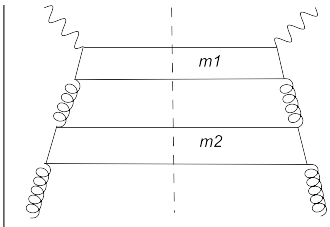	$c_{a,g}^{FC_2^g,T_3}(\hat{\zeta}(2(m_1+m_2)))$
FC_{11}^g	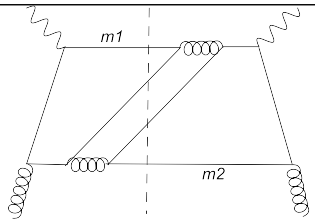	$c_{a,g}^{FC_{11}^g,T_2}(\hat{\zeta}(2(m_1+m_2)))$

Table 9.3: Summary of the generalized rescaling variables for different types of flavor classes.

9.3.4 Scale dependence of N3LO structure functions in the IM scheme

The previous subsection presented approximate IM expressions for the 3-loop coefficient functions in neutral-current DIS at the factorization scale $\mu = Q$. We will now derive logarithmic contributions to these functions that arise when $\mu \neq Q$.

We have introduced the perturbative expansion of the DGLAP equation in Section 8.2.3 and the singlet and non-singlet flavor basis in Section 9.3.1. Extending perturbative expansions for the PDFs and splitting functions in Equation (8.70) to N3LO, we obtain their 3-loop perturbative coefficients as

$$\begin{aligned} f_i^{(3)} = &\left[-\frac{1}{6}L^3 P_{ij}^{(0)} \otimes P_{jk}^{(0)} \otimes P_{kl}^{(0)} + \frac{1}{2}\beta_0 L^3 P_{ij}^{(0)} \otimes P_{jl}^{(0)} + L^2 P_{ij}^{(0)} \otimes P_{jl}^{(1)}\right. \\ &\left. - (\frac{1}{3}\beta_0^2 L^3 + \frac{1}{2}\beta_1 L^2) P_{il}^{(0)} - \beta_0 L^2 P_{il}^{(1)} - L P_{il}^{(2)}\right] \otimes f_{l,0}^{(0)} \\ &+ \left(\frac{1}{2}L^2 P_{ij}^{(0)} \otimes P_{jk}^{(0)} - \frac{1}{2}\beta_0 L^2 P_{jk}^{(0)} - L P_{ik}^{(1)}\right) \otimes f_{k,0}^{(1)} - L P_{ij}^{(0)} \otimes f_{j,0}^{(2)} + f_{i,0}^{(3)}. \end{aligned} \tag{9.68}$$

Also, the scale-dependent parts of Wilson coefficient functions in Equation (8.75) can be extended to N3LO as

$$\begin{aligned} c_i^{(3,1)} &= c_j^{(0)} \otimes P_{ji}^{(2)} + c_j^{(1)} \otimes (P_{ji}^{(1)} - \beta_1 \delta_{ji}) + c_j^{(2)} \otimes (P_{ji}^{(0)} - 2\beta_0 \delta_{ji}), \\ c_i^{(3,2)} &= \frac{1}{2}\left\{ c_j^{(1,1)} \otimes (P_{ji} - \beta_1 \delta_{ji}) + c_j^{(2,1)} \otimes (P_{ji}^{(0)} - 2\beta_0 \delta_{ji}\right\}, \\ c_i^{(3,3)} &= \frac{1}{3} c_j^{(2,2)} \otimes (P_{ji}^{(0)} - 2\beta_0 \delta_{ji}). \end{aligned} \tag{9.69}$$

Next, we decompose the DGLAP equations in the singlet, non-singlet basis as in Equation (9.45). From Equation (9.69), we can obtain all coefficients of the scale-dependent logarith-

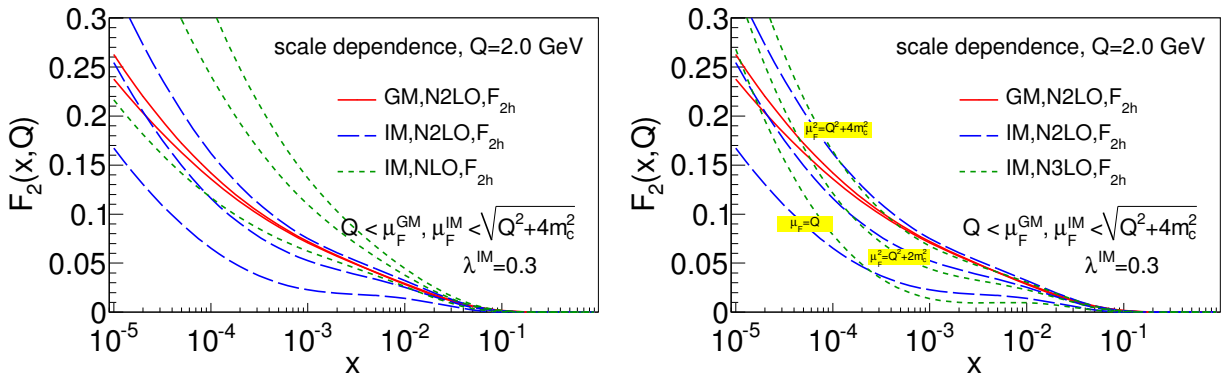

Figure 9.11: The μ dependence in the IM and GM scheme up to NNLO (left) and N3LO (right).

mic terms at 3 loops, composed from non-singlet, pure singlet, and gluon components. Full expressions of the 3-loop scale-dependent terms for $\mu \neq Q$ can be found in Ref. [154].

From the results presented in the last two subsections, we can construct full coefficient functions with heavy-quark mass dependence in the intermediate-mass scheme up to N3LO. The upside of the IM scheme is that allows to construct massive N3LO terms that exactly coincide with the ZM-VFN result when $Q^2 \gg m_q^2$, and they retain a plausible (but not exact) dependence on massive terms of order $\mathcal{O}(m_q^2/Q^2)$ when $Q^2 \approx m_q^2$. The downside of the IM approach is that, since its mass-dependence expression for N3LO DIS structure functions is still approximate, the dependence on the factorization scale and rescaling variable at N3LO DIS is not reduced in the IM scheme compared to NNLO. In contrast, when we construct S-ACOT-χ functions with the exact massive FC terms, by construction the dependence on the factorization scale and the form of rescaling variable in the FE terms are systematically reduced when higher-order terms in α_s are included. See numerical examples of such reduction in the S-ACOT-χ scheme at NNLO in Ref. [153].

Let us illustrate this discussion by showing numerical results for DIS structure functions in the GM and IM schemes. In Figure 9.11, we first show the scale dependence of the NNLO and N3LO predictions in the intermediate-mass scheme. We fix $\lambda = 0.3$ for this comparison, and show predictions for the factorization scales $\mu^2 = Q^2, Q^2 + 2m_c^2, Q^2 + 4m_c^2$. We can see the scale uncertainty is slightly reduced when increasing the perturbative order from the IM NLO to N2LO and N3LO. But it converges much slower than the GM N2LO results, which

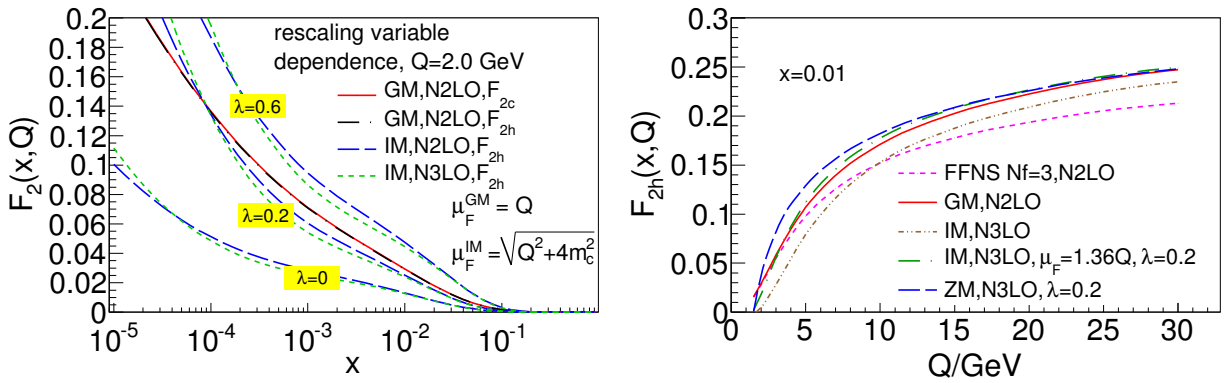

Figure 9.12: The λ dependence in the IM scheme (left) and the Q dependence in the FFN, ZM, IM and GM schemes (right).

means that the incomplete dependence on terms of order m_c^2 play an important role near the threshold region. The strong coupling α_s and the PDFs are only evolved up to NNLO, introducing a mismatch in the N3LO coefficient functions.

In the left plots of Figure 9.12, we show the λ dependence in the IM scheme. The $\lambda = 0$ corresponds to the rescaling χ variable in the S-ACOT-χ scheme. We see that the NNLO IM scheme with $\lambda = 0.2 \sim 0.3$ reproduces the GM NNLO results. Knowing that the best $\lambda \simeq 0.2$ value captures the missing mass effect in the IM scheme at NNLO, we use the same λ value at N3LO, and we compare the structure functions in various schemes in the right subfigure of Figure 9.12. We see that the FFN scheme underestimates the GM VFN structure function at large Q, because the FFN structure function totally misses the higher-order logarithmic terms resummed in the charm PDF in the GM VFN scheme. At small Q values of a few GeV, the ZM scheme overestimates the massive predictions for $F_2(x, Q)$ because it does have proper energy-momentum conservation in the heavy-quark threshold production region. Our intermediate-mass scheme for the first time estimates the mass effect on the heavy flavor structure function at the N3LO level.

Chapter 10

Heavy-flavor production at hadron colliders

In Chapter 9, we reviewed factorization schemes for QCD processes with heavy quarks and applied the S-ACOT-χ and intermediate-mass schemes to describe deep inelastic scattering at NNLO and approximate N3LO, respectively. The massive factorization schemes such as S-ACOT-χ have been most extensively studied in the context of charm and bottom quark production in deep inelastic scattering, the process in which typical photon virtuality Q accessible in the experiments are of the same order as heavy-quark masses, $m_{c,b}$. In the last few years, measurements of heavy-quark production at hadron-hadron colliders become increasingly precise, and the relevant NNLO computations are anticipated in the near future. As in the case of DIS, perturbative convergence of QCD calculations in the ACOT and other GM-VFN schemes at small momenta comparable to m_Q can be significantly improved by physical treatment of kinematics in flavor-excitation and subtraction terms. This consideration gives rise to the SACOT-MPS (SACOT with massive space) factorization framework for heavy-quark scattering processes at hadron-hadron colliders. The SACOT-MPS scheme is an equivalent of the SACOT-χ scheme, but applied to hadron-hadron, rather than lepton-hadron kinematics. In this chapter, we will introduce the SACOT-MPS scheme on the example of single-inclusive heavy-flavor production at the LHC.

10.1 Hadroproduction of heavy flavors

LHC measurements of heavy-flavor production, $pp \to QX$, provide very interesting information to test various aspects of quantum chromodynamics (QCD). The cross section for this process is perturbatively calculable due to the presence of heavy-quark mass (m_Q) which pushes the physical energy scale up to the perturbative region of QCD. In a typical measurement of this kind, either a heavy meson or a hadronic jet containing a displaced decay vertex is observed in the detector. Main features of experimentally observed cross sections can be understood by computing heavy-quark production cross sections at the par-

ton level, the approach that we will adopt in this paper. To obtain the observable cross sections, the parton-level cross section must be combined with a fragmentation function of a fragmentation model describing the decay of the heavy quark into the observed final state.

When the final-state heavy quark has a relatively small transverse momentum, ($p_T \lesssim m_Q$), the p_T distribution can be computed in the fixed-flavor number (FFN) scheme [159, 160, 161, 162], because the heavy quark can be treated as an inactive parton, and only emerges in the final state, which means that the power terms $(p_T^2/m_Q^2)^p$ can be treated correctly in the perturbative series for the hard-scattering cross section. However, this FFN scheme calculation becomes unreliable when $p_T \gg m_Q$, where terms of order $\alpha_s^m \log^n(p_T^2/m_Q^2)$ need to be resummed to all orders to get the reliable predictions. In this case, the Zero-Mass (ZM) Scheme [163] applies, in which the large logarithms of this kind are resummed inside the initial-state parton distribution functions (PDFs) and final-state fragmentation functions (FFs). In this kinematic region, the heavy quark is treated as an active parton that contributes to the scale dependence of the running QCD coupling as well as the PDFs. In the intermediate region ($p_T \sim m_Q$), several composite schemes that retain key mass dependence, resum collinear logarithms, and thus match the FFN and ZM schemes, were developed, including the Fixed-Order plus Next-to-Leading Logarithms (FOFLL) [164, 165] and an ACOT-like General-Mass Variable Flavor Number Scheme (GM-VFNS) [163, 166]. Recently, I. Helenuis and H. Paukkenen [167] introduced the SACOT-m_T scheme to treat the D-meson hadroproduction that follows the organizing principles of the Simplified-ACOT scheme [141, 142] in DIS.

So far, the LHC Run I data on heavy-flavor production rates [168, 169, 170, 171] demonstrate good agreement with theoretical predictions within the estimated systematic uncertainties [165, 166, 172, 173]. Since a significant reduction of the statistical uncertainties is expected as more data are accumulated in high-luminosity LHC runs, the theoretical uncertainties gradually become a limiting factor both for precision tests of the Standard Model and searches for new physics. Some theoretical uncertainties include dependence on the choices of the renormalization and factorization scales, uncertainties in the heavy-quark mass and PDFs, as well as (in the case of composite schemes) dependence on the matching prescription between N_F and $N_F + 1$ flavors. Specifically, at a small transverse momentum ($p_T \sim m_Q$,

$Q = c, b$), the NLO scale uncertainties on c, b hadroproduction cross sections estimated with FONLL may reach 100 (50)% [174]. At such p_T, the QCD coupling is usually evaluated at low renormalization scale such as $\mu_R \sim \sqrt{p_T^2 + m_Q^2}$, and varies rapidly when μ_R changes. In traditional VFN scheme such as the ACOT, the NLO scale dependence remains sizable also at $p_T^2 \gg m_Q^2$.

Measurements of charm and bottom production cross sections in the regions of small p_T and large rapidity y of the heavy quark are sensitive to the PDFs at both small and large momentum fractions ($x_{1,2} \sim \frac{\sqrt{p_T^2+m_Q^2}}{\sqrt{S}} e^{\pm y}$), where the PDFs may not be covered well by by other experiments. For example, the charm or bottom quark produced in the rapidity range $4 < |y| < 4.5$ in a pp collision at $\sqrt{s} = 13$ TeV can probe the momentum fraction region $x \lesssim 10^{-5}$, and, for $p_T \gtrsim 40$ GeV, this kind of data can probe $x \gtrsim 0.2$. The precision measurement of heavy flavor production at pp collider can provide especially sensitive constraints on the gluon PDF since the relevant production channels are dominated by gg initial states. Ref. [173] recommends presenting heavy-flavor production data in the form of normalized cross sections for purposes of PDF studies, since the absolute cross section suffers large theoretical uncertainties due to the uncalculated higher-order corrections beyond NLO. On the contrary, the normalized cross section can provide a significant cancellation of the theoretical uncertainties. Another similar idea is to constrain the PDFs using the ratios $\sigma(X, E_2)/\sigma(X, E_1)$ of cross sections at different collision energies [175], which cancels the luminosity uncertainties on the experimental side and some theoretical effects, such as dependence on the fragmentation $b \to B$ in bottom meson production. We can even take a double ratio to normalize the 13-over-7 TeV cross section ratio to some fixed rapidity value, combining the advantages of normalized cross sections and the ratio variables between 2 different center-of-mass energies. This idea is exploited in Ref. [174], which shows a significant reduction of theoretical uncertainties in the ratio of LHC forward heavy quark production cross sections at $\sqrt{s} = 7$ and 13 TeV. As a result of cancelation of QCD scale dependence in the cross section ratios, the PDF uncertainty dominates above other unknown factors, which provides a good chance to constrain the gluon PDF by including the experimental data on the ratios into the global PDF fits. Now, $B^{\pm}$ production cross section in the format of cross section ratios has become available, e.g., from LHCb collaboration [169].

Heavy-quark-mass dependence is important at small p_T and, in general, in kinematic regions sensitive to mass-dependent modifications in phase space available for radiation of $Q\bar{Q}$ pairs. In theoretical computations, threshold suppression of the phase space is controlled by a factor $\beta = \sqrt{1 - 4m_{Q^2}/\hat{s}}$. The FFNS presents the most economical theoretical approach to describe these special regions. A viable GM-VFN scheme must be constructed so that it reduces, in a robust way, to FFNS in these limits, it resums collinear logarithms away from the threshold region, and any differences between the GM-VFN and FFN schemes are systematically suppressed by including higher-order terms in α_s.

In this chapter, we construct such a streamlined and systematic general-mass scheme for heavy-flavor hadroproduction, called the **S-ACOT with Massive Phase Space** (SACOT-MPS) scheme. We follow principles of the S-ACOT-χ method originally developed for deep inelastic scattering [140, 153] but extend the consideration to the case of hadron-hadron scattering kinematics. Then, we apply the SACOT-MPS formalism to make predictions for the LHC. The results are presented at the next-to-leading order (NLO) in the QCD coupling strength, but the extension to higher orders is straightforward.

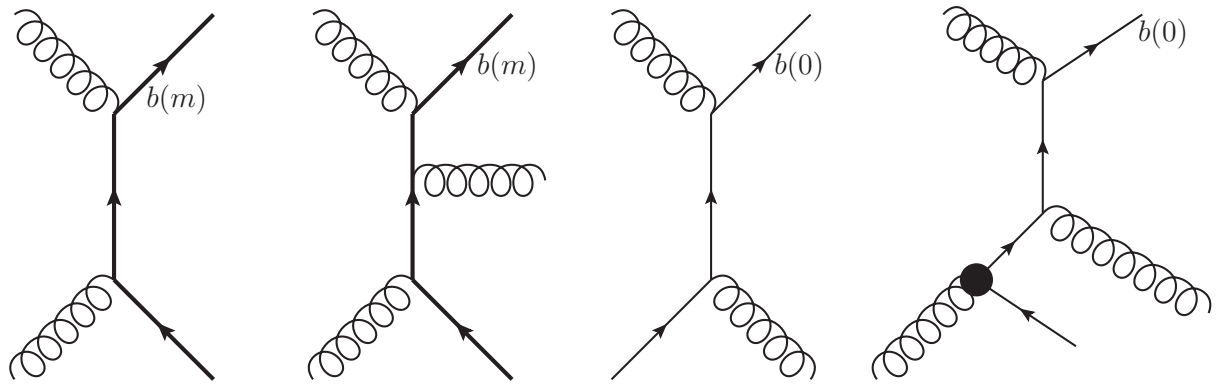

Figure 10.1: The representative Feynman diagrams for $pp \to QX$ production: (a) LO Flavor Creation (FC) terms; (b) NLO FC; (c) Flavor Excitation (FE); (d) subtraction (SB) terms. The thick (thin) lines indicate massive (massless) propagators and external-state spinors for heavy quarks. The black blob indicates a collinear splitting term for $g \to Q\bar{Q}$.

In the ACOT approach, we classify the relevant Feynman diagrams into **flavor creation** (FC) and **flavor excitation** (FE) contributions. The representative diagrams are shown in Fig. 10.1. The overlapping heavy flavor-initial parton generated by the gluon splitting at this order (NLO) is subtracted out in order to avoid double counting. In the Flavor Creation

terms, the heavy quark only appears in the final state, which enables us to use the full quark-mass dependence calculations both in the phase space and the matrix elements. The hard cross sections can be simplified in the FE channels by neglecting the m_Q dependence without loss in precision, which corresponds to the approach of S-ACOT scheme [141, 142]. Similarly to the χ variable introduced in S-ACOT-χ scheme [140], we invoke the massive phase space in the Flavor Excitation term to approximate suppression of the available phase space near the heavy-quark production threshold. We dub this novel scheme as **SACOT-MPS scheme**, in which MPS is short for **Massive Phase Space**. Here MPS plays a similar role as m_T in the SACOT-m_T scheme [167].

At the NLO, the Feynman subgraphs of heavy flavor coming from the collinear gluon splitting appear in the Flavor Creation terms, in which they are resummed as a part of the heavy-quark PDF, and in the Subtraction (SB) terms, defined as the perturbative expansion of the respective FE terms to the same order in α_s as the FC terms. The full cross section takes the generic form:

$$\sigma = \text{FC} \ + \text{FE} - \text{SB}. \tag{10.1}$$

The SB term is *subtracted* from the sum of the FC and FE terms to eliminate double-counting of collinear-splitting contributions. In the high-energy limit ($\hat{s} \gg m_Q^2$ or $p_T^2 \gg m_Q^2$), the SB term is expected to cancel enhanced collinear contributions in the Flavor Creation, in order to reproduce the ZM scheme calculations in this region. Conversely, in the threshold region ($\hat{s} \gtrsim 4m_Q^2$ or $p_T \lesssim m_Q$), the FE terms that contain the initial heavy-flavor PDF generated perturbatively by DGLAP equation will cancel the SB terms, so that the cross section reduces to the FC contribution, which is equivalent to the FFNS cross section up to a small higher-order correction.

The remainder of this chapter is organized as follows. In Sec. 10.2, we describe the framework of our theoretical calculations and compare it with the other available calculations, such as FFNS, FONLL, GM-VFM, and NLO+PS approaches. Our theoretical predictions for LHCb $B^{\pm}$ production are presented in Sec. 10.3. We will also discuss the potential impact of experimental heavy-flavor production data on the PDF global fitting in this section. Finally, we conclude in Sec. 10.4.

10.2 Theoretical calculations

The fixed-flavor-number scheme (FFNS) calculation of heavy quark pair production was first achieved at the Next-to-Leading Order in Refs. [159, 160] and repeated in Refs. [161, 162]. As its name indicates, the FFNS assumes a fixed number N_F of active parton flavors. The heavy-quark species of our interest is consistently treated in the FFNS as an inactive flavor in the running coupling, masses of active partons, initial-state PDFs, and final-state fragmentation functions. Take $pp \to bX$ as an example. The inactive b-quark means no b-quark PDF in the initial proton at all. Meanwhile, the strong coupling should be renormalized in the $N_F = 4$ $\overline{\text{MS}}$ scheme. As discussed in Sec. 10.1, this calculation for the p_T distribution is reliable only when $p_T \lesssim m_Q$. In the Feynman graphs like the one in Figure 10.2, the b quark that runs in a virtual loop contributes to the hard partonic cross section in the NLO $N_F = 4$ FFNS calculations. In such a calculation, both the $\alpha_s(\mu)$

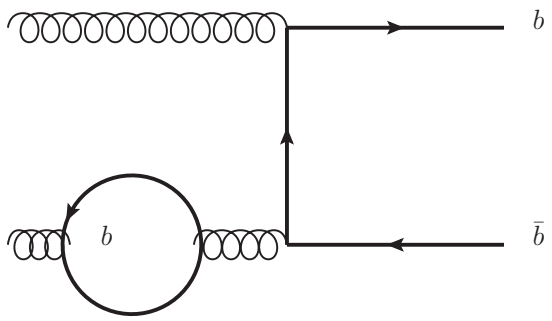

Figure 10.2: The heavy quark running the virtual loops whose contribution should be added back to the hard partonic cross section in the NLO $N_F = 4$ FFNS calculations.

and PDFs $f_{a/p}(x, \mu)$ are consistently evolved using $N_F = 4$ active flavors. However, some of the available calculations in literature were performed by taking $\alpha_s(N_F = 5)$ while using $N_F = 4$ PDFs. This mismatch creates a conceptual inconsistency between the N_f values of the strong coupling used in the hard cross section, on one hand, and in the DGLAP evolution of PDFs, on the other. As already mentioned in the Sec. 10.1, the FFNS is only valid when $p_T^2 \lesssim m_b^2$.

To predict cross sections at all p_T values, including the $p_T^2 \gg m_b^2$ region where FFNS eventually becomes inadequate, several general-mass VFN schemes are available on the market. In FONLL [164, 165], the NLO massive and massless calculations are matched in terms

of

$$\text{FONLL} = \text{FO} + (\text{RS} - \text{FOM0}) \times G(m, p_T). \tag{10.2}$$

Here FO is the Fixed-Order calculation in the massive scheme. FOM0 represents the Fixed-Order results in massless limit, which is analogous to the subtraction term in SACOT. RS is resummed cross section by using the formalism of "perturbative" fragmentation functions (PFFs), $D_{i\to Q}(x,\mu)$ [176, 177], which describe a light parton i goes into the heavy quark. The behavior at intermediate p_T is determined, in part, by a matching function, which is chosen to be

$$G(m, p_T) = \frac{p_T^2}{p_T^2 + c^2 m_Q^2}, \tag{10.3}$$

with $c = 5$ in order to suppress RS-FOM0 for $p_T < 5m_Q$. $G(m, p_T)$ approaches 1 at large p_T and 0 at small p_T. Here, FO differs from the FFNS in that its running couplings and gluon evolution are computed assuming $N_F = 5$ rather than $N_F = 4$ consistently for bottom production.

Differently from FONLL, the GM-VFNS is designed to resum large logarithms as heavy-flavor PDFs. The general structure of the GM-VFNS cross section from Refs. [163, 166] can be expressed as

$$\sigma = \sigma_m + \sigma_0 - \sigma_0^{\Delta}, \quad \text{or} \quad \sigma = \sigma_m + \sigma_0 - \sigma_m^{\Delta}. \tag{10.4}$$

Here σ_m is the massive FFN calculation, while σ_0 is the same cross-section in the limit $m \to 0$, in which m is kept in the logarithmic terms. The $\sigma_0^{\Delta}(\sigma_m^{\Delta})$ are the massless (massive) subtraction terms deduced by a comparison between the heavy flavor hadroproduction and massless QCD jet production at the same order. The original version of GM-VFNS [163], which should have been called ZM-VFNS at that time, performs the calculations of subtraction terms σ_0^{Δ} in the massless limit, which is valid at high p_T. Subsequently, it was extended to include the finite mass effect by evaluating the massive subtraction term σ_m^{Δ} [166]. In addition, the GM-VFNS has embedded fragmentation functions, such as $f_{b\to B^{\pm}}(z,\mu)$, in order to deal with cross sections for hadronic final states.

In contrast to the GM-VFN and FONLL's resummation calculations for the inclusive production of heavy quarks and mesons, Monte Carlo generators based on Parton Showers

(PS) and string (PYTHIA [178]) or cluster (HERWIG [179]) hadronization models can describe completely exclusive final states. The NLO calculation with showering effects was performed with MC@NLO [180] by combining the NLO QCD corrections in the hard part with the improved leading-logarithmic parton shower in HERWIG and subtracting the double-counted terms properly. This approach was further developed in POWHEG [181], which simplifies the subtraction terms, avoids the negative-weight events possible in MC@NLO, and allows one to match to the PYTHIA parton shower as an option. However, both MC@NLO and POWHEG are based on massive $N_F = 4$ NLO calculations, which treats heavy quark as an inactive parton in the PDFs. But both codes adopt $N_F = 5$ in the running of strong coupling, which gives a mismatch, similarly to the FFNS, as we discussed above. As a result, this approach can be only applied to the small and moderate p_T ranges, since it is inconsistent in computing the large logarithms when $p_T \gg m_Q$.

In this work, following the idea of Simplified-ACOT-χ scheme in DIS case [140, 153], we develop the S-ACOT-MPS scheme for the heavy flavor production in the hadron collisions, which is closely similar to GM-VFN calculations [166]. A similar scheme has been proposed under the name of the SACOT-m_T scheme [167], but our MPS scheme differs in two aspects. Firstly, we take a massive phase space for the flavor excitation and subtraction terms in order to closely capture the threshold behavior of massive heavy-flavor production. In contrast, SACOT-m_T scheme just substitutes p_T with m_T in the $x_{1,2}$ integration limits and scaling variables $\tau_{1,2}$ [167]. By its construction, the SACOT-MPS cross section smoothly approaches the FFNS calculation in the $p_T \to 0$ limit. The SACOT-m_T calculation is undefined in the $p_T \to 0$ limit and takes a hard cut for $\sigma_{\rm FE}(p_T < m_Q\sqrt{1/\xi^2 - 1}) = 0$, by setting the heavy-flavor PDF to be zero when $\mu_F = \xi\sqrt{p_T^2 + m_Q^2} < m_Q$. Needless to say, SACOT-m_T scheme only works for the choice of the scale factor to be $\xi < 1$. Secondly, we introduce the concept of a **residual PDF** as the difference between the heavy-flavor PDF and the convolution of a light-flavor PDF with the corresponding splitting function, which simplifies the calculation of the Flavor Excitation and subtraction terms.

For the inclusive hadronic heavy flavor production $pp \to QX$, we can write the cross section in a factorized form,

$$\sigma(pp \to QX) = \sum_{i,j} \int \mathrm{d}x_1 \mathrm{d}x_2 f_i(x_1, \mu_F) f_j(x_2, \mu_F) \hat{\sigma}_{ij}(\hat{s}, \hat{t}, \hat{u}, \alpha_s(N_f, \mu_R^2), m_Q). \tag{10.5}$$

Here $f_i(x, \mu_F)$ is a PDF for flavor $i = g, q, Q$. $\hat{\sigma}_{ij}(\hat{s}, \hat{t}, \hat{u}, \alpha_s(N_f, \mu_R^2), m_Q)$ is the partonic cross section, where $\alpha_s(N_f, \mu_R)$ depends on the active flavor number N_f and renormalization scale μ_R. Here we take $Q = b$ as an example to illustrate. The SACOT-MPS is applicable to the charm-flavor production as well. We can expand the partonic cross section and the PDF in terms of the strong couplings $\alpha_s/2\pi$ as

$$\sigma(pp \to bX) = \sum_{i,j} \sum_{n=0} \left(\frac{\alpha_s}{2\pi}\right)^{n+2} \int \mathrm{d}x_1 \mathrm{d}x_2 f_i(x_1, \mu_F^2) f_j(x_2, \mu_F) \hat{\sigma}_{ij}^{(n)}(\hat{s}, \hat{t}, \hat{u}, m_Q). \tag{10.6}$$

Representative Feynman diagrams are shown in Fig. 10.1. The thick (thin) propagators and external legs indicate the massive (massless) quarks, which will be calculated with (without) mass dependence in our approximation. The leading order only contains Flavor Creation term $gg \to Q\bar{Q}$ shown in Fig. 10.1(a). It can be written as

$$\sigma^{(0)} = \int \mathrm{d}x_1 \mathrm{d}x_2 g(x_1, \mu_F) g(x_2, \mu_F) \hat{\sigma}_{gg}^{(0)}(\hat{s}, \hat{t}, \hat{u}, \alpha_s(N_f, \mu_R^2), m_Q). \tag{10.7}$$

At the next-to-leading order, the Flavor Excitation diagrams involving the heavy flavor as initial partons begin to show up, such as Fig. 10.1(c). In the FE diagrams, the heavy-flavor PDF generated from evolution of DGLAP equation resums the $(\alpha_s^m \log^n \mu_F^2/m_Q^2)$ terms to all order in α_s. At a specific fixed order, overlap terms, such as Fig. 10.1(d), which are included both in the FC terms, such as Fig. 10.1(b), and the Flavor Excitation terms, such as Fig. 10.1(c), should be subtracted in order to avoid double counting. The full contribution of order $O(\alpha_s^3)$ [1] can be written as

$$\begin{aligned}
\sigma^{(1)} = & \int \mathrm{d}x_1 \mathrm{d}x_2 g(x_1, \mu_F) f_i(x_2, \mu_F) \hat{\sigma}_{gi}^{(1)}(\hat{s}, \hat{t}, \hat{u}, \alpha_s(N_f, \mu_R^2), m_b) \\
& + \int \mathrm{d}x_1 \mathrm{d}x_2 \frac{b(x_1, \mu_F)}{\alpha_s/2\pi} f_i(x_2, \mu_F) \hat{\sigma}_{bi}^{(0)}(\hat{s}, \hat{t}, \hat{u}, \alpha_s(N_f, \mu_R^2), m_b = 0) \\
& - \int \mathrm{d}x_1 \mathrm{d}x_2 \log \frac{\mu_F^2}{m_b^2} [P_{b \leftarrow g} \otimes g](x_1, \mu_F) f_i(x_2, \mu_F) \hat{\sigma}_{bi}^{(0)}(\hat{s}, \hat{t}, \hat{u}, \alpha_s(N_f, \mu_R^2), m_b = 0) \\
& + (1 \leftrightarrow 2),
\end{aligned} \tag{10.8}$$

where $f_i(x, \mu_F)$ can be the PDF for gluon or light quarks. The real and virtual corrections to the partonic cross section are included in the $\hat{\sigma}^{(1)}$ term. The convolution is defined as

[1] The LO cross section of $pp \to bX$ is order of $O(\alpha_s^2)$.

$[P \otimes f](x) = \int_x^1 \frac{\mathrm{d}\xi}{\xi} P(\frac{x}{\xi}) f(\xi)$. $P_{b\leftarrow g}(x) = \frac{1}{2}[x^2 + (1-x)^2]$ is the leading order Altarelli-Parisi splitting function for $g \to b\bar{b}$. The denominator $\alpha_s/2\pi$ results from the prefactor that has been factored out in front of Eq. (10.6). The partonic cross section $\hat{\sigma}_{gg}^{(0)}$ and $\hat{\sigma}_{gi}^{(1)}$ for Flavor Creation terms retain full m_b dependence, which is known from in the NLO FFNS calculations [162, 159, 160, 161].

In the hard matrix elements of the Flavor Excitation terms, the heavy quark is treated as massless; but the full mass dependence is retained in the phase space of the FE terms. This setup resolves the technical difficulty that the total cross section of Flavor Excitation terms over the full phase space is diverging due to the forward-backward collinear divergence, which is regulated by fiducial cuts, such as transverse momentum $p_T > 20$ GeV or the pseudorapidity $2.0 < \eta < 4.5$, in the experimental measurement. Following the philosophy of the χ variable introduced in the S-ACOT-χ scheme [140], we adopt the massive phase space of $Q\bar{Q}$ production to capture the threshold effect. As a result, we obtain a finite cross section at all p_T. The details of our implementation and the comparison of massless and massive phase space results can be found in Sec. B.1.

At each order of α_s, the Subtraction (SB) terms and the corresponding FE terms share the same hard-scattering cross section, with the heavy-quark mass ignored in both. In light of this feature, at NLO, we define the **subtraction** heavy-flavor PDF as

$$\tilde{b}(x,\mu) = \frac{\alpha_s(\mu)}{2\pi} \log\frac{\mu^2}{m_b^2} \int_x^1 \frac{\mathrm{d}\xi}{\xi} P_{b\leftarrow g}(\frac{x}{\xi}) g(\xi,\mu). \tag{10.9}$$

With the DGLAP evolution code `HOPPET` [182], we perform this convolution and save $\tilde{b}(x,\mu)$ as an `LHAPDF` [183] format table. Afterwards, the SB terms can be written in a similar way as the corresponding FE terms,

$$\begin{aligned} \sigma_{\mathrm{FE}} &= b(x_1,\mu) f_i(x_2,\mu) \otimes \hat{\sigma}_{bi}^{(0)} + (1 \leftrightarrow 2), \\ \sigma_{\mathrm{SB}} &= \tilde{b}(x_1,\mu) f_i(x_2,\mu) \otimes \hat{\sigma}_{bi}^{(0)} + (1 \leftrightarrow 2). \end{aligned} \tag{10.10}$$

The subtraction terms are now calculated in the same way as Flavor Excitation terms, just by replacing the heavy flavor PDF by the subtraction PDF. Using this subtraction PDF, we compute the subtraction terms much faster than by the standalone computation of the convolution integrals. In fact, we can now compute the FE-SB difference in one step, by convoluting the FE hard cross section with the **residual** PDF $b(x,\mu) - \tilde{b}(x,\mu)$, also provided

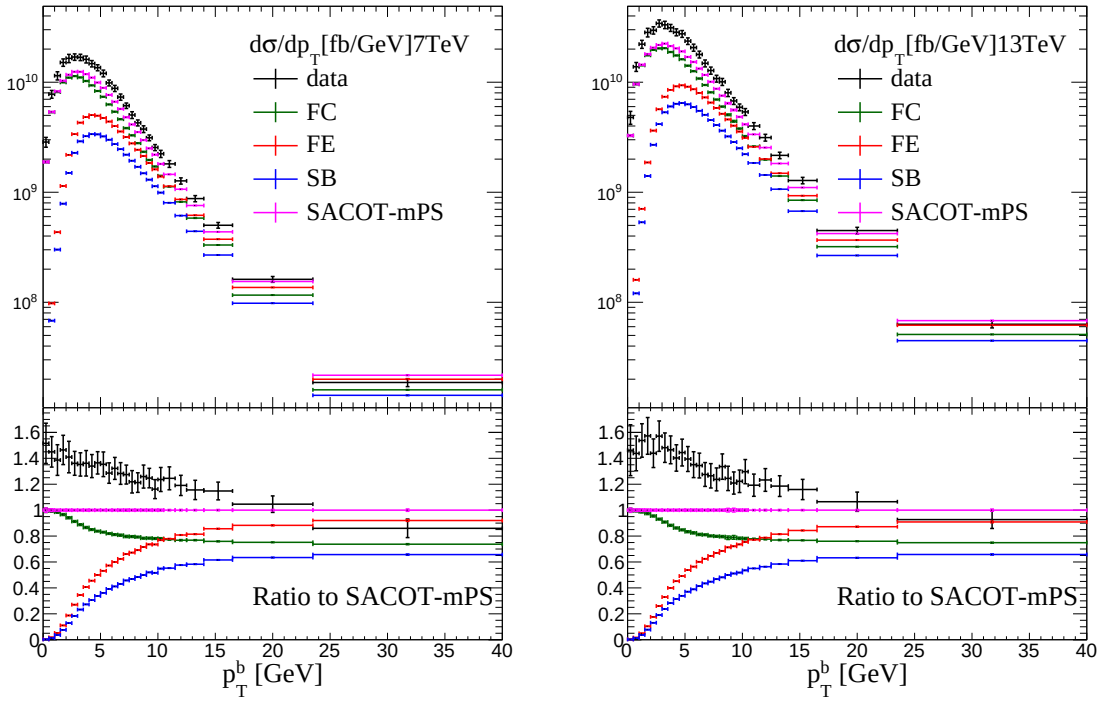

Figure 10.3: The Flavor Excitation (FE) terms, subtracted double counting terms (SB) and Flavor Creation (FC) terms in the forward ($2.0 < |y| < 4.5$) b production at LHCb 7 and 13 TeV [169] and the respectively ratios to the SACOT-MPS calculation values. We corrected the $B^{\pm}$-meson back to b-quark with $f(b \to B^{\pm}) = 0.407$ [184]. Here we take CT14 NNLO central PDF, $m_b = 4.75$ GeV, and scale choice as $\mu_R = \mu_F = \sqrt{m_b^2 + p_T^2}$.

in the form of an `LHAPDF` table. As an illustration, the FC, FE and SB terms for b production at LHCb 7 TeV can be viewed in Figure 10.3.

So far, our SACOT-MPS calculations have been performed for the inclusive b-quark production. In order to perform a fast computation in our global PDF fitting, we generate look-up tables called `APPLgrid` [185] with an interface package `mcfm-bridge`, which allows us a posteriori variations of PDFs, strong couplings, renormalization, and factorization scale and center-of-mass energies. Within the same framework, our calculations can be applied to charm production as well. Equipped with the subtracted PDFs, we can easily extend our calculations to other heavy flavor production processes, such as W/Z or Higgs boson associated with heavy flavor production, which is left to the future work. Another future direction is to extend our calculations to the Next-to-Next-to Leading order, whenever the

public code for NNLO calculations of the fully differential cross section in heavy flavor production is available.

10.3 A phenomenological application to LHCb $B^{\pm}$ production

The first b-flavored hadron measurement performed by LHCb Collaboration is the cross section of $pp \to H_b X$ at 7 TeV reconstructed with events containing a D^0 meson and a muon in the final states [186]. Afterward, LHCb published the 7 TeV $B^{\pm}$ production cross section reconstructed exclusively with the decay mode $B^{\pm} \to J/\psi K^{\pm}$ and $J/\psi \to \mu^+\mu^-$ [187]. These measured total and differential cross sections show good agreement with the FFNS [159, 160] (implemented in the `MCFM` code [188]) and FONLL [189] predictions, within the systematic uncertainties. As we already mentioned, and as is seen in Ref. [174, 165], the theoretical uncertainties are large (about 50%) for both for the total and differential cross sections, mostly reflecting large scale uncertainties. PROSA Collaboration suggests to use a normalized differential cross section for the global QCD analysis [173], in which the large scale dependence is absorbed by the normalization. Another similar idea is to cancel the scale uncertainties by computing cross section ratios between different CM energies [175], or between different rapidity bins [173]. These ideas are implemented in Ref. [174], which projected, based on an analysis using the FONLL program, that the ratio of forwarding heavy quark production at LHCb $\sqrt{s} = 7$ and 13 TeV would provide good sensitivity to the gluon distribution function. Recently, the $B^{\pm} \to J\psi(\to \mu^+\mu^-)K^{\pm}$ analysis at LHCb at 13 TeV [169] becomes available, so that the data on the 13-to-7 ratios can now indeed be compared to theoretical predictions.

We will now present the differential cross section $\mathrm{d}\sigma/\mathrm{d}p_T^b$ of $pp \to bX$ and its corresponding ratio between $\sqrt{s} = 7$ and 13 TeV, and compare it to the LHCb measurements. The central renormalization and factorization scales are set to be the transverse mass of b quark, $\mu = m_T^b = \sqrt{m_b^2 + p_T^2}$. The scale uncertainty is estimated by varying the renormalization and factorization scale independently up and down by a factor of two from the central values, that is, by computing an envelope of a 7-point scale variation:

$$(\mu_R, \mu_F) = \left\{(\frac{1}{2}, \frac{1}{2}), (\frac{1}{2}, 1), (1, \frac{1}{2}), (1, 1), (1, 2), (2, 1), (2, 2)\right\} \times m_T^b. \tag{10.11}$$

We drop two points $(\mu_R, \mu_F) = \{(\frac{1}{2}, 2), (2, \frac{1}{2})\}$ to eliminate particularly large logarithmic variations that may still be present at NLO. We take CT14 NNLO [190] as our PDF set, and estimate the PDF uncertainties with the symmetrical Hessian method [191, 192],

$$\delta^H_{\rm PDF}(X) = \frac{1}{2}\sqrt{\sum_{i=1}^{N_{\rm eig}}(X_i^+ - X_i^-)^2}. \tag{10.12}$$

The CT14 NNLO PDFs generate a nonzero b-quark parton distribution function perturbatively via DGLAP evolution that switches from $N_F = 4$ to $N_F = 5$ at scale $\mu = m_b = 4.75$ GeV. We use the b quark pole mass with $m_b = 4.75$ GeV as the central value and vary it within the $m_b \in [4.5, 5.0]$ GeV range to estimate the quark-mass dependence. Note that, in principle, the variation of m_b in the Flavor Creation terms $\hat{\sigma}_{gi}(m_b)$ and subtraction terms $\log \frac{\mu_F^2}{m_b^2} P_{b\leftarrow g}\hat{\sigma}_{bi}(m_b = 0)$ is not fully consistent with the perturbative b-quark PDF in CT14 NNLO due to this discrepancy. However, as our numerical results will show, this mass dependence can be ignored, when compared to the scale uncertainties, and practically cancels out in the cross section ratios.

LHCb measured the $B^\pm$ meson production over the range $0 < p_T < 40$ GeV and $2.0 < y < 4.5$ at 7 and 13 TeV [169]. With the fragmentation fraction $f(b \to B^\pm) = 0.407$ [184], we obtain the b-quark cross sections and compare against our theoretical predictions. The central values of the SACOT-MPS calculations of the FC, FE and SB contributions to the transverse momentum distribution, $\mathrm{d}\sigma/\mathrm{d}p_T^b$, are displayed in Fig. 10.3. As shown in Fig. 10.3, the Flavor Creation terms make up $60 \sim 80\%$ of the experimental data over the full p_T range. In comparison, the Flavor Excitation terms make a big contribution in the high-p_T region ($p_T \gg m_b$), while its low-p_T ($p_T \lesssim m_b$) contribution is negligible because of mass-dependent phase space suppression. When subtracting the overlapping contribution, we get the total theoretical prediction in a good agreement with data. As we expected, when $p_T \gg m_b$, the b-quark mass can be ignored, and the massive FC terms approach their massless limit. The SB terms cancel the mass logarithms in the FC terms. The FE terms dominate in this region, while the difference FC-SB contributes a smaller finite correction that is effectively one high-order compared to the FE terms. Conversely, when $p_T \lesssim m_b$, we obtain a good cancellation between the Flavor Excitation terms and Subtraction terms.

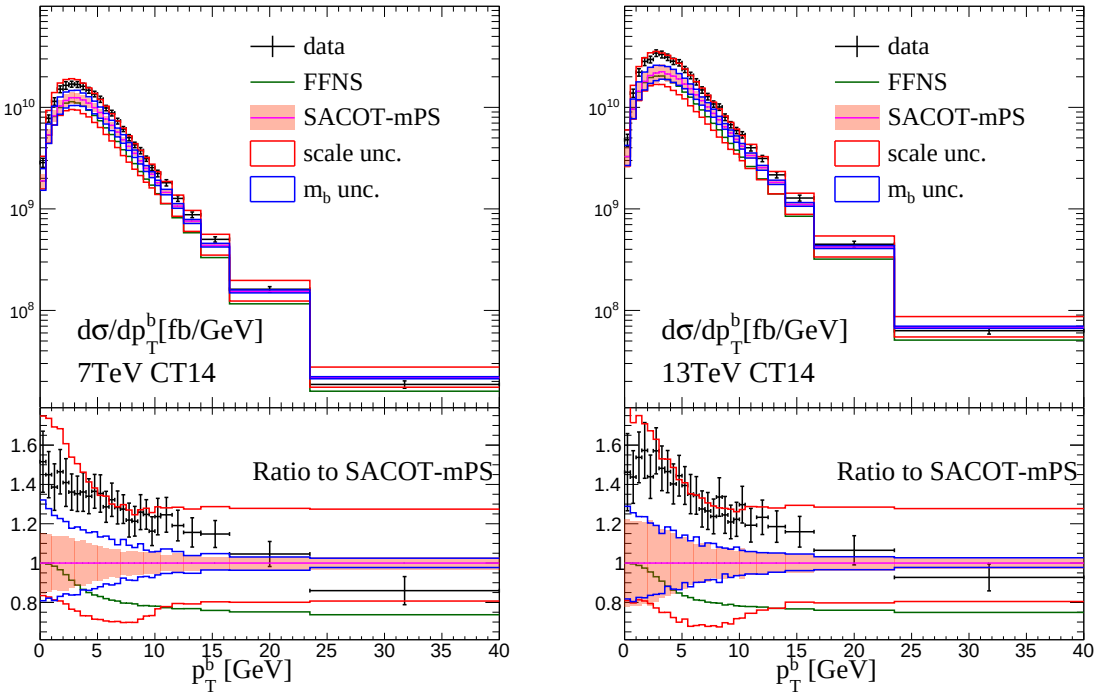

Figure 10.4: The SACOT-MPS calculations for forward ($2.0 < |y| < 4.5$) partonic b-jet production at LHCb $\sqrt{s} = 7$ (left) and 13 (right) TeV [169]. The experimental data for $B^{\pm}$ meson were corrected back to the b-quark level with the fragmentation fraction $f(b \to B^{\pm}) = 0.407$ [174].

The total theoretical predictions (FC+FE-SB) with various theoretical uncertainties are compared against the experimental data in Fig. 10.4. We see that the experimental data fits fully within the theoretical error bands. As we expected, the dominant theoretical uncertainties come from scale variations. In the moderate transverse momentum region ($p_T \sim m_b$), the scale uncertainty can even exceed 50%, while at even higher p_T, it stabilizes around $20 \sim 30\%$, which is consistent with the observations in Ref. [174]. It means the unknown NNLO corrections are non-negligible for $pp \to bX$ process at the LHC collision energy. The PDF uncertainty is about 15% at moderate p_T, while it is a few percent at high p_T. The quark-mass dependence is 10% at low p_T, i.e., slightly smaller than the PDF uncertainty, but it is damped much faster with increasing p_T due to the suppression of mass-dependent terms in the cross section. In comparison, the experimental uncertainties stay below 10% for the whole p_T range.

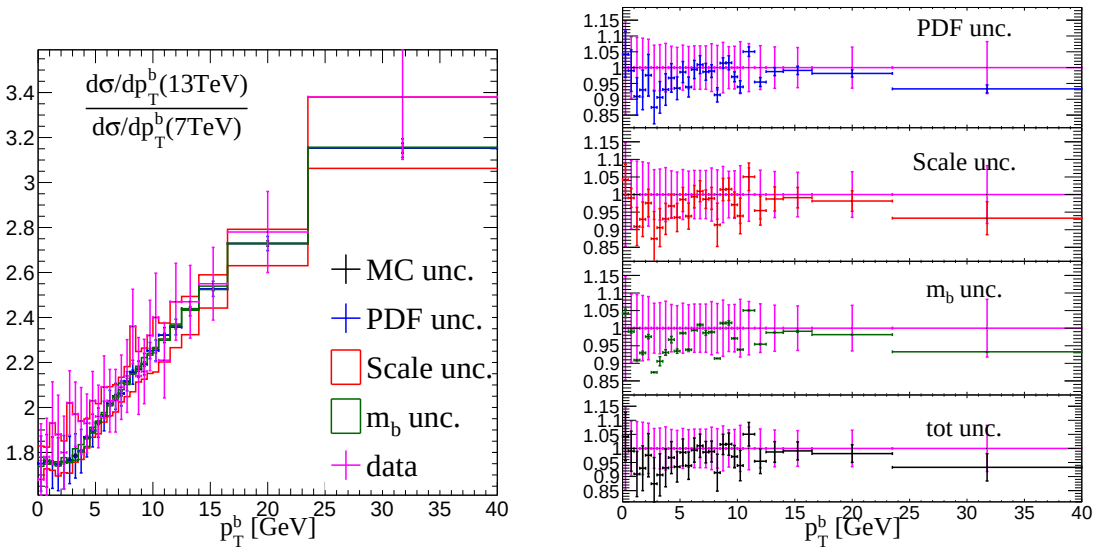

Figure 10.5: Left: the ratio of LHCb p_T distributions at two different collider energies, $\frac{\mathrm{d}\sigma/\mathrm{d}p_T(13\mathrm{TeV})}{\mathrm{d}\sigma/\mathrm{d}p_T(7\mathrm{TeV})}$. Right: the PDF, scale, m_b, and total uncertainties of the cross section ratio.

As suggested in Ref. [175], the ratios of cross sections at different collision energies can cancel the correlated theoretical uncertainties to a large degree, which may improve sensitivity to detailed dynamics in the Standard Model and beyond. Here we consider the ratios of p_T distributions at $\sqrt{s} = 7$ and 13 TeV for B-meson production at LHCb,

$$R(p_T) = \frac{\mathrm{d}\sigma/\mathrm{d}p_T(13\mathrm{TeV})}{\mathrm{d}\sigma/\mathrm{d}p_T(7\mathrm{TeV})}, \tag{10.13}$$

which is shown in Fig. 10.5. As we expected, the scale uncertainties cancel to a large extent in the ratio, down to within 10%. The b-quark-mass dependence is almost cancelled out, with less than 2% left. As a result, the PDF uncertainties turn out to be about the the same size as the scale uncertainties for this ratio observable. The big reduction of the scale uncertainty reflects the assumption that the scale uncertainties are highly correlated at different collider energy. In comparison, the mild cancellation of PDF uncertainties implies that the ratio is sensitivity to the PDFs, especially the gluon PDF that is constrained in different x ranges in this process.

We repeat our calculation for the double differential cross section $\mathrm{d}^2\sigma/(\mathrm{d}p_T\mathrm{d}y)$, shown in Fig. 10.6, and the corresponding cross section ratio between $\sqrt{s} = 7$ and 13 TeV, shown in Fig. 10.7. The theoretical uncertainties for this double differential cross section are larger than the experimental uncertainties throughout the whole p_T. In the cross section ration

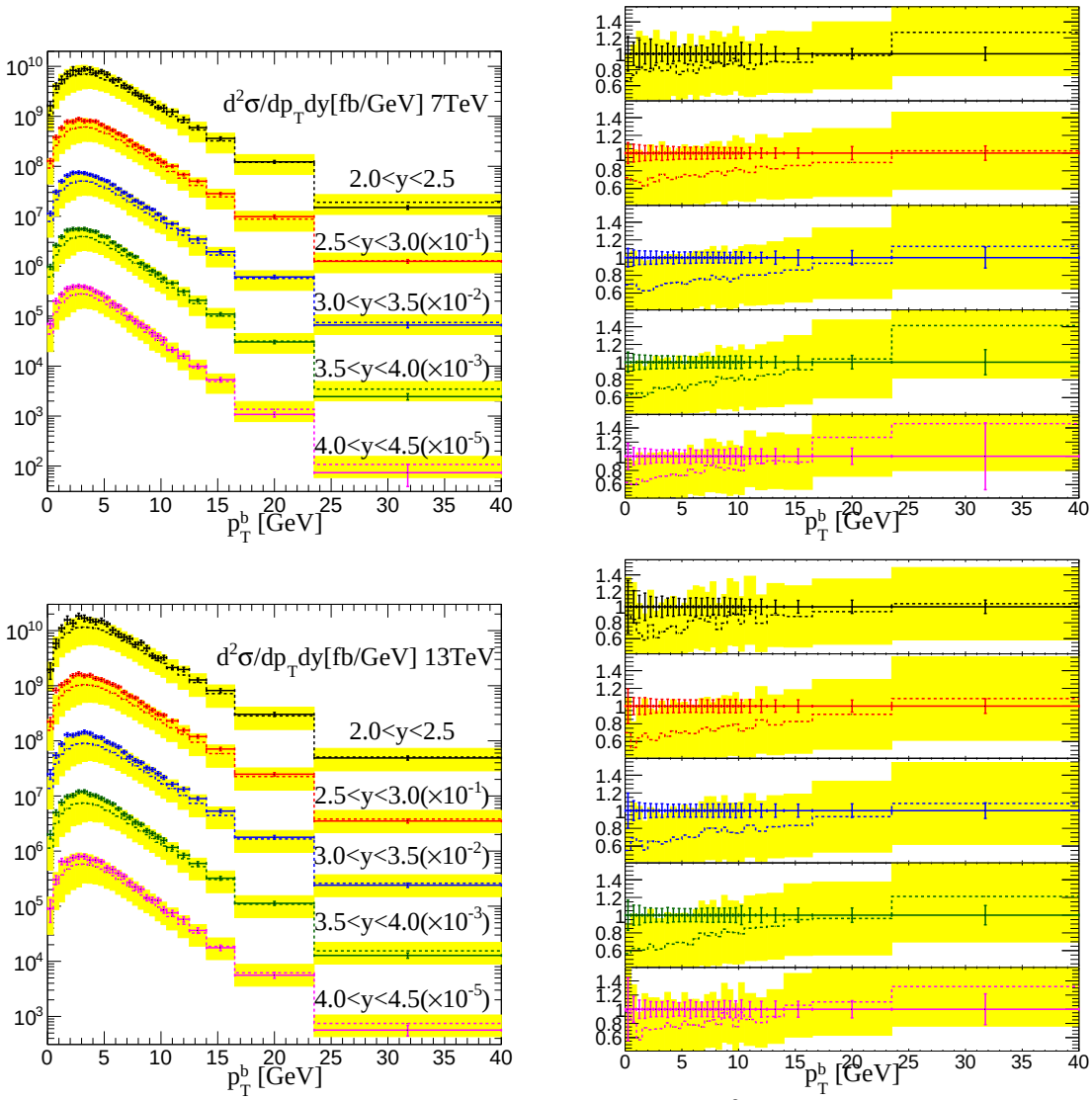

Figure 10.6: Left: the double differential cross section $\frac{\mathrm{d}^2\sigma}{\mathrm{d}p_T\mathrm{d}y}$ for b-meson production. The dashed lines with yellow error bands indicate SACOT-MPS NLO theoretical predictions, while the solid lines with error bars represent experimental data corrected back to parton level [169]. Right: ratios ($R = T/D$) of experimental data (D) to theory calculations (T). Here theoretical errors are given the quadrature sum of PDF, scale, and m_b uncertainties.

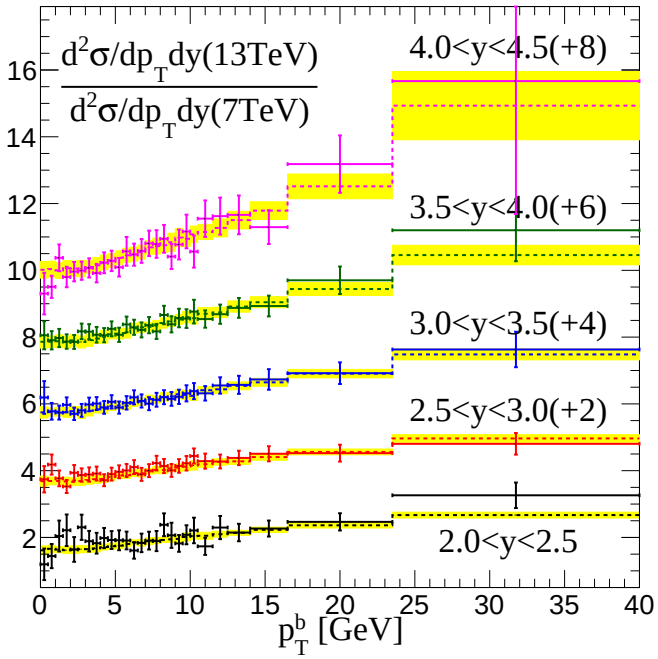

Figure 10.7: The cross section ratio of double differential cross section $\frac{\mathrm{d}^2\sigma/(\mathrm{d}p_T\mathrm{d}y)(13\mathrm{TeV})}{\mathrm{d}^2\sigma/(\mathrm{d}p_T\mathrm{d}y)(7\mathrm{TeV})}$. Same as Fig. 10.6, the dashed lines with yellow error bands are SACOT-MPS NLO theory predictions while the solid lines with error bars represent data. Here the experimental errors are calculated with $\delta R/R = \sqrt{(\delta X_{13}/X_{13})^2 + (\delta X_7/X_7)^2}$, with $X_{13}(X_7)$ and $\delta X_{13}(\delta X_7)$ as the experimental measured value and the corresponding uncertainty for 13 (7) TeV.

in Figure 10.7, the theoretical uncertainties are reduced compared to the cross sections themselves in Figure 10.6. On the other hand, the experimental uncertainties has increased, rather than decreased. We propagate the experimental uncertainties into the cross section ration R according to the formula

$$\frac{\delta R}{R} = \sqrt{\left(\frac{\delta X_{13}}{X_{13}}\right)^2 + \left(\frac{\delta X_7}{X_7}\right)^2}, \quad \text{with} \quad R = \frac{X_{13}}{X_7}, \tag{10.14}$$

where X stands for the double differential cross section $\mathrm{d}^2\sigma/(\mathrm{d}p_T\mathrm{d}y)$. It means the experimental uncertainties are accumulated in Fig. 10.7, while the theoretical uncertainties cancel.

With the typical momentum fractions estimated to be roughly $x_{1,2} = \frac{\sqrt{m^2+p_T^2}}{\sqrt{s}}e^{\pm y}$, we know that the data at high p_T (such as $p_T = 40$ GeV) and high rapidity (such as $y = 4.5$) can probe the gluon PDF at a large momentum fraction ($x \sim \frac{\sqrt{5^2+40^2}}{7000}e^{4.5} \simeq 0.5$). On the contrary, the low p_T with high rapidity can probe the small momentum fraction down to $x \sim \frac{\sqrt{5^2+5^2}}{13000}e^{-4.5} \simeq 6 \times 10^{-6}$. These extremely large and extremely small x domains are out of reach of other measurements.

10.4 Conclusions

In this chapter, we propose a heavy-flavor general-mass factorization scheme SACOT-MPS of the ACOT family [193, 141, 140, 153] for a broad class of processes involving massive quark production and scattering at hadron colliders. This scheme reduces to the fixed-flavor-number scheme near the kinematical threshold for heavy quark production, and it resums heavy-quark mass logarithms in the regions where the quark masses are negligible. We systematically classify the radiative contributions into Flavor Creation (FC) and Flavor Excitation (FE) categories, then consistently subtract the double-counted terms, dubbed as Subtraction (SB) terms. Following the insights from using a rescaling χ-variable in the S-ACOT-χ scheme, the SACOT-MPS scheme evaluates integrals of the Flavor Excitation and Subtraction terms using massless hard-scattering matrix elements combined with the mass-dependent, rather than massless, phase space. This prescription results in a smooth, stable matching of the full SACOT-MPS cross section onto the FFNS result in the regions where the threshold kinematics is important. To demonstrate the potential of the SACOT-MPS scheme, we apply our theoretical calculations at NLO to the (double) differential cross

section dependent on the transverse momentum (p_T) and rapidity y of the $B^{\pm}$ meson in LHCb measurement at $\sqrt{s} = 7$ and 13 TeV [169].

The SACOT-MPS calculation demonstrates clockwork cancellations among its constituent parts (between the FE and SB terms at small p_T, and between the SB and logarithmically-enhanced FC terms at large p_T) that lead to stable predictions across the full p_T range and guarantee systematic improvement in the theoretical accuracy from including even higher-order perturbative QCD corrections.

We investigate the renormalization and factorization uncertainties by varying the central scale value $\mu_R = \mu_F = \sqrt{m_b^2 + p_T^2}$ up and down by a factor of 2, computing the PDF uncertainties with the symmetric Hessian method, and varying the b-quark mass. The SACOT-MPS NLO theoretical predictions agree well with the experimental data within the uncertainties. The scale uncertainty is a dominant resource that limits the predictivity power of the NLO QCD theory. By taking the ratios of cross sections at different center-of-mass energies, we may obtain some reduction of theoretical uncertainties, especially the cancellation of the QCD scale dependence, if the variations of the renormalization and factorization scales are assumed to be correlated in the numerator and denominator. More precise experimental measurements of these ratios, combined with the envisioned NNLO calculations for the respective theoretical predictions, open the possibility to constrain the gluon PDF in both the high- and low-x regions, thanks to the forward configuration of the LHCb detector, and it can offer valuable inputs for future global PDF analyses.

Chapter 11

Summary

11.1 The SGM model

In this dissertation, we started with the discussion of the electroweak sector in the Standard Model in Chapter 2. Motivated by neutrino masses, we discussed several possible solutions, known as the seesaw mechanism, in Chapter 3. We reviewed three types of seesaw mechanism, based on different particle fields to be added into the Standard Model. Type I seesaw mechanism corresponds to right-handed Majorana neutrinos. Alternatively, we considered scalar triplets Δ to realize the Type-II seesaw mechanism. If a hypercharge $Y = 2$ is assigned to the triplet, we can couple it to the leptonic doublet, $l_L = (\nu_L, e_L)^T (Y = -1)$, in the Yukawa way $y l_L^T C i\tau_2 \Delta l_L$. After this triplet develops a VEV in the SSB (or induced by the VEV of the SM Higgs), the left-handed neutrinos acquire Majorana masses.

However, there is no such thing as a free lunch. The triplet VEVs have a contribution to electroweak symmetry breaking (EWSB), which is strongly constrained by precision measurements. The ρ parameter [44] is one of the strongest constraints. The Standard Model predicts $\rho = 1$ at the tree level, and the current precision measurements constrain the deviation within $\Delta\rho \lesssim 10^{-3}$ [23]. This small number implies a fine-tuning on the triplet VEVs. We introduce a custodial symmetry, which strongly weakens the ρ parameter constraint. The custodial symmetry requires at least 2 triplets: a complex ($Y = \pm 2$) one, χ, and a real ($Y = 0$) one, η. This is the well-known **Georgi-Machacek** (GM) Model. Under the custodial symmetry, the triplet VEVs are aligned, i.e., $v_\chi = v_\eta$. As a result, $\Delta\rho = 0$ is recovered at the tree level.

But situations are not so simple when we go one step further. We have to keep it in mind that the custodial symmetry is not a priori requirement of the Standard Model or its extension. It is an accidental symmetry that the SM Higgs potential automatically satisfies.

Moreover, the custodial symmetry is only approximate, which is violated already in the Standard Model, due to two sources: nonzero hypercharge gauge interaction and unequal Yukawa couplings between up- and down-type fermions. First, the nonzero hypercharge gauge introduces mass splitting between the neutral and charged weak gauge bosons, that is, $M_Z \neq M_W$. We saw this mass splitting happened twice in the supersymmetric custodial triplet model in Chapter 5. It is not a big issue, at least at the tree level, as it is compensated by the Weinberg angle θ_W in the ρ parameter definition. However, the situation changes because of quantum corrections. The nonzero hypercharge interaction introduces a quadratic divergence in the ρ parameter, starting at the one-loop level [60]. A similar divergence occurs in the mass splitting of the up- and down-type fermions. Numerically, the big difference between the top and bottom quarks contributes to the biggest part of nonzero $\Delta\rho$. A lesson here is that the custodial symmetry will be recovered in the limit of zero hypercharge, $g_Y \to 0$, and equal Yukawa couplings, $y_t \to y_b$.

This the hierarchy problem associated with the quadratic divergence in the loop corrections to the squared masses of scalars fields, can be solved by supersymmetry (SUSY). Therefore, we introduced the supersymmetry to obtain the Supersymmetric Custodial Triplet Model (SCTM), which eliminated both quadratic divergences simultaneously. We first reviewed the basic ingredients of supersymmetry and its extension of the Standard Model in Chapter 4. We limited ourselves to the Minimal Supersymmetric Standard Model (MSSM). We focused on the Higgs sector as one specific example of the Two-Higgs-Doublet Model (2HDM), which was also briefly discussed there.

Afterward, we moved forward to the SCTM in Chapter 5. We derived the F- and D-term potentials of the SCTM. So far, no supersymmetric particles have been discovered yet, which means the SUSY must be broken. People have come up with several mechanisms to break the SUSY, mediated by gravity [84], gauge [194], gaugino [195], or anomaly [85]. We parameterized the soft SUSY breaking in an effective way, which breaks SUSY explicitly. With F-, D- and soft breaking terms, we fully determined the mass spectrum of the SCTM. We focused on the electroweak sector, including scalars and their fermionic superpartners (gauginos and higgsinos). When comparing the SCTM spectrum with the GM one, we obtained a decoupling limit when the dimensionful parameters, B-terms, become large

($|B_{\mu,\Delta}| \to \infty$). In such a limit, all the GM-like particles in the SGM and GM models share the same masses at the energies in the TeV range, while all the *mirror*-GM particles become heavy, and therefore, are decoupled. We dubbed this decoupling limit of the SCTM as the Supersymmetric GM (SGM) model. It gives a weakly coupled origin for the ordinary GM model at the EW scale.

The next natural question is whether we can distinguish the SGM from the GM models, even though the GM-like spectrum is the same. In Chapter 6, we realized that the key was to observe the superpartners, especially higgsinos. When the Lightest Supersymmetric Particle (LSP) becomes light, the GM-like particles can decay into the LSP or other light superpartners, which lowers down the branching ratios of the GM-like particles into the SM particles, such as diboson (WW, ZZ) or diphoton. In contrast, if the LSP is heavy, all the superpartners are decoupled from the GM sector, which leaves the SGM model the same as the GM model. In Chapter 7, we took the GM and SGM models as examples to show how light exotic Higgs bosons could escape the current experimental constraints, through the cancellation of different loops and via the invisible decays.

11.2 Heavy-particle production

The most powerful machines to produce the massive particles predicted by the GM and SGM models are hadron colliders. The physics at hadron colliders is based on our understanding of Quantum Chromodynamics (QCD). In Chapter 8, we started with the Higgs production through gluon fusion as an example to demonstrate the QCD factorization theorem. Then, we generalized the factorization formalism and discussed the higher-order corrections. We applied the factorization to the Drell-Yan process and deep inelastic scattering.

In Chapter 9, we discussed the heavy-flavor production in DIS. First, we compared two heavy-flavor treatments: the **fixed-flavor-number** (FFN) and **zero-mass** (ZM) schemes. When the physical energy scale characterized by the photon virtuality ($Q^2 = -q^2$) is not so high compared to the heavy-quark mass ($Q^2 \sim m_q^2$), the heavy quark can be treated as inactive. The heavy quark can be only produced through **flavor creation** (FC), in which the heavy quark must be treated as massive. In contrast, when the physical energy becomes much larger than the heavy-quark mass ($Q^2 \gg m_q^2$), the heavy quark can be treated as

massless in hard scattering processes. We have to resum large logarithms, $\alpha_s^m \log^n(Q^2/m_q^2)$, into the heavy-flavor PDF. In such a case, the dominant contribution to the heavy-flavor production comes from the **flavor excitation** (FE) term.

When the physical energy Q spans both the low and the high energy regions, we need a composite scheme to encompass the merits of the FFN and ZM schemes in their own valid ranges. That is the idea of the **general-mass variable-flavor-number** (GM-VFN) scheme. However, the subprocesses corresponding to the diagrams of gluon splitting into heavy quark are counted twice, both in the FC and FE channels. We need to subtract the double-counted terms systematically, which is the key point of the ACOT scheme [135, 136, 137, 138, 139]. The ACOT scheme allows us to deal with the heavy-quark mass consistently. In the FC terms, the heavy-quark mass is kept. In the FE and subtraction terms, we can take the zero-mass approximation to simplify the calculation significantly, which is the idea of the simplified-ACOT (S-ACOT) scheme [141, 142]. In the high-energy limit, the subtraction terms are expected to cancel the FC terms, which leaves the FE terms to remain. That is, the S-ACOT scheme then coincides the ZM scheme in this region. In the low-energy limit, the subtraction terms cancel the FE terms, leaving the S-ACOT scheme to be equivalent to the FFN scheme. However, in the threshold region, the cancellation between the FE and subtraction terms is unstable due to the divergence behavior of the zero-mass approximation. Wu-Ki Tung *et al.* proposed the S-ACOT-χ scheme [140], in which the momentum fraction x was replaced by a rescaling variable $\chi = x(1 + 4m_q^2/Q^2)$. It enforces the momentum conservation and stabilizes the cancellation between FE and subtraction terms when $Q^2 \sim m_q^2$.

However, when extending the S-ACOT-χ scheme to a higher order, we face difficulty in calculating the full mass-dependent coefficient functions. In contrast, the zero-mass coefficient functions are much easier to obtain. Inspired by the χ variable, Pavel Nadolsky and Wu-Ki Tung introduced the **intermediate-mass** (IM) scheme [152] to approximate the mass-dependence of the full GM scheme. In the IM scheme, we introduce a more general rescaling variable $\zeta(\lambda)$ with a free parameter λ. We can extract λ from the exact mass dependence at a lower order and apply it to higher orders. Equipped with the tools of the IM scheme, we extended the calculation of DIS heavy-flavor structure functions to N3LO.

In Chapter 10, we applied the idea of the S-ACOT scheme to heavy-flavor production at hadron colliders. Similarly to the χ prescription in SACOT-χ scheme, we introduced the **massive phase space** (MPS) for the FE and subtraction terms to capture the mass dependence, and we dubbed it as the SACOT-MPS scheme. Furthermore, we constructed the subtraction and residual PDFs which simplify the calculation of the FE and subtraction terms. We also proposed to do QCD calculations with the subtracted and residual PDFs, which simplify the computations for the FE and subtraction terms. When describing the data of $B^{\pm}$ meson production at LHCb, we found large theoretical uncertainties, especially the scale uncertainties. Therefore, we took a ratio variable, defined as the ratio of cross sections at different collision energies. The theoretical uncertainties on this ratio variable cancel significantly. In such a way, the SACOT-MPS calculation provides a good prescription for the LHCb data.

Appendix A

Dimensional regularization

A.1 One-Loop Integrals

Considering a general one-loop diagram shown Figure A.1, we have the corresponding loop integral tensor written as

$$T^N_{\mu_1\cdots\mu_P} = \frac{\mu^{4-D}}{i\pi^{D/2} r_\Gamma} \int \mathrm{d}^D q \frac{q_{\mu_1}\cdots q_{\mu_P}}{[q_1 - m_1^2][(q+k_1)^2 - m_2^2]\cdots[(q+k_{N-1})^2 - m_N^2]}, \tag{A.1}$$

where

$$r_\Gamma = \frac{\Gamma^2(1-\epsilon)\Gamma(1+\epsilon)}{\Gamma(1-2\epsilon)},\ D = 4 - 2\epsilon. \tag{A.2}$$

where the momentum k_i is defined as Figure A.1,

$$\begin{aligned} &p_1 = k_1,\ p_2 = k_2 - k_1,\ \cdots\ p_N = k_N - k_{N-1}, \\ &k_1 = p_1,\ k_2 = p_1 + p_2,\ \cdots\ k_N = \sum_i^N p_i. \end{aligned} \tag{A.3}$$

These integral tensor can be reduced to linear combinations of Lorentz covariant tensors, which can be constructed from $g_{\mu\nu}$ and $k_{i\mu}k_{j\nu}$, etc [196]. This reduction procedure is not unique, and we following the conventions in `LoopTools` [78]. The tensor integrals showing up in this dissertation reads explicitly as

$$\begin{aligned} B_\mu &= k_{1\mu} B_1, \\ B_{\mu\nu} &= g_{\mu\nu} B_{00} + k_{1\mu}k_{1\nu} B_{11}, \\ C_\mu &= k_{1\mu} C_1 + k_{2\mu} C_2 = \sum_{i=1}^2 k_{i\mu} C_i \\ C_{\mu\nu} &= g_{\mu\nu} C_{00} + \sum_{i,j=1}^2 k_{i\mu}k_{j\nu} C_{ij}, \\ C_{\mu\nu\rho} &= \sum_{i=1}^2 (g_{\mu\nu}k_i\rho + g_{\nu\rho}k_{i\mu} + g_{\mu\rho}k_{i\nu}) C_{00i} + \sum_{i,j,l=1}^2 k_{i\mu}k_{j\nu}k_{l\rho} C_{ijl}. \end{aligned} \tag{A.4}$$

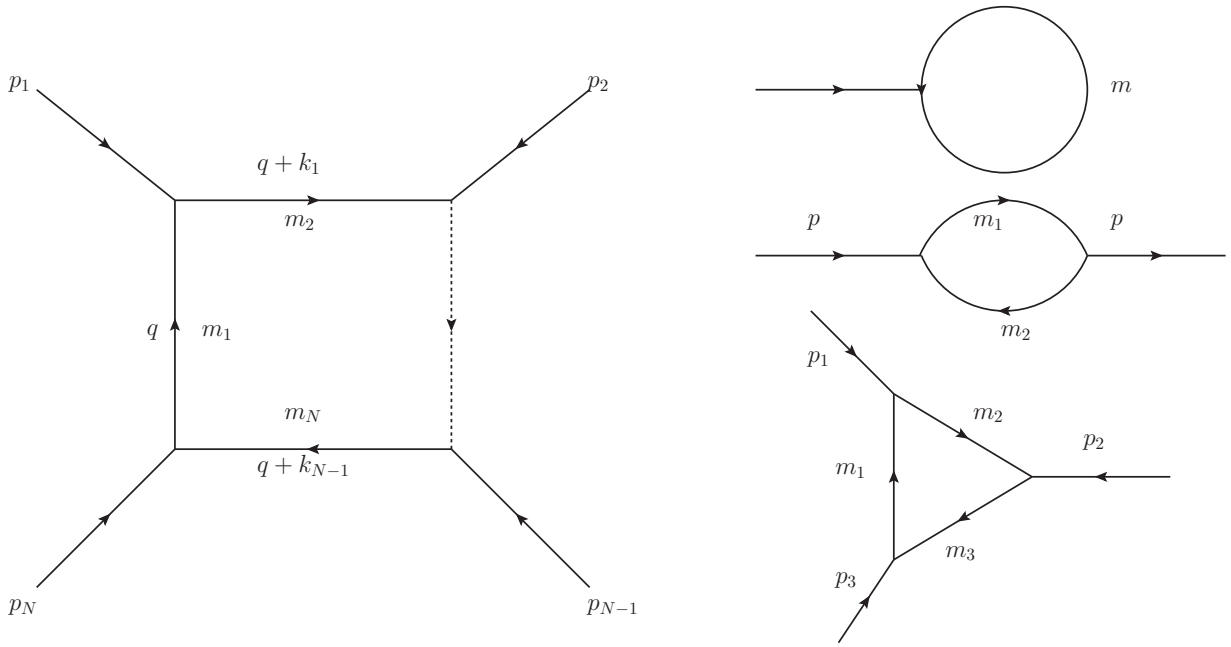

Figure A.1: A general loop integral tensor, and the A, B, C functions.

We have use the following conventions for momenta inside of the parentheses,

$$\begin{aligned} A(a) &: a = m^2, \\ B(a) &: a = p^2, m_1^2, m_2^2, \\ C(a) &: a = p_1^2, p_2^2, (p_1 + p_2)^2, m_1^2, m_2^2, m_3^2. \end{aligned} \tag{A.5}$$

Appendix B

Massless partonic cross sections

B.1 Flavor Excitation terms

When heavy quarks are treated as active partons inside the proton, the cross section for $pp \to QX$ contains nonzero Flavor Excitation (FE) terms – Feynman graphs with initial-state heavy quarks. The FE terms and respective SB terms are approximate and are introduced to resum large logarithms in the limit when $p_T^2 \gg m_Q^2$. The coefficient functions and phase space for the FE and SB terms are not unique and may include mass-dependent terms that always cancel up to one higher-order in α_s [153]. This flexibility can be put to advantage to simplify the functional form of the FE and SB coefficient functions, and at the same time to improve the cancellation of the FE and SB near the threshold for heavy-quark production, where both terms become unphysical. The SACOT-MPS scheme builds on these principles by evaluating the FE and SB terms using *massless* hard-scattering cross sections and *exact phase space* with full mass dependence. As a result, the SACOT-MPS cross sections are easy to implement and demonstrate fast perturbative convergence at all p_T.

In our specific application to inclusive b-meson hadroproduction, the $\mathcal{O}(\alpha_s)$ matrix elements for the FE and SB terms in the SACOT-MPS scheme are exactly the same as the leading order of $bg \to bg$ and $bq \to bq$ in dijet production, shown in Fig. B.1. By summing over 3 channels of $b(k_1)g(k_2) \to b(k_3)g(k_4)$, we obtain the squared amplitude as

$$|\mathcal{M}_{bg\to bg}|^2 = \frac{64\pi^2}{9}\alpha_s^2(t^2+u^2)(-\frac{1}{ut}+\frac{9}{4s^2}). \tag{B.1}$$

The partonic Mandelstam variables [1] are defined as

$$s = (k_1+k_2)^2 = 2k_1\cdot k_2, \quad t = (k_1-k_3)^2 = -2k_1\cdot k_2, \quad u = (k_1-k_4)^2 = -2k_1\cdot k_4, \tag{B.2}$$

[1] Typically, the partonic parameter is denoted with a hat above, such as $\hat{s}, \hat{t}, \hat{u}$. But we leave out the hat here for simplicity.

and satisfy $s+t+u=0$. The tree-level diagram $b(k_1)q(k_2) \to b(k_3)q(k_4)$ renders a squared amplitude

$$|\mathcal{M}_{bq\to bq}|^2 = \frac{64\pi^2}{9}\alpha_s^2 \frac{s^2+u^2}{t^2}. \tag{B.3}$$

In these diagrams, spins and colors are averaged for the initial states and summed over for the final states.

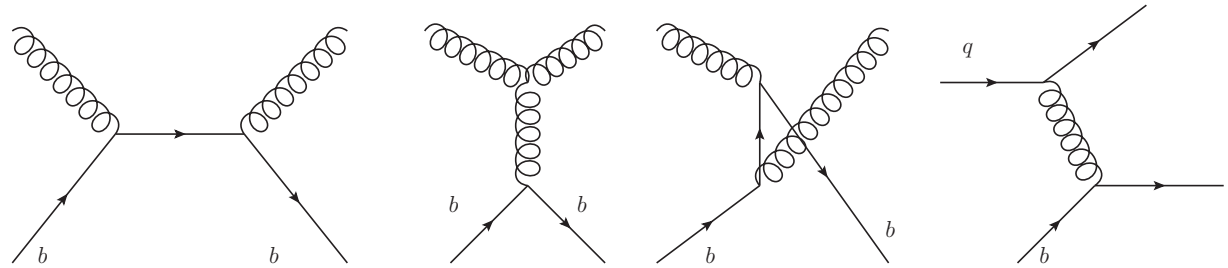

Figure B.1: Feynman diagrams for scattering processes $bg \to bg$, (a) s-channel, (b) t-channel, (c) u-channel, and (d) $bq \to bq$.

In the center-of-mass frame, partonic momenta take the form

$$\begin{aligned} k_1 &= \frac{Q}{2}(1,0,0,1), & k_2 &= \frac{Q}{2}(1,0,0,-1), \\ k_3 &= \frac{Q}{2}(1,\sin\theta,0,\cos\theta), & k_4 &= \frac{Q}{2}(1,-\sin\theta,0,-\cos\theta), \end{aligned} \tag{B.4}$$

if the momenta of the final-state particles are in the O-xz plane. The Mandelstam variables become

$$s = Q^2, \quad t = -\frac{Q}{2}(1-\cos\theta), \quad u = -\frac{Q^2}{2}(1+\cos\theta). \tag{B.5}$$

The two-body phase space can be written as

$$\mathrm{d}\Phi_2 = (2\pi)^4\delta^{(4)}(k_1+k_2-k_3-k_4)\frac{\mathrm{d}^3k_3}{(2\pi)^3 k_3^0}\frac{\mathrm{d}^3k_4}{(2\pi)^3 2k_4^0} = \frac{\mathrm{d}\Omega}{32\pi^2}. \tag{B.6}$$

Therefore, we get the total partonic cross section for $gb \to gb$ as

$$\begin{aligned} \hat{\sigma}(gb\to gb) &= \frac{1}{2s}\int \mathrm{d}\Phi_2 |\mathcal{M}_{gb\to gb}|^2 \\ &= \frac{4\pi}{3Q^2}\alpha_s^2\left[10 + \frac{72}{1-x} + x(11+x) + 36\log(1-x) + 8\log(1+x)\right]\Big|_{-1+\delta}^{1-\delta}, \end{aligned} \tag{B.7}$$

where $x = \cos\theta \in [-1+\delta, 1-\delta]$. Similarly, we get the $bq \to bq$ cross section in the full phase space as

$$\hat{\sigma}(bq\to bq) = \frac{2\pi}{9Q^2}\alpha_s^2\left[\frac{8}{1-x} + x + 4\log(-1+x)\right]\Big|_{-1+\delta}^{1-\delta}. \tag{B.8}$$

We can see clearly that the full phase space cross section is divergent in the forward collinear limit $\delta \to 0$ and soft limit $Q^2 \to 0$, which is regulated by the fiducial cuts such as $p_T > p_T^{\mathrm{cut}}$

or $|\eta| < \eta^{\rm cut}$ in the practical experimental measurements. Let us consider the differential cross section $\mathrm{d}\sigma/\mathrm{d}p_T$ in the $p_T \to 0$ limit. In the partonic center-of-mass frame at LO, the $p_T = \frac{Q}{2}\sin\theta = \frac{\sqrt{x_1 x_2 S}}{2}\sin\theta$. Therefore, two limits $\hat{s} = x_1 x_2 S \to 0$ and $\theta \to 0, \pi$ will lead to $p_T \to 0$. As we discussed above, the $\theta \to 0, \pi$ limit leads to a collinear divergence, which is regulated by the experimental rapidity cut. The limit $x_1 x_2 S \to 0$ violates the threshold constraint, which invalidates the massless assumption. In other words, the Flavor Excitation calculations break down when $\hat{s} = x_1 x_2 S < 4m_Q^2$. Together with the threshold constraint $x_1 x_2 S > 4m_b^2$ and the rapidity cut $|y| < y^{\rm cut}$, we will get an effective cut for in the FE and SB terms,

$$\begin{aligned} 4m_b^2 < x_1 x_2 S = 2p_T^2(1+\cosh\Delta y) < 2p_T^2(1+\cosh 2y^{\rm cut}) \\ \Longrightarrow p_T > \sqrt{\frac{2m_b^2}{1+\cosh 2y^{\rm cut}}} \approx 2m_b e^{-y^{\rm cut}}, \end{aligned} \tag{B.9}$$

where $x_{1,2} = \frac{p_T}{\sqrt{S}}(e^{\pm y_1} + e^{\pm y_2})$. For the typical LHCb measurement, the fiducial volume satisfies $|y| < 4.5$, which gives $p_T^b > 2 \cdot 4.75 \cdot e^{-4.5} \approx 0.1$ GeV, and avoids the $p_T^b \to 0$ limit.

In order to implement this threshold constraint naturally, the SACOT-MPS approach evaluates all three types of terms (FC, FE, and SB) using the massive phase space. The difference between the cancellations of the FE and SB terms in the region $p_T^2 \sim m_b^2$, when those are evaluated using the massless and massive phase spaces, is illustrated in the example of the LHCb forward ($2.0 < y < 4.5$) $B^{\pm}$ production at 7 TeV [169], shown in Figure B.2. In the high-p_T region, the massive phase space approaches its massless limit. At $p_T^2 \gg m_b^2$, the FE and SB terms computed with the massive phase space (indicated by mFE and mSB) are essentially identical to their counterparts computed with the zero-mass space, 0FE and 0SB. Besides, the SB term approaches and nearly cancels the full FC term (or rather, it exactly cancels the logarithmically enhanced part of the FC term). In the same region, the FE term is somewhat larger than the FC term, indicating that the higher-order contributions introduced as a part of the b-quark PDF in the FE term, but missing in the FC term, cannot be omitted in this case.

Conversely, in the low-p_T limit, the Flavor Creation contribution to the differential cross section $\mathrm{d}\sigma/\mathrm{d}p_T$ converges well, since the heavy quark mass m_b serves a natural regulator. In sharp contrast, the 0FE and 0SB with massless phase space diverge in this limit, because

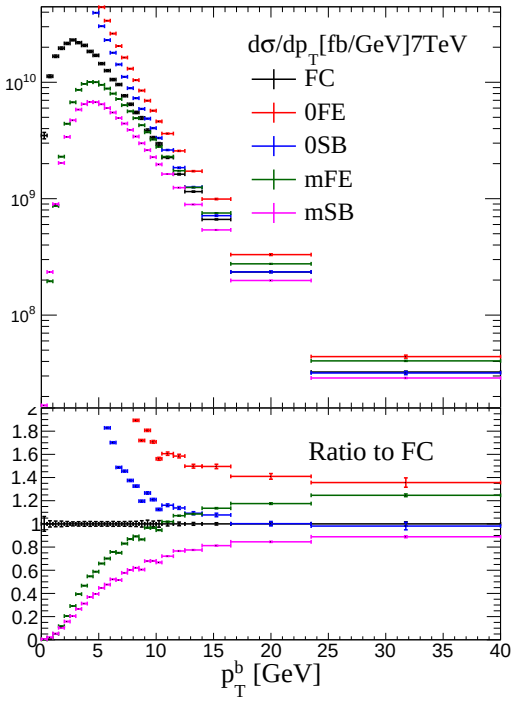

Figure B.2: The massive and massless phase space results for Flavor Excitation and Subtraction terms when compared to the Flavor Creation terms. Here we take the fiducial volume of the LHCb 7 TeV measurement of $B^{\pm}$ production [169] as an example to demonstrate.

of the collinear and soft singularities present at $p_T \to 0$. Ideally, we expect the 0FE and the 0SB to cancel in the $p_T \to 0$ limit. But the divergence destabilizes this cancellation. However, after adopting the massive phase space, the divergent behavior gets tamed by the phase space suppression. We get a stable good cancellation between the mFE and mSB terms in this region, which leaves the FC terms to dominate.

REFERENCES

[1] J. Roche, "What is strongly interacting matter." `https://inpp.ohio.edu/~roche/group_page/strongly_interacting.html`, January, 2014.

[2] A. Pais and S. B. Treiman, *How many charm quantum numbers are there?*, *Phys. Rev. Lett.* **35** (Dec, 1975) 1556–1559.

[3] S. Weinberg, *A Model of Leptons*, *Phys. Rev. Lett.* **19** (1967) 1264–1266.

[4] C. N. Yang and R. L. Mills, *Conservation of isotopic spin and isotopic gauge invariance*, *Phys. Rev.* **96** (Oct, 1954) 191–195.

[5] Y. Nambu, *Quasi-particles and gauge invariance in the theory of superconductivity*, *Phys. Rev.* **117** (Feb, 1960) 648–663.

[6] J. Goldstone, *Field Theories with Superconductor Solutions*, *Nuovo Cim.* **19** (1961) 154–164.

[7] F. Englert and R. Brout, *Broken symmetry and the mass of gauge vector mesons*, *Phys. Rev. Lett.* **13** (Aug, 1964) 321–323.

[8] P. W. Higgs, *Broken symmetries and the masses of gauge bosons*, *Phys. Rev. Lett.* **13** (Oct, 1964) 508–509.

[9] G. S. Guralnik, C. R. Hagen and T. W. B. Kibble, *Global conservation laws and massless particles*, *Phys. Rev. Lett.* **13** (Nov, 1964) 585–587.

[10] UA1 collaboration, G. Arnison et al., *Experimental Observation of Isolated Large Transverse Energy Electrons with Associated Missing Energy at s**(1/2) = 540-GeV*, *Phys. Lett.* **B122** (1983) 103–116.

[11] UA1 collaboration, G. Arnison et al., *Experimental Observation of Lepton Pairs of Invariant Mass Around 95-GeV/c**2 at the CERN SPS Collider*, *Phys. Lett.* **B126** (1983) 398–410.

[12] UA2 collaboration, M. Banner et al., *Observation of Single Isolated Electrons of High Transverse Momentum in Events with Missing Transverse Energy at the CERN anti-p p Collider*, *Phys. Lett.* **B122** (1983) 476–485.

[13] UA2 collaboration, P. Bagnaia et al., *Evidence for Z0 —¿ e+ e- at the CERN anti-p p Collider*, *Phys. Lett.* **B129** (1983) 130–140.

[14] ATLAS collaboration, G. Aad et al., *Observation of a new particle in the search for the Standard Model Higgs boson with the ATLAS detector at the LHC*, *Phys. Lett.* **B716** (2012) 1–29, [1207.7214].

[15] CMS collaboration, S. Chatrchyan et al., *Observation of a new boson at a mass of 125 GeV with the CMS experiment at the LHC*, *Phys. Lett.* **B716** (2012) 30–61, [1207.7235].

[16] M. Magg and C. Wetterich, *Neutrino Mass Problem and Gauge Hierarchy*, *Phys. Lett.* **94B** (1980) 61–64.

[17] R. N. Mohapatra and G. Senjanovic, *Neutrino Masses and Mixings in Gauge Models with Spontaneous Parity Violation*, *Phys. Rev.* **D23** (1981) 165.

[18] J. C. Pati and A. Salam, *Lepton Number as the Fourth Color*, *Phys. Rev.* **D10** (1974) 275–289.

[19] A. D. Sakharov, *Violation of CP Invariance, C asymmetry, and baryon asymmetry of the universe*, *Pisma Zh. Eksp. Teor. Fiz.* **5** (1967) 32–35.

[20] M. Fukugita and T. Yanagida, *Baryogenesis Without Grand Unification*, *Phys. Lett.* **B174** (1986) 45–47.

[21] E. W. Kolb and S. Wolfram, *Baryon Number Generation in the Early Universe*, *Nucl. Phys.* **B172** (1980) 224.

[22] J. A. Harvey and M. S. Turner, *Cosmological baryon and lepton number in the presence of electroweak fermion number violation*, *Phys. Rev.* **D42** (1990) 3344–3349.

[23] Particle Data Group collaboration, M. Tanabashi et al., *Review of Particle Physics*, *Phys. Rev.* **D98** (2018) 030001.

[24] H. Georgi and M. Machacek, *DOUBLY CHARGED HIGGS BOSONS*, *Nucl. Phys.* **B262** (1985) 463–477.

[25] A. Delgado, M. Garcia-Pepin and M. Quiros, *GMSB with Light Stops*, *JHEP* **08** (2015) 159, [1505.07469].

[26] S. W. Herb, D. C. Hom, L. M. Lederman, J. C. Sens, H. D. Snyder, J. K. Yoh et al., *Observation of a dimuon resonance at 9.5 gev in 400-gev proton-nucleus collisions*, *Phys. Rev. Lett.* **39** (Aug, 1977) 252–255.

[27] CDF collaboration, F. Abe et al., *Observation of top quark production in $\bar{p}p$ collisions*, *Phys. Rev. Lett.* **74** (1995) 2626–2631, [hep-ex/9503002].

[28] D0 collaboration, S. Abachi et al., *Observation of the top quark*, *Phys. Rev. Lett.* **74** (1995) 2632–2637, [hep-ex/9503003].

[29] C. S. Li, *Lecture notes on quantum gauge field theory*, July, 2000.

[30] F. Englert and R. Brout, *Broken symmetry and the mass of gauge vector mesons*, *Phys. Rev. Lett.* **13** (Aug, 1964) 321–323.

[31] Wikipedia, "Standard Model." `https://en.wikipedia.org/wiki/Standard_Model`, June 30, 2019.

[32] Wikipedia, "Spontaneous symmetry breaking." `https://en.wikipedia.org/wiki/Spontaneous_symmetry_breaking`, July 6, 2019.

[33] J. H. Christenson, J. W. Cronin, V. L. Fitch and R. Turlay, *Evidence for the* 2π *decay of the* k_2^0 *meson*, *Phys. Rev. Lett.* **13** (Jul, 1964) 138–140.

[34] B. Pontecorvo, *Mesonium and anti-mesonium*, *Sov. Phys. JETP* **6** (1957) 429.

[35] B. Pontecorvo, *Neutrino Experiments and the Problem of Conservation of Leptonic Charge*, *Sov. Phys. JETP* **26** (1968) 984–988.

[36] Super-Kamiokande collaboration, Y. Fukuda et al., *Evidence for oscillation of atmospheric neutrinos*, *Phys. Rev. Lett.* **81** (1998) 1562–1567, [`hep-ex/9807003`].

[37] SNO collaboration, Q. R. Ahmad et al., *Measurement of the rate of* $\nu_e + d \to p + p + e^-$ *interactions produced by* ^8B *solar neutrinos at the Sudbury Neutrino Observatory*, *Phys. Rev. Lett.* **87** (2001) 071301, [`nucl-ex/0106015`].

[38] B. Pontecorvo, *Neutrino Experiments and the Problem of Conservation of Leptonic Charge*, *Sov. Phys. JETP* **26** (1968) 984–988.

[39] B. Pontecorvo, *Mesonium and anti-mesonium*, *Sov. Phys. JETP* **6** (1957) 429.

[40] B. Pontecorvo, *Inverse beta processes and nonconservation of lepton charge*, *Sov. Phys. JETP* **7** (1958) 172–173.

[41] Z. Maki, M. Nakagawa and S. Sakata, *Remarks on the unified model of elementary particles*, *Prog. Theor. Phys.* **28** (1962) 870–880.

[42] R. P. Feynman and M. Gell-Mann, *Theory of Fermi interaction*, *Phys. Rev.* **109** (1958) 193–198.

[43] E. C. G. Sudarshan and R. e. Marshak, *Chirality invariance and the universal Fermi interaction*, *Phys. Rev.* **109** (1958) 1860–1860.

[44] D. A. Ross and M. J. G. Veltman, *Neutral Currents in Neutrino Experiments*, *Nucl. Phys.* **B95** (1975) 135–147.

[45] M. J. G. Veltman, *Limit on Mass Differences in the Weinberg Model*, *Nucl. Phys.* **B123** (1977) 89–99.

[46] V. M. Lobashev, *The search for the neutrino mass by direct method in the tritium beta-decay and perspectives of study it in the project KATRIN*, *Nucl. Phys.* **A719** (2003) 153–160.

[47] Troitsk collaboration, V. N. Aseev et al., *An upper limit on electron antineutrino mass from Troitsk experiment*, *Phys. Rev.* **D84** (2011) 112003, [1108.5034].

[48] C. Kraus et al., *Final results from phase II of the Mainz neutrino mass search in tritium beta decay*, *Eur. Phys. J.* **C40** (2005) 447–468, [hep-ex/0412056].

[49] K. N. Abazajian et al., *Cosmological and Astrophysical Neutrino Mass Measurements*, *Astropart. Phys.* **35** (2011) 177–184, [1103.5083].

[50] Planck collaboration, P. A. R. Ade et al., *Planck 2015 results. XIII. Cosmological parameters*, *Astron. Astrophys.* **594** (2016) A13, [1502.01589].

[51] S. Weinberg, *Baryon- and lepton-nonconserving processes*, *Phys. Rev. Lett.* **43** (Nov, 1979) 1566–1570.

[52] H. Georgi and S. L. Glashow, *Unified weak and electromagnetic interactions without neutral currents*, *Phys. Rev. Lett.* **28** (May, 1972) 1494–1497.

[53] T. D. Lee, *CP Nonconservation and Spontaneous Symmetry Breaking*, *Phys. Rept.* **9** (1974) 143–177.

[54] T. D. Lee, *A theory of spontaneous t violation*, *Phys. Rev. D* **8** (Aug, 1973) 1226–1239.

[55] P. Sikivie, L. Susskind, M. B. Voloshin and V. I. Zakharov, *Isospin Breaking in Technicolor Models*, *Nucl. Phys.* **B173** (1980) 189–207.

[56] K. Hartling, K. Kumar and H. E. Logan, *The decoupling limit in the Georgi-Machacek model*, *Phys. Rev.* **D90** (2014) 015007, [1404.2640].

[57] M. S. Chanowitz, M. A. Furman and I. Hinchliffe, *Weak Interactions of Ultraheavy Fermions*, *Phys. Lett.* **78B** (1978) 285.

[58] M. S. Chanowitz, M. A. Furman and I. Hinchliffe, *Weak Interactions of Ultraheavy Fermions. 2.*, *Nucl. Phys.* **B153** (1979) 402–430.

[59] M. B. Einhorn, D. R. T. Jones and M. J. G. Veltman, *Heavy Particles and the rho Parameter in the Standard Model*, *Nucl. Phys.* **B191** (1981) 146–172.

[60] J. F. Gunion, R. Vega and J. Wudka, *Naturalness problems for ρ=1 and other large one-loop effects for a standard-model higgs sector containing triplet fields*, *Phys. Rev.* **D43** (1991) 2322–2336.

[61] M. E. Peskin and D. V. Schroeder, *An Introduction to quantum field theory*. Addison-Wesley, Reading, MA, USA, 1995.

[62] T. P. Cheng and L. F. Li, *GAUGE THEORY OF ELEMENTARY PARTICLE PHYSICS*. 1984.

[63] N. Seiberg, *Naturalness versus supersymmetric nonrenormalization theorems*, *Phys. Lett.* **B318** (1993) 469–475, [hep-ph/9309335].

[64] M. Drees, R. Godbole and P. Roy, *Theory and phenomenology of sparticles: An account of four-dimensional N=1 supersymmetry in high energy physics*. 2004.

[65] S. Weinberg, *The quantum theory of fields. Vol. 3: Supersymmetry*. Cambridge University Press, 2013.

[66] I. Jack, D. R. T. Jones and P. C. West, *Not the no - renormalization theorem?*, *Phys. Lett.* **B258** (1991) 382–385.

[67] M. Bershadsky, S. Cecotti, H. Ooguri and C. Vafa, *Holomorphic anomalies in topological field theories*, *Nucl. Phys.* **B405** (1993) 279–304, [hep-th/9302103].

[68] M. Carena, I. Low, N. R. Shah and C. E. M. Wagner, *Impersonating the Standard Model Higgs Boson: Alignment without Decoupling*, *JHEP* **04** (2014) 015, [1310.2248].

[69] J. Bernon, J. F. Gunion, H. E. Haber, Y. Jiang and S. Kraml, *Scrutinizing the alignment limit in two-Higgs-doublet models: m_h=125 GeV*, *Phys. Rev.* **D92** (2015) 075004, [1507.00933].

[70] J. Bernon, J. F. Gunion, H. E. Haber, Y. Jiang and S. Kraml, *Scrutinizing the alignment limit in two-Higgs-doublet models. II. m_H=125 GeV*, *Phys. Rev.* **D93** (2016) 035027, [1511.03682].

[71] L. Cort, M. Garcia and M. Quiros, *Supersymmetric Custodial Triplets*, *Phys. Rev.* **D88** (2013) 075010, [1308.4025].

[72] R. Vega, R. Vega-Morales and K. Xie, *The Supersymmetric Georgi-Machacek Model*, *JHEP* **03** (2018) 168, [1711.05329].

[73] W. Porod, *SPheno, a program for calculating supersymmetric spectra, SUSY particle decays and SUSY particle production at e+ e- colliders*, *Comput. Phys. Commun.* **153** (2003) 275–315, [hep-ph/0301101].

[74] W. Porod and F. Staub, *SPheno 3.1: Extensions including flavour, CP-phases and models beyond the MSSM*, *Comput. Phys. Commun.* **183** (2012) 2458–2469, [1104.1573].

[75] J. Alwall, R. Frederix, S. Frixione, V. Hirschi, F. Maltoni, O. Mattelaer et al., *The automated computation of tree-level and next-to-leading order differential cross sections, and their matching to parton shower simulations*, *JHEP* **07** (2014) 079, [1405.0301].

[76] NNPDF collaboration, R. D. Ball et al., *Parton distributions from high-precision collider data*, *Eur. Phys. J.* **C77** (2017) 663, [1706.00428].

[77] T. Hahn, *Generating Feynman diagrams and amplitudes with FeynArts 3*, *Comput. Phys. Commun.* **140** (2001) 418–431, [hep-ph/0012260].

[78] T. Hahn and M. Perez-Victoria, *Automatized one loop calculations in four-dimensions and D-dimensions*, *Comput. Phys. Commun.* **118** (1999) 153–165, [hep-ph/9807565].

[79] D. M. Gingrich, *Practical Quantum Electrodynamics (Pure and Applied Physics)*. CRC Press, Inc., Boca Raton, FL, USA, 2006.

[80] A. Djouadi, *The Anatomy of electro-weak symmetry breaking. I: The Higgs boson in the standard model*, *Phys. Rept.* **457** (2008) 1–216, [hep-ph/0503172].

[81] A. Djouadi, M. Spira and P. M. Zerwas, *QCD corrections to hadronic Higgs decays*, *Z. Phys.* **C70** (1996) 427–434, [hep-ph/9511344].

[82] F. Staub, *Exploring new models in all detail with SARAH*, *Adv. High Energy Phys.* **2015** (2015) 840780, [1503.04200].

[83] A. Vicente, *Computer tools in particle physics*, 1507.06349.

[84] H. P. Nilles, *Supersymmetry, Supergravity and Particle Physics*, *Phys. Rept.* **110** (1984) 1–162.

[85] S. P. de Alwis, *On Anomaly Mediated SUSY Breaking*, *Phys. Rev.* **D77** (2008) 105020, [0801.0578].

[86] D. Gonçalves, T. Han, F. Kling, T. Plehn and M. Takeuchi, *Higgs boson pair production at future hadron colliders: From kinematics to dynamics*, *Phys. Rev.* **D97** (2018) 113004, [1802.04319].

[87] A. Delgado, M. Garcia-Pepin, M. Quiros, J. Santiago and R. Vega-Morales, *Diphoton and Diboson Probes of Fermiophobic Higgs Bosons at the LHC*, *JHEP* **06** (2016) 042, [1603.00962].

[88] G. Brooijmans et al., *Les Houches 2015: Physics at TeV colliders - new physics working group report*, in *9th Les Houches Workshop on Physics at TeV Colliders (PhysTeV 2015) Les Houches, France, June 1-19, 2015*, 2016. 1605.02684.

[89] T. Cao and S. Sekula, *Measurements of the Properties of the Higgs-Like Boson in the Four Lepton Decay Channel with the ATLAS Detector*, Apr, 2016.

[90] A. Djouadi, J. Quevillon and R. Vega-Morales, *Into the multi-TeV scale with a Higgs golden ratio*, *Phys. Lett.* **B757** (2016) 412–419, [1509.03913].

[91] A. G. Akeroyd, M. A. Diaz and F. J. Pacheco, *Double fermiophobic Higgs boson production at the CERN LHC and LC*, *Phys. Rev.* **D70** (2004) 075002, [hep-ph/0312231].

[92] CMS collaboration, V. Khachatryan et al., *Constraints on the spin-parity and anomalous HVV couplings of the Higgs boson in proton collisions at 7 and 8 TeV*, *Phys. Rev.* **D92** (2015) 012004, [1411.3441].

[93] LHC Higgs Cross Section Working Group collaboration, S. Dittmaier et al., *Handbook of LHC Higgs Cross Sections: 1. Inclusive Observables*, 1101.0593.

[94] S. Dittmaier et al., *Handbook of LHC Higgs Cross Sections: 2. Differential Distributions*, 1201.3084.

[95] LHC Higgs Cross Section Working Group collaboration, J. R. Andersen et al., *Handbook of LHC Higgs Cross Sections: 3. Higgs Properties*, 1307.1347.

[96] A. Arhrib, R. Benbrik, M. Chabab, G. Moultaka and L. Rahili, *Higgs boson decay into 2 photons in the type II Seesaw Model*, *JHEP* **04** (2012) 136, [1112.5453].

[97] S. Kanemura and K. Yagyu, *Radiative corrections to electroweak parameters in the Higgs triplet model and implication with the recent Higgs boson searches*, *Phys. Rev.* **D85** (2012) 115009, [1201.6287].

[98] CMS collaboration, V. Khachatryan et al., *Search for a Higgs boson in the mass range from 145 to 1000 GeV decaying to a pair of W or Z bosons*, *JHEP* **10** (2015) 144, [1504.00936].

[99] ATLAS collaboration, G. Aad et al., *Search for Scalar Diphoton Resonances in the Mass Range* $65 - 600$ *GeV with the ATLAS Detector in pp Collision Data at* $\sqrt{s} = 8$ *TeV*, *Phys. Rev. Lett.* **113** (2014) 171801, [1407.6583].

[100] CMS collaboration, C. Collaboration, *Search for new resonances in the diphoton final state in the mass range between 70 and 110 GeV in pp collisions at* $\sqrt{s} = 8$ *and 13 TeV*, .

[101] ATLAS collaboration, T. A. collaboration, *Search for resonances in the 65 to 110 GeV diphoton invariant mass range using 80* fb^{-1} *of pp collisions collected at* $\sqrt{s} = 13$ *TeV with the ATLAS detector*, .

[102] R. Vega, R. Vega-Morales and K. Xie, *Light (and darkness) from a light hidden Higgs*, *JHEP* **06** (2018) 137, [1805.01970].

[103] S. Dawson et al., *Working Group Report: Higgs Boson*, in *Proceedings, 2013 Community Summer Study on the Future of U.S. Particle Physics: Snowmass on the Mississippi (CSS2013): Minneapolis, MN, USA, July 29-August 6, 2013*, 2013. 1310.8361.

[104] J. M. Campbell, J. W. Huston and W. J. Stirling, *Hard Interactions of Quarks and Gluons: A Primer for LHC Physics*, *Rept. Prog. Phys.* **70** (2007) 89, [hep-ph/0611148].

[105] J. D. Bjorken, *Asymptotic Sum Rules at Infinite Momentum*, *Phys. Rev.* **179** (1969) 1547–1553.

[106] R. P. Feynman, *Very high-energy collisions of hadrons*, *Phys. Rev. Lett.* **23** (1969) 1415–1417.

[107] J. D. Bjorken and E. A. Paschos, *Inelastic Electron Proton and gamma Proton Scattering, and the Structure of the Nucleon*, *Phys. Rev.* **185** (1969) 1975–1982.

[108] S. D. Drell and T.-M. Yan, *Partons and their Applications at High-Energies*, *Annals Phys.* **66** (1971) 578.

[109] V. N. Gribov and L. N. Lipatov, *Deep inelastic e p scattering in perturbation theory*, *Sov. J. Nucl. Phys.* **15** (1972) 438–450.

[110] L. N. Lipatov, *The parton model and perturbation theory*, *Sov. J. Nucl. Phys.* **20** (1975) 94–102.

[111] G. Altarelli and G. Parisi, *Asymptotic Freedom in Parton Language*, *Nucl. Phys.* **B126** (1977) 298–318.

[112] Y. L. Dokshitzer, *Calculation of the Structure Functions for Deep Inelastic Scattering and e+ e- Annihilation by Perturbation Theory in Quantum Chromodynamics.*, *Sov. Phys. JETP* **46** (1977) 641–653.

[113] J. C. Collins and D. E. Soper, *The Theorems of Perturbative QCD*, *Ann. Rev. Nucl. Part. Sci.* **37** (1987) 383–409.

[114] J. C. Collins, D. E. Soper and G. F. Sterman, *Factorization of Hard Processes in QCD*, *Adv. Ser. Direct. High Energy Phys.* **5** (1989) 1–91, [hep-ph/0409313].

[115] J. Prentki and J. Steinberger, eds., *Proceedings, 14th International Conference on High-Energy Physics (ICHEP 68)*, (Geneva), CERN, CERN, 1968.

[116] E. D. Bloom, D. H. Coward, H. DeStaebler, J. Drees, G. Miller, L. W. Mo et al., *High-energy inelastic $e-p$ scattering at 6° and 10°*, *Phys. Rev. Lett.* **23** (Oct, 1969) 930–934.

[117] M. Breidenbach, J. I. Friedman, H. W. Kendall, E. D. Bloom, D. H. Coward, H. DeStaebler et al., *Observed behavior of highly inelastic electron-proton scattering*, *Phys. Rev. Lett.* **23** (Oct, 1969) 935–939.

[118] A. De Roeck and R. S. Thorne, *Structure Functions*, *Prog. Part. Nucl. Phys.* **66** (2011) 727–781, [1103.0555].

[119] S. L. Adler, *Adler sum rule*, 0905.2923.

[120] D. J. Gross and C. H. Llewellyn Smith, *High-energy neutrino - nucleon scattering, current algebra and partons*, *Nucl. Phys.* **B14** (1969) 337–347.

[121] K. Gottfried, *Sum rule for high-energy electron - proton scattering*, *Phys. Rev. Lett.* **18** (1967) 1174.

[122] New Muon collaboration, M. Arneodo et al., *A Reevaluation of the Gottfried sum*, *Phys. Rev.* **D50** (1994) R1–R3.

[123] New Muon collaboration, M. Arneodo et al., *Accurate measurement of F2(d) / F2(p) and R**d - R**p*, *Nucl. Phys.* **B487** (1997) 3–26, [hep-ex/9611022].

[124] New Muon collaboration, M. Arneodo et al., *A Reevaluation of the Gottfried sum*, *Phys. Rev.* **D50** (1994) R1–R3.

[125] T. Sloan, R. Voss and G. Smadja, *The Quark Structure of the Nucleon from the CERN Muon Experiments*, *Phys. Rept.* **162** (1988) 45–167.

[126] BCDMS collaboration, A. C. Benvenuti et al., *A High Statistics Measurement of the Proton Structure Functions F(2) (x, Q**2) and R from Deep Inelastic Muon Scattering at High Q**2*, *Phys. Lett.* **B223** (1989) 485–489.

[127] BCDMS collaboration, A. C. Benvenuti et al., *A High Statistics Measurement of the Deuteron Structure Functions F2 (X, Q^2) and R From Deep Inelastic Muon Scattering at High Q^2*, *Phys. Lett.* **B237** (1990) 592–598.

[128] New Muon collaboration, M. Arneodo et al., *Measurement of the proton and deuteron structure functions, F2(p) and F2(d), and of the ratio sigma-L / sigma-T*, *Nucl. Phys.* **B483** (1997) 3–43, [hep-ph/9610231].

[129] H1, ZEUS collaboration, H. Abramowicz et al., *Combination of measurements of inclusive deep inelastic $e^{\pm}p$ scattering cross sections and QCD analysis of HERA data*, *Eur. Phys. J.* **C75** (2015) 580, [1506.06042].

[130] W. Furmanski and R. Petronzio, *Lepton - Hadron Processes Beyond Leading Order in Quantum Chromodynamics*, *Z. Phys.* **C11** (1982) 293.

[131] H1, ZEUS collaboration, S. V. Chekanov, *Open charm production in DIS at HERA*, *Eur. Phys. J.* **C33** (2004) S488–S490, [hep-ex/0309004].

[132] J. C. Collins, F. Wilczek and A. Zee, *Low-Energy Manifestations of Heavy Particles: Application to the Neutral Current*, *Phys. Rev.* **D18** (1978) 242.

[133] S. Bethke, *The 2009 World Average of alpha(s)*, *Eur. Phys. J.* **C64** (2009) 689–703, [0908.1135].

[134] JADE collaboration, S. Bethke, S. Kluth, C. Pahl and J. Schieck, *Determination of the Strong Coupling alpha(s) from hadronic Event Shapes with O(alpha**3(s)) and resummed QCD predictions using JADE Data*, *Eur. Phys. J.* **C64** (2009) 351–360, [0810.1389].

[135] M. A. G. Aivazis, F. I. Olness and W.-K. Tung, *QCD formulation of charm production in deep inelastic scattering and the sea quark - gluon dichotomy*, *Phys. Rev. Lett.* **65** (1990) 2339–2342.

[136] M. A. G. Aivazis, F. I. Olness and W.-K. Tung, *Leptoproduction of heavy quarks. 1. General formalism and kinematics of charged current and neutral current production processes*, *Phys. Rev.* **D50** (1994) 3085–3101, [hep-ph/9312318].

[137] M. A. G. Aivazis, J. C. Collins, F. I. Olness and W.-K. Tung, *Leptoproduction of heavy quarks. 2. A Unified QCD formulation of charged and neutral current processes from fixed target to collider energies*, *Phys. Rev.* **D50** (1994) 3102–3118, [hep-ph/9312319].

[138] J. C. Collins and W.-K. Tung, *Calculating Heavy Quark Distributions*, *Nucl. Phys.* **B278** (1986) 934.

[139] F. I. Olness and W.-K. Tung, *When Is a Heavy Quark Not a Parton? Charged Higgs Production and Heavy Quark Mass Effects in the QCD Based Parton Model*, *Nucl. Phys.* **B308** (1988) 813.

[140] W.-K. Tung, S. Kretzer and C. Schmidt, *Open heavy flavor production in QCD: Conceptual framework and implementation issues*, *J. Phys.* **G28** (2002) 983–996, [hep-ph/0110247].

[141] M. Kramer, 1, F. I. Olness and D. E. Soper, *Treatment of heavy quarks in deeply inelastic scattering*, *Phys. Rev.* **D62** (2000) 096007, [hep-ph/0003035].

[142] J. C. Collins, *Hard scattering factorization with heavy quarks: A General treatment*, *Phys. Rev.* **D58** (1998) 094002, [hep-ph/9806259].

[143] M. Cacciari, S. Frixione and P. Nason, *The p(T) spectrum in heavy flavor photoproduction*, *JHEP* **03** (2001) 006, [hep-ph/0102134].

[144] B. A. Kniehl, M. Kramer, G. Kramer and M. Spira, *Cross-sections for charm production in e p collisions: Massive versus massless scheme*, *Phys. Lett.* **B356** (1995) 539–545, [hep-ph/9505410].

[145] M. Buza, Y. Matiounine, J. Smith and W. L. van Neerven, *Charm electroproduction viewed in the variable flavor number scheme versus fixed order perturbation theory*, *Eur. Phys. J.* **C1** (1998) 301–320, [hep-ph/9612398].

[146] M. Buza, Y. Matiounine, J. Smith and W. L. van Neerven, *Comparison between the various descriptions for charm electroproduction and the HERA data*, *Phys. Lett.* **B411** (1997) 211–217, [hep-ph/9707263].

[147] R. S. Thorne and R. G. Roberts, *A Practical procedure for evolving heavy flavor structure functions*, *Phys. Lett.* **B421** (1998) 303–311, [hep-ph/9711223].

[148] R. S. Thorne and R. G. Roberts, *An Ordered analysis of heavy flavor production in deep inelastic scattering*, *Phys. Rev.* **D57** (1998) 6871–6898, [hep-ph/9709442].

[149] A. Chuvakin, J. Smith and W. L. van Neerven, *Comparison between variable flavor number schemes for charm quark electroproduction*, *Phys. Rev.* **D61** (2000) 096004, [hep-ph/9910250].

[150] M. Cacciari, M. Greco and P. Nason, *The P(T) spectrum in heavy flavor hadroproduction*, *JHEP* **05** (1998) 007, [hep-ph/9803400].

[151] B. W. Harris and J. Smith, *Heavy quark correlations in deep inelastic electroproduction*, *Nucl. Phys.* **B452** (1995) 109–160, [hep-ph/9503484].

[152] P. M. Nadolsky and W.-K. Tung, *Improved formulation of global qcd analysis with zero-mass hard cross sections*, *Phys. Rev. D* **79** (Jun, 2009) 113014.

[153] M. Guzzi, P. M. Nadolsky, H.-L. Lai and C. P. Yuan, *General-Mass Treatment for Deep Inelastic Scattering at Two-Loop Accuracy*, *Phys. Rev.* **D86** (2012) 053005, [1108.5112].

[154] B. Wang, *Applications of QCD factorization in multiscale Hadronic scattering.* PhD thesis, Southern Methodist University, 2015.

[155] W. Furmanski and R. Petronzio, *Lepton - Hadron Processes Beyond Leading Order in Quantum Chromodynamics*, *Z. Phys.* **C11** (1982) 293.

[156] J. A. M. Vermaseren, A. Vogt and S. Moch, *The Third-order QCD corrections to deep-inelastic scattering by photon exchange*, *Nucl. Phys.* **B724** (2005) 3–182, [hep-ph/0504242].

[157] S. A. Larin, P. Nogueira, T. van Ritbergen and J. A. M. Vermaseren, *The Three loop QCD calculation of the moments of deep inelastic structure functions*, *Nucl. Phys.* **B492** (1997) 338–378, [hep-ph/9605317].

[158] S. Moch, J. A. M. Vermaseren and A. Vogt, *The Longitudinal structure function at the third order*, *Phys. Lett.* **B606** (2005) 123–129, [hep-ph/0411112].

[159] P. Nason, S. Dawson and R. K. Ellis, *The One Particle Inclusive Differential Cross-Section for Heavy Quark Production in Hadronic Collisions*, *Nucl. Phys.* **B327** (1989) 49–92.

[160] P. Nason, S. Dawson and R. K. Ellis, *The Total Cross-Section for the Production of Heavy Quarks in Hadronic Collisions*, *Nucl. Phys.* **B303** (1988) 607–633.

[161] W. Beenakker, W. L. van Neerven, R. Meng, G. A. Schuler and J. Smith, *QCD corrections to heavy quark production in hadron hadron collisions*, *Nucl. Phys.* **B351** (1991) 507–560.

[162] W. Beenakker, H. Kuijf, W. L. van Neerven and J. Smith, *QCD Corrections to Heavy Quark Production in p anti-p Collisions*, *Phys. Rev.* **D40** (1989) 54–82.

[163] B. A. Kniehl, G. Kramer, I. Schienbein and H. Spiesberger, *Inclusive D*+- production in p anti-p collisions with massive charm quarks*, *Phys. Rev.* **D71** (2005) 014018, [hep-ph/0410289].

[164] M. Cacciari, M. Greco and P. Nason, *The P(T) spectrum in heavy flavor hadroproduction*, *JHEP* **05** (1998) 007, [hep-ph/9803400].

[165] M. Cacciari, S. Frixione, N. Houdeau, M. L. Mangano, P. Nason and G. Ridolfi, *Theoretical predictions for charm and bottom production at the LHC*, *JHEP* **10** (2012) 137, [1205.6344].

[166] B. A. Kniehl, G. Kramer, I. Schienbein and H. Spiesberger, *Inclusive B-Meson Production at the LHC in the GM-VFN Scheme*, *Phys. Rev.* **D84** (2011) 094026, [1109.2472].

[167] I. Helenius and H. Paukkunen, *Revisiting the D-meson hadroproduction in general-mass variable flavour number scheme*, *JHEP* **05** (2018) 196, [1804.03557].

[168] ALICE collaboration, B. Abelev et al., *Measurement of prompt J/ψ and beauty hadron production cross sections at mid-rapidity in pp collisions at $\sqrt{s} = 7$ TeV*, *JHEP* **11** (2012) 065, [1205.5880].

[169] LHCb collaboration, R. Aaij et al., *Measurement of the $B^{\pm}$ production cross-section in pp collisions at $\sqrt{s} = 7$ and 13 TeV*, 1710.04921.

[170] ATLAS collaboration, G. Aad et al., *Measurement of the inclusive and dijet cross-sections of b^- jets in pp collisions at $\sqrt{s} = 7$ TeV with the ATLAS detector*, *Eur. Phys. J.* **C71** (2011) 1846, [1109.6833].

[171] CMS collaboration, S. Chatrchyan et al., *Inclusive b-jet production in pp collisions at $\sqrt{s} = 7$ TeV*, *JHEP* **04** (2012) 084, [1202.4617].

[172] B. A. Kniehl, G. Kramer, I. Schienbein and H. Spiesberger, *Inclusive Charmed-Meson Production at the CERN LHC*, *Eur. Phys. J.* **C72** (2012) 2082, [1202.0439].

[173] PROSA collaboration, O. Zenaiev et al., *Impact of heavy-flavour production cross sections measured by the LHCb experiment on parton distribution functions at low x*, *Eur. Phys. J.* **C75** (2015) 396, [1503.04581].

[174] M. Cacciari, M. L. Mangano and P. Nason, *Gluon PDF constraints from the ratio of forward heavy-quark production at the LHC at $\sqrt{S} = 7$ and 13 TeV*, *Eur. Phys. J.* **C75** (2015) 610, [1507.06197].

[175] M. L. Mangano and J. Rojo, *Cross Section Ratios between different CM energies at the LHC: opportunities for precision measurements and BSM sensitivity*, *JHEP* **08** (2012) 010, [1206.3557].

[176] B. Mele and P. Nason, *The Fragmentation function for heavy quarks in QCD*, *Nucl. Phys.* **B361** (1991) 626–644.

[177] M. Cacciari and M. Greco, *Large p_T hadroproduction of heavy quarks*, *Nucl. Phys.* **B421** (1994) 530–544, [hep-ph/9311260].

[178] T. Sjostrand, S. Mrenna and P. Z. Skands, *A Brief Introduction to PYTHIA 8.1*, *Comput. Phys. Commun.* **178** (2008) 852–867, [0710.3820].

[179] G. Corcella, I. G. Knowles, G. Marchesini, S. Moretti, K. Odagiri, P. Richardson et al., *HERWIG 6: An Event generator for hadron emission reactions with interfering gluons (including supersymmetric processes)*, *JHEP* **01** (2001) 010, [hep-ph/0011363].

[180] S. Frixione, P. Nason and B. R. Webber, *Matching NLO QCD and parton showers in heavy flavor production*, *JHEP* **08** (2003) 007, [hep-ph/0305252].

[181] S. Frixione, P. Nason and G. Ridolfi, *A Positive-weight next-to-leading-order Monte Carlo for heavy flavour hadroproduction*, *JHEP* **09** (2007) 126, [0707.3088].

[182] G. P. Salam and J. Rojo, *A Higher Order Perturbative Parton Evolution Toolkit (HOPPET)*, *Comput. Phys. Commun.* **180** (2009) 120–156, [0804.3755].

[183] A. Buckley, J. Ferrando, S. Lloyd, K. Nordström, B. Page, M. Rüfenacht et al., *LHAPDF6: parton density access in the LHC precision era*, *Eur. Phys. J.* **C75** (2015) 132, [1412.7420].

[184] Particle Data Group collaboration, C. Patrignani et al., *Review of Particle Physics*, *Chin. Phys.* **C40** (2016) 100001.

[185] T. Carli, D. Clements, A. Cooper-Sarkar, C. Gwenlan, G. P. Salam, F. Siegert et al., *A posteriori inclusion of parton density functions in NLO QCD final-state calculations at hadron colliders: The APPLGRID Project*, *Eur. Phys. J.* **C66** (2010) 503–524, [0911.2985].

[186] LHCb collaboration, R. Aaij et al., *Measurement of $\sigma(pp \to b\bar{b}X)$ at $\sqrt{s} = 7$ TeV in the forward region*, *Phys. Lett.* **B694** (2010) 209–216, [1009.2731].

[187] LHCb collaboration, R. Aaij et al., *Measurement of the $B^{\pm}$ production cross-section in pp collisions at $\sqrt{s} = 7$ TeV*, *JHEP* **04** (2012) 093, [1202.4812].

[188] R. Boughezal, J. M. Campbell, R. K. Ellis, C. Focke, W. Giele, X. Liu et al., *Color singlet production at NNLO in MCFM*, *Eur. Phys. J.* **C77** (2017) 7, [1605.08011].

[189] M. Cacciari, "FONLL Heavy Quark Production." http://www.lpthe.jussieu.fr/~cacciari/fonll/fonllform.html, June, 2017.

[190] S. Dulat, T.-J. Hou, J. Gao, M. Guzzi, J. Huston, P. Nadolsky et al., *New parton distribution functions from a global analysis of quantum chromodynamics*, *Phys. Rev.* **D93** (2016) 033006, [1506.07443].

[191] J. Pumplin, D. Stump, R. Brock, D. Casey, J. Huston, J. Kalk et al., *Uncertainties of predictions from parton distribution functions. 2. The Hessian method*, *Phys. Rev.* **D65** (2001) 014013, [hep-ph/0101032].

[192] J. Pumplin, D. R. Stump, J. Huston, H. L. Lai, P. M. Nadolsky and W. K. Tung, *New generation of parton distributions with uncertainties from global QCD analysis*, *JHEP* **07** (2002) 012, [hep-ph/0201195].

[193] W.-K. Tung, S. Kretzer and C. Schmidt, *Open heavy flavor production in QCD: Conceptual framework and implementation issues*, *J. Phys.* **G28** (2002) 983–996, [hep-ph/0110247].

[194] M. Dine and A. E. Nelson, *Dynamical supersymmetry breaking at low-energies*, *Phys. Rev.* **D48** (1993) 1277–1287, [hep-ph/9303230].

[195] Z. Chacko, M. A. Luty, A. E. Nelson and E. Ponton, *Gaugino mediated supersymmetry breaking*, *JHEP* **01** (2000) 003, [hep-ph/9911323].

[196] G. Passarino and M. J. G. Veltman, *One Loop Corrections for e+ e- Annihilation Into mu+ mu- in the Weinberg Model*, *Nucl. Phys.* **B160** (1979) 151–207.